The Dynamics and Function of the Endolysosomal/Lysosomal System

Luther John Davis

University of Cambridge

Homerton College

This dissertation is submitted for the degree of Doctor of Philosophy

September 2018

Acknowledgements

Firstly, I would like to thank Prof. J Paul Luzio for his invaluable guidance and effort towards the production and proofreading of this thesis. I would also like to thank Chloe Taylor, Ian Baines, Theo Dare, and Ashley Broom for their expertise, assistance and reassurance. I am grateful to the BBSRC and GSK for funding my project for four years. I thank Sally Gray, Nick Bright, and Lena Wartosch for their technical assistance and support. Finally I would like to express my gratitude to Matthew Gratian and Mark Bowen for training and assistance with microscopy, as well as Reiner Schulte, Chiara Cossetti, and Gabriela Grondys-Kotarba for their help with flow cytometry and cell sorting.

Preface

This dissertation is the result of my own work and includes nothing which is the outcome of work done in collaboration except as declared in the Preface and specified in the text. It is not substantially the same as any that I have submitted, or, is being concurrently submitted for a degree or diploma or other qualification at the University of Cambridge or any other University or similar institution except as declared in the Preface and specified in the text. I further state that no substantial part of my dissertation has already been submitted, or, is being concurrently submitted for any such degree, diploma or other qualification at the University of Cambridge or any other University or similar institution except as declared in the Preface and specified in the text. This dissertation does not exceed the word limit of 60,000 words, as stipulated by the School of Clinical Medicine.

Thesis Summary

Lysosomes are intracellular organelles that were considered for a long time to be simply an acidic and hydrolytically active end point of trafficking routes for degradation, in the last 20 years, light has been shed on their functional heterogeneity and striking role in signalling and nutrient homeostasis. While the dynamic nature and variety of lysosomal functions are now better appreciated, the mechanisms governing lysosomal fusion, reformation, signalling, and homeostasis remain to be fully elucidated, and are investigated here.

In this study, endolysosomes which formed by fusion of late endosomes with lysosomes and are thought to be the predominant site of hydrolytic activity, were further characterised. Using live cell imaging and fluorescent labelling, the proportion of endolysosomes in the total pool of lysosomes was estimated using probes to their acidity and cathepsin activity, and their larger size compared to storage lysosomes was observed. The endolysosomal membrane was also shown to be marked by Rab7, Rab9, $PI(3,5)P_2$ supporting the role of endolysosomes a highly active and dynamic principal site of hydrolase activity.

The contributions of VAMP7 and VAMP8 to endolysosome fusion, measured by delivery of endocytosed cargo from late endosomes to endolysosomes, were analysed by CRISPR-Cas9 mediated knockout. Cells lacking VAMP7 and VAMP8 had no effect on delivery to endolysosomes, however at EM level, they displayed extensive tethering between late endocytic organelles, and accumulated small tethered vesicles. YKT6 knockdown impeded delivery to endolysosomes in VAMP7+VAMP8 knockout cells, which was rescued by VAMP7 expression, suggesting YKT6 substituted for VAMP7 in lysosome fusion.

Following the hypothesis that reversible dissociation of V1 and Vo sectors of the V-ATPase may control the increase in pH of reforming storage lysosomes, cells expressing tagged V1G1 and Voa3 were generated. These markers of both sectors are present on endolysosomal membranes, and on the emerging endolysosomal tubules, suggesting the V1 and Vo sectors remain associated at this earliest stage of lysosome reformation, but these markers are still in development.

Two assays were developed to give a readout of, and assess lysosomal stress. Firstly, an assay measuring TFEB-GFP translocation to the nucleus gave a robust and quantifiable readout of lysosomal perturbation. Secondly, a qPCR assay was developed to measure lysosomal gene upregulation as a downstream reporter of TFEB-activating lysosomal perturbations, however this assay, despite being more lysosome-specific, lacked the consistency and dynamic range of the TFEB translocation quantification.

In summary, lysosomes are a heterogeneous collection of organelles, which have been better characterised primarily according to their acidity and hydrolytic capacity. Additionally, more SNAREs appear to be involved in lysosome fusion in cells than suggested by cell free assays, and I have developed tools to trace the V-ATPase during reformation of lysosomes after fusion to form endolysosomes. Lastly, I have developed a robust, reporter for a range of lysosomal stress-inducing conditions, providing a broad indication of their effects on lysosomal signalling and homeostasis.

Abbreviations

AKT	Protein kinase B
AMP	Adenosine monophosphate
ANOVA	Analysis of variance
AP	Adaptor protein
APS	Ammonium persulfate
Arf	ADP-ribosylation factor
Arp	Actin-related proteins
ATP	Adenosine triphosphate
BafA1	Bafilomycin A1
BAR	Bin/amphiphysin/rvs
BCA	Bicinchoninic acid
BHK	Baby hamster kidney
BSA	Bovine serum albumin
CCV	Clathrin coated vesicle
Cdc42	Cell division control protein 42 homolog
CFTR	Cystic fibrosis transmembrane conductance regulator
CLEAR	Coordinated lysosomal expression and regulation
CLEM	Correlative light and electron microscopy
CLIC	Clathrin independent carrier
CME	Clathrin mediated endocytosis
CORVET	Class C core/vacuole tethering
CQ	Chloroquine
CRISPR	Clustered regularly interspaced short palindromic repeats
CTxB	Cholera toxin B-subunit
DAB	Diaminobenzidine
DexA488	Dextran AlexaFluor™ 488 10,000 MW
DexA647	Dextran AlexaFluor™ 647 10,000 MW
DIC	Differential interference contrast
DMEM	Dulbecco’s Modified Eagle’s Medium
DNA	Deoxyribonucleic acid
dNTP	Deoxynucleotide triphosphate
DRM	Detergent-resistant membrane
DTT	Dithiothreitol
EBSS	Earle’s balanced salt solution
EEA1	Early endosome antigen 1
EGFR	Epidermal Growth Factor Receptor
EM	Electron microscopy
Eps15	Epidermal growth factor receptor pathway substrate 15
Eps15R	Epidermal growth factor receptor pathway substrate 15R
ER	Endoplasmic Reticulum

ESCRT	Endosome sorting complexes required for transport
FACS	Fluorescence-activated cell sorting
FCS	Foetal calf serum
G418	Geneticin
GAP	GTPase-activating protein
GEEC	GPI-enriched endocytic compartment
GEF	Guanine nucleotide exchange factor
GFP	Green fluorescent protein
GGA	Golgi-localised gamma-ear-containing Arf-binding protein
GPCR	G-protein coupled receptor
GPI	Glycosylphosphatidylinositol
GTP	Guanosine triphosphate
HA	Haemagglutinin
HEK	Human embryonic kidney
HOPS	Homotypic fusion and vacuole protein sorting
HRP	Horseradish peroxidase
Hsc70	Heat shock cognate protein 70
IFITM3	Interferon-inducible transmembrane protein 3
ILV	Intraluminal vesicle
KD	Knock down
KO	Knock out
LAMP	Lysosome-associated membrane protein
LBPA	Lysobisphosphatidic acid
LC3	Microtubule-associated protein light chain 3
LDL	Low density lipoprotein
LDLR	Low density lipoprotein receptor
lgp120	Lysosomal membrane glycoprotein 120kDa
LM	Light microscopy
LRO	Lysosome-related organelle
LTG	LysoTracker® Green DND-26
LTR	LysoTracker® Red DND-99
LYST	Lysosomal trafficking regulator
M6PR	Mannose-6-phosphate receptor
MCF7	Michigan Cancer Foundation-7
MCS	Membrane contact sites
MEM	Minimum Essential Medium
MRB	Magic Red™ Cathepsin B-substrate
MRL	Magic Red™ Cathepsin L-substrate
mTOR	mechanistic target of rapamycin
mTORC1	mTOR complex 1
MVB	Multivesicular body
Mvb12	Multivesicular body sorting factor 12
MW	Molecular weight
NAADP	Nicotinic acid adenine dinucleotide phosphate
NRK	Normal rat kidney

Ostm1	Osteopetrosis associated transmembrane protein 1
PBS	Phosphate buffered saline
PCR	Polymerase chain reaction
PERK	Protein kinase RNA-like endoplasmic reticulum kinase
PFA	Paraformaldehyde
PI(3)K	Phosphoinositide 3-kinase
PI(3)P	Phosphatidylinositol-3-phosphate
$PI(3,4,5)P_2$	Phosphatidylinositol-3,4,5-trisphosphate
$PI(3,5)P_2$	Phosphatidylinositol-3,5-bisphosphate
$PI(4,5)P_2$	Phosphatidylinositol-4,5-bisphosphate
PIP	Phosphatidylinositol phosphate
PNK	Polynucleotide Kinase
PS	Phosphatidyl Serine
PVDF	Polyvinylidene difluoride
RILP	Rab-interacting lysosomal protein
RNA	Ribonucleic acid
RPMI	Roswell Park Memorial Institute
SDS-PAGE	Sodium dodecyl sulfate–polyacrylamide gel electrophoresis
SEM	Standard error of the mean
SERCA	Sarco/endoplasmic reticulum Ca^{2+}-ATPase
SH3	SRC homology 3
siRNA	Small interfering RNA
SNAP29	Synaptosome associated protein 29
SNARE	Soluble NSF attachment protein receptor
Snf7	Sucrose non-fermenting protein 7
Snx	Sorting nexin
Snx1	Sorting nexin 1
SV40	Simian vacuolating virus 40
TAE	Tris-acetic acid-EDTA
TBS-T	Tris buffered saline-tween 20
TEM	Transmission electron microscopy
TEMED	Tetramethylethylenediamine
TFEB	Transcription factor EB
TfR	Transferrin receptor
TGN	Trans-Golgi Network
TLR9	Toll-like receptor 9
TPC	Two pore channel
TSE	Tubular sorting endosomes
UIM	Ubiquitin interacting motif
VAMP4	Vesicle associated membrane protein 4
Vap	Virulence-associated protein
V-ATPase	Vacuolar H+-ATPase
VPS	Vacuolar protein sorting-associated protein
Vti1a	Vesicle transport through interaction with t-SNAREs homolog 1A

Vti1b	Vps10 tail interactor 1b
WASH	WASP and Scar homolog
WAVE	WASP-family verprolin-homologous protein
WT	Wild type
ZKSCAN3	Zinc finger with KRAB and SCAN domains 3

Publications

Publications to which I have contributed during the period of the work for this thesis:

Bright NA, Davis LJ and Luzio JP. (2016) Endolysosomes Are the Principal Intracellular Sites of Acid Hydrolase Activity. *Curr Biol.* **26**:2233-2245. doi: 10.1016/j.cub.2016.06.046.

Rapiteanu R, Davis LJ, Williamson JC, Timms RT, Paul Luzio J and Lehner PJ. (2016) A Genetic Screen Identifies a Critical Role for the WDR81-WDR91 Complex in the Trafficking and Degradation of Tetherin. *Traffic* **17**:940-958. doi: 10.1111/tra.12409.

Rofe AP, Davis LJ, Whittingham JL, Latimer-Bowman EC, Wilkinson AJ and Pryor PR. (2017) The *Rhodococcus equi* virulence protein VapA disrupts endolysosome function and stimulates lysosome biogenesis. *MicrobiologyOpen* **6**: e00416 doi: 10.1002/mbo3.416.

Hesketh GG, Wartosch L, Davis LJ, Bright NA, Luzio JP. (2018) The Lysosome and Intracellular Signalling. *Prog Mol Subcell Biol.* **57**:151-180. doi: 10.1007/978-3-319-96704-2_6.

Table of Contents

Chapter 1 - Introduction

1.1 Endocytic pathway summary

The endocytic pathway is a trafficking route through which cells can internalise macromolecules from the plasma membrane. Many are subsequently sorted and recycled back to the cell surface. A proportion of endocytosed material, however, is destined for degradation to regulate certain cellular functions and provide the cell with nutrients. This degradation requires the lysosome, a membrane bound organelle discovered in the 1950s (de Duve, 2005) which contains a wide array of digestive enzymes and has been described as having a luminal pH between 4.6 and 5.0 (MellmanFuchs and Helenius, 1986) permitting its digestion of a range of substrates.

Intracellular membrane trafficking, including transport of macromolecules to lysosomes, generally occurs through a number of distinct and sequential processes, beginning with vesicle formation (reviewed in (Mellman and Warren, 2000; Bonifacino and Glick, 2004). Regions within a membrane can assemble protein coats, which deform the membrane while incorporating cargo proteins into a forming pit. This pit within the membrane eventually buds off, generating a cargo-laden coated vesicle. The coat is rapidly disassembled, allowing the vesicle to be directed to its destination by interactions of intracellular proteins with the vesicle's Rab GTPase proteins. Rab proteins on the surface of the vesicle determine its destination by interacting with a number of Rab-specific effectors such as motor proteins, which drive long distance movement along cytoskeletal filaments using the energy from the hydrolysis of ATP. Rab proteins can undergo further specific interactions with tether proteins, which are long-reaching protein complexes bound to the target membrane, which link the two membranes together in close proximity. After being tethered to the target membrane, the vesicle can finally deliver its contents via membrane fusion which requires soluble N-ethylmaleimide-sensitive factor attachment protein receptor (SNARE) proteins. SNAREs are transmembrane proteins containing helical domains which, in specific combinations, are able to form trans-SNARE complexes between vesicle and target membranes (reviewed in (WangLi and Hong, 2017)). Trans-SNARE complexes are formed between a single R-SNARE (named for the critical Arg residue in the helical domain) on the vesicle with three Q-SNAREs (Qa, Qb, and Qc, named for the critical Glu residue) on the target membrane. As these domains bind and zipper together into a four-helix bundle, the opposing membranes are

thought to be brought close enough to exclude water and mediate movement of lipids between the membranes before full membrane fusion (Figure 1.1).

Figure 1.1

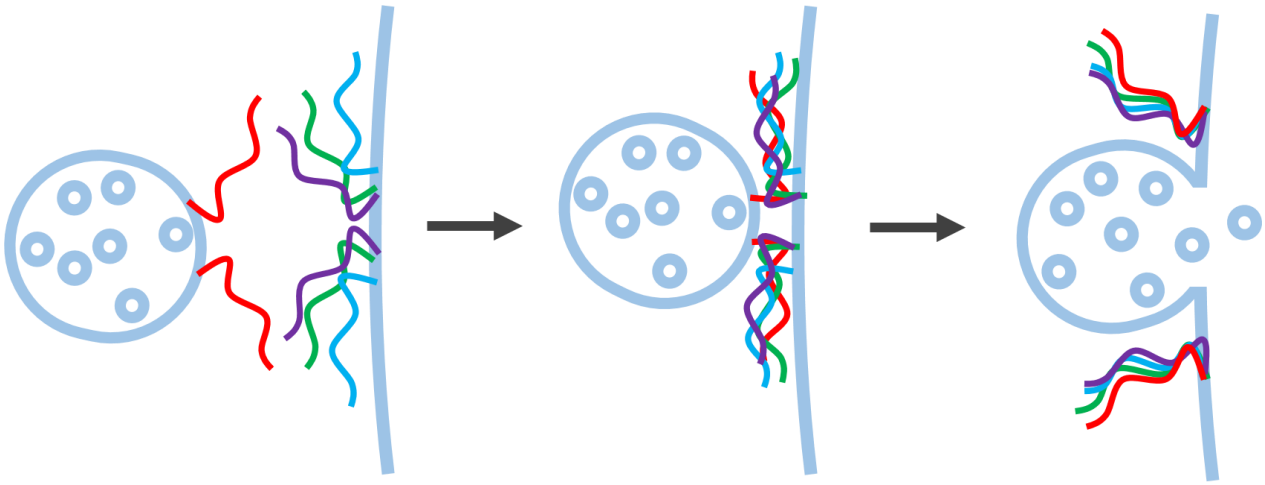

Figure 1.1: SNARE-mediated fusion

Diagram depicting the formation of trans-SNARE complexes between the R-SNAREs (red) on an oncoming organelle, with the Qa, Qb, and Qc SNAREs on the target membrane (green, blue and purple). The trans-SNARE complexes zipper up, pulling the phospholipid bilayers of the organelle and target membrane close enough to promote membrane fusion.

Through a number of mechanisms, specific cargo-enriched regions of the plasma membrane can be invaginated and pinched off to generate endocytic vesicles which fuse with early endosomes. The Golgi apparatus can deliver proteins important to lysosomal function via this route, or through more direct routes whereby Golgi-derived vesicles fuse with early endosomes, as is the case for many hydrolases, or with late endosomes, as has been demonstrated for lysosome-associated membrane proteins (LAMPs) (Pols *et al.*, 2013b). In the lumen of early endosomes, the lower pH causes some ligands to dissociate from their receptors, which can cause a cessation of signalling, and frees the receptor to be recycled back to the plasma membrane or Golgi apparatus. Early endosomes mature into, or bud off, late endosomes which are generally marked by the switch from Rab5 to Rab7, lower pH, and fewer recycling proteins, and hence less tubulation. Proteins in the limiting membrane of the early endosome which are destined for degradation are marked by ubiquitination, which acts as a signal for their incorporation into intraluminal vesicles (ILVs) by the endosome sorting complexes required for transport (ESCRT). This gives rise to the characteristic numerous vesicles of the late endosome/multi-vesicular body (MVB). Late endosomes deliver lysosomal proteins and degradation substrates to the lysosomes by transient exchanges of luminal content, or direct fusions resulting in a hybrid endolysosome compartment (Mullock *et al.*, 1998) from which lysosomes may be reformed (Pryor *et al.*, 2000). The overall architecture of the endocytic pathway is shown in Figure 1.2.

Figure 1.2

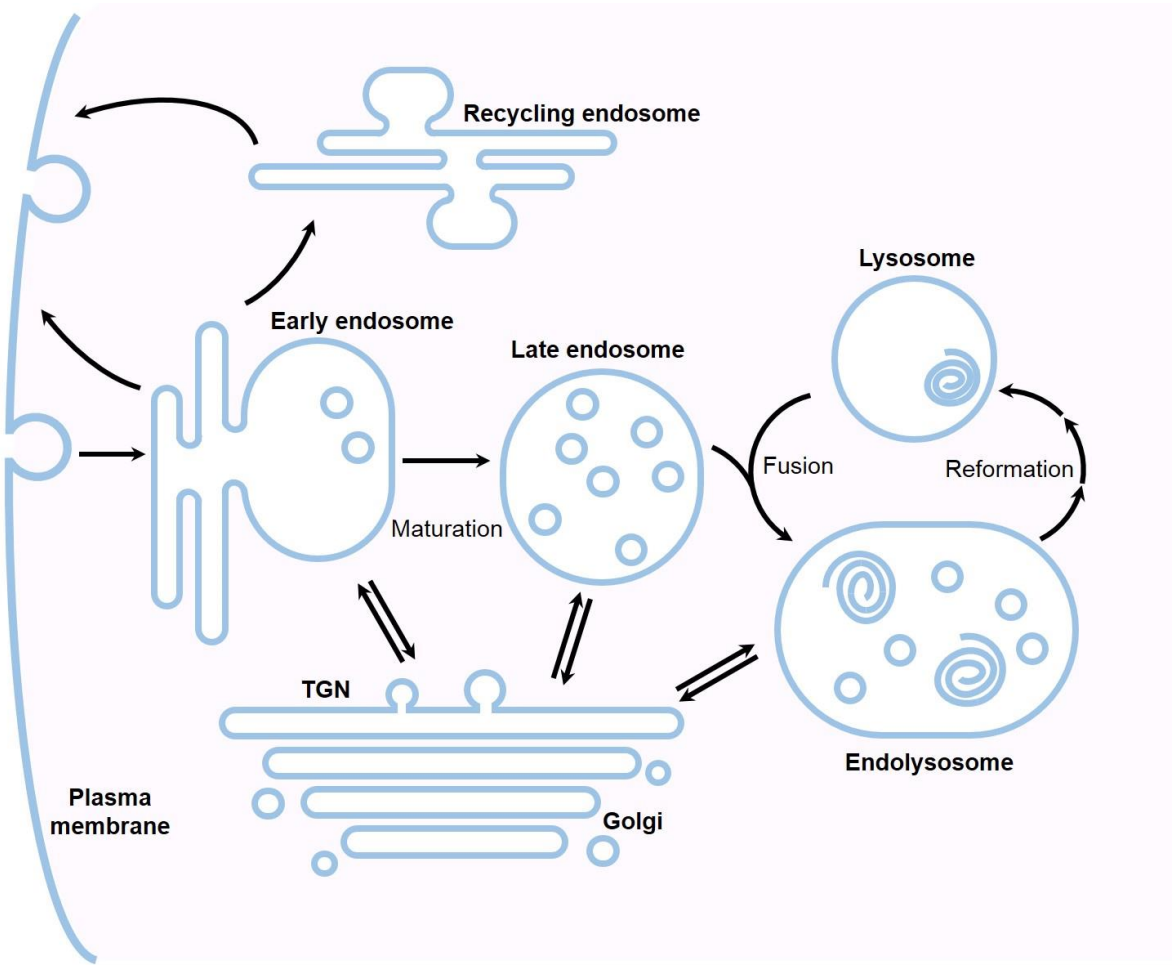

Figure 1.2: The endocytic pathway

Scheme showing the trafficking route of the endocytic pathway from plasma membrane through to endolysosomes. Also depicted is the recycling from early endosomes back to the membrane, and the bidirectional trafficking between the Golgi and early endosomes, late endosomes, or endolysosomes.

1.2 Clathrin-mediated endocytosis

Endocytosis is a process by which receptor-bound or fluid phase macromolecules, larger solutes, lipids, and ions are internalised into the cell, providing substrates for lysosomal digestion, maintaining membrane homeostasis, and regulating the composition and function of the plasma membrane. This occurs at distinct regions of the plasma membrane where integral cargo proteins are accumulated by cytosolic proteins organised at the intracellular face of the membrane, leading to reshaping, invagination, and ultimately fission to release an endocytic vesicle.

Clathrin-mediated endocytosis (CME) is the best studied and most predominant mechanism of endocytosis (Watts and Marsh, 1992; BitsikasCorrêa and Nichols, 2014). Clathrin itself does not recognise cargo, so the endocytic process begins with the recruitment of adaptor proteins to the plasma membrane. Adaptor proteins for CME localise to the plasma membrane by interactions with PI(4,5)P2 and specific signals or motifs on cargo proteins which designate them for internalisation. Adaptor complex AP2 is the most abundant clathrin adaptor, recognising both YxxΦ and acidic di-leucine sequence motifs on the cytosol-accessible regions of cargo proteins (Kelly and Owen, 2011; Bonifacino and Traub, 2003), which together comprise the majority of internalisation signals in mammalian cells.

Ubiquitination of proteins is a widely used internalisation signal in yeast, and is also present in mammalian cells, where it is not recognised by AP2, but is bound by Eps15, Eps15R, and epsin via their ubiquitin-interacting motifs (UIM) (Polo *et al.*, 2002; Barriere *et al.*, 2006). These proteins in turn bind clathrin, inducing coated pit formation. Phosphorylation of the cytoplasmic domain of receptors represents another signal for CME, and is exemplified by the internalisation of G-Protein Coupled Receptors (GPCR). Ligand binding causes conformational changes which allow the GPCR to become phosphorylated. In this phosphorylated state, the receptor can be bound by its adaptors, β-arrestins 1 and 2 which in turn recruit AP2 and clathrin (Traub and Bonifacino, 2013). However, it is not yet understood how these adaptors distinguish GPCRs from the range of other phosphorylated proteins at the cell surface.

Cargo-bound adaptors bind clathrin subunits in the form of triskelia, each comprised of three heavy chains and three light chains (Edeling *et al.*, 2006). Many clathrin

subunits polymerise together, forming a cage-like coat around a budding region of membrane where cargo proteins are then accumulated. For a long time it remained unclear whether pre-existing flat arrays of clathrin on membranes change shape to form the coated pits destined to become clathrin-coated vesicles (CCV) or if sequential recruitment of clathrin subunits helps drive the pit formation (Mousavi *et al.*, 2004). Recent use of combined fluorescence microscopy and electron tomography has shown that during invagination the curvature of the clathrin coat increases, but the coated surface area remains nearly constant. Moreover, clathrin rapidly exchanges at all stages of CME, so that coated vesicle budding involves bending of a dynamic preassembled clathrin coat (Avinoam *et al.*, 2015). Simultaneous to the recruitment of clathrin, additional accessory proteins such as epsin, and the Bin/amphiphysin/Rvs (BAR) domain-containing proteins amphiphysin and endophilin, are recruited to, and induce the bending of, the membrane (PopovaDeyev and Petrenko, 2013). The clathrin lattice is thought to stabilise this curvature of the forming pit.

The GTPase, dynamin, is recruited to the membrane by the Src Homology (SH3) domain of amphiphysin, self-assembles into rings around the neck of the forming pit, and along with endophilin, facilitates fission, releasing a clathrin coated vesicle (CCV) (SchmidMcNiven and De Camilli, 1998). Following scission of the coated vesicle from the membrane, clathrin needs to be released to recycle its subunits, and to expose the membrane proteins of the vesicle required for proper trafficking. This occurs when auxilin binds to assembled clathrin, and recruits Hsc70, the ATPase activity of which disrupts clathrin-clathrin interactions (Lemmon, 2001).

1.3 Clathrin Independent Endocytosis

Although CME can account for the majority of endocytosis and fluid-phase uptake in many cell types, macropinocytosis can make an important contribution (Buckley and King, 2017). Cells spontaneously construct circular or linear ruffles by locally coordinated membrane extensions, for which small GTPase Rac1 activation is necessary and sufficient. Rac1 must then be deactivated to allow ruffle collapse to enclose and capture extracellular fluid. Throughout the process of macropinocytic cup formation, levels of different phosphatidylinositol phosphates (PIP)s, primarily phosphatidylinositol-4,5-bisphosphate (PI(4,5)P2) and phosphatidylinositol-3,4,5-

trisphosphate ($PI(3,4,5)P_3$), are modulated however the timing of each peak is inconsistent between cell types. Patches of active Ras and $PI(3,4,5)P_3$ recruit SCAR/WAVE proteins, which in turn activate Arp2/3 complex to drive actin polymerisation and membrane protrusion at the lip. Progressive $PI(3,4,5)P_2$ dephosphorylation is important for the closure of the protruded macropinocytic cup, possibly by PI(3)P-mediated K^+-channel activation (Maekawa *et al.*, 2014). Macropinosomes mature through condensation of their contents and receiving delivery of enzymes and V-ATPases, mediated by Rab5 recruitment, and later Rab5-Rab7 exchange (reviewed in (Egami, 2016). The mechanisms of late maturation of macropinosomes are not well defined, but macropinosomes can acquire LAMP1 through fusion with degradative/lysosomal compartments. The parallels between macropinosomes and endosomes, with the advantage of their larger dimensions, makes macropinosomes potential models for live cell studies of endosomal dynamics and function (Kerr and Teasdale, 2009).

A proportion of Epidermal Growth Factor Receptor (EGFR) can be endocytosed in certain cell types via coat-free vesicles in a dynamin-dependent manner (Sorkin and Goh, 2009). EGFR can accumulate in caveolae, which are pits in the plasma membrane formed by association of proteins CAV1, 2, or 3, and cavins 1, 2, 3, or 4 (depending on cell type) with phosphatidyl serine (PS), PI(4,5)P2, and cholesterol-rich lipid rafts on the plasma membrane (Sigismund *et al.*, 2005; PartonTillu and Collins, 2018). The lack of known caveolae-exclusive cargo makes their endocytic function difficult to trace, but it is generally accepted that they form endocytic vesicles, requiring dynamin, Src kinase, and protein kinase C (Parton and Simons, 2007) and contain cargoes such as SV40 virions, cholera toxin B subunit (CTxB), and glycosylphosphatidylinositol (GPI)-linked proteins. Unlike clathrin, caveolae-derived endocytic vesicles retain their cavin coat proteins through to fusion with early endosomes, from which they are recycled to the plasma membrane. Another endocytic route, which does not depend on clathrin or caveolin, is the clathrin-independent carrier/GPI-enriched endocytic compartment (CLIC/GEEC), which shares some cargoes with caveolae, is cholesterol-dependent and seems to be regulated by cdc42 (Doherty and McMahon, 2009). It is hypothesised that enriched GPI-linked protein cargoes in the membrane may be sufficient to induce curvature which could then be recognised by proteins which facilitate budding and scission,

such as BAR-domain proteins and dynamin, releasing endocytic compartments destined for GEECs.

1.4 Early Endosomes

Endocytic, and Golgi-derived vesicles converge at the early endosome in the periphery of the cell, where they undergo SNARE-mediated fusion with the early endosome membrane to deliver their contents. Early endosomes undergo further homotypic fusions mediated by the SNAREs syntaxin 13, syntaxin 6, vti1a, and VAMP4, however these SNAREs alone do not confer specificity to this fusion (Rink *et al.*, 2005; Brandhorst *et al.*, 2006). The early endosome is a hub for the sorting and trafficking of internalised proteins to their appropriate destinations, be it recycling to the plasma membrane, delivery to the TGN, or to the lysosome (Jovic *et al.*, 2010). The functions and identity of the early endosome are largely determined by the presence of Rab5, its regulators, and its effectors on the organelle surface, including VPS34/p150 which functions as a PI 3-kinase (PI(3)K) to generate PI(3)P in the membrane (Zerial and McBride, 2001). The predominant trafficking route from the early endosome is recycling to the plasma membrane via tubular sorting endosomes (TSE) which concentrate membrane proteins by the nature of their surface area:volume ratio. This route is used to return receptors, such as low density lipoprotein (LDL) receptors (LDLR), to the cell surface after their internalisation and ligand dissociation due to the lower pH of the endosome, to allow for further rounds of ligand binding (Saftig and Klumperman, 2009). Cell surface recycling of these integral proteins is mediated by the similar but distinct coat protein complexes retromer, which can bind cytosolic domains directly or via adaptor protein sorting nexin-27 (SNX27) (Burd and Cullen, 2014), and retriever, which binds cargo via it's adaptor, sorting nexin-17 (SNX17) (McNally *et al.*, 2017). Both retromer and retriever associate with WASH complex to activate Arp2/3-dependent actin polymerisation and drive extrusion from the membrane. Similarly to LDL, acid hydrolases dissociate from the mannose-6-phosphate receptor (M6PR) after delivery from the TGN to the early endosome, constituting a major delivery route for lysosomal enzymes. M6PR is recycled via endosome-to-TGN carriers from the endosome body, requiring retromer subunit sorting nexin 1 (SNX1), or from the TSE where retromer subunit VPS26 colocalises with clathrin (Seaman, 2004; Arighi *et al.*, 2004; Carlton *et al.*, 2004). Clathrin coated vesicles also appear to contribute to M6PR recycling to the TGN, as

AP-1 is required (Meyer *et al.*, 2000) and depends on binding and vesicle incorporation by Golgi-localized, γ-ear-containing, Arf (ADP-ribosylation factor)-binding proteins (GGAs) (Doray *et al.*, 2002). Ubiquitination of membrane proteins acts as a signal for endosomal retention and eventual delivery to lysosomes. This can act as a regulatory mechanism to stop signalling of receptors which do not dissociate from their ligands in the endosomal pH, such as EGFR, or to down regulate the total amounts of available receptors at the cell surface. Ubiquitinated proteins are concentrated into a subdomain of the early endosome (Saftig and Klumperman, 2009), where they are sorted into intra-luminal vesicles (ILV) by the sequential actions of five cytosolic complexes: ESCRT-0, -I, -II, -III, and Vps4 complex (Schmidt and Teis, 2012) as depicted in Figure 1.3. The constituent proteins of these complexes were first identified in yeast genetic screens for vacuole defects (Raymond *et al.*, 1992) and their roles are conserved in mammalian cells. Multiple monoubiquitination or polyubiquitination of the cytosolic domains of membrane proteins is recognised as a signal for ILV incorporation. ILV formation is initiated by ESCRT-0, which is comprised of Vps27 and Hse1, and binds both ubiquitin and PI(3)P on the endosome membrane. ESCRT-0 recruits, and transfers cargo to ESCRT-I, a rod-like hetero-tetramer of Vps23, Vps28, Vps37, and Mvb12, also capable of binding ubiquitinated cargo. ESCRT-I in turn recruits and transfers cargo to ESCRT-II, which consists of Vps22, Vps36, and two Vps25 proteins, and is also able to bind ubiquitin moieties. Unlike ESCRT-0, -I, and –II, ESCRT-III is only transiently assembled onto the membrane and lacks any ubiquitin binding. The subunits of ESCRT-III are Vps2, Vps20, Vps24, and Snf7, with the homo-oligomerisation of the latter thought to play an important role in the invagination of the membrane to form a cargo-laden ILV (Henne *et al.*, 2012). Finally, Vps4 and cofactor Vta1 are recruited onto ESCRT-III where they employ energy from ATP hydrolysis to disassemble ESCRT-III subunits from the membrane, terminating ILV formation. In mammalian cells, the ESCRT-0 protein HRS recruits clathrin to form a flat lattice on endosomes. This clathrin is necessary for ESCRT-0 dissociation thus regulating waves of ESCRT sub-complex recruitment and dissociation and playing an important role in efficient ILV formation (Wenzel *et al.*, 2018). ESCRT-independent mechanisms of ILV formation also exist, although the molecular details of these are less well described. These different mechanisms of ILV formation can give rise to different sizes of ILVs within MVBs and sub-populations of MVBs with

different functions (White *et al.*, 2006; Woodman and Futter, 2008; EdgarEden and Futter, 2014).

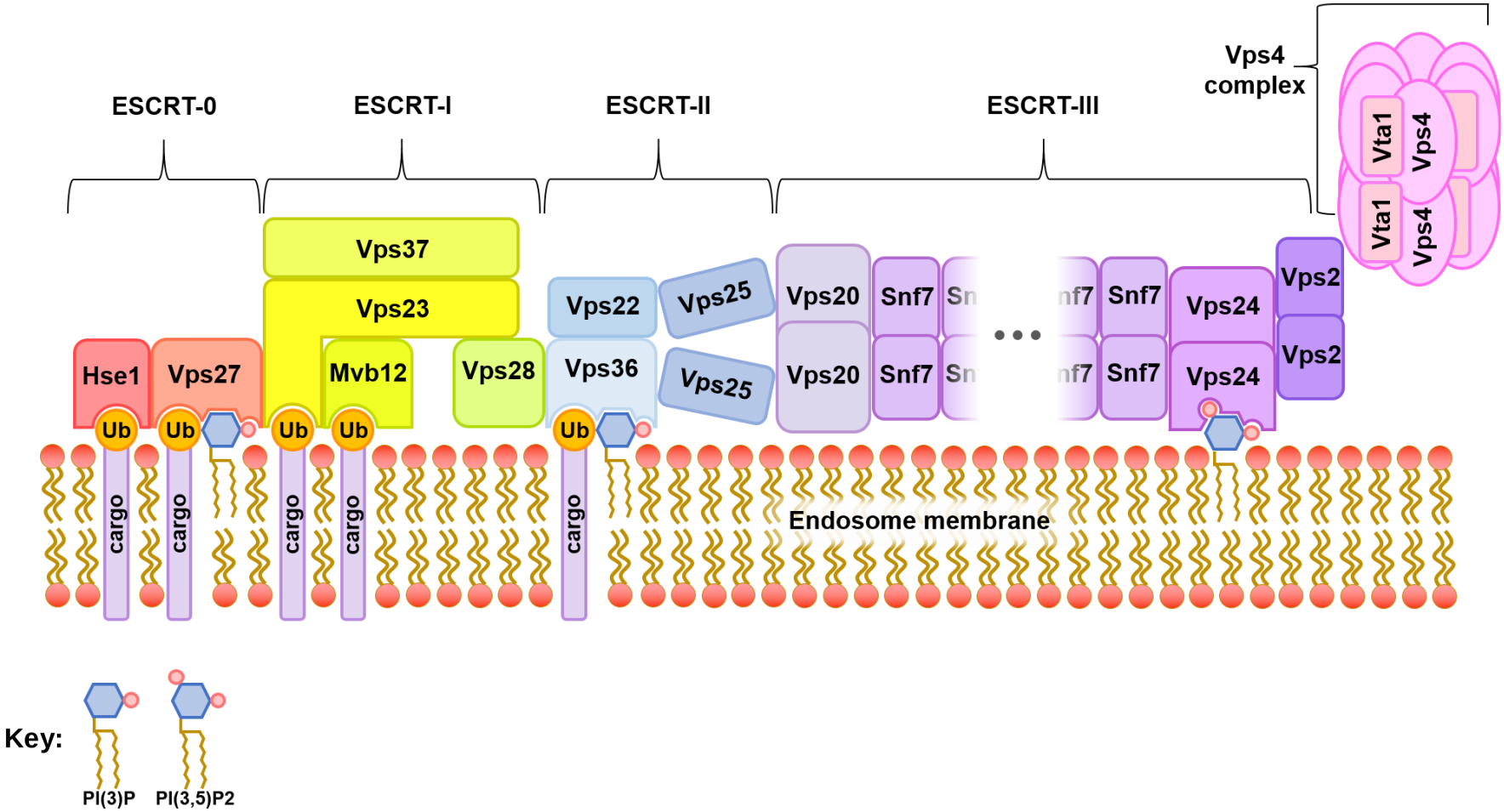

Figure 1.3 Schematic of the ESCRT

Diagram showing the ESCRT complexes which are sequentially recruited to the surface of endosomes, in order from left to right. Subunits of each complex are shown in contact with proteins or elements of the membrane with which they can interact.

1.5 Late Endosomes / Multivesicular Bodies

Late endosomes are generated by maturation of early endosomes, by gradual changes of their morphology and function. Most strikingly, late endosomes tend to contain a much greater number of ILVs than early endosomes, indicating an enrichment of membrane proteins destined for degradation and coining the term multi-vesicular body (Woodman and Futter, 2008). Late endosomes also have a lower luminal pH, reside mostly in the perinuclear region of the cell, and exhibit less recycling of cargo to the plasma membrane, however recycling to the TGN remains intact (LuzioPryor and Bright, 2007). Perhaps the most discrete and significant change marking the maturation of an endosome is the switching of Rab5 to Rab7 on the membrane (Rink *et al.*, 2005). On early endosomes, a complex of the Rab5-GEF, Rabex-5 and Rab5-effector, Rabaptin-5, is recruited to the membrane, activating Rab5 and promoting further Rab5 recruitment (Lippé *et al.*, 2001). Disrupting this feedback loop by removing the activating machinery or deactivating Rab5 directly is necessary to allow the transition to Rab7 recruitment. Evidence from C.elegans suggests that the Mon1-Ccz1 complex may play a central role in the Rab switch. Mon1-Ccz1 can bind to Rab5-GTP and PI(3)P, which may represent a mechanism through which the Rab conversion is coordinated to happen after sufficient time, maturation, and Rab5/PI(3)P accumulation on the early endosome membrane. The complex is able to displace Rabex-5, interrupting the Rab5 recruitment feedback loop, recruit Rab7 to the membrane (Kinchen and Ravichandran, 2010; Poteryaev *et al.*, 2010) and activate Rab7 by acting as a Rab7-GEF (Nordmann *et al.*, 2010). Identification of a Rab5 GAP has been complicated by differential targets of candidate GAPs between different studies or species. Additionally, ESCRT complex components have been shown to be involved in the Rab5-to-7 switch via activation of Rab7 (Karim *et al.*, 2018). Once Rab7 is recruited and active on the now-late endosome, it can begin recruiting Rab7-specific effectors to establish late endosomal characteristics, such as fusion specificity for late endosomes or lysosomes, and recruitment of dynein-dynactin motor complexes via RILP (Jordens *et al.*, 2001), for directed movement along microtubules toward lysosome-dense regions of the cell. The lipid environment also matures as a reduction of VPS34 association stops PI(3)P production. PIKfyve binds to, and

converts the pool of PI(3)P to PI(3,5)P_2, which may be important for late endocytic fusion events.

1.6 Late endosome-lysosome fusion

Late endosomes/MVBs deliver their cargo to lysosomes by transient 'kiss-and-run' events or by full fusions with lysosomes (Bright Gratian and Luzio, 2005; Futter *et al.*, 1996; van Deurs *et al.*, 1995). In order for a late endosome/MVB to be capable of fusion with a lysosome, it must have sufficiently matured by way of removing the majority of its recycling proteins and sorting its ubiquitinated cargo into ILVs (reviewed in (Metcalf and Isaacs, 2010)). A number of studies link subunits of the final ESCRT complex, ESCRT-III to MVB-lysosome fusion, where depletion or mutation of different ESCRT-III components lead to impeded fusion and altered endosomal morphology (Bache *et al.*, 2006; Shim *et al.*, 2006; Urwin *et al.*, 2010).

Fusion of these compartments to form a hybrid endolysosome involves tethering and docking before fusion of the phospholipid bilayers. These fusions are highly specific, and this strict targeting is conferred by organelle-specific tethering complexes and SNARE proteins.

1.7.1 HOPS complex

The HOPS (homotypic fusion and vacuole protein sorting) complex is comprised of a core of four subunits, VPS11, VPS16, VPS18, and VPS33, with two associated accessory subunits VPS39 and VPS41. The function of HOPS in mammalian cells has been less well studied than in yeast, however overexpression of VPS39 or VPS41 has been shown to cause clustering of late endosomes/lysosomes, and VPS18 depletion causes a dispersion of lysosomes (Poupon *et al.*, 2003), providing early evidence of the function of HOPS in endosome-lysosome tethering. Indeed, the whole HOPS complex has been shown to be required for endosome-lysosome fusion (Wartosch *et al.*, 2015). In yeast, HOPS is recruited directly to the Rab7 orthologue Ypt7p (Hickey and Wickner, 2010), but in mammalian cells RILP (Lin *et al.*, 2014; van der Kant *et al.*, 2015) and the small GTPase Arl8b (Khatter *et al.*, 2015) are required for HOPS assembly on late endosomes/lysosomes. HOPS is closely related to the Class C core/vacuole tethering (CORVET) complex that functions on early endosomes and shares the four core subunits VPS11, VPS16, VPS18, and VPS33, with two different accessory subunits, VPS 8 and

BRAP1/TRAP1 (homolog of yeast Vps3) replacing VPS39 and VPS41 (Perini *et al.*, 2014).

1.7.2 SNAREs

Once tethered together, the opposing late endosome and lysosome membranes must undergo trans-SNARE complex formation for fusion to occur. Cell free assays including antibody inhibition experiments identified the Qa-, Qb-, Qc-, and R-SNAREs involved in late endosome-lysosome fusion in mammalian cells to be syntaxin7, VPS10 tail interactor 1b (Vti1b), syntaxin8, and vesicle associated membrane protein 7 (VAMP7) respectively (Pryor *et al.*, 2004). The same Q-SNAREs with VAMP8 constitute the SNARE complex for homotypic late endosome fusion.

1.7.3 Calcium

In cell-free experiments release of Ca^{2+} from an intra-lysosomal pool was shown to be required for maximum late endosome-lysosome fusion, but the mechanistic reason for this requirement remains unclear (Pryor *et al.*, 2000). It is also unclear which Ca^{2+} channel(s) in the lysosome membrane is most important in release of this luminal Ca^{2+}, with evidence that mucolipins (especially transient receptor potential mucolipin 1, also known as transient receptor potential cation channel mucolipin subfamily, member 1 (TRPML1) (Dong *et al.*, 2010), two-pore channels (especially TPC2) (Grimm *et al.*, 2014), a voltage-gated calcium channel (Tian *et al.*, 2015) and/or the purinergic receptor, P2X4 (Cao *et al.*, 2015), may be involved.

1.8 Endolysosomes and lysosome reformation

In contrast to the molecular machinery of fusion, less is known about the mechanism(s) by which lysosomes are re-formed from endolysosomes and autolysosomes. In both cases, tubulation and fission events have been suggested to occur. Some of these events are likely concerned with the recycling of membrane components e.g. SNAREs that should not be present on the re-formed lysosomes. However, others are necessary in the formation and scission, along their length, of proto-lysosomal tubules from which mature re-formed lysosomes are generated. In the re-formation of lysosomes from autolysosomes, the formation of protolysosomal tubules is regulated by mammalian target of rapamycin complex 1 (mTORC1) (Yu *et*

al., 2010; Rong *et al.*, 2011) and their scission/vesiculation is mediated by the GTPase dynamin2 (Schulze *et al.*, 2013). Currently, the best model for re-formation of lysosomes from autolysosomes comes from the results of experimental manipulations, which suggest that localized phosphoinositide generation on the autolysosome membrane causes the recruitment of the sorting adaptors AP-2 and AP-4, clathrin and the kinesin motor KIF5B to microdomains enriched in PI(4,5)P2, which then results in the formation and extension of protolysosomal tubules along microtubules (Rong *et al.*, 2012; Du *et al.*, 2016). One note of caution about this model is that much earlier experiments showed how easy it was to mis-target AP-2 and clathrin to intracellular compartments and away from the plasma membrane, where their recruitment and function is well understood, simply by adding GTPγS or excess Ca^{2+} (SeamanBall and Robinson, 1993). Recently, it has been suggested that it is not alterations in mTORC1 activity per se that induces lysosome reformation, but the delivery to the autolysosome of mitochondrial DNA, which binds to TLR9 (toll-like receptor 9). This triggers an increase in local PI(4,5)P2 concentration, resulting in the recruitment of AP-2 and clathrin (De Leo *et al.*, 2016). Additional clues about the machinery of lysosome re-formation have come from the study of cells from patients with lysosomal storage diseases. These are rare, inherited genetic defects, in many cases causing deficiencies in specific lysosomal acid hydrolases, but in others resulting in defects in lysosomal membrane proteins or nonenzymatic soluble lysosomal proteins. Cells from such patients contain membrane-bound, heterogeneous storage lesions, most probably abnormal endolysosomes/autolysosomes, filled with different contents in different diseases (PlattBoland and van der Spoel, 2012). Amongst lysosomal disease-associated proteins implicated in lysosome re-formation are Niemann–Pick type-C2 (Goldman and Krise, 2010) , LYST (lysosomal trafficking regulator) (Holland *et al.*, 2014), the sorting adaptor AP-5 along with its associated proteins spatacsin and spastizin (Hirst *et al.*, 2015), and also the cation channel TRPML1 (Miller *et al.*, 2015), but molecular mechanisms remain elusive. In the case of TRPML1, it has been proposed that this channel is responsible for the release of luminal Ca^{2+} and earlier in vitro experiments had shown that luminal Ca^{2+} is necessary for the reformation of lysosomes from endolysosomes (Pryor *et al.*, 2000). PI(3,5)P_2 is an activator, and PI(4,5)P_2 is an inhibitor of TRPML1, which suggests tight spatiotemporal control of the concentrations of these phosphoinositides on the lysosomal membrane if fusion

events and reformation events are to be properly coordinated. Depletion or pharmacological inhibition of PIKfyve, the enzyme synthesizing $PI(3,5)P_2$ results in the formation of enlarged endocytic compartments with many characteristics of endolysosomes (reviewed in (Dove *et al.*, 2009)) and small molecule activators of TRPML1 can reverse the enlarged endolysosomal phenotype observed when a protein acting as a scaffold for PIKfyve is depleted (Zou *et al.*, 2015). The Ca^{2+} released through TRPML1 may be required for the extension and/or scission of the membrane bridges connecting endolysosomes to nascent lysosomes in the protolysosomal tubules (Miller *et al.*, 2015). It has been argued that a good candidate for a Ca^{2+}-regulated target is actin (Miller *et al.*, 2015), the polymerisation state of which can also be affected by PI(4,5)P2 (SaarikangasZhao and Lappalainen, 2010).

1.9 Acidification in the endosomal-lysosomal system

Compartmentalisation of cells allows a variety of different environments to be maintained within them, allowing for organised domains of specialised function. One particularly important environmental aspect in the endocytic pathway is the intraluminal pH. Starting at the early endosome, of pH ~6.5, the endocytic pathway compartments progressively acidify, culminating in the endolysosome, at a pH between 4 and 5, before reformation of lysosomes of neutral pH.

The mild acidity of the early endosome permits the dissociation of bound ligands from their receptors, such as LDL being released from LDLR, which can then be recycled to continue signalling, or hydrolases from M6PR, allowing them to be trafficked to the lysosome. pH may also play a role in the regulation of PI(3)P in the membrane, as a recent study showed acidification of the phagosome resulted in dissociation of the Vps34 class III phosphatidylinositol-3-kinase (PI3K) (Naufer *et al.*, 2018). Reduced PI(3)P production, combined with continued conversion of remaining of PI(3)P to phosphatidylinositol-3,5-bisphosphate ($PI(3,5)P_2$) by PIKfyve shifts the identity of the membrane more towards that of the late endosome/lysosome.

Organelle pH appears to play a role in fusion, as treatment with Bafilomycin A1 (BafA1), an inhibitor of the vacuolar H^+-ATPase (V-ATPase), has been shown to impede homotypic vacuole fusion in yeast (UngermannWickner and Xu, 1999) as

well as trafficking from early endosomes to late endosomes (Clague *et al.*, 1994; Baravalle *et al.*, 2005), or from late endosomes to lysosomes (van Weert *et al.*, 1995), although this latter effect may be independent of V-ATPase-mediated acidification (Mullock *et al.*, 1998). The effect of pH on autophagosome-lysosome fusion is unclear due to some conflicting evidence. A study in Drosophila showed BafA1 treatment to inhibit autophagosome-lysosome fusion, independent of V-ATPase, via inhibition of the calcium channel, sarco/endoplasmic reticulum Ca^{2+}-ATPase (SERCA) (Mauvezin *et al.*, 2015). A study in mammalian cells showed increase of pH by BafA1 and V-ATPase independent mechanisms to block autophagosome-lysosome fusion (Kawai *et al.*, 2007). The variation in reported effects of BafA1 may result from species differences between the studies, or from other indirect/off target effects of BafA1 itself. The low pH of lysosomes is crucial to the maturation (Richo and Conner, 1994) and function of many, but not all (Butor *et al.*, 1995) lysosomal enzymes responsible for degradation, and was required for the reformation of lysosomes from endolysosomes in a cell free system (Bright *et al.*, 1997). The primary driving force behind the acidification of the endosomal-lysosomal system is the V-ATPase complex which is discussed below.

1.10.1 V-ATPase complex

The V-ATPase is a large multi-subunit complex consisting of a membrane-embedded Vo sector, responsible for translocation of protons across the membrane, coupled to a peripheral V1 sector which hydrolyses ATP to provide energy for the structural rotation necessary for proton transport (Figure 1.4). The V1 sector is composed of 8 different subunits, while the Vo sector is comprised of 6, with known stoichiometry (Marshansky and Futai, 2008). The V1 subunits are the catalytic subunits A and B, V1Vo-connecting central stalk subunits D and F, and stator subunits C, E, G, and H which keep the V1 sector stationary relative to the Vo a subunit while the proteolipid ring rotates. The Vo sector subunits are c, c', and c'' which comprise the hydrophobic ring in the membrane, subunit a, which plays roles in complex localisation and regulation, subunit d of the central stalk, and subunit e. Close to half of these subunits have two or three isoforms, one of which is usually ubiquitously expressed, while the expression of the other isoforms is tissue/cell type specific. The quantity of component proteins, and its central role in the acidification and hence degradative function of lysosomes, implicates the V-ATPase complex in a

number of neurodegenerative diseases (Colacurcio and Nixon, 2016). V-ATPase proteins may be involved in other functions independent of acidification. It has been proposed that trans complexes of Vo sectors play a role in forming the initial pore in yeast vacuole fusion, independent of any role in acidification (Peters *et al.*, 2001; Bayer *et al.*, 2003). However, this is contested by in vivo experiments in which V-ATPase-independent vacuole acidification permitted vacuole fusion in the absence of V-ATPase, suggesting that acidic pH, rather than the presence of Vo, is required for fusion (Coonrod *et al.*, 2013).

Figure 1.4

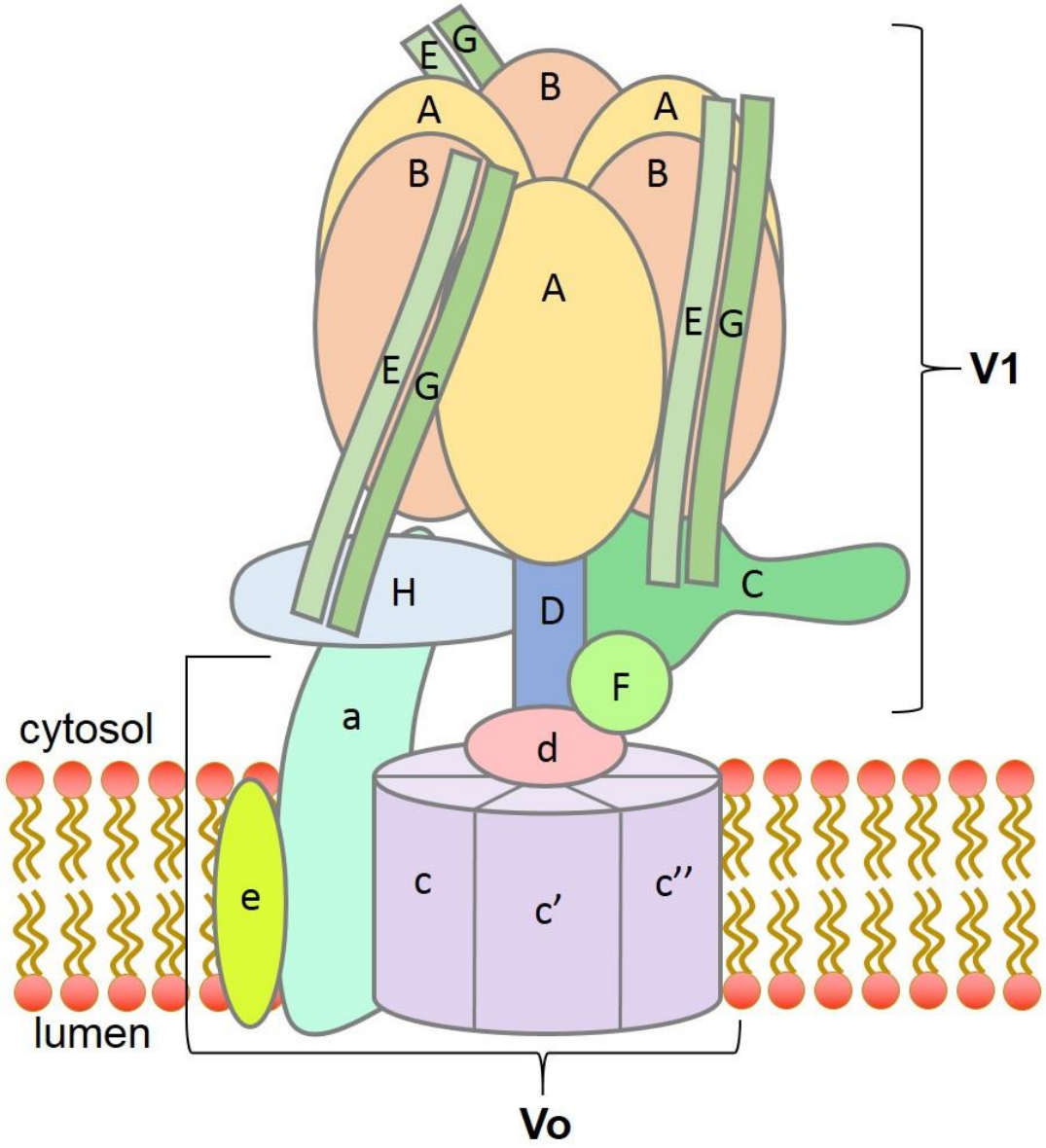

Figure 1.4 Schematic of the V-ATPase complex

Diagram of the assembled V-ATPase complex depicting its constituent subunits A, B, C, D, E, F, G and H of the V1 sector, and subunits a, c', c'', c''', d and e of the V0 sector.

1.10.2 V-ATPase regulation

Given the controlled and relatively discrete pH values in early endosomes, late endosomes, endolysosomes, and lysosomes, as well as the importance of pH in a number of functions, it is unsurprising that the proton pumping ability of the V-ATPase and the organelle proton concentration can be regulated in a number of ways.

Trafficking and distribution of V-ATPase complexes to membranes affects the V-ATPase density of organelles, and thus affects acidification. The subcellular localisation of V-ATPases is controlled in part by the subunit composition, and in particular, the isoform of the Voa subunit. Different isoforms of V-ATPase subunits, while retaining similar kinetics and affinities to one another (Rahman *et al.*, 2016) can affect the coupling efficiency, showing significant variation in proton translocation per unit of ATP hydrolysis (Kawasaki-NishiNishi and Forgac, 2001). A Rab7 effector, Rab-interacting lysosomal protein (RILP), while bound to Rab7, was shown to regulate the recruitment of V1G1 to late endosomes and lysosomes, supporting V-ATPase assembly. Unbound RILP, however, induces proteasomal degradation of V1G1, thus downregulating acidification (De Luca *et al.*, 2014). Another protein observed to bind V-ATPase and potentially regulate activity is the interferon-induced protein IFITM3 (interferon-inducible transmembrane protein 3), which may be particularly important in regulating lysosomal acidity and function following viral infection (Wee *et al.*, 2012).

Perhaps the most dramatic means by which the V-ATPase is regulated is by dissociation of the Vo and V1 sectors. First observed in moulting *Manduca sexta* larvae (Sumner *et al.*, 1995), and later in glucose-deprived yeast (Kane, 1995) the V1 sector is released from the Vo sector which remains on the membrane. The cytosolic dissociated V1 sectors are auto-inhibited by the V1H subunit, preventing aberrant ATP hydrolysis in the cytosol (ParraKeenan and Kane, 2000) and the absence of ATP-hydrolysis and rotor machinery prevents the remaining Vo sector from pumping protons. This dissociation is also seen in some mammalian cell types, for example in baby hamster kidney (BHK) cell endosomes, where the proportion of V1 sectors associated with Vo correlates with their acidity (Lafourcade *et al.*, 2008). An example of re-association occurs during the maturation of dendritic cells, where

recruitment of V1 sectors onto lysosomal membranes increases the acidification capacity of these organelles (Trombetta *et al.*, 2003). This dissociation/re-association mechanism provides a rapid mechanism for altering the rate of acidification that doesn't rely directly on protein synthesis or trafficking events.

Some evidence suggests that the local lipid environment is another means by which the V-ATPase is regulated. All V-ATPase subunits in BHK cell late endosomes were found in a detergent-resistant membrane (DRM) fraction, suggesting their association with lipid-raft-like membrane domains (Lafourcade *et al.*, 2008) although a caveat is that not all proteins found in DRMs are necessarily in physiologically relevant lipid microdomains (Munro, 2003). Lafourcade *et al*. also observed that manipulated levels of cholesterol correlated with BafA1-sensitive changes in endosomal pH. In yeast, the Vo subunit Vph1p was shown to interact with $PI(3,5)P_2$ and stabilise Vo-V1 sector assembly. Additionally, transient increase of $PI(3,5)P_2$ levels showed increased recruitment of the N-terminal domain of Vph1p to intracellular membranes (Li *et al.*, 2014).

Whilst the reversible dissociation of the Vo and V1 sectors of the V-ATPase may be the most likely way of regulating V-ATPase function during the lysosome regeneration cycle, other possibilities include recycling of the intact V-ATPase, as has been proposed for the generation of neutral post-lysosome compartments in a slime mould (Carnell *et al.*, 2011).

1.10.3 Counter-ion conductance

The unidirectional nature of proton pumping by the V-ATPase generates an electrochemical gradient across its resident membrane. The building positive charge resulting from proton accumulation would, in isolation, reach a threshold where the voltage would inhibit further proton pumping, hence limiting acidification. In the context of the endolysosome/lysosome, the charge inside must be dissipated to allow continued acidification for proper lysosomal function. This may occur by counter-ion movement across the membrane, either in the form of cation egress, anion ingress, or a combination of both, possibly represent another mode of regulating organelle pH.

Early experiments on isolated lysosomes showed an important role of Cl^- ions, as their removal or replacement with membrane impermeant ions of similar charge slowed or inhibited acidification (Dell'Antone, 1979), and were unable to reverse the V-ATPase-mediated positive shift in membrane potential. While experiments with sequentially added K^+ or H^+-specific ionophores demonstrated the limited permeability of lysosomes to K^+ (OhkumaMoriyama and Takano, 1982), there is evidence that anions also play, in part, a role in counter-ion movement. Addition of K^+ had a measurable effect on dissipation of membrane potential of lysosomes loaded with voltage sensitive dye (Harikumar and Reeves, 1983), however there is conflicting evidence on whether K^+ ion replacement affects acidity (OhkumaMoriyama and Takano, 1982; Van Dyke, 1993). Analysing the effects of counter-ions on acidification in whole cells is difficult as it requires manipulation of the intracellular ionic environment while maintaining the integrity of the plasma membrane. Through careful application of conditions to equilibrate cells with the external medium, and to equilibrate the lysosomes with the cytosol, counter-ion effects have been studied in live macrophages (Steinberg *et al.*, 2010). These experiments showed little requirement for cytosolic Cl^-, and a dependence on K^+ for lysosomal acidification, but any inferences about the role of Cl^- must take into account the imperfect cytosolic equilibration achieved.

Provided the strong evidence from isolated lysosomes that Cl^- is the central counter-ion involved in acidification, it is a reasonable assumption that a Cl^- channel or transporter is responsible. One such candidate is the cystic fibrosis transmembrane conductance regulator (CFTR) which is a well-studied Cl^- channel due to its disease association, and its role in counter-ion conductance and acidification is hypothesised to be the route through which cystic fibrosis mutations lead to pathogenesis (Deriy *et al.*, 2009). Evidence for CFTR's effect on lysosomal acidification is disputed (Haggie and Verkman, 2009a) and neither pharmacological nor genetic inhibition of CFTR could significantly affect lysosomal pH in a number of cell types (Haggie and Verkman, 2007; Haggie and Verkman, 2009b) using more appropriate imaging methods and fluorophores for lysosomes (DiCiccio and Steinberg, 2011).

The CLC family of Cl^- channels and transporters contains a likely candidate for counter-ion transport in the lysosome-localised $2Cl^-/H^+$ antiporter ClC-7. ClC-7 knock-out was shown to cause osteoclast malfunction by preventing acidification of

the ruffled order (Kornak *et al.*, 2001), providing the first link between ClC-7 and acidification. This was supported by a study of HeLa cells in which ClC-7 siRNA-mediated knockdown reduced LysoTracker staining, indicating reduces acidity in lysosomes (Graves *et al.*, 2008) however the incomplete knockdown combined with the suboptimal methodology lends credence to other studies which refute this effect. Quantitative methods to measure pH were used to show that knockout of ClC-7 or Ostm1, a β-subunit responsible for the lysosomal localisation and stability of ClC-7, had no effect on lysosomal pH (Kasper *et al.*, 2005; Steinberg *et al.*, 2010; Lange *et al.*, 2006). The weight of evidence against the two best Cl^- transporter candidates may indicate a more significant contribution of cation egress from lysosomes in counter-ion movement, perhaps from the lysosomal Ca^{2+} channels described in sections 1.7.3 and 1.12.2.

1.11 Lysosomal signalling

Over the past ten years it has been increasingly recognised that in addition to its role in degradation of macromolecules delivered through the endocytic and autophagic pathways, the lysosome is a multifunctional signalling hub, which integrates the cell's response to nutrient status and growth factor/hormone signaling. The cytosolic surface of the limiting membrane of the lysosome is the site of activation of the multi-protein complex mTORC1, which phosphorylates numerous cell growth-related substrates, including transcription factor EB (TFEB) (Sancak *et al.*, 2008; Sardiello *et al.*, 2009; Settembre *et al.*, 2012; Eltschinger and Loewith, 2016; Perera and Zoncu, 2016). Under conditions in which mTORC1 is inhibited including starvation, TFEB becomes dephosphorylated and translocates to the nucleus where it functions as a master regulator of lysosome biogenesis. In addition, lysosomes act as an intracellular Ca^{2+} store, which can release Ca^{2+} into the cytosol for local effects on membrane fusion, lysosome reformation and pleiotropic effects within the cell (Morgan *et al.*, 2011).

1.12.1 TFEB and the CLEAR network

Active Rag GTPases promote recruitment of the transcription factor TFEB to the lysosome membrane in an amino acid-dependent manner (Martina and Puertollano, 2013). In fully fed cells, TFEB continuously cycles between lysosomes and the cytosol, such that when associated with the lysosome it can be phosphorylated by

mTORC1 at several sites, including residue S211 (Settembre *et al.*, 2012; Vega-Rubin-de-Celis *et al.*, 2017). Phosphorylation at S211 promotes interaction with the cytosolic chaperone 14-3-3, resulting in a steady state in which the majority of TFEB is in the cytosol (Roczniak-Ferguson *et al.*, 2012). Nutrient withdrawal or other treatments leading to lysosomal stress e.g. V-ATPase inhibition, lead to inactivation of mTORC1, since it is released from the lysosomal surface, thus reducing phosphorylation of TFEB. Nutrient withdrawal/lysosomal stress also cause the dephosphorylation of TFEB by the calcium-dependent phosphatase calcineurin, dissociation from 14-3-3 and transport into the nucleus (Figure 1.5). Activation of calcineurin results from the release of luminal Ca^{2+} from the lysosome via TRPML1 (Medina *et al.*, 2015). TFEB is a basic helix-loop-helix transcription factor which binds to a palindromic 10-bp (base pair) nucleotide motif, GTCACGTGAC, present (often in multiple copies) in the promoter region of many genes encoding lysosomal enzymes. The palindromic nucleotide motif has been named the CLEAR (coordinated lysosomal expression and regulation) element (Sardiello *et al.*, 2009) and the extensive number of genes affected, the CLEAR network (Palmieri *et al.*, 2011). This network provides a system that regulates the expression, import and activity of lysosomal enzymes, which control the degradation of proteins, glycosaminoglycans, sphingolipids and glycogen, is involved in the regulation of autophagy, exo- and endocytosis, phagocytosis and the immune response, as well as regulating some non-lysosomal enzymes/proteins involved in protein degradation and lipid metabolism (Palmieri *et al.*, 2011; Settembre *et al.*, 2013). Other members of the members of the MiTF/TFE transcription factor family, in particular TFE3 which also binds CLEAR elements, are regulated in a very similar way to TFEB (reviewed in (Raben and Puertollano, 2016; Napolitano and Ballabio, 2016)). TFEB and TFE3 are partially redundant in their ability to induce lysosome biogenesis in response to starvation and both are necessary for a maximal response. However, overall MiTF/TFE transcription factors appear to have limited redundancy and some specific functions. Their ability to heterodimerize with each other has been a complication in studies of their function.

It should be noted that lysosome biogenesis is also affected by mTORC1 independent mechanisms. Thus, protein kinase C couples activation of TFEB with inactivation of the transcriptional repressor ZKSCAN3 via parallel signaling cascade (Li *et al.*, 2016) and an mTORC1-independent pathway mediated via PERK (protein

kinase RNA-like endoplasmic reticulum kinase), has been shown to regulate TFEB/TFE3 translocation to the nucleus in response to ER stress (Martina *et al.*, 2016). Recently, it has been demonstrated that AKT modulates TFEB activity by phosphorylation at S467 and that trehalose, an mTOR-independent autophagy enhancer, promotes nuclear translocation of TFEB by inhibiting AKT (Palmieri *et al.*, 2017). These observations are especially interesting because they have suggested that AKT control of TFEB activity may be a useful mTORC1-independent target for pharmacological treatment of neurodegenerative lysosomal storage diseases to stimulate cellular clearance of the storage material.

Figure 1.5

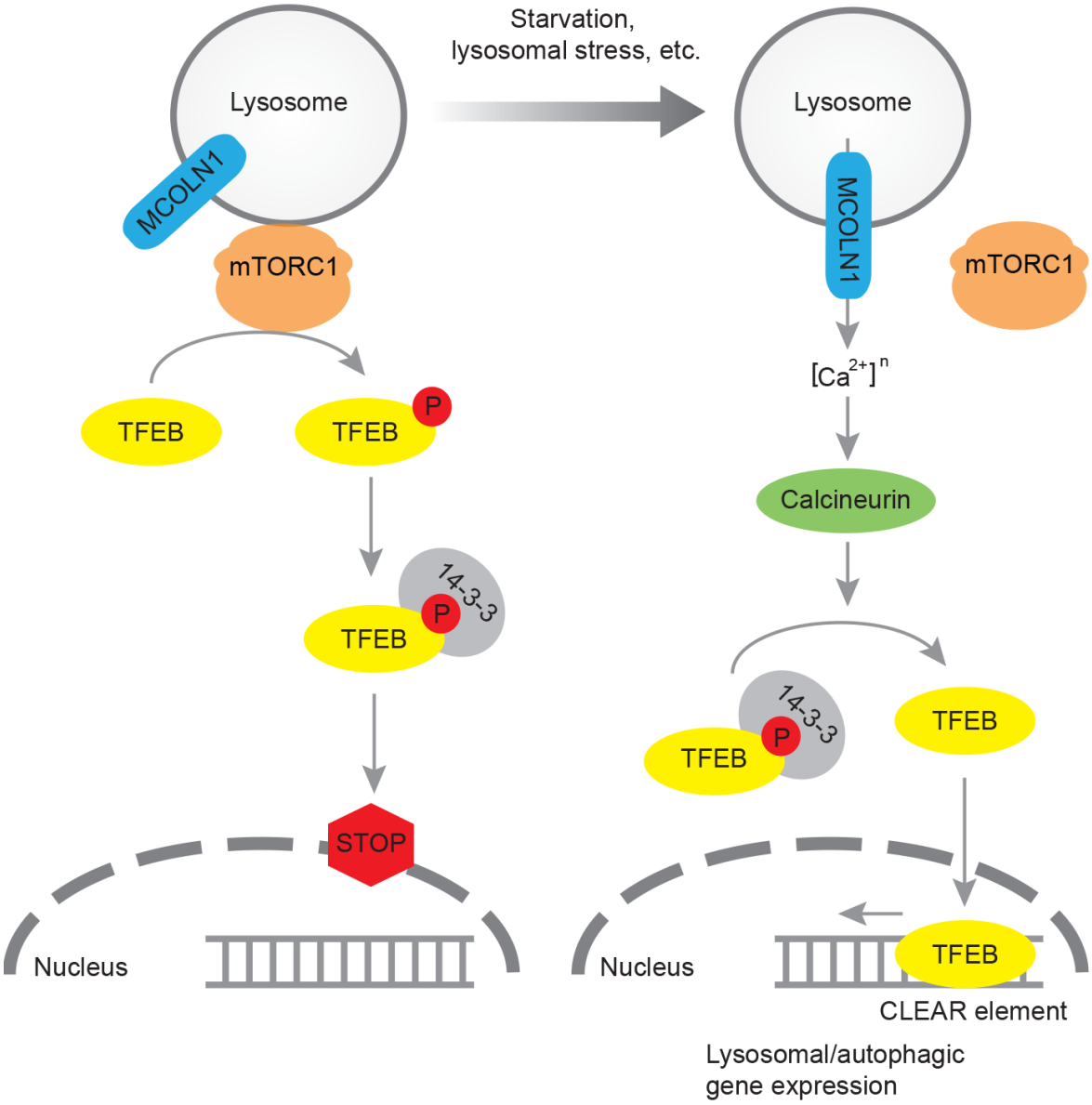

Figure 1.5 Schematic of TFEB dynamics in the cell

This schematic depicts the fed-cell state of TFEB undergoing phosphorylation by mTORC1, leading to its cytosolic sequestration by 14-3-3, compared to in lysosomal stress conditions, in which mTORC1 is no longer active or on the lysosomal membrane, and TFEB is no longer phosphorylated. TFEB dephosphorylation by TRPML1/MCOLN1-activated calcineurin is also depicted.

1.12.2 Calcium

Mammalian, acidic lysosomes/endolysosomes contain a significant store of intracellular free Ca^{2+}, measured as being ~0.5mM (ChristensenMyers and Swanson, 2002; Lloyd-Evans *et al.*, 2008; Ronco *et al.*, 2015). This is within the range of estimates of the steady state luminal free concentration in the ER, and is >3 orders of magnitude higher than the cytosolic Ca^{2+} concentration. Thus, release of Ca^{2+} through any of the identified lysosomal channels has the potential to affect a range of cytosolic functions. As described above, regulated release of lysosomal Ca^{2+} is implicated in both fusion and fission events, as well as the activation of calcineurin to dephosphorylate TFEB and upregulate genes with CLEAR elements. However, the effect of releasing lysosomal Ca^{2+} on cytosolic Ca^{2+} concentration can be amplified by stimulation of ER Ca^{2+} release, facilitating its involvement in a range of other cellular processes including muscle contraction, neurite extension and differentiation (reviewed in (Morgan *et al.*, 2011; Penny *et al.*, 2015)). Ca^{2+} release from the endolysosomal system has also been implicated in metastasis (Nguyen *et al.*, 2017) and in Ebola virus entry into host cells (Sakurai *et al.*, 2015). Defects in lysosomal Ca^{2+} signaling and homeostasis have been suggested to play a role in lysosomal storage disease pathogenesis (Lloyd-Evans and Platt, 2011). One of the most significant developments in understanding a role for lysosomes in intracellular signalling came from the discovery that release of Ca^{2+} from acidic lysosome related organelles (LROs) in sea urchin eggs is stimulated by the pyridine nucleotide metabolite Nicotinic acid adenine dinucleotide phosphate (NAADP) (Clapper *et al.*, 1987). Whilst the physiological production and degradation of NAADP is not fully understood, it clearly functions as an intracellular second messenger in mammalian cells (Yamasaki *et al.*, 2005), not just in sea urchin eggs, and a major intracellular target activated by NAADP is the lysosomal two pore channel TPC2 (Pitt *et al.*, 2010). The regulation of the release of Ca^{2+} through TPC2 is also be affected by lysosomal Ca^{2+} concentration and lysosomal pH. As discussed above, the acidic lysosomal pH is generated through the activity of the lysosomal V-ATPase, with charge compensation provided via unspecified cation channels, the lysosomal Cl^-/H^+ antiporter ClC-7/Ostm1 and/or alternative counter-ion pathways (Steinberg *et al.*, 2010). In some cell types lysosomal pH can be regulated by signaling pathways affecting V-ATPase trafficking or charge compensation e.g. pathways involving a cell

surface G protein-coupled receptor, cyclic AMP and protein kinase A (Lassen *et al.*, 2016; Folts *et al.*, 2016), thus potentially also affecting lysosomal Ca^{2+} release. Re-filling of lysosomal Ca^{2+} stores may also play a role in signaling. The lysosomal Ca^{2+}/H^{+} exchanger CAX has been shown to play a role in cell migration during frog development, but does not appear to have an ortholog in placental mammals (Melchionda *et al.*, 2016). In mammalian cells the ER is the primary source of Ca^{2+} for the lysosome (Garrity *et al.*, 2016) and it has been proposed that selective accumulation of Ca^{2+} released from the ER may allow lysosomes to play a role in shaping cytosolic Ca^{2+} signals caused by release of ER Ca^{2+} (López-Sanjurjo *et al.*, 2013). The functional relationship(s) between lysosomal and ER Ca^{2+} stores are likely affected by the close physical proximity of these organelles and the formation of ER-lysosome contact sites (Penny *et al.*, 2015; López-Sanjurjo *et al.*, 2013; Ronco *et al.*, 2015; Sbano *et al.*, 2017). Membrane contact sites (MCSs) between intracellular organelles, especially those involving the ER, are currently the subject of much investigation (Gatta and Levine, 2017; Zhang and Hu, 2016; Hariri *et al.*, 2016; Raffaello *et al.*, 2016; Kilpatrick *et al.*, 2013)), since they enable nonvesicular communication, for example for the transfer of cholesterol between endolysosomes and the ER (Du *et al.*, 2011), as well as marking sites of organelle fission of both mitochondria (Friedman *et al.*, 2011) and endosomes (Rowland *et al.*, 2014) and regulating the final steps of autophagy (Wijdeven *et al.*, 2016). In the context of lysosomal signaling, one especially interesting observation was the induction of NAADP-dependent microdomains of high Ca^{2+} concentration between lysosomes and the sarcoplasmic reticulum in response to beta-adrenoceptor activation in cardiac myocytes (Capel *et al.*, 2015).

1.13 Pharmacological agents and lysosomal health

As described above, TFEB translocates to and functions in the cell nucleus to upregulate lysosomal and autophagic genes in response to conditions of lysosomal stress or dysfunction. This often occurs in cells treated with cationic amphiphilic drugs, including chloroquine, which accumulate in the acidic lumen of lysosomes (Kazmi *et al.*, 2013; Settembre *et al.*, 2012). Over half of all commercially available drugs contain at least one basic amine (Goldman *et al.*, 2009). These basic amphipathic compounds can freely diffuse into acidic endolysosomal compartments

where they become protonated, preventing their diffusion out. The accumulation of weak basic drugs in the endolysosome sequesters them away from their target, over-distributes them in lysosome-rich tissues (DanielBickel and Honegger, 1995; Daniel and Wójcikowski, 1999; Kazmi *et al.*, 2013), and is linked to the development of phospholipidosis; an acquired lysosomal storage disease (Shayman and Abe, 2013). This concentration of weak basic drugs in lysosomes and its impact on phospholipid homeostasis represents a common side effect that must be considered in drug development.

1.14 Thesis Aims

My overarching aim was to gain a better insight into the mechanisms and proteins involved in maintaining the dynamic endo-lysosomal system.

The specific aims of the experiments described in this thesis were:

1. To test the hypothesis that endolysosomes are the principal intracellular sites of acid hydrolase activity (Chapter 3):
2. To determine the role of the R-SNAREs VAMP7 and VAMP8 in delivering endocytosed cargo to lysosomes in cultured cells (Chapter 4):
3. To develop tools to study the dynamics and function of V-ATPase throughout the lysosome fusion/regeneration cycle (Chapter 5):
4. To assess whether lysosomal signalling to the cell nucleus could be used to assess lysosomal health in cells treated with toxins, drugs, or drug precursors.

Chapter 2 – Materials and Methods

2.1 Cell culture

HeLa M epithelial cells and Phoenix cells were cultured in Roswell Park Memorial Institute medium (RPMI 1640), Normal rat kidney (NRK) fibroblasts and MCF7 human breast adenocarcinoma cells were cultured in Dulbecco's Modified Eagle's Medium (DMEM), and HEK293 cells were cultured in Minimum Essential Medium (MEM) GlutaMAX™. RPMI and DMEM media were supplemented with 4.5 g/l glucose and 2mM L-glutamine. All media was supplemented with 10% (v/v) foetal calf serum (FCS), 100 IU/ml penicillin, and 100µg/ml streptomycin. NRK cells expressing TFEB-GFP, V1G1-GFP, or V1G1-mOrange2 M163K, HeLa cells expressing TFEB-GFP, or V1G1-GFP, and MCF7 cells expressing TFEB-GFP were cultured in medium supplemented additionally with 0.5 mg/ml Geneticin (G418). HEK293 cells expressing TFEB-GFP were cultured in medium supplemented additionally with 2.0 mg/ml Geneticin (G418). NRK cells expressing Voa3-GFP, or Voa3-RFP were cultured in medium supplemented additionally with 0.2 mg/ml hygromycin B. All cells were incubated at 37ºC and 5% CO_2.

2.2 Transient transfection

HeLa M and NRK cells were transiently transfected with plasmid DNA using Lipofectamine® 2000 (Invitrogen). For HeLa M cells, 4µg of DNA, or for NRK cells, 3µg of DNA was added to 250µl Opti-MEM™ (Gibco) and incubated for 5 minutes at room temperature. Simultaneously, 10µl of Lipofectamine® 2000 was added to 250µl Opti-MEM™ and incubated for 5 minutes at room temperature. After incubation, the two solutions were combined in one tube, gently mixed, and incubated for 20 minutes at room temperature. The DNA-lipid complex solution was then added dropwise to >80% confluent cells in 2ml of serum-free culture medium in 6 well plates, and the cells were incubated at 37ºC in 5% CO_2 overnight. The next day, the media was replaced with 2ml of normal culture medium. Cells were harvested or processed between 24 and 36 hours post-transfection.

2.3 Generating stable cell lines

All stable cells lines (Table 2.1) were generated using the Phoenix cell packaging system (Swift *et al.*, 2001) with either a modified pLXIN or a pBMN construct,

resulting in overexpression levels not far from endogenous due to the relatively weak promoter (Gordon *et al.*, 2009).

Day 1: ~5.0 x 10^6 Phoenix cells were seeded in a 10cm dish in 10ml antibiotic-free RPMI and incubated at 37ºC in 5% CO_2 for 4 hours to settle. 10µg of pLXIN or pBMN construct plasmid DNA was added to 1.5ml Opti-MEM™ and incubated at room temperature. Simultaneously, 25µl of Lipofectamine® 2000 was added to 1.5ml Opti-MEM™ and incubated for 5 minutes at room temperature. After incubation, the two solutions were combined in one tube, gently mixed, and incubated for 20 minutes at room temperature. The DNA-lipid complex solution was then added dropwise to the 10ml of RPMI in the dish of Phoenix cells, which were then incubated at 37ºC in 5% CO_2 overnight.

Day 2: The media on the Phoenix cells was replaced with 12ml antibiotic-free RPMI and the cells were incubated at 32ºC in 5% CO_2 overnight to produce virus.

Day 3: ~3x10^6 NRK or HeLa M cells were trypsinized, resuspended in normal culture medium, pelleted at 900rpm for 3 minutes in a swinging-bucket rotor, and the supernatant aspirated off. The entirety of the media from the Phoenix cells was passed through a 0.45µm filter to remove loose Phoenix cells, and added alongside 12µl of 5mg/ml polybrene to the cell pellet to resuspend the cells. The cells and retrovirus resuspension was seeded into a T75 cell culture flask and incubated at 37ºC in 5% CO_2 overnight.

Day 4: The media in the flask was replaced with 12ml fresh RPMI, and returned to incubate at 37ºC in 5% CO_2 overnight.

Day 5: The cells were trypsinized and divided equally into 4 flasks containing 12ml culture medium with either G418 (using pLXIN) or HygroB (using pBMN) to begin selection of successfully transduced cells.

Selection medium was replaced every two days until there was no further observable cell death, leaving a mixed-population stable cell line. Clonal lines were generated by single cell fluorescence-activated cell sorting (FACS) using a Becton Dickinson Influx cell sorter, and the stably expressed fluorophore as a positive marker and wild type cells as a negative control.

Table 2.1 Stable cell lines

Stable cell line generated	Contruct used	Cell line used
NRK TFEB-GFP	pLXIN TFEB-GFP	NRK
HeLa TFEB-GFP	pLXIN TFEB-GFP	HeLa
MCF7 TFEB-GFP	pLXIN TFEB-GFP	MCF7
HEK TFEB-GFP	pLXIN TFEB-GFP	HEK293
NRK V1G1-GFP	pLXIN V1G1-GFP	NRK
HeLa V1G1-GFP	pLXIN V1G1-GFP	HeLa
NRK Voa3-GFP	pBMN Voa3-GFP	NRK
NRK V1G1-TagRFP	pLXIN V1G1-TagRFP	NRK
NRK Voa3-TagRFP	pBMN Voa3-TagRFP	NRK
NRK Voa3-GFP V1G1-TagRFP	pLXIN V1G1-TagRFP	NRK Voa3-GFP
NRK Voa3-TagRFP V1G1-GFP	pBMN Voa3-TagRFP	NRK V1G1-GFP
NRK Voa3-GFP V1G1-mOrange2 M163K	pLXIN V1G1-mOrange2 M163K	NRK Voa3-GFP

2.4 RNA interference

All siRNA oligonucleotides (Table 2.2) were purchased as either ON-TARGET plus pools, or custom synthesised oligos from GE Healthcare Dharmacon. All siRNA had 3' UU modification, a 5'phosphate modification, and were made up to a final concentration of 50nM in siRNA buffer (Dharmacon). VPS33A SMARTpool: ON-TARGETplus oligonucleotides were used previously (Wartosch *et al.*, 2015). VAMP7, VAMP8 and YKT6 target sequences were a gift from Andrew Peden.

2.4.1 Five-day double hit siRNA knockdown

Day 1: 3.0 x 10^5 cells were seeded in a 6-well plate in 2ml normal culture medium and incubated at 37ºC in 5% CO_2 for 4 hours to settle. 4µl of siRNA solution was added to 160µl Opti-MEM™ and incubated at room temperature. Simultaneously, 10µl of Oligofectamine® (Invitrogen) was added to 20µl Opti-MEM™ and incubated for 5 minutes at room temperature. After incubation, the siRNA solution was added dropwise to the Oligofectamine® solution gently mixed, and incubated for 20 minutes at room temperature. The media on the settled cells was aspirated off, and a further 800µl Opti-MEM™ was added to the siRNA-Oligofectamine® solution before applying directly to the cells. An additional 1ml of antibiotic-free medium was added to the wells before returning the cells to the incubator at 37ºC in 5% CO_2 overnight.

Day 2: The media on the cells was replaced with 2ml normal culture media before returning the cells to the incubator at 37ºC in 5% CO_2 overnight.

Day 3: The cells were trypsinized, resuspended in 4ml normal culture medium, seeded into a 6cm dish and incubated at 37ºC in 5% CO_2 for 4 hours to settle. The cells were then transfected exactly as on Day 1, but with 2x the volumes of siRNA, Oligofectamine®, Opti-MEM™, and antibiotic-free medium.

Day 4: The media on the cells was replaced with 4ml normal culture media before returning the cells to the incubator at 37ºC in 5% CO_2. At the end of the day, cells were trypsinized, resuspended in normal culture medium, and seeded into plates with or without coverslips for cell lysates or microscopy respectively.

Day 5: The cells were harvested for lysates, or prepared for microscopy.

2.4.2 Five-day single hit siRNA knockdown

Cells were treated the same as the five-day double hit siRNA knockdown, except the Day 3 transfection is omitted.

Table 2.2 siRNA oligonucleotides

Gene	Oligo type	Target Sequence	Accession number	Dharmacon catalogue number
VPS33A	SMARTpool: ON-TARGETplus	Pool of oligos 1-4 Sequences listed below	NM_001351019	L-013339-01
VPS33A	ON-TARGET plus oligo 1	GGGCGUAACC UUCGCUGAA	NM_001351019	J-013330-09
VPS33A	ON-TARGET plus oligo 2	GAAGAAACGUC AACCGGGA	NM_001351019	J-013330-10
VPS33A	ON-TARGET plus oligo 3	AGGAGAAUGC GCUCGGCAA	NM_001351019	J-013330-11
VPS33A	ON-TARGET plus oligo 4	UUACCCAACUA UACGGAAA	NM_001351019	J-013330-12
VAMP7 oligo B	Custom siRNA	AACGTTCCCGA GCCTTTAATT	N/A	N/A
VAMP8 oligo B	Custom siRNA	AAGCCACATCT GAGCACTTCA	N/A	N/A
YKT6 oligo A	Custom siRNA	GCUCAAAGCCG CAUACGAU	N/A	N/A
YKT6 oligo C	Custom siRNA	AUACCAGAACC CACGAGAA	N/A	N/A

2.5 CRISPR-Cas9 knockout

2.5.1 Cloning CRISPR-Cas9 Constructs

Guides for CRISPR were generated by finding the target gene on the Ensembl genome database (Human genome assembly GRCh38.p12), searching the first 5' constitutively expressed exon for appropriate guide sequences, as is targetted in CRISPR-Cas9 knockout screening (Shalem *et al.*, 2014), using the Zhang lab CRISPR design tool (crispr.mit.edu). Guides were selected largely by the off-target-dependent score, with preference for targets earlier in the coding sequence. Complementary guide oligo pairs were designed to include the selected guide sequence flanked by overhangs that, after oligo dimerization, resemble a BbsI restriction cut site. Complementary guide oligo pair duplexing reaction was set up as follows:

CRISPR Guide Oligo-Pair Duplexing Reaction

1.0µl 10X T4 DNA ligase Buffer (New England Biolabs)

10µM Oligo 1

10µM Oligo 2

0.5µl T4 Polynucleotide Kinase (PNK) (New England Biolabs)

H_2O up to 10µl

The reaction was incubated at 37ºC for 30 minutes, followed by 95ºC for 5 minutes, and cooled at approximately -0.5ºC/minute down to room temperature. The CRISPR-Cas9 vector was digested at 37ºC for 3 hours as follows:

pX330 BbsI Restriction Digest Reaction

2µl 10X Buffer 2.1 (New England Biolabs)

500ng pX330 vector plasmid DNA

1µl BbsI (New England Biolabs)

H_2O up to 20µl

The restriction digest reaction was run on a 0.8% agarose gel and BbsI-cut pX330 was isolated from the gel (as detailed in chapter 2.8.1). The duplexed guide oligos

were then ligated into the BbsI-cut pX330 with complementary sticky ends at 37ºC for 1 hour as follows:

pX330 Guide Oligo Duplex Ligation Reaction

1µl 10X T4 DNA ligase buffer (New England Biolabs)

1µl [1/200 diluted in H_2O] Guide oligo duplex

1µl BbsI-cut pX330 vector

1µl T4 DNA ligase (New England Biolabs)

H_2O up to 10µl

Next, 2.5µl of the ligation reaction was transformed into competent bacteria, plated on selection medium, colonies were picked, cultured overnight, and sequenced (as detailed in chapter 2.8.2).

Table 2.3 CRISPR-Cas9 guide oligos

Guide	Sequence
VAMP7_Exon2 sense	5'-CAC CGA ACA AAC TAA CGT ACT CAC A-3'
VAMP7_Exon2 antisense	5'-AAA CTG TGA GTA CGT TAG TTT GTT C-3'
VAMP8_Exon2 sense	5'-CAC CGT GGA GGA AAT GAT CGT GTG-3'
VAMP8_Exon2 antisense	5'-AAA CCA CAC GAT CAT TTC CTC CAC-3'

2.5.2 Generating CRISPR-Cas9 Knockout Cells

HeLa M cells were transiently transfected (as described in section 2.2) with guide-incorporated pX330 construct and pIRES-GFP-Puro selection reporter construct at a ratio of 5:1. 48 hours post-transfection, individual successfully transfected GFP-positive cells were sorted by FACS into 96 well plates to grow into clonal populations.

2.6 Immunofluorescence

2.6.1 Fixation

Cells were grown on 13mm glass coverslips in 24-well plates to 40-60% confluency. The wells were rinsed with phosphate buffered saline (PBS) before fixing either in chilled methanol at -20ºC for 5 minutes immediately before staining, or in PBS with 4% PFA (w/v) at room temperature for 20 minutes followed by quenching in PBS with 30mM glycine.

2.6.2 Permeabilisation

Paraformaldehyde-fixed cells were permeabilised by incubating coverslips for 5 minutes at room temperature in either PBS with 0.1% Triton X-100 and 3% BSA, or in PBS with 0.05% saponin (w/v) and 3% BSA. Cells permeabilised with saponin maintained 0.05% saponin in every staining solution.

2.6.3 Staining

Methanol-fixed cells were rinsed with PBS, and incubated for 1 hour at room temperature with primary antibodies diluted in PBS with 3% BSA (w/v). Following permeabilisation, paraformaldehyde-fixed cells were incubated for 1 hour at room temperature with primary antibodies (Table 2.4) diluted in the same buffer used for permeabilisation. Primary antibody solutions were aspirated off, and the coverslips were washed three times in PBS for 5 minutes at room temperature. The coverslips were then incubated with AlexaFluor-conjugated secondary antibodies (Table 2.5) diluted in the same solution as the primary antibodies for 1 hour at room temperature. The coverslips were then washed three times in PBS for 5 minutes at room temperature, nuclei were stained by incubation for 10 minutes at room temperature in 1µg/ml Hoechst 33342 (ThermoFisher Scientific) then coverslips were rinsed in distilled water and mounted onto glass slides with ProLong™ Gold Antifade Mountant (ThermoFisher Scientific). Mountant was left to set overnight at room temperature then slides were stored at 4ºC in the dark.

Table 2.4 Primary antibodies for immunofluorescence microscopy

Antigen	Antibody I.D.	Host species	Source	Dilution
Human LC3	4E12	Mouse monoclonal	MBL International	1:400
Human LAMP1	H4A3	Mouse monoclonal	AbCam	1:1000
LBPA	6C4	Mouse monoclonal	Merck Millipore	1:1000
Human EEA1	C45B10	Rabbit polyclonal	Cell Signalling Technology	1:1000
Human TGN46	GB2	Rabbit polyclonal	Gift from George Banting (Bristol)	1:400
Human YKT6	N/A	Rabbit polyclonal	Gift from Andrew Peden (Sheffield)	1:500
Rat lgp120	GM10	Mouse monoclonal	Gift from Ken Siddle (Cambridge)	1:500
Mouse Voa3	N/A	Rabbit polyclonal	Gift from Thomas Jentsch (Berlin)	1:250

Table 2.5 Secondary antibodies for immunofluorescence microscopy

Antigen	Antibody I.D.	Host species	Source	Dilution
Rabbit IgG	Donkey anti-rabbit Alexa-488	Donkey polyclonal	ThermoFisher Scientific	1:1000
Rabbit IgG	Donkey anti-rabbit Alexa-594	Donkey polyclonal	ThermoFisher Scientific	1:1000
Mouse IgG	Donkey anti-mouse Alexa-488	Donkey polyclonal	ThermoFisher Scientific	1:1000
Mouse IgG	Donkey anti-mouse Alexa-488	Donkey polyclonal	ThermoFisher Scientific	1:1000
Guinea pig IgG	Goat anti-guinea pig Alexa-594	Goat polyclonal	ThermoFisher Scientific	1:1000

2.7 Western blotting

2.7.1 Generating cell lysates

Whole cell lysates were prepared by first rinsing the cells in 6-well plates twice with ice cold PBS. The PBS was removed before adding 100µl of lysis buffer (50mM Tris pH 7.4, 50mM NaCl, 2% sodium dodecyl sulfate (SDS), 1X cOmplete™ Protease Inhibitor Cocktail (Roche)) to each well. Cells were then scraped off the plate, resuspended in the lysis buffer, and transferred to a QIAshredder (QIAGEN) column which was centrifuged at 16,000g for 2 minutes at room temperature. The lysate in the collection tube was passed through the QIAshredder column a second time at 16,000g for 2 minutes at room temperature

Cell lysate protein concentration was measured by Pierce BCA (bicinchoninic acid) assay in a 96-well plate using a standard curve of BSA dilutions (Table 2.6).

Table 2.6 BSA standard curve

BSA 1mg/ml (µl)	0	1	2	5	10	15	20
H_2O (µl)	20	19	18	15	10	5	0
[BSA] (mg/ml)	0.00	0.05	0.10	0.25	0.50	0.75	1.00

Each lysate was diluted 1:20 in H_2O, in triplicate wells. Every well of the protein standard curve and samples was incubated with 200µl Pierce BCA protein assay solution (BCA Protein Assay Reagent A (Thermo) with 4% $CuSO4*5H_2O$ at 50:1) for 30 minutes at 37ºC. The plate was read at 562nm on an Anthos HT II plate reader to calculate the lysate protein concentration (mg/ml per well). Each cell lysate was then diluted 2:1 with 3X sample buffer (200mM Tris pH 6.8, 5mM EDTA (Ethylenediaminetetraacetic acid), 0.1% bromophenol blue, 1M sucrose, 4% SDS, 300mM DTT (dithiothreitol) to run on self-cast gels, or 3:1 with 4X TruPAGE™ LDS Sample Buffer (Sigma-Aldrich) to run on TruPAGE™ Precast gels (Sigma-Aldrich). Diluted lysates were denatured by incubation at 95ºC for 5 minutes before gel loading alongside 5µl PageRuler™ Prestained Protein Ladder (26616, Thermo).

2.7.2 SDS-PAGE

Polyacrylamide gels were either purchased precast (TruPAGE™, Sigma-Aldrich) or resolving gels were made as follows (Table 2.7)

Table 2.7 SDS-PAGE resolving gels

Resolving gel	8% gel	10% gel	15% gel
30% Acrylamide stock (ml)	1.6	2.0	3.0
1.68M Tris pH 8.8 (ml)	1.5	1.5	1.5
H_2O (ml)	2.9	2.5	1.5
20% w/v SDS (µl)	30.0	30.0	30.0
10% w/v Ammonium persulfate (APS) (µl)	24.0	24.0	24.0
Tetramethylethylenediamine (TEMED) (µl)	4.8	4.8	4.8

The top of the gel mix was covered with 100µl isopropanol to exclude air and allow the gel to set. Once set, the resolving gel was rinsed to remove isopropanol and unpolymerised resolving gel mix before casting a stacking gel with a comb to form appropriate number and volume of wells as follows (Table 2.8)

Table 2.8 SDS-PAGE stacking gels

Stacking gel	5% gel
30% Acrylamide stock (µl)	415.0
1M Tris pH 6.8 (µl)	175.0
60% w/v Sucrose (µl)	625.0
H_2O (µl)	1285.0
20% w/v SDS (µl)	12.5
10% w/v Ammonium persulfate (APS) (µl)	25.0
Tetramethylethylenediamine (TEMED) (µl)	2.5

Once the stacking gel has set, wells were washed with running buffer to remove unpolymerised acrylamide, samples were loaded, and the gel run with running buffer (H_2O with 6g/litre Trizma® base (Sigma-Aldrich), 383mM glycine, 0.1% SDS) at 200V in a vertical electrophoresis gel tank (Sigma).

2.7.3 Transfer

Proteins were transferred to Immobilon®-P (Merck-Millipore) PVDF membranes for chemiluminescence detection, or Immobilon®-FL PVDF membranes for fluorescence

detection. The PVDF membrane was first activated by incubating in methanol for 5 minutes at room temperature. The PVDF membrane was then rinsed in H_2O and briefly incubated in transfer buffer (H_2O with 3g/litre Trizma® base (Sigma-Aldrich),191.5mM glycine, 20% (v/v) methanol) before being placed on a stack of three pieces of filter paper and a sponge, all saturated with transfer buffer and flattened to remove air pockets. The protein gel was briefly washed in transfer buffer before being placed on top of the PVDF membrane, and flattened to remove air pockets and ensure complete contact with the membrane. Another transfer buffer-saturated stack of filter paper, followed by a sponge were placed on top of the gel, and the whole stack was held together in a locked cassette before loading into a transfer tank (BioRad) with an ice pack and filled with transfer buffer. Protein transfer was run at 100V for 1 hour.

2.7.4 Immunoblotting

After the transfer was complete, the membrane was blocked in TBS-T (20mM Tris, pH 7.4, 0.9% NaCl, 0.1% tween 20) with 5% skimmed milk powder (w/v) for either 1 hour at room temperature, or overnight at 4ºC. Membranes were probed for proteins of interest by incubating with primary antibodies (Table 2.9) diluted in 5% milk TBS-T overnight at 4ºC. The antibody solution was then removed, membranes washed three times for 10 minutes each with TBS-T, then incubated with species-appropriate anti-IgG secondary antibodies (Table 2.9), tagged with horse radish peroxidase (HRP) for chemiluminescence or fluorescent dyes for fluorescence detection, diluted in 5% milk TBS-T for 1 hour at room temperature, protected from light. The membranes were washed three times for 10 minutes each with TBS-T then rinsed in PBS. For blots with HRP, membranes were incubated in enhanced chemiluminescent (ECL) solution (ECL reagent A with ECL reagent B at 1:1) for 2 minutes at room temperature before exposing to film initially for 1 minute, then developing the film. Blots with fluorescent dyes were scanned in a shallow pool of PBS using an Odyssey® CLx imaging system (LI-COR Biosciences). Blots were quantified using Image Studio software tools, with background correction based on the median background in regions above and below the selected band region, to avoid signal from adjacent lanes.

Table 2.9 Primary and secondary antibodies for immunoblotting

Antigen	Antibody I.D.	Host species	Source	Dilution
Human β -Actin	A2066	Rabbit polyclonal	Sigma-Aldrich	1:6000
Human LC3	NB100-2220	Rabbit polyclonal	Novus Biologicals	1:1000
Human VAMP7	N/A	Mouse monoclonal	Gift from Andrew Peden (Sheffield)	1:1000
Human VAMP8	N/A	Rabbit polyclonal	Gift from Andrew Peden (Sheffield)	1:1000
Human YKT6	N/A	Rabbit polyclonal	Gift from Andrew Peden (Sheffield)	1:1000
Human SEC22b	N/A	Rabbit polyclonal	Gift from Andrew Peden (Sheffield)	1:500
Human V1G1	16143-1-AP	Rabbit polyclonal	ProteinTech	1:500
Rabbit IgG	Anti-rabbit-HRP	Goat polyclonal	Sigma-Aldrich	1:8000
Mouse IgG	Anti-mouse-HRP	Rabbit polyclonal	Sigma-Aldrich	1:8000
Rabbit IgG	Anti-rabbit-IRDye 680	Goat polyclonal	LI-COR Biosciences	1:8000
Mouse IgG	Anti-mouse-IRDye 800	Goat polyclonal	LI-COR Biosciences	1:8000
Rabbit IgG	Anti-rabbit-IRDye 800	Goat polyclonal	LI-COR Biosciences	1:8000

2.8 Molecular biology

2.8.1 Cloning

All constructs were cloned from pre-existing constructs containing the cDNA of interest, or from an integrated molecular analysis of genomes and their expression (IMAGE) clone. Primers were designed to have at least 15 base pairs complementary to the target cDNA before incorporating a desired restriction site, and

were used to incorporate modifications into, and amplify the target cDNA. PCR reaction was set up as follows:

PCR Reaction

5µl 10X Buffer for KOD Hot Start DNA Polymerase

200µM of each deoxynucleotide triphosphate (dNTP)

1.5mM $MgSO_4$

300nM Forward primer

300nM Reverse primer

2µl DMSO

1µl KOD Hot Start DNA Polymerase

10ng Plasmid DNA template

H_2O up to 50µl

PCR Programme

1. 95ºC for 2 minutes
2. 95ºC for 20 seconds
3. (Tm-5)ºC for 10 seconds
4. 70ºC for 10 seconds/kilobase [<500bp product]
   15 seconds/kilobase [500-1000bp product]
   20 seconds/kilobase [1000-3000bp product]
5. Go to 2. x29
6. 70ºC for 3 minutes
7. 4ºC indefinitely

PCR products were mixed with 9:1 with 10X sample buffer (0.4% Xylenol orange (Sigma-Aldrich), 1mM EDTA pH 8.0, 50% (v/v) glycerol) and run by gel electrophoresis on a gel of 0.8%, 1.0% or 1.2% agarose (Fisher Bioreagents) (w/v) in Tris pH 8.0, acetic acid, EDTA (TAE), alongside GeneRuler 1kb DNA ladder (Thermo) at 60V. DNA was extracted from gels by cutting out bands and using a QIAquick gel extraction kit (QIAGEN) to purify the DNA. Vectors and PCR products were restriction digested at 37ºC for 3 hours as follows:

Restriction Digest Reaction

2µl 10X NEBuffer™ or CutSmart® buffer (New England Biolabs)

500ng DNA

1µl Restriction enzymes (New England Biolabs)

H_2O up to 20µl

Restriction digested vectors were run on a 1% agarose gel then purified using a QIAquick gel extraction kit as before. Restriction digested PCR products were directly purified using a QIAquick kit, taking the reaction volume as a proxy for gel volume. DNA concentrations were measured using a nano-drop, then ligations performed at room temperature for 1 hour as follows:

Ligation reaction

1µl 10X T4 DNA ligase buffer (New England Biolabs)

~25ng vector DNA

3:1 molar ratio of insert:vector DNA

1µl T4 DNA ligase (New England Biolabs)

H_2O up to 10µl

2.8.2 Transformation

2.5µl of the ligation product was added to 50µl of DH5α-T1 competent *E. coli* cells and incubated on ice for 20 minutes. The competent cells were then heat shocked in a 42ºC water bath for 45 seconds before returning to ice for 3 minutes. 200µl super optimal broth with catabolite repression (SOC) was added to the cells which were

then incubated at 37ºC for 1 hour in a shaker. Separately, 50µl and 200µl of the cell suspension was plated on lysogeny broth (LB) agarose plates with the appropriate antibiotic (ampicillin 100µg/ml, kanamycin 40µg/ml) to select for the vector. The plates were incubated at 37ºC overnight, resultant colonies were picked with sterile 20ul pipette tips and used to inoculate 5ml LB cultures with appropriate antibiotics, which were grown for 16 hours at 37ºC in a shaker. Overnight cultures were pelleted by centrifuging at 3,000g for 10 minutes, the supernatants were removed, and DNA isolated using a QIAprep® Spin Miniprep Kit (QIAGEN). Constructs were analysed by restriction digest as detailed above, and successful ligations were sequenced by Source BioScience.

2.8.3 Mutagenesis

Mutations were introduced into DNA using QuikChange (Agilent) site-directed mutagenesis PCR. Forward and reverse primers were designed to have at least 15 base pairs complementary to the target cDNA surrounding the target sequence, and to include the desired mutation in between the regions of homology. The PCR reaction was set up as follows:

Mutagenesis PCR Reaction

5µl 10X PfuTurbo Buffer

200µM of each deoxynucleotide triphosphate (dNTP)

300nM Forward primer

300nM Reverse primer

50ng Plasmid DNA template

1µl PfuTurbo DNA Polymerase **OR** 1µl H_2O (negative control)

H_2O up to 50µl

The reaction mix was divided equally into three tubes to reduce the risk of unintended mutation contamination, and run as follows:

Mutagenesis PCR Programme

1. 95ºC for 45 seconds

2. 95ºC for 45 seconds

3. 55ºC for 60 seconds

4. 68ºC for 60 seconds/kilobase of template

5. Go to 2. X17

6. 4ºC indefinitely

After PCR, the PCR product was pooled together, and 10µl was run on a 1% agarose gel as detailed before. The remaining 40µl of PCR product was incubated with 2µl DpnI enzyme (New England Biolabs) at 37ºC for 2 hours to digest methylated template DNA, while leaving PCR product intact. 2µl of DpnI-digested PCR product was then transformed into 50µl competent bacteria as detailed before.

2.9 Drugs, reagents, and constructs

For amino acid and serum starvation conditions, cells were washed with PBS 3 times before incubation with EBSS (Sigma). For amino acid starvation cells were washed with PBS 3 times before incubation with amino acid-free DMEM (US Biological) supplemented with dialysed FBS (Gibco). For sucrose uptake, cultured cells' medium was replaced with their regular culture medium further supplemented with sucrose to make a 30mM solution. Dextran loading was performed with 0.5mg/ml fluorescently conjugated dextran in solution in supplemented DMEM described in section 2.1. LysoTracker® Green DND-26 or Red DND-99 was made to 50nM in CO_2-independent medium supplemented with FCS (10% v/v). Magic Red™ cathepsin substrates were made to 1:2600 from stock (solid dissolved in 50µl DMSO) in CO_2-independent medium supplemented with FCS (10% v/v). Poly-L-lysine (Sigma-Aldrich) was made to 0.1mg/ml in PBS. The following drugs were used: Torin1 (Tocris Bioscience), BafA1 (Alfa Aesar), CQ (Sigma-Aldrich), ML-SA1 (Tocris Bioscience), Acetaminophen (Sigma-Aldrich), Leptomycin B (LKT Laboratories).

TFEB-GFP construct in pEGFP was a gift from Andrea Ballabio (Telethon Institute of Genetics and Medicin, Pozzuoli, NA, Italy). TFEB-GFP was subcloned into a

modified version of pLXIN retroviral expression vector (Clontech, Mountain View, CA, USA). TFEB is attached to GFP by a linker: CCGGTCGCCACC.

An IMAGE clone of V1G1 (accession number NM_004888) was amplified by PCR incorporating an AgeI site for cloning into pEGFP with the same linker as for TFEB-GFP. V1G1-GFP was subcloned into a modified pLXIN vector. mOrange2 vector was purchased from Addgene.

Table 2.10 PCR primers

Primer	Sequence	Function
V1G1 FOR	ATGGCTAGTCAGTCTCAGGG	PCR out V1G1 IMAGE clone
V1G1 REV	CTATCCATTTATGCGGTAGTT	PCR out V1G1 IMAGE clone
V1G1 GFP FOR	ATATATGTCGACGCCACCATGGCTAGTCAGTCTCAGGGG	Cloning into pEGFP-N1
V1G1 GFP REV	AAATTTACCGGTCCTCCATTTATGCGGTAGTTTTCATGG	Cloning into pEGFP-N1
mOr M163K quickchange FOR	GAAGGGCAAGATCAAGAAGAGGCTGAAGCTGAAGG	M163K mutagenesis
mOr M163K quickchange REV	CCTTCAGCTTCAGCCTCTTCTTGATCTTGCCCTTC	M163K mutagenesis

2.10 Assessing autophagy and TFEB translocation in cultured cells

2.10.1 Assessing LC3 accumulation

To assess autophagy by immunofluorescence, cells were seeded on to 13mm glass coverslips, fixed after treatment in 4% PFA, and permeabilised in PBS with 0.1% Triton X-100 and 3% BSA before staining with primary LC3 antibody (MBL) followed by AlexaFluor488-conjugated secondary antibody and Hoechst 33342 as described in section 2.6.3. Images were acquired on a Zeiss LSM880 confocal microscope with Zeiss ZEN software. Mean LC3 fluorescence intensity from at least 10 fields (≥5 cells per field) for each of three independent experiments was measured using IMAGEJ software and normalized to cell area.

To assess autophagy by Western blotting, cell lysates were ran on a 15% polyacrylamide gel before transferring to PVDF membrane, blocking, and probing

with primary LC3 antibody (Novus Biologicals) followed by washes and incubation with an IRDye-conjugated secondary antibody as described in section 2.7.4. LC3 bands were quantified using Image Studio software to measure the signal of the band and subtract local background levels. The fluorescence output (arbitrary units) is then normalised to either β-actin band intensity or REVERT™ Total Protein Stain intensity.

2.10.2 Quantifying nuclear translocation of TFEB

Cells stably expressing TFEB-GFP were seeded at $1x10^4$ cells per well for fixing in 2 days, or $3x10^4$ cells per well for fixing the subsequent day, into glass-bottom black-wall 96-well plates (Perkin Elmer). To promote the adhesion of HEK293 cells, plates were coated with 0.1 mg/ml poly-L-lysine for 1 hour, washed twice with PBS and left to air dry before seeding cells. After treatment conditions, cells were washed once with PBS, fixed in 4% PFA for 10 minutes at room temperature, incubated in 1µg/ml Hoechst 33342 for 10 minutes at room temperature, washed with PBS twice and finally imaged in PBS. To quantify nuclear translocation, I used a modified version of the default nuclear translocation protocol in HCS Studio software used to operate a Cell Insight CX7 High Content Screening microscope (Thermo). This programme detects cells and autofocusses using the Hoechst channel which reveals stained nuclei. The area of the nucleus is mapped and outlined producing an area referred to as Nuc (nucleus). The region just outside of Nuc, extending outward by an adjustable number of pixels is referred to as the Cyt (cytoplasm). The amount of fluorophore being detected is recorded on a pixel-by-pixel scale, giving an intensity value per pixel in each of the Nuc, representing the nucleus, and the Cyt, representing a significant portion of the cytoplasm. Nuclear translocation data is presented as the mean intensity of pixels in the Circ region after subtracting the mean intensity of pixels in the Ring region, representing the difference between nuclear and cytoplasmic concentrations of fluorophore in arbitrary units (A.U.). All data are presented as mean ± SEM of 3 experiments, each with >750 cells per condition.

2.11 Measuring delivery of endocytosed cargo to endolysosomes/lysosomes

To measure the extent of delivery of endocytosed cargo from endosomes to

endolysosomes, a content mixing assay was performed on cells, essentially as described by Wartosch et al., Traffic 2015. In brief this assay was based on the visualization and quantification of delivery of endocytosed fluorescent-labelled dextran to enzymatically active endolysosomal/lysosomal compartments. The latter were identified with Magic Red™ which is a membrane permeable substrate for the lysosomal acid hydrolase Cathepsin B (ImmunoChemistry Technologies) The bi-substituted cresyl violet groups in Magic Red™ are non-fluorescent until they are cleaved at one or both arginine amide linkage sites by Cathepsin B in lysosomes. After cleavage mono- and non-substituted cresyl violet emits red fluorescence when exited at 550–590nm. In the assay described below Magic Red™ cathepsin substrates were made to 1:2600 from stock (solid dissolved in 50μl DMSO) in CO_2-independent medium with FCS (10% v/v). Cells were incubated with Magic Red™ substrates for a minimum of 2 minutes, to a maximum of 30 minutes to minimise imaging of cleaved fluorophore after trafficking to non-active compartments. Previous work by Nick Bright (Bright, Davis and Luzio, 2016) showed overlap of Magic Red™ Cathepsin-B substrate with pre-loaded dextran to not change between 2 minutes and 2 hours Magic Red™ incubation.

To perform the assay, cells were first seeded sparsely onto 25mm glass coverslips in normal growth medium and left to adhere and grow overnight at 37ºC and 5% CO_2. The cells were loaded by incubation for 2 hours at 37ºC and 5% CO_2 in DMEM with 0.5mg/ml dextran Alexa Fluor® 488 10,000 molecular weight (MW), anionic, fixable (Life Technologies). The cells were then chased for 1 hour in dextran-free normal growth medium, rinsed in CO_2-independent medium (Gibco), then the coverslips were mounted in a cell chamber and transferred to an incubated microscope stage. The cells were incubated in CO_2-independent medium (Gibco) with 673nM Magic Red™ Cathepsin B substrate (ImmunoChemistry Technologies) for at least 2 minutes at 37ºC and 5% CO_2 in the incubated stage chamber. After this incubation with Magic Red™ substrate, and the cell chamber acclimatising to the incubated stage chamber temperature, confocal images were captured. Cells were randomly selected and 1-2 cells were imaged per field using a Zeiss LSM780 confocal microscope, with a pinhole of 1 Airy unit, and digital gain adjusted such that both channels were just below saturation. Three independent experiments were performed with 20 fields captured per condition. These images were then analysed

to determine the colocalisation of dextran Alexa Fluor® 488 and Magic Red™ as a measure of the proportion of endolysosomes to which dextran has been delivered from endosomes. Colocalisation was measured by Manders colocalisation coefficients using Zen software (ZEISS).

2.12 pH clamping of cultured cells

Ionophores nigericin and monensin were reconstituted in ethanol as 10mM stock solutions and stored at -20ºC. pH clamping was performed using modification of a previously described method (Lange *et al.*, 2006). A pH5 clamping solution was prepared using 25mM sodium acetate buffer pH5, containing 5mM NaCl, 1mM CaCl2, 115mM KCl, 1.2mM $MgSO_4$, 10mM glucose, 10µM nigericin and 10µM monensin. For fluorescence confocal microscopy, cells were incubated with the pH 5 clamping for 5 minutes before imaging.

2.13 Quantitative polymerase chain reaction

To analyse changes in gene regulation at the transcript level, mRNA was isolated from cells, converted to cDNA by reverse transcription, then amplified using quantitative PCR. Gene-specific probes bind the cDNA, and upon extension of the polymerase up to the bound-probe, a reporter dye is cleaved and released into the reaction solution. Through repeated cycles, the increasing intensity of the released dye is measured and used to calculate the original number of mRNA transcripts.

2.13.1 RNA isolation

After treatment, cells were washed with PBS, aspirated, and lysed using SV RNA isolation kit (Promega). The cells are lysed in 175µl SV RNA Lysis Buffer, and transferred to a fresh tube before adding 350µl SV RNA Lysis Dilution Buffer and inverting 4 times. The solution was then incubated at 70ºC for no longer than 3 minutes, and centrifuged at 14,000 x g for 10 minutes at room temperature. The supernatant of the lysis solution was transferred to a fresh tube, 200µl 95% ethanol was added, mixed, and the whole solution was transferred to a Spin Column Assembly which was centrifuged at 14,000 x g for 1 minute at room temperature. The column was then washed with 600µl SV RNA Wash Solution, and centrifuged at 14,000 x g for 1 minute at room temperature. The column was then incubated in 50µl DNase Incubation mix (40µl Yellow Core Buffer, 5µl 0.09M MnCl2, and 5µl DNase I

enzyme) for 15 minutes at room temperature. 200µl of SV DNase Stop Solution was added to the column and incubated for 1 minute before centrifuging at 14,000 x g for 1 minute. The column was washed with 600µl, and again with 250µl of SV RNA Wash Solution before centrifuging at 14,000 x g for 2 minutes to remove residual wash buffer. The RNA was eluted by adding 100µl nuclease-free water to the column which was placed in an elution tube and centrifuged at 14,000 x g. RNA concentration was determined using a NanoDrop™ Microvolume Spectrophotometer (Thermo Scientific) and stored at -70ºC.

2.13.2 Reverse transcription

All RNA samples were diluted to 50ng/µl before undergoing reverse transcription with a High Capacity cDNA Reverse Transcription Kit (Applied Biosystems) set up per reaction as follows:

2.50µl 10X RT Buffer

1.00µl 25X dNTP Mix (100nM)

2.50µl 10X RT random primers

1.25µl MultiScribe Reverse Transcriptase

2.75µl H_2O

The 10µl reverse transcription master mix was added to 15µl RNA sample in 96-well TaqMan optimal plates then the wells were sealed with a thermal seal, centrifuged at 1000 rpm for 1 minute to bring the contents to the bottom of the wells, and run on a Tetrad PCR thermal cycler with the following steps:

<u>Reverse transcription programme</u>

1. 25ºC for 10 minutes

2. 37ºC for 120 minutes

3. 85ºC for 5 minutes

4. 4ºC indefinitely

The resulting 30ng/µl cDNA samples are diluted down with molecular grade water to 2ng/µl for use in TaqMan array cards, or to 6ng/µl for TaqMan custom arrays.

2.13.3 TaqMan real time PCR

For TaqMan array cards, the PCR reaction mix was made by mixing 50µl of 2ng/µl cDNA sample, or 50µl H_2O for a non-template control, with 50µl 2X TaqMan Universal PCR Master Mix with AmpErase® UNG. This 100µl reaction mix was pipetted into the fill port on the array card, and centrifuged at 1200 rpm for 2 minutes to distribute the PCR reaction mix to every reaction well before sealing the array card. For custom arrays, PCR master mix was made by combining 12.5µl 2X TaqMan Universal PCR Master Mix with AmpErase® UNG with 1.25µl individual gene assay solution and 6.25µl H_2O. This 20µl master mix was added to 5µl of 6ng/µl cDNA sample, or 5µl of H_2O for a non-template control, in wells of a 96-well TaqMan optimal plate, and sealed with a thermal seal. Array cards and custom arrays were run on a QuantStudio 7 Flex Real-Time PCR System (ThermoFisher).

2.13.4 Transcript quantification

The amount of transcript was quantified using the standard curve-based relative quantification method (LarionovKrause and Miller, 2005). The number of cycles each reaction requires to reach a fluorescence threshold (CT), and the CT values of a standard curve generated by serial dilution of cDNA, are plotted as a function of Log10(Relative Quantity) against CT. From this plot, the CT values, the gradient, and the Y-intercept values were then used to normalise CT values, using the equation: (1^10*gradient*CT) / Y-intercept. For each experimental sample, the transcript value is divided by the endogenous/untreated control. All samples were measured in triplicate, allowing mean and SEM to be calculated, which was presented as fold change from the control condition in bar graphs to allow easy comparison between conditions.

2.14 Confocal microscopy

Live-cell confocal microscopy was performed with an incubated stage Zeiss LSM780 microscope, using a x63 1.4 NA Plan Apochromat oil-immersion lens. A 488nm Argon laser was used to excite eGFP, a 543nm HeNe laser was used to excite cresyl violet, and a 633nm HeNe laser was used to excite Alexa647. Laser power was kept at 2% to reduce photobleaching of samples, and the detector pinhole diameter was adjusted to image an optical slice of 0.7-1.2µm depth. Images were

taken with 4x line averaging. Fixed-cell confocal microscopy was performed with a Zeiss LSM880 microscope using the same settings as described for the LSM780.

2.15 Colocalisation analyses

Colocalisation data used to estimate proportions of lysosomes which are Magic Red™- or LysoTracker®-positive were generated through Imaris software using its automated thresholding algorithm on confocal images with detectors adjusted such that the peak intensity in each channel was just below saturation. Pearson's colocalisation coefficient gives a single-value measure of colocalisation between two fluorophores/channels ranging from -1 (complete separation of signals) to +1 (complete colocalisation of signals). Manders' overlap coefficient gives values representing the proportion of each channel's signal which is overlapped by signal from the other channel being compared (DunnKamocka and McDonald, 2011). In the experiments described here, Manders' overlap coefficient was used for estimations of lysosomes with or without staining, as the directionality of the overlap values provides useful information in these experiments with organelle-confined punctate signals.

In the quantification of delivery of endocytosed cargo to endolysosomes/lysosomes, the extent of colocalisation of dextran Alexa Fluor 488 with Magic Red™ was measured by calculating Manders' M1/M2 coefficients (Manders EMM, Verbeek FJ, Aten JA. Measurement of colocalization of objects in dual-color confocal images. J Microsc (Oxf) 1993;169:375–382) using ZEN software (ZEISS). These data were all presented as fold change in the colocalisation of dextran Alexa Fluor 488 with Magic Red™.

2.16 Statistics

The statistical significance of variations between population means was determined using unpaired T-tests. The unpaired T-test is applicable when, and works on the assumption that, the data fit a normal distribution, and the compared groups have equal variance. The unpaired T-test was applied as independent, unrelated sets of samples with the same distribution are generally being compared, for example untreated vs knockdown cells. To assess statistical significance between treatment conditions in qPCR quantification, one-way Analysis of variance (ANOVA)

calculation was performed, with subsequent Dunnett's multiple comparisons tests, comparing treatment conditions to the vehicle control.

2.17 Cell viability assay

To ensure conditions of lysosomal perturbation were not causing more than 20% cell death, after treatments of HEK293 cells in 96-well plates, an equal volume of PrestoBlue™ Cell Viability Reagent (ThermoFisher) was added to the medium in the wells containing cells, and wells without cells as a control, then incubated for 15 minutes at 37ºC before reading absorbance at 570nm. The average reading from medium-only cells is subtracted as background from all wells, and the resulting absorbance represents cell survival, which is compared to untreated cells.

Chapter 3 – Endolysosomes are the principal sites of acid hydrolase activity

3.1 Introduction

Since their discovery in the 1950s, lysosomes were largely considered to simply be degradative termini of the endocytic and autophagic pathways, despite the relatively early establishment of the morphological heterogeneity of lysosomes (reviewed in Holtzman, E. (1989) Lysosomes, Plenum Publishing Co., New York). It is only in the last 20 years that the dynamics and diverse range of functions of lysosomes have begun to be fully appreciated, and that they play important roles in nutrient sensing and signalling. The heterogeneity of lysosomes may represent the continuum of organelles in a lysosome regeneration cycle. In this model, late endosomes/MVBs deliver endocytic cargo for degradation by fusion with lysosomes (reviewed in (LuzioPryor and Bright, 2007)), forming late endosome-lysosome hybrid organelles, now called endolysosomes (Huotari and Helenius, 2011) from which lysosomes can be reformed.

The dynamic nature of the relationship between lysosomes and endolysosomes in mammalian cells can often be demonstrated and manipulated by incubating cells with sucrose. This manipulation was first introduced almost 50 years ago (Cohn and Ehrenreich, 1969). The sucrose is taken up by fluid phase endocytosis and, in the absence of any enzyme to degrade it, causes the cells to form osmotically swollen sucrosome compartments. Subsequent endocytosis of invertase, which degrades the sucrose, reverses the phenotype. Using electron microscopy (EM), it was later shown in NRK cells that the formation of sucrosomes can be explained by the swelling of compartments which can be morphologically defined as endolysosomes (with markers from both late endosomes and lysosomes) (Bright *et al.*, 1997). During their formation over several hours, the sucrosomes continue to grow as the result of further fusions, resulting in a greatly reduced number of lysosomes in the cell. Adding invertase to the cells breaks down the sucrose, which eventually permits tubules to extend from the collapsing sucrosomes, leading to continued lysosome reformation (Bright *et al.*, 1997).

When I started my PhD work, the extent to which endolysosomes, or more terminal lysosomal compartments were involved in hydrolysis of macromolecules had not been established. Clearly the differences in morphology between endolysosomes and lysosomes, and the selective/regulated reformation of nascent lysosomes

suggested that there could be differences in the functions of these related organelles. Earlier EM and cell-free experiments had also led to the idea that the organelles identified in both NRK cells and hepatocytes as dense-core lysosomes, with condensed contents, could be storage compartments for hydrolytic enzymes that are delivered to the endolysosome during fusion of lysosomes with late endosomes to enable the commencement of hydrolysing endocytosed macromolecules (LuzioBright and Pryor, 2007). The availability of synthetic, membrane-permeable cathepsin substrates (commercially available as Magic Red™ compounds), which liberate fluorescent cresyl violet that remains within acidic organelles upon proteolytic cleavage, allowed the development of assays to identify the principal sites of cathepsin activity in cultured mammalian cells. In initial experiments, using NRK cells in which all of the lysosomes and endolysosomes had been pre-loaded with fluorescent dextran (4h fluid phase uptake, followed by 20h chase of Oregon green-dextran, DexOG), Dr Nick Bright demonstrated that only some of the organelles contained active cathepsin B (Figure 3.1A and 3.1B). Correlative light and electron microscopy (CLEM) showed that the cathepsin-active organelles had heterogeneous morphology. These were subsequently, identified as endolysosomes and contained the pre-lysosomal endosome marker cation-independent M6PR. CLEM also identified fluorescent dextran loaded lysosomes, which did not contain active cathepsin B (Figure 3.1). Subsequent immuno-EM of MCF7 cells, carried out by Dr Bright showed that both Magic Red™-positive endolysosomes and Magic Red™-negative lysosomes contain cathepsins (Bright, Davis and Luzio, 2016). I set out to extend these observations to test the hypothesis that endolysosomes are the principal sites of acid hydrolase activity in mammalian cells. Data from these experiments are published in Bright et al., 2016.

A

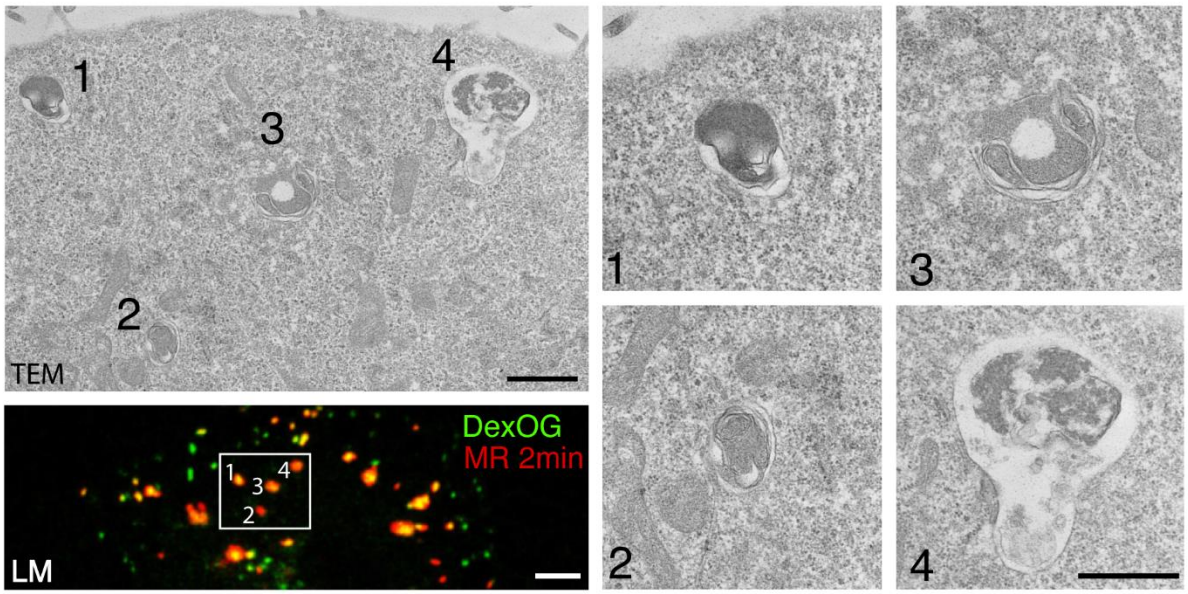

B

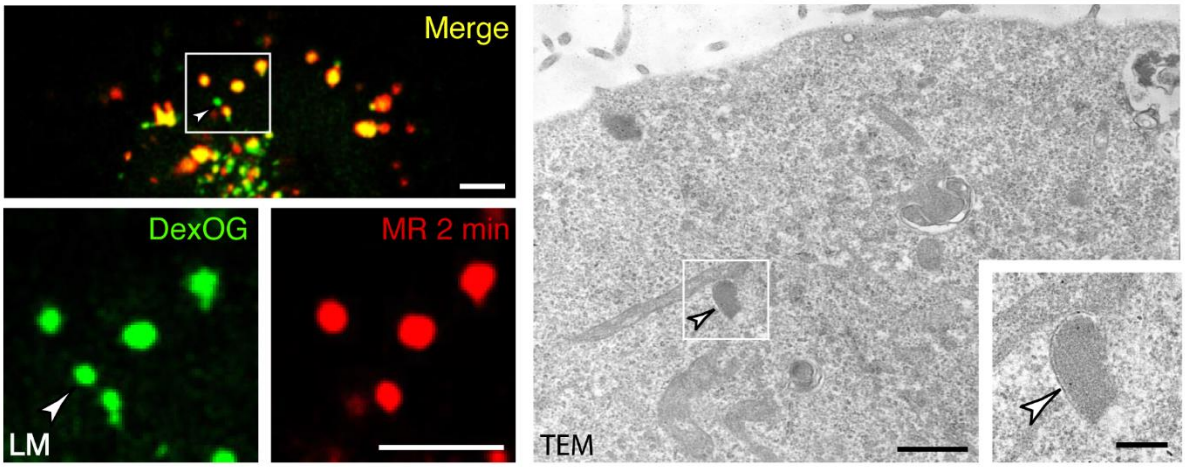

Figure 3.1: Endolysosomes are the principal sites of cathepsin B catalytic activity in NRK cells (Images from Dr Nick Bright, (Bright, Davis and Luzio, 2016))

Terminal endocytic compartments of NRK cells were loaded with DexOG for 4 hours followed by a 20 hour chase in DexOG-free medium.

(A) DexOG- and Magic Red™ Cathepsin B substrate (MRB)-positive organelles were identified by confocal microscopy then processed for transmission electron microscopy (TEM) to show their ultrastructure. The boxed region of the light microscopy (LM) image and corresponding section in the TEM shows the

ultrastructure of four cathepsin B-active endolysosomes. The enlargements show that these organelles contain multi-lamellar intralumenal membranes and electron dense content. Scale bars represent 5µm (light microscopy (LM)), 1µm (TEM), and 500nm (TEM enlargements).

(B) An image from an adjacent confocal plane to that shown in (A) with enlargements and corresponding TEM image of the boxed region identifying a DexOG-positive, MRB-negative terminal endocytic organelle (arrowhead) amongst endolysosomes. The TEM image of this organelle reveals it to be a granular dense core lysosome. Scale bars represent 5µm (LM), 1µm (TEM), and 200nm (TEM inset).

3.2 Results

3.2.1 Endolysosomes are the principal sites of Cathepsin L catalytic activity and are acidic in mammalian cells

To address the different characteristics of lysosomes and endolysosomes, NRK cells were first loaded with Alexa-647 Dextran (DexA) using a 4 hour pulse, 20 hour chase protocol, as previously described (BrightGratian and Luzio, 2005), to label all terminal endocytic organelles. The cells were then incubated with membrane-permeable cathepsin L Magic Red™ substrate (MRL), which after cleavage by active cathepsin L, releases membrane-impermeable cresyl violet fluorophore which accumulates in the compartment where cathepsin L is active. Next, the cells were incubated with LysoTracker Green (LTG) which is a membrane-permeable acidotropic probe which accumulates and fluoresces in acidic compartments. Live cell confocal microscopy of these cells showed only a subpopulation of dextran-loaded terminal endocytic compartments to be marked by cresyl violet and lysotracker, revealing a population of lysosomes which were neither acidic nor cathepsin L-active (Figure 3.2 A). Using the same method, distinct populations of dextran-loaded terminal endocytic compartments which are positive or negative for Magic Red™ and LysoTracker were observed in HeLa cells (Figure 3.2 B) and MCF7 cells (Figure 3.2 C), indicating that this is not a species- or cell line-specific characteristic. Together with the data from CLEM using cathepsin B Magic Red™ substrate (Figure 3.1), as well as immunofluorescence and immuno-EM data from Dr Nick Bright (Bright, Davis and Luzio, 2016), my data were consistent with the Magic Red™-marked compartments being endolysosomes. Moreover, my data with LTG showed that these compartments, but not Magic Red-negative lysosomes, were acidic. My data also showed that the distinction between the hydrolytically active endolysosomes and hydrolytically inactive lysosomes could be shown with a substrate for cathepsin L, just as it had been shown initially for cathepsin B.

To measure the proportion of dextran-loaded terminal endocytic compartments that are cathepsin-active and acidic endolysosomes, colocalisation of Dextran and Magic Red™ or LysoTracker® was analysed in confocal microscopy images using Pearson's and Manders' coefficients. Manders' values were used to estimate the proportion of dextran-loaded organelles that were Magic Red™-positive

endolysosomes to be 67.4% ± 4.6% in NRK cells, 46.8% ± 8.7% in HeLa cells, and 64.1% ± 3.3% in MCF7 cells (M1, Figure 3.2 D). Using the same method, the proportion of dextran-loaded organelles that are acidic was estimated to be 47.4% ± 0.057% in NRK cells, 46.4% ± 0.043% in HeLa cells, and 58.8% ± 0.002% in MCF7 cells (M1, Figure 3.2 E). The remaining proportion of dextran-loaded organelles in both instances may be considered to represent the proportion of reusable terminal, acid hydrolase-storage lysosomes.

Figure 3.2 A

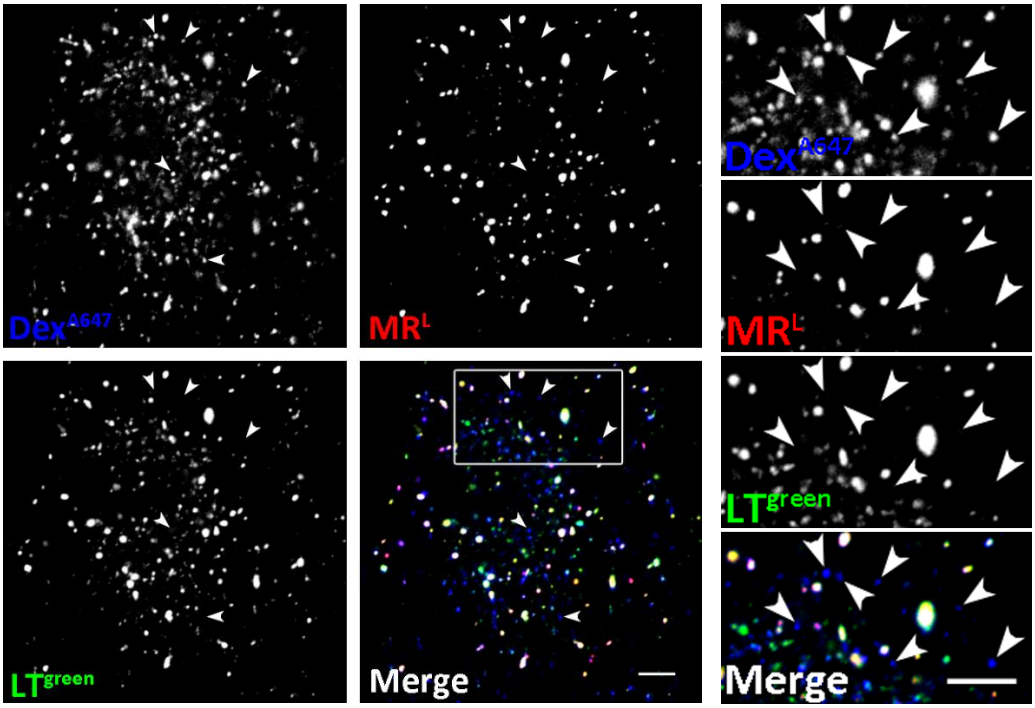

B

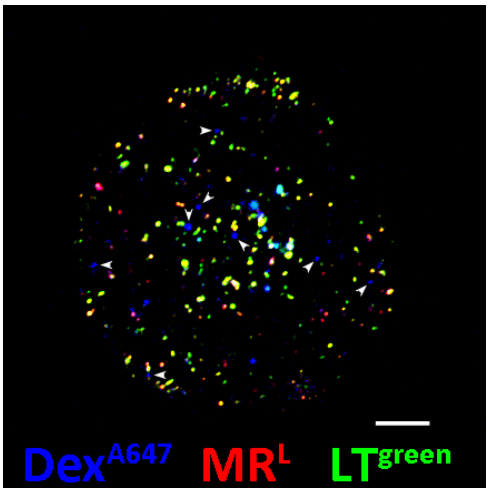

C

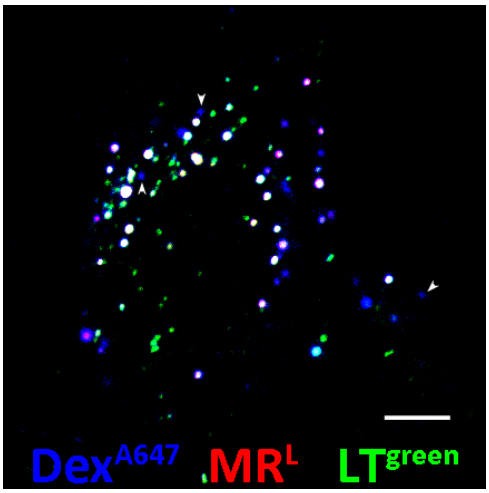

D

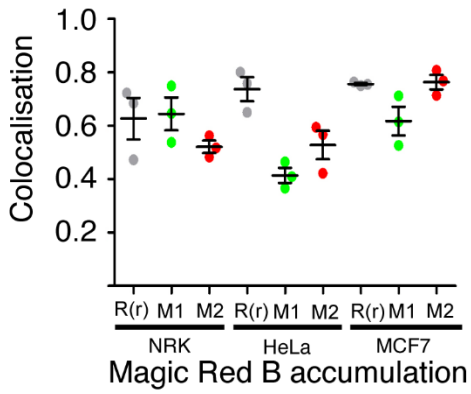

E

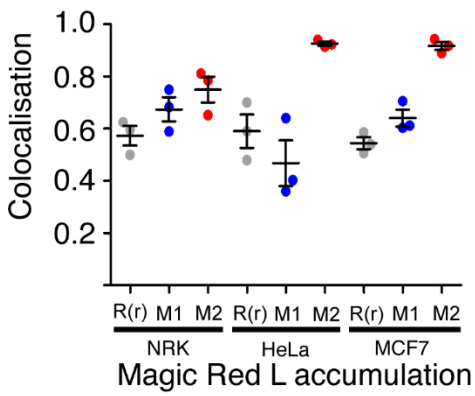

Figure 3.2: Endolysosomes are the principal sites of Cathepsin L catalytic activity and are acidic in NRK cells

Terminal endocytic compartments were loaded with DexA as for Figure 3.1.

(A) Confocal fluorescence microscopy representative images of NRK cells preloaded with DexA, to label terminal endocytic compartments, and incubated for 2 min with MRL followed by addition of 50nM LTG for 5 min. Enlargements of the boxed region in the cell show DexA-positive terminal endocytic organelles that were negative for both MRL and LTG (arrowheads). Scale bars represent 5µm.

(B) Confocal fluorescence microscopy image of a HeLa cell preloaded with DexA, and incubated with MRL and LTG as for (A) showing DexA-positive terminal endocytic organelles that were negative for both MRL and LTG (arrowheads). Scale bars represent 5µm.

(C) Confocal fluorescence microscopy image of a MCF7 cell as per (B). Scale bars represent 5µm.

(D) Pearson's (R(r); gray) and Mander's (M1, blue, DexA:MRL and M2, red, MRL:DexA) correlation coefficients for colocalisation of pre-loaded DexA and 2 min incubated MRL in NRK, HeLa and MCF7 cells. Error bars represent the mean ± SEM of 3 experiments.

(E) Pearson's (R(r); gray) and Mander's (M1, blue, DexA:LTG and M2, green, LG:DexA) correlation coefficients for colocalisation of pre-loaded DexA and 5 min incubated LTG in NRK, HeLa or MCF7 cells. Error bars represent the mean ± SEM of 3 experiments.

3.2.2 Further characterisation of endolysosomes

Using Magic Red™ as a marker of endolysosomes, live-cell confocal microscopy was used to further characterise the compartment. Confocal slices of NRK cells pre-loaded with fluorescent dextran and incubated with the Magic Red™ cathepsin B substrate were analysed using an automated spot detection programme to measure the areas of all visible dextran- or Magic Red™-positive organelles (Figure 3.3). Given that dextran-positive compartments represent the total of all endolysosomes and terminal lysosomes, the similarity to the size distribution of Magic Red™-positive endolysosomes is unsurprising. To estimate the sizes of terminal lysosomes, dextran-positive organelles with Magic Red™ fluorescence below 2x background levels were isolated (Black bars) showing a simultaneous decrease in the proportion of larger organelles, and increase in the proportion of smaller organelles, compared to endolysosomes. This difference is in agreement with Dr Bright's qualitative TEM observations of the relative sizes of endolysosomes and terminal/dense core lysosomes (Figure 3.1, (Bright, Davis and Luzio, 2016).

As discussed in chapter 1, Rab proteins confer identity and largely determine functions of organelles. HeLa cells stably expressing EGFP-tagged Rab5, Rab7, or Rab9 were a gift from Dr Matthew Seaman, and were incubated with MRB then imaged using live-cell confocal microscopy. Rab5 was distributed throughout the cytosol and in puncta around the periphery of the cell, seemingly separate from the Magic Red™-positive endolysosomes (Figure 3.4A). Rab7 and Rab9 were also partially cytosolic, and concentrated in puncta clustered in the perinuclear region, overlapping with almost all Magic Red™-positive endolysosomes. To quantify the observed absence of Rab5, and presence of Rab7 and Rab9 on endolysosomes, the colocalisation of each EGFP-tagged Rab with Magic Red™ was analysed using Pearson's correlation coefficient (Figure 3.4B). Rab5 showed an almost complete lack of colocalisation, whereas both Rab7 and Rab9 showed a strong positive colocalisation with Magic Red™, indicating that the endolysosome membrane is marked by Rab7 and Rab9, but not Rab5, consistent with the identity of the endolysosome as a hybrid of late endosomes and lysosomes.

The low abundance phosphoinositide $PI(3,5)P_2$ is predicted to localise to yeast vacuoles, endosomes, and lysosomes, based on the localisation of $PI(3,5)P_2$-generating PIKfyve (reviewed in (HasegawaStrunk and Weisman, 2017)). $PI(3,5)P_2$

plays an important role in endolysosomal trafficking through its activation of TRPML1 (Dong *et al.*, 2010) and the subsequent release of lysosomal Ca^{2+}. To investigate whether Magic Red™-positive endolysosomes are marked by this phosphoinositide, NRK cells were transiently transfected with ML1Nx2-GFP, a proposed $PI(3,5)P_2$-specific probe, based on the cytosolic N-terminal region of TRPML1 (Li *et al.*, 2013). Transfected cells were incubated with MRB before imaging, and showed almost complete colocalisation between ML1Nx2-GFP and MRB (Figure 3.4C). This suggests that all endolysosomal membranes contain $PI(3,5)P_2$, which may be expected given the localisation of PIKfyve to both late endosomes and lysosomes. However, results obtained using this probe should be interpreted with caution given the reported concerns over the specificity and off rate of the probe (Hammond *et al.*, 2015).

Figure 3.3

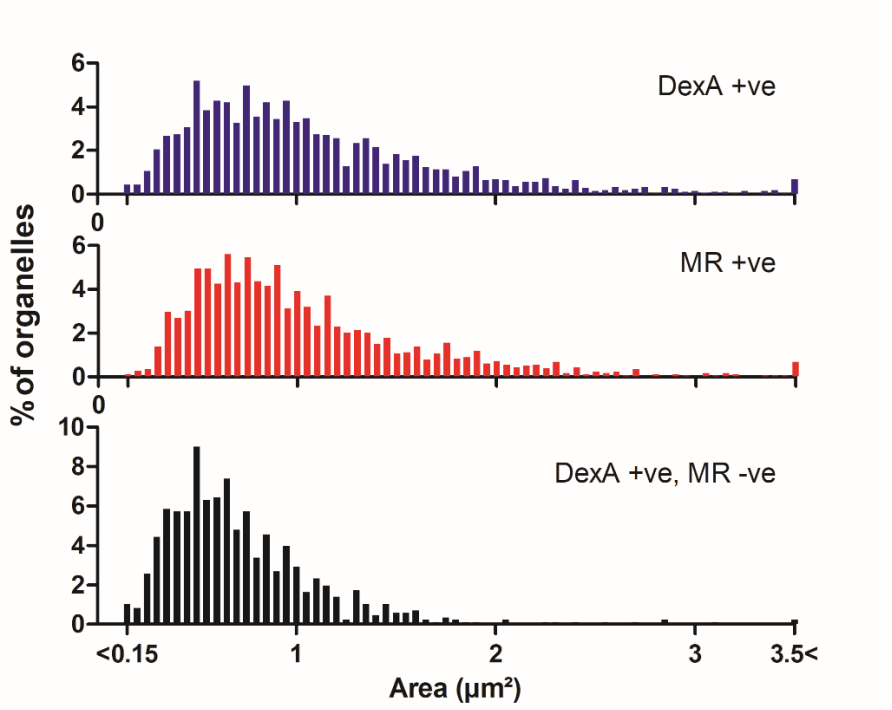

Figure 3.3 Characterisation of endolysosome and lysosome size

NRK cells were pre-loaded with DexA, as for figure 3.1, and incubated with MRB for 2 minutes. Size distribution of DexA-positive MR-positive, and DexA-positive MRB-negative organelles from 15 confocal slices containing 1927 DexA +ve spots, in NRK cells (single experiment).

Figure 3.4

A

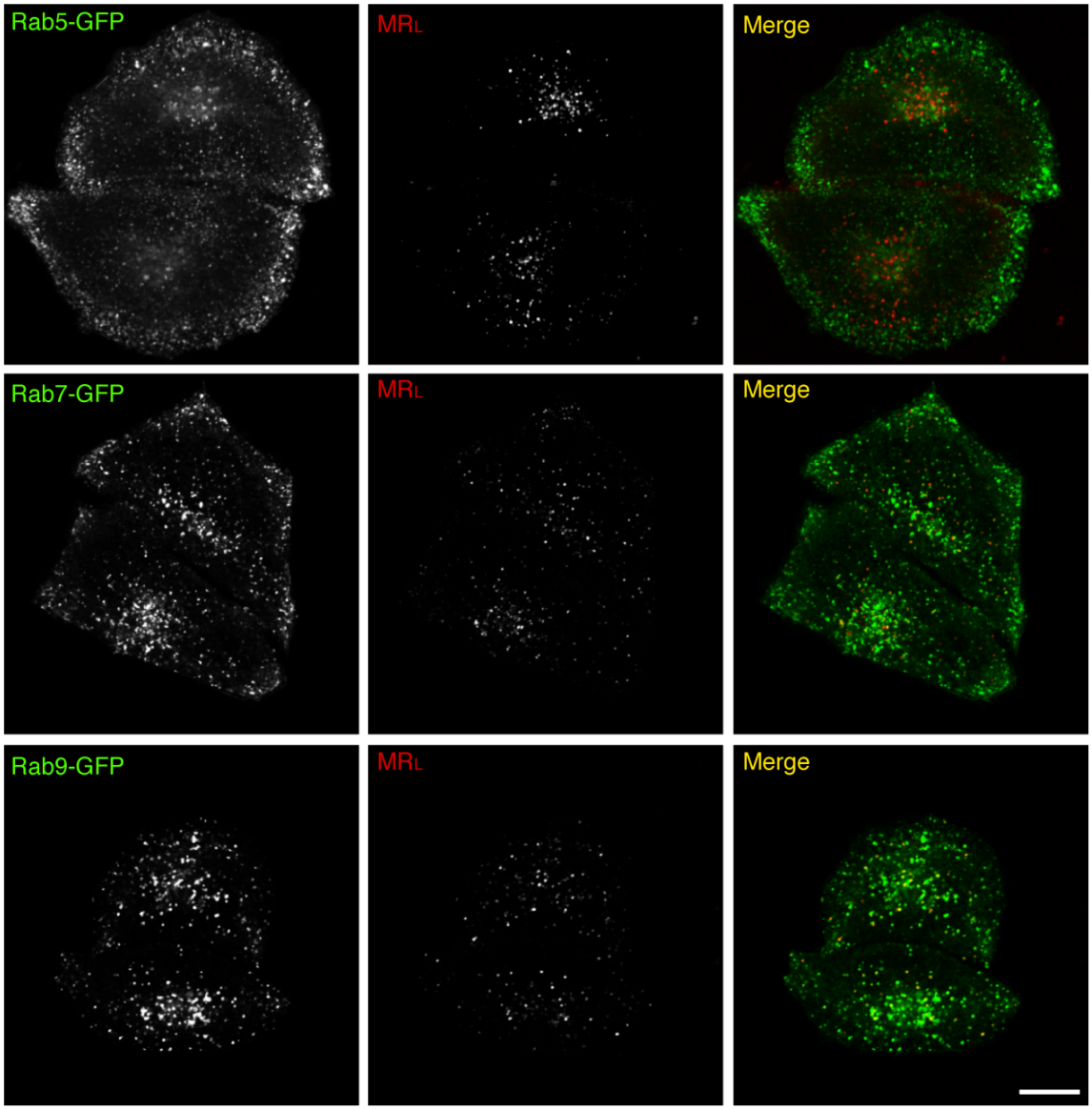
Rab5-GFP
MRL
Merge
Rab7-GFP
MRL
Merge
Rab9-GFP
MRL
Merge

B

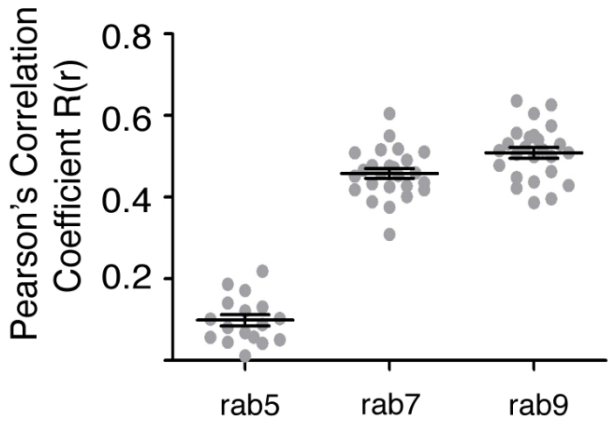
Pearson's Correlation Coefficient R(r)
0.8
0.6
0.4
0.2
rab5
rab7
rab9

C

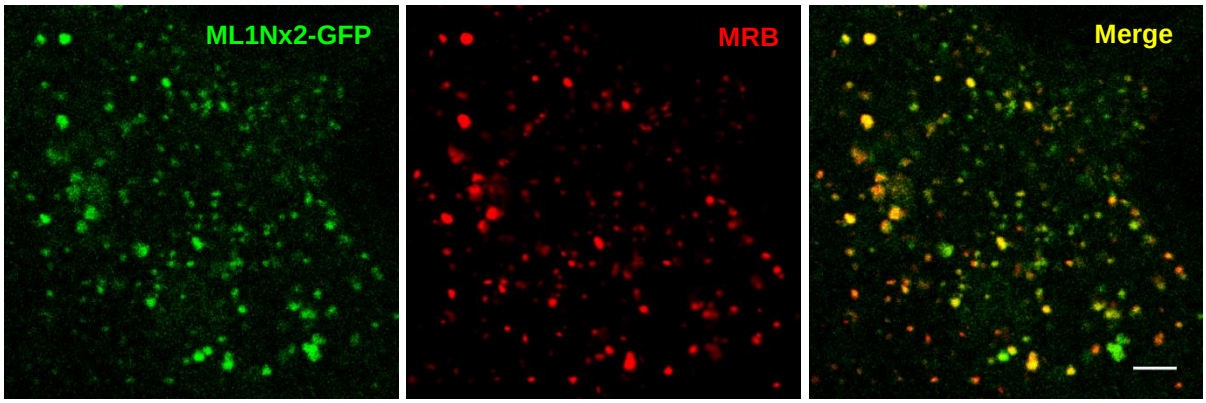

Figure 3.4: Further characterisation of endolysosomes

(A) Confocal fluorescence microscopy representative images of HeLa cells stably expressing either GFP-labelled Rab5, Rab7 or Rab9 after 2 min incubation with MRL. Scale bar represents 10µm.

(B) Pearson's colocalisation analysis for colocalisation of GFP-labelled Rab5, Rab7, or Rab9 with MRL after 2 min incubation (single experiment, ≥17 cells). Error bars represent the mean ± SEM.

(C) Confocal fluorescence microscopy representative image of NRK cells transiently transfected with ML1Nx2-GFP, after 2 min incubation with MRB. Scale bar represents 5µm.

3.2.3 Sucrosomes are cathepsin-active endolysosomes which do not upregulate TFEB signalling or autophagy in NRK cells

In NRK cells incubated with sucrose, then with MRB, it was observed that the swollen sucrosome compartments, which form after prolonged fluid phase uptake of indigestible sucrose, accumulated cresyl violet, confirming their identity as a swollen endolysosome with retained hydrolytic activity (Figure 3.5).

3.2.4 The formation of sucrosomes in NRK cells does not upregulate autophagy or TFEB signalling in NRK cells

To confirm that the effect of sucrosome formation on the equilibrium of endolysosomes and terminal lysosomes was not being affected by the autophagic pathway, LC3 levels were analysed by immunofluorescence. NRK cells were incubated with sucrose or Bafilomycin A1 (BafA1) as a positive control before fixation, immunostaining for LC3, and imaging by confocal microscopy (Figure 3.6A). The pixel intensity of LC3 staining was quantified in each condition and no change was measured between untreated and sucrose-incubated cells (Figure 3.6B), showing that sucrosome formation did not upregulate autophagy after 24 hours of sucrose uptake. To further ensure that the equilibrium of endolysosomes and terminal lysosomes was not being impacted by lysosome biogenesis signalling, NRK cells stably expressing TFEB-GFP were incubated with or without sucrose for 24 hours, with or without torin1 as a positive control. These cells were then incubated with Magic Red™ to mark sucrosomes, and imaged by live-cell confocal microscopy, showing negligible translocation of TFEB to the nucleus in cells incubated with sucrose alone (Figure 3.7A). The degree of TFEB translocation was quantified by incubating NRK cells stably expressing TFEB-GFP with or without sucrose before imaging using an automated high-throughput widefield microscope and analysing the difference between nuclear and cytosolic TFEB-GFP fluorescence in each condition. Incubation with sucrose had no effect on the translocation of TFEB-GFP to the nucleus (Figure 3.7B) suggesting that sucrosome formation in NRK cells does not activate lysosomal signalling or upregulate lysosome biogenesis. This is not the case for all mammalian cells, as MCF7 cells stably expressing TFEB-GFP were treated as per the NRK cells in Figure 3.7A, and showed dramatic translocation of TFEB-GFP to the nucleus (Figure 3.8).

Figure 3.5

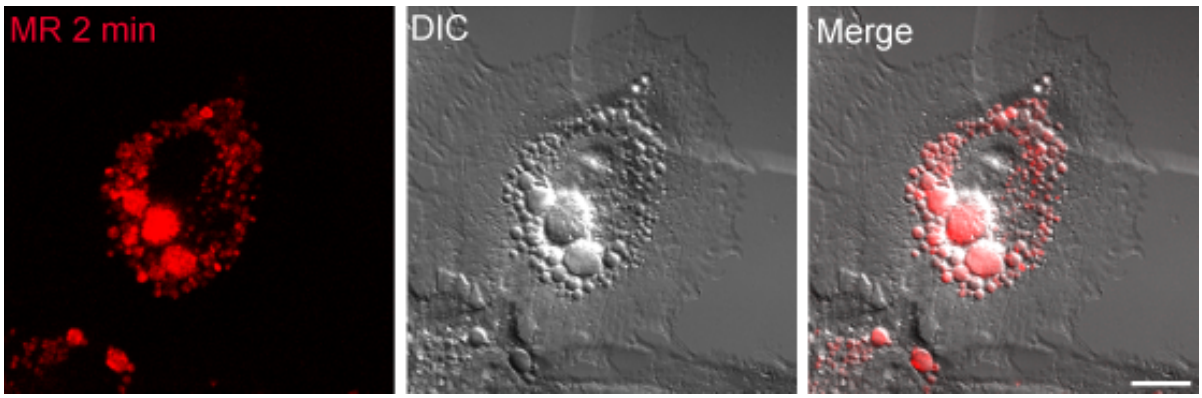

Figure 3.5: Sucrosomes are swollen cathepsin-active endolysosomes in NRK cells

Sucrosomes were formed in all cells by endocytosis of 30mM sucrose for 24 hours. Incubation of NRK cells with MRB for 2 min showed that the swollen vacuoles seen by differential interference contrast (DIC) microscopy were cathepsin B-active. Scale bar represents 10um.

Figure 3.6

A

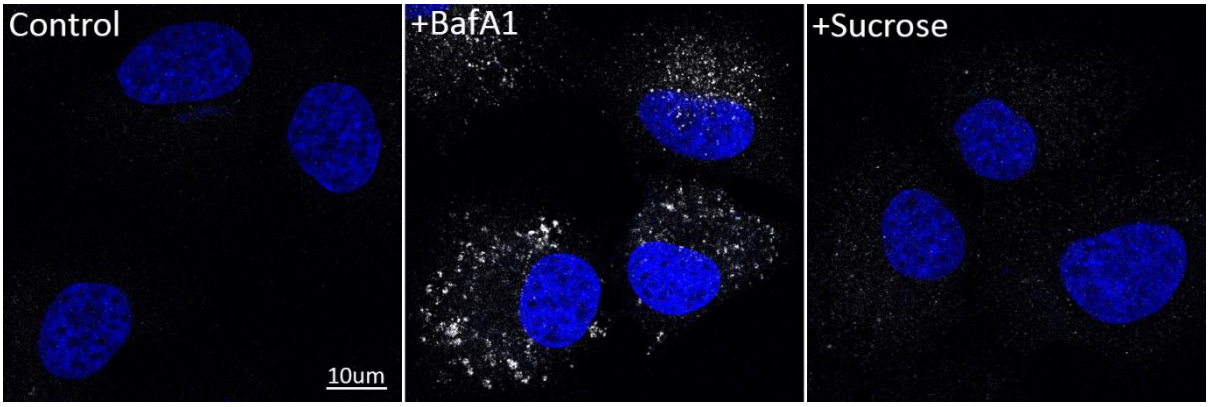

B

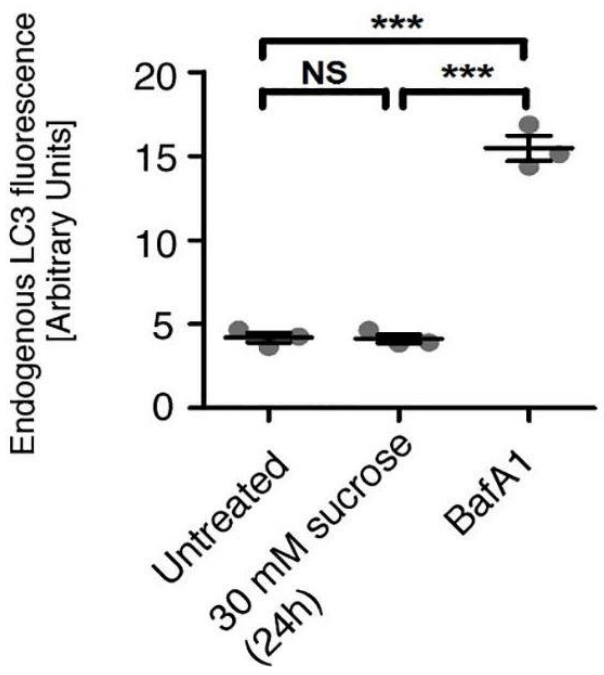

Figure 3.6: The formation of sucrosomes does not upregulate autophagy in NRK cells

Sucrosomes were formed in all cells by endocytosis of 30mM sucrose for 24 hours.

(A) Confocal immunofluorescence microscopy images of NRK cells using anti-LC3 immunoreactivity as a marker of autophagosome accumulation following sucrosome

formation. 400nM BafA1 for 8 hr was used as a positive control for autophagosome accumulation. Nuclei were identified by Hoechst 33342 staining.

(B) Quantification of mean LC3 immunofluorescence intensity in NRK cells treated as in (B). Error bars represent the mean ± SEM of 3 experiments. ***p < 0.001, NS, not significant (Two tailed unpaired t test).

Figure 3.7

A

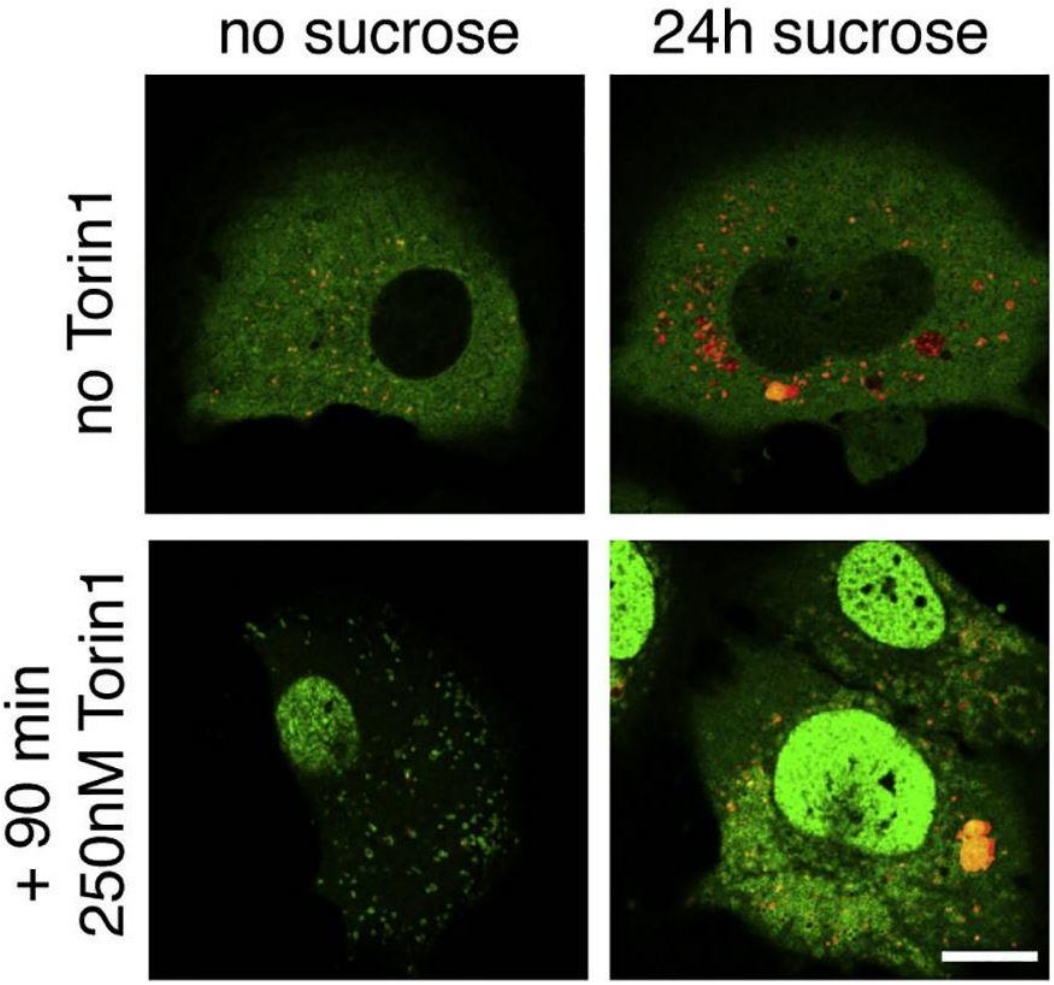
no sucrose
24h sucrose
no Torin1
+ 90 min
250nM Torin1

B

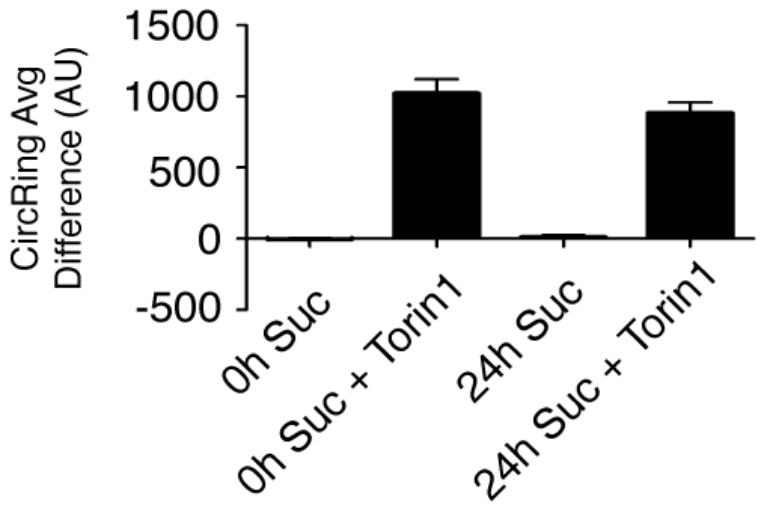
CircRing Avg
Difference (AU)
1500
1000
500
0
-500
0h Suc
0h Suc + Torin1
24h Suc
24h Suc + Torin1

Figure 3.7: The formation of sucrosomes does not upregulate TFEB translocation or autophagy in NRK cells

(A) Confocal fluorescence microscopy images of NRK cells stably expressing TFEB-GFP which were incubated with or without 30mM sucrose for 24 hr and subsequently with or without 250nM Torin 1 for 90 min (used as a positive control for TFEB-GFP translocation to the nucleus). The cells were then incubated with MRB for 2 min prior to imaging to mark cathepsin B- active organelles. Scale bar represents 10um.

(B) Quantification of the translocation of stably expressed TFEB-GFP to the nucleus of NRK cells which were incubated with sucrose and Torin 1 as in (A). TFEB translocation is presented as NucCyt difference, which is the mean pixel fluorescence intensity in the nuclei (Nuc) after subtracting the mean pixel intensity of the cytoplasm (Cyt) in a.u. Error bars represent the mean + SEM of 3 experiments.

Figure 3.8

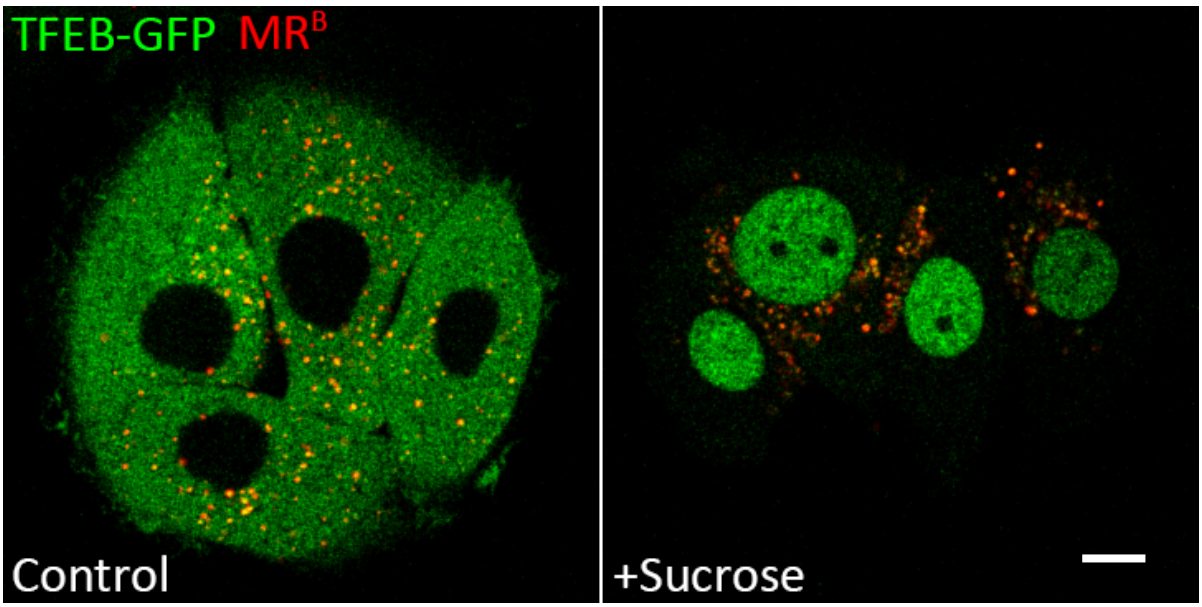

Figure 3.8: The formation of sucrosomes upregulates TFEB translocation in MCF7 cells

Confocal fluorescence microscopy images of MCF7 cells stably expressing TFEB-GFP, which were incubated with or without 30mM sucrose for 24 hr and subsequently with MRB for 2 min prior to imaging to mark cathepsin B- active organelles. Scale bar represents 10um

3.3 Discussion

Taken together with data generated by Dr Nick Bright (Bright, Davis and Luzio, 2016), the experiments reported in this chapter provide evidence that in mammalian cells endolysosomes are the principal sites of intracellular acid hydrolase activity and can be distinguished from acid-hydrolase-inactive terminal lysosomes, which likely act as a store of acid hydrolases. My experiments demonstrated that Dr Bright's initial observations on NRK cells with a Magic Red™ cathepsin B substrate could be extended to other cell types (HeLa and MCF7) and the use of a Magic Red™ cathepsin L substrate. Further, I was able to quantitate, using fluorescence light microscopy, the proportion of the total endolysosomal/lysosomal pool which was cathepsin-active endolysosomes and that which was cathepsin-inactive terminal lysosomes. In addition, it was observed that the cathepsin-active endolysosomes were LysoTracker®-positive i.e. acidic, whereas the terminal lysosomes were not. This was not due to lack of cathepsins, since Dr Bright showed by immuno-EM that in human, MCF-7 cells, for which a usable anti-cathepsin D antibody was available, both the endolysosomes and lysosomes contained cathepsin (Bright, Davis and Luzio, 2016).

A recent study showed cresyl violet to be a lipophilic weak base capable of permeating membranes in its unprotonated state, and accumulating in acidic compartments (Ostrowski *et al.*, 2016) Given this potent ability of cresyl violet to act as an acidotropic dye, the accuracy of cresyl violet accumulation as a marker of cathepsin activity, following treatment of cells with Magic Red™ cathepsin substrates, is brought into question. Following cleavage of Magic Red™ substrates, cresyl violet is released into the cathepsin-active compartment, but is only trapped within the membrane if it is in a protonated state. If a fraction of liberated cresyl violet could potentially evade protonation, it would be capable of diffusing out of the compartment it was generated in, and into other acidic compartments where it could accumulate as a result of protonation and trapping. This could hypothetically cause an under-representation of cathepsin activity in less acidic endolysosomes where cresyl violet is less rapidly protonated, and an over- or mis-representation of cathepsin activity in any sufficiently acidic compartments. Two observations made by Dr Bright make this unlikely (Bright, Davis and Luzio, 2016). Firstly, following formaldehyde fixation and incubation with antibodies in the presence of mild

detergent for immunofluorescence localisation of markers, the Magic Red™-positive compartments were still visible for 45-60min after fixation, despite the expected loss of pH gradients. Secondly, in live cell experiments in which endosome-lysosome fusions were followed by measuring the mixing of two fluorescent dextrans, the appearance of the cresyl violet fluorescence occurred after initial mixing and developed within the new endolysosomal compartment over time. It is therefore thought unlikely that unprotonated cresyl violet would escape in any detectable quantity in the experiments described and would preferentially diffuse away and accumulate in other acidic compartments, rather than where it was generated.

The experiments shown in this chapter also expanded the characterization of endolysomes and terminal lysosomes. Using the fluorescent probes in live cells, the endolysosomes were measurably larger in size than terminal lysosomes, consistent with Dr Bright's qualitative observations by TEM. The Magic Red™-positive endolysosomes were also observed to be positive for the late endosomal small GTPases Rab7, Rab9, but negative for the early endosomal GTPase Rab5. Use of the ML1Nx2 probe also showed that endolysosomes were positive for the phosphoinositide PI(3,5)P_2. This observation was consistent with the same probe being previously reported to identify a rapid increase in the concentration of PI(3,5)P_2 on the membranes of LAMP1-positive compartments immediately before they fuse (Li *et al.*, 2013). However, it should be noted that the specificity of this PI(3,5)P_2 probe has been questioned, because its subcellular localisation is largely unchanged following pharmacological or genetic interventions blocking PI(3,5)P_2 synthesis (Hammond *et al.*, 2015).

Although it has been known for over 30 years that lysosomes exhibit a wide range of pH (Yamashiro and Maxfield, 1987; Butor *et al.*, 1995), it wasn't until recently that Johnson et al., (2016) showed that less acidic lysosomes are preferentially distributed closer to the cell periphery. The subcellular localization of lysosomes is determined by the balance between the small GTPases Rab7 and Arl8 which interact with kinesin and dynein microtubule motors via different effectors (Jordens *et al.*, 2001; Rosa-Ferreira and Munro, 2011; Pu *et al.*, 2015; Guardia *et al.*, 2016; Fujiwara *et al.*, 2016), as well as an ER-located ubiquitin ligase system that contributes to their immobilisation in the perinuclear region (Jongsma *et al.*, 2016). Johnson et al. (2016) showed that if cells were experimentally manipulated to drive

more lysosomes to the periphery, there was a reduction in their acidity. Conversely, if lysosomes were driven towards the microtubule organising centre/nucleus, there was an increase in acidity. Whereas Johnson et al (2016) concluded that lysosome position within the cell determines acidity, my work together the experiments of Dr Bright suggests that it is the stage of the lysosome fusion/regeneration cycle that is important, but the different conclusions are not incompatible. Thus, more acidic endolysosomes are likely to be closer to the microtubule organising centre/nucleus and less acidic, reusable terminal lysosomes, more peripheral. Johnson *et al.* (2016) also provided evidence that the reduced acidity of some lysosomes is due to an increased passive (leak) permeability to protons together with reduced V-ATPase activity (a subject discussed further in Chapter 5).

A further important observation from my experiments was that sucrosomes formed in NRK cells, which had previously been shown to be endolysosomes (i.e hybrid organelles formed as a result of late endosome-lysosome fusion;(Bright *et al.*, 1997)), were Magic Red™-positive. This provides further evidence that endolysosomes rather than terminal lysosomes are acid hydrolase-active. An interesting feature of these experiments was that the sucrose treatment of NRK cells necessary to form sucrosomes appeared to have no effect on autophagy or the translocation of TFEB to the nucleus. Others have previously reported that sucrose treatment of mouse embryonic fibroblasts stimulates autophagy in a time- and sucrose concentration-dependent manner, causing an accumulation of autophagosomes (HiguchiNishikawa and Inoue, 2015). In HeLa cells sucrose treatment has been shown to cause nuclear translocation of TFEB (Sardiello *et al.*, 2009), just as I showed in MCF7 cells. At present, the molecular mechanisms underlying these differences in the effects of sucrose treatment on different cell types are unknown.

The data shown in this chapter, together with the additional data presented and discussed in Bright et al., 2016 have led me, together with my colleagues Professor Luzio (my supervisor) and Dr Bright to propose the lysosome regeneration cycle shown in Figure 3.9. In this cycle, what we call terminal, re-usable, acid hydrolase-storage lysosomes fuse with late endosomes to form endolysosomes, which become more acidic and in which acidic hydrolysis of endocytosed macromolecules commences. Further fusions of both late endosomes and lysosomes with the

endolysosomes can occur (BrightGratian and Luzio, 2005). Terminal, re-usable, storage lysosomes can then be re-formed from endolysosomes. This likely occurs via tubulation, loss of endosomal markers, recycling of SNARE proteins and condensation of content. It clearly involves loss of luminal acidity. The re-formation process is a maturation process and it is likely that macromolecule digestion continues as the pH increases. Indeed, lysosomal enzymes that are more active at less acidic pH, such as some enzymes involved in oligosaccharide degradation (Butor *et al.*, 1995), are predicted to be more effective as the pH rises during lysosome re-formation.

Figure 3.9

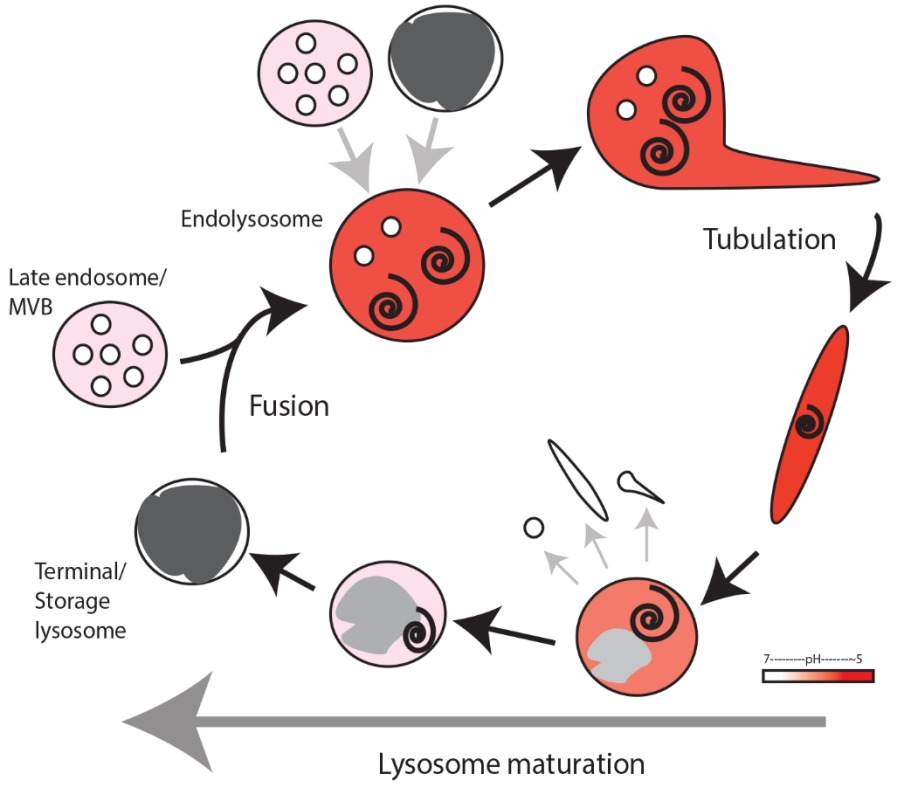

Figure 3.9 The lysosome regeneration cycle

Schematic showing the fusion of terminal storage lysosomes with late endosomes to form endolysosomes, which can undergo further fusions with late endosomes and with terminal storage, or undergo tubulation and content condensation in the process of reforming terminal storage lysosomes. The pink to red colour gradient represents the change from endosomal to endolysosomal (~5) pH, and gray regions represent electron-dense matter.

Chapter 4 – The mechanism of endosome-lysosome fusion in cultured mammalian cells

4.1 Introduction

Delivery of endocytosed macromolecules and cargo destined for degradation through the endosomal system to lysosomes requires kiss-and-run or full fusion events to occur between late endosomes and lysosomes, as discussed in Chapter 1. The fusion between late endosomes and lysosomes requires the sequential steps of tethering, trans-SNARE complex formation, and the merging of the opposing phospholipid bilayers. The SNAREs Vti1b, Syntaxin7, Syntaxin8 with either VAMP8 or VAMP7 were shown to be required for homotypic late endosome fusion or late endosome-lysosome fusion respectively by antibody inhibition studies (Antonin *et al.*, 2000; Ward *et al.*, 2000; Pryor *et al.*, 2004). Despite these data, knockout mice lacking VAMP7 or VAMP8 show no significant defects in their endosomal/lysosomal systems (Wang *et al.*, 2004; Sato *et al.*, 2011; Danglot *et al.*, 2012). This negligible effect of VAMP7 depletion is mirrored in cultured cells where siRNA-mediated knockdown of VAMP7 does not affect delivery of endocytosed cargo to lysosomes (Pols *et al.*, 2013a). The differences between the cell-free and whole cell studies may indicate that an alternative R-SNARE is compensating for the lack of VAMP7. Indeed, it has been reported that concomitant knockdown of both VAMP7 and VAMP8 impedes delivery of endocytosed cargo suggesting that there may be some functional redundancy between VAMP7 and VAMP8. Another SNARE that may potentially compensate for depletion of VAMP7 is YKT6, which like VAMP7, is a longin domain-containing R-SNARE. YKT6 is a promiscuous SNARE, localising to a number of intracellular compartments due to its lipid anchor-mediated membrane attachment rather than proteinaceous transmembrane domain. YKT6 has been shown to play a role in a number of different fusion events in yeast including vacuole homotypic fusion, in which Ykt6p can replace the VAMP7-orthologue Nyv1. (Thorngren *et al.*, 2004). Recently, the R-SNARE YKT6 has also been shown to be involved in autophagosome-lysosome fusion in human cultured cells (Matsui *et al.*, 2018) and fruit fly cells (Takáts *et al.*, 2018) where it replaces VAMP7/VAMP8 in the trans SNARE complex. Together, these data suggest that the current understanding of the roles of R-SNAREs in late endocytic pathway fusions is incomplete.

4.2 Results

4.2.1 Knockout of R-SNAREs VAMP7 and VAMP8 in HeLaM cells

Given the viability and only minor defects in VAMP7 or VAMP8 knockout mice, HeLa cells were knocked out for VAMP7 or VAMP8 using CRISPR-Cas9 technology for analysis of the effects of full depletion rather than siRNA mediated knockdown which can leave functional residual amounts of SNAREs as observed for endosome fusion (Bethani *et al.*, 2009). Using guide RNAs targeted to the first protein encoding exons of each sequence, the VAMP7 and VAMP8 were knocked out of HeLa cells, clonal lines were selected, and protein expression was analysed by Western blot (Figure 4.1A). The genotypes of VAMP7-knockout clone 2 and VAMP8-knockout clone A were determined by sequencing, and all allele variations are shown compared to the wild type gene (Figure 4.1B). VAMP7-knockout clone 2 cells contain either an 11-base or 25-base deletion, while VAMP8-knockout clone A cells contain only a single base insertion.

Figure 4.1

A

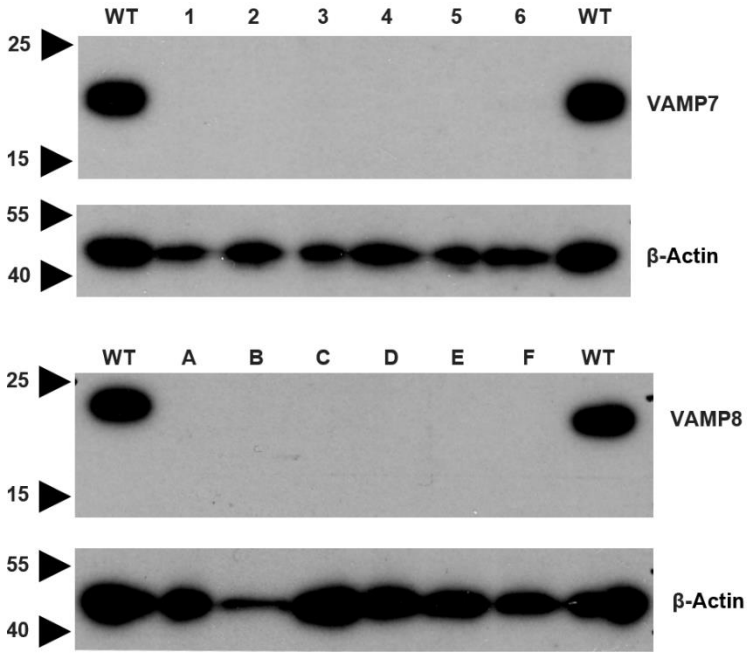

B

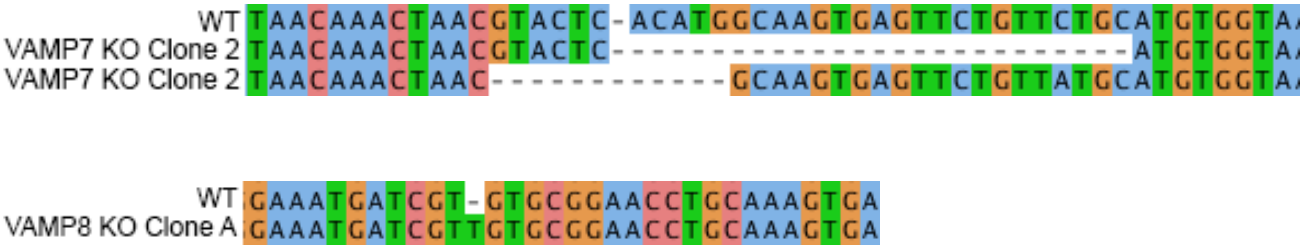

Figure 4.1: Knockouts of VAMP7 and VAMP8 in HeLa cells

(A) HeLa cells were co-transfected with the SpCas9 and guide RNA-containing plasmid and a GFP reporter plasmid in a 1:5 ratio. After 48 hours, single cells of successful transfectants were sorted by FACS for clonal populations. Six clonal lines of VAMP7 or VAMP8 knockout cells were analysed by Western blot to confirm knockout of protein expression. Cell lysates were run on a 15% polyacrylamide SDS gel, and transferred to PVDF membrane before immunoblotting with antibodies to VAMP7 and VAMP8. Anti-β-actin antibody was used to assess the levels of protein loading of each clonal line.

(B) The genomic region targeted by guide RNAs to human VAMP7 and VAMP8, aligned with the mutations introduced by CRISPR-Cas9 in the clonal lines used for further experiments. Genomic DNA was isolated from cells, amplified by PCR, and TA cloned into pCR2.1 vector before Sanger sequencing.

4.2.2 The effect of VAMP7 or VAMP8 depletion on endolysosome dynamics

To address the relative impacts of VAMP7 or VAMP8 depletion on the integrity of the endolysosomal system, particularly the balance of lysosomes and endolysosomes, the proportions of dextran pre-loaded lysosomes containing LysoTracker Green or Magic Red™ Cathepsin B were analysed. Colocalisation of dextran and LysoTracker or Magic Red™ was analysed in confocal microscopy images using Manders' coefficient. Neither VAMP7 knockout nor VAMP8 knockout had a significant effect on the proportion of lysosomes that were marked with either LysoTracker or Magic Red™ (Figure 4.2A). As a measure of late endosome-lysosome fusion, the delivery of endocytosed fluorescent dextran to catalytically active endolysosomes was analysed in each knockout cell line compared to wild type cells. Again, no significant effect was seen in either knockout cell line (Figure 4.2 B), indicating that there is no major impediment to late endosome-lysosome fusion.

Figure 4.2

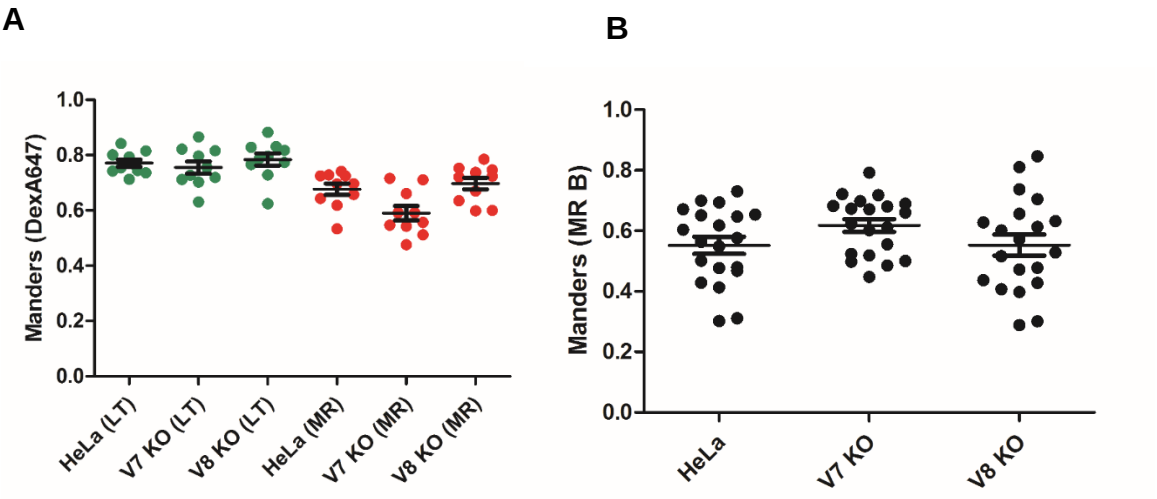

Figure 4.2: The effect of VAMP7 or VAMP8 depletion on endolysosome dynamics

(A) Cells were preloaded with DexA for 4 hours, chased with dextran-free medium for 20 hours and incubated with Magic Red™ Cathepsin B for 2 minutes before capturing confocal images which were analysed for colocalisation analysis. Mander's (green, DexA:LTG and red, DexA:MRB) correlation coefficients for colocalisation of preloaded DexA and LTG or MRB in HeLa, HeLa VAMP7-knockout, and HeLa VAMP8-knockout cells are shown for a single experiment.

(B) Cells were pulsed with 2 hours uptake of Dex488 followed by 1 hour chase in dextran-free medium, and incubated with Magic Red™ Cathepsin B for 2 minutes before capturing confocal images which were analysed for colocalisation analysis. Mander's (Dex488: MRB) correlation coefficients for colocalisation of pulsed Dex488 and MRB in HeLa, HeLa VAMP7-knockout, and HeLa VAMP8-knockout cells are shown for a single experiment.

4.2.3 Localisation of intracellular markers are unaffected after knockout of VAMP7 or VAMP8

To assess if the knockout of VAMP7 and VAMP8 had caused any major disruptions to organelles of the endocytic or biosynthetic pathways, their morphology and localisation were analysed by confocal microscopy. Imaging reagents and antibodies to key markers of early endosomes, late endosomes, lysosomes, and trans Golgi network were used to stain the compartments. The size and distribution of each marker seemed unaffected by either VAMP7 or VAMP8 knockout (Figure 4.3) indicating that the compartments remain largely unaffected by depletion of each R-SNARE.

Figure 4.3

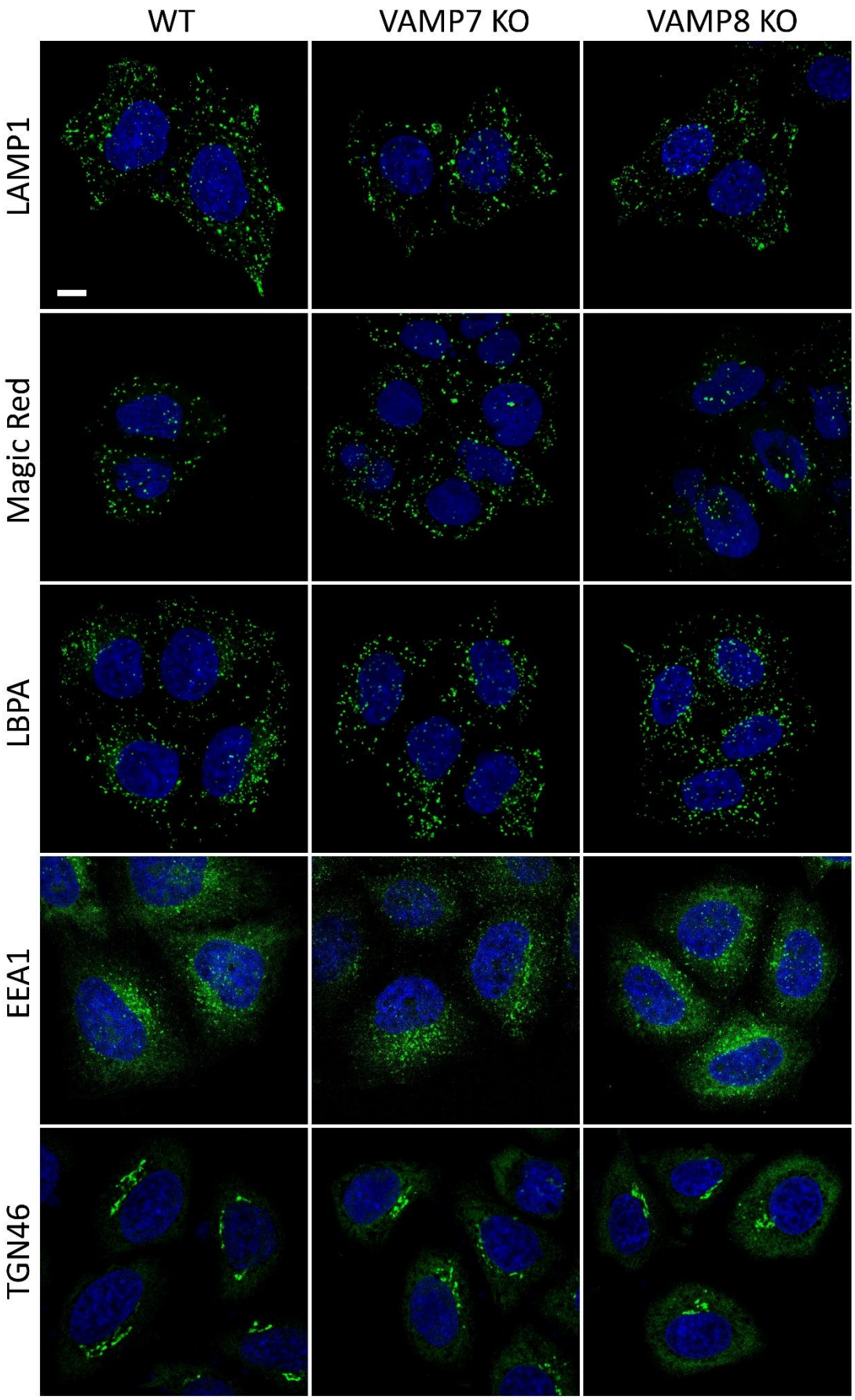

Figure 4.3: Immunofluorescence of intracellular markers after knockout of VAMP7 or VAMP8

(A) Anti-LAMP1, anti-LBPA, anti-EEA1, and anti-TGN46 immunoreactivity in fixed HeLa cells was used to mark lysosomes, late endosomes, early endosomes, and trans Golgi network respectively. Magic Red™ was used in live cells to mark endolysosomes. Nuclei were identified by Hoechst 33342 staining. Scale bar represents 10µm.

4.2.4 Generation of VAMP7 and VAMP8 double knockout HeLa cells

The combination of the lack of effect seen in the individual R-SNARE knockout cells, and the potential complication of insufficient SNARE knockdown by siRNA to affect fusion (Bethani *et al.*, 2009) provided the basis to study the simultaneous depletion of VAMP7 and VAMP8 by generating a double-knockout cell line. VAMP7 was knocked out of VAMP8-knockout clone A background cells using CRISPR-Cas9. Clonal lines of double VAMP7 and VAMP8 knockout were selected and VAMP7 and VAMP 8 protein expression was analysed by Western blot (Figure 4.4).

Figure 4.4

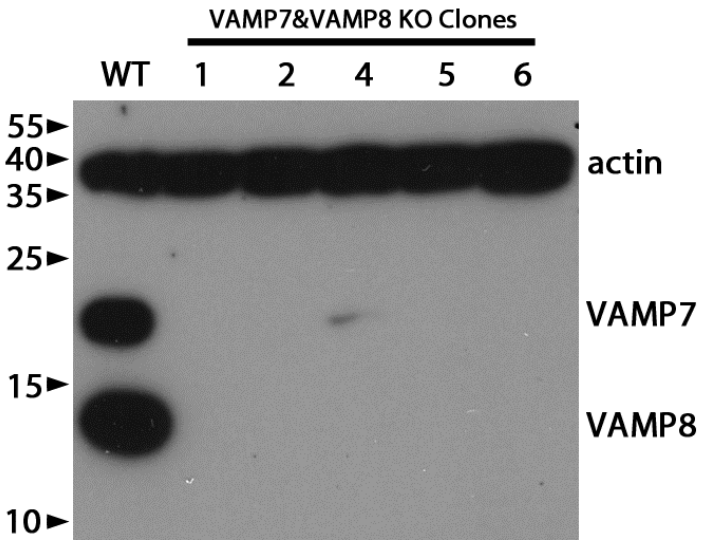

Figure 4.4: Double knockout of VAMP7 and VAMP8 in HeLa cells

HeLa VAMP8-knockout clone A cells were co-transfected with the SpCas9 and guide RNA-containing plasmid and a GFP reporter plasmid in a 1:5 ratio. After 48 hours, single cells of successful transfectants were sorted by FACS for clonal populations. Six clonal lines of VAMP7+VAMP8 double knockout cells were analysed by western blot to confirm knockout of protein expression. Cell lysates were run on a 15% polyacrylamide SDS gel, and transferred to PVDF membrane before immunoblotting with antibodies to VAMP7 and VAMP8. Anti-β-actin antibody was used to assess the levels of protein loading of each clonal line.

4.2.5 Delivery of endocytosed cargo to endolysosomes is unaffected in VAMP7 and VAMP8 double knockout cells

Given the possibility that VAMP8 compensates for the lack of VAMP7 in VAMP7-knockout cells, the effects of the double knockout on fluid phase cargo delivery of endocytosed dextran to Magic Red™-positive lysosomes was analysed as in Figure 4.2. No significant change was observed between wild type cells and VAMP7+VAMP8 double knockout cells (Figure 4.5A and B). siRNA-mediated knockdown of VPS33A was used as a positive control, showing that it is possible to block delivery of dextran to endolysosomes in wild type and double knockout cells (Figure 4.5A and B). These data indicate that either VAMP8 does not play a significant role in the compensation for VAMP7 depletion, or that the presence of another R-SNARE is capable of facilitating late endosome-lysosome fusion events.

Figure 4.5

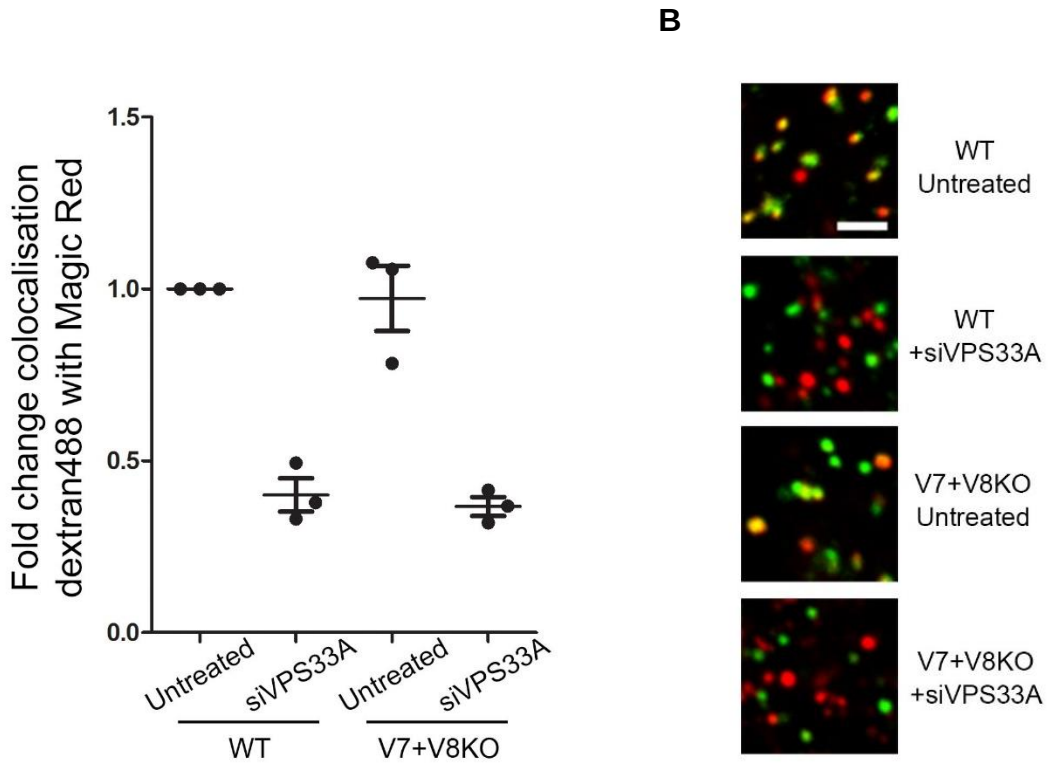

Figure 4.5: Endocytosed cargo delivery to endolysosomes in VAMP7 and VAMP8 double knockout cells

(A) Cells were pulsed with 2 hours uptake of Dex488 followed by 1 hour chase in dextran-free medium, and incubated with Magic Red™ Cathepsin B for 2 minutes before capturing confocal images which were analysed for colocalisation analysis. Mander's (MRB: Dex488) correlation coefficients for colocalisation of pulsed Dex488 and MRB in wild type and VAMP7+VAMP8 double knockout cells are shown. Error bars represent the mean ± SEM of 3 experiments.

(B) Live cell confocal image sections of cells analysed for colocalisation in (A), showing Dex488 in green and MRB in red. Scale bar represents 2.5µm.

4.2.6 Immunofluorescent staining of LAMP1 and not of other intracellular markers is affected by double knockout of VAMP7 and VAMP8

To address the state of intracellular organelles after VAMP7+VAMP8 double knockdown, markers of organelles of the endocytic and biosynthetic pathways were analysed by immunofluorescence as in Figure 4.3. While markers for endolysomes and trans Golgi network appeared to be unaffected, there was a mild effect on LAMP1 staining (Figure 4.6). In VAMP7+VAMP8 double knockout cells, there appeared to be fewer LAMP1-positive puncta per cell, and the puncta seemed to be larger on average than those in wild type cells.

Figure 4.6

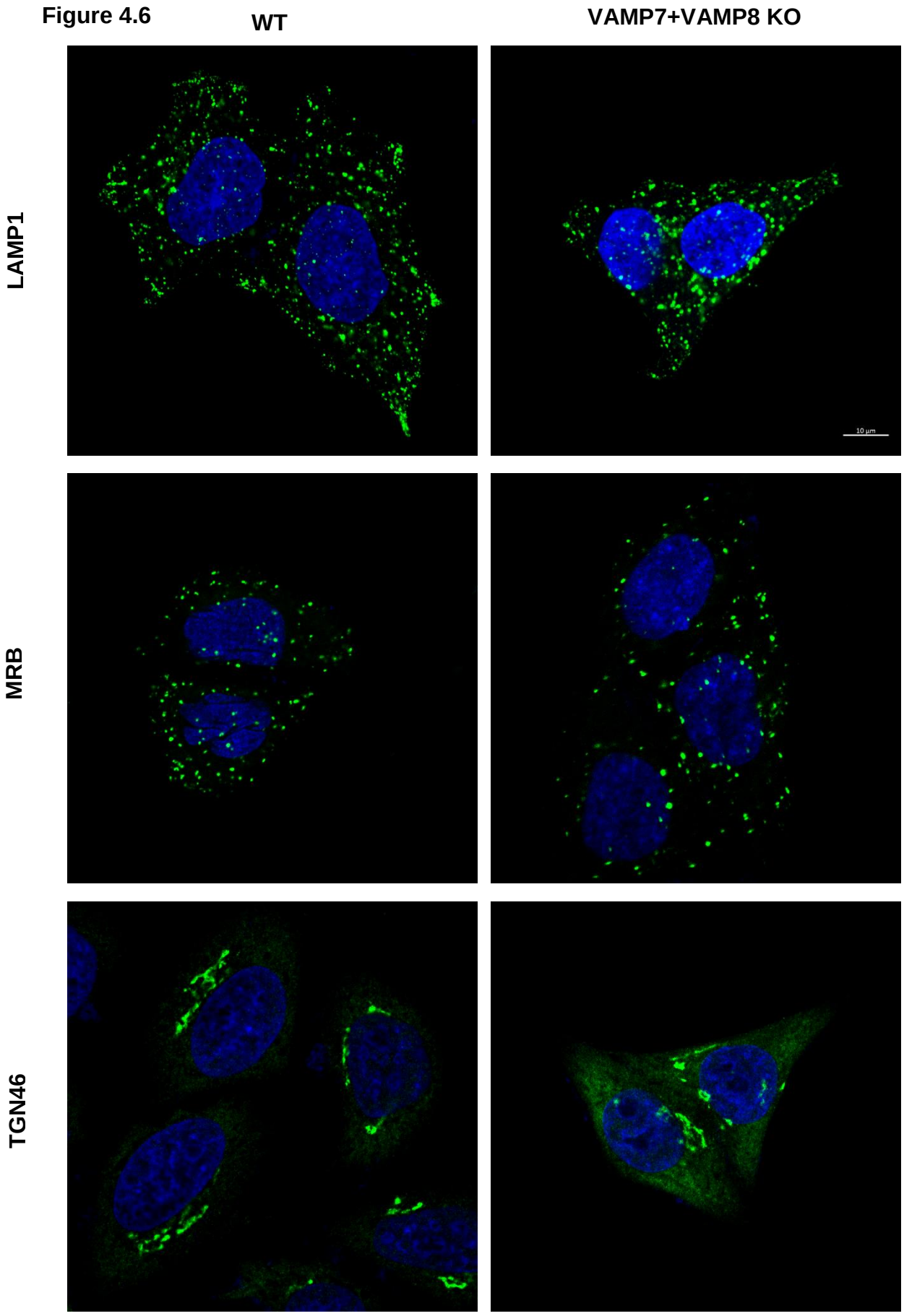

Figure 4.6: Immunofluorescence of intracellular markers after knockout of VAMP7 and VAMP8 in HeLa cells

Anti-LAMP1 and anti-TGN46 immunoreactivity in fixed cells was used to mark lysosomes and trans Golgi network respectively. Magic Red™ was used in live cells to mark endolysosomes. Nuclei were identified by Hoechst 33342 staining. Scale bar represents 10µm.

4.2.7 The appearance of LAMP1-positive organelles in control, individual, and double knockout of VAMP7 and VAMP8

While the individual knockdowns of VAMP7 and VAMP8 had little effect on the immunofluorescent labelling of the endosomal and biosynthetic organelles, the VAMP7+VAMP8 double knockout cells presented fewer and larger LAMP1 stained puncta. The LAMP1-positive puncta in double knockout cells also appeared less rounded or uniform in shape, possibly indicating a minor aberration in morphology, or a clustering of LAMP1-containing organelles (Figure 4.7A). To quantify and measure this perceived difference in LAMP1 staining, wild type, VAMP7-knockout, VAMP8-knockout, and VAMP7+VAMP8 double knockout cells were immunolabelled for LAMP1 as before, and confocal images were taken and analysed to determine the diameter of LAMP1-positive puncta in each condition. This revealed a slight upward shift in the size distribution of LAMP1-positive puncta in VAMP7-knockout cells, and a greater shift in VAMP7+VAMP8 double knockout cells (Figure 4.7B). The data also showed the mean number of LAMP1-positive puncta per cell to be similar between wild type cells and individual knockout cells, whereas double knockout cells showed a steep decline in the mean number of puncta per cell (Figure 4.7C).

Figure 4.7

A

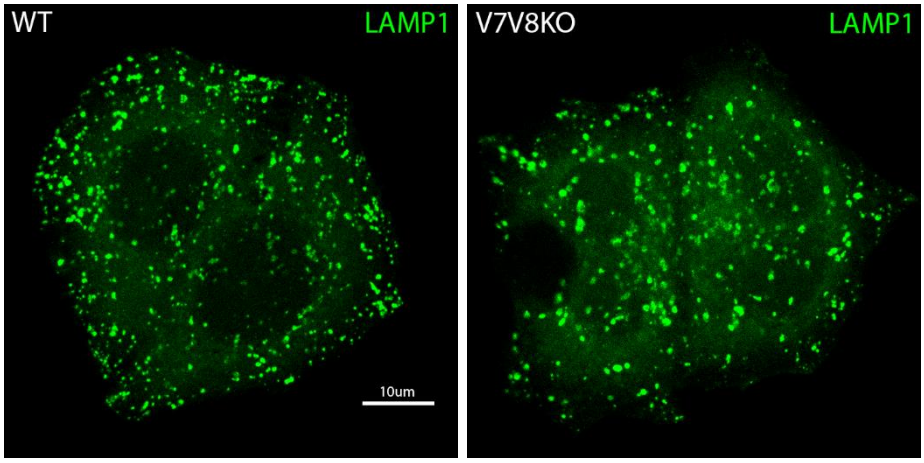

B

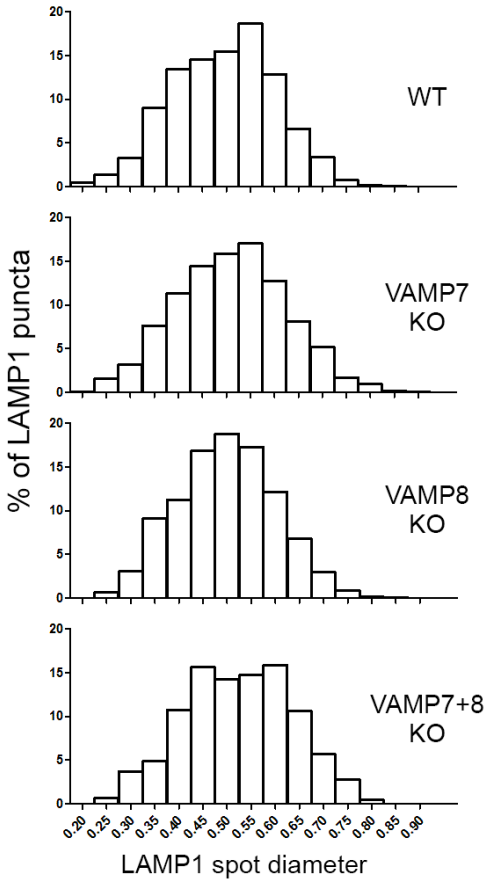

C

	HeLa M WT	HeLa M VAMP7 KO	HeLa M VAMP8 KO	HeLa M VAMP7& VAMP8 KO
Mean lysosomes per cell	160.2	181.2	174.6	89.6
Mean lysosome diameter	0.497	0.512	0.499	0.524
Standard deviation of lysosome diameter	0.106	0.114	0.101	0.111

Figure 4.7: LAMP1-positive organelles in control, individual, or double knockout of VAMP7 and VAMP8

(A) Confocal fluorescence images of anti-LAMP1 immunolabelling in fixed cells of wild type or VAMP7+VAMP8 double knockout cells. Scale bar represents 10µm.

(B) Confocal images of 10 LAMP1-stained cells were processed using Imaris software to analyse the number and size of LAMP1-positive puncta. Histograms show the percentage of puncta in each bin for diameter, increasing in increments of 0.05µm.

(C) Number of lysosomes per cell, mean lysosome diameter and standard deviation of the diameter, derived from the Imaris analysis of spot size in each condition.

4.2.8 Increased tethering between late endocytic organelles and with peripheral vesicles in double knockout of VAMP7 and VAMP8

To better understand the morphological effects observed by LAMP1-immunofluorescence in the VAMP7+VAMP8 double knockout cells, EM was performed by Nick Bright to analyse the ultrastructure of late endocytic organelles in thin sections. In these sections of double knockout cells, there was an unusual degree of filamentous tethering and pore formation between late endocytic organelles (Figure 4.8A) and which was not observed in wild type cells. Additionally, VAMP7+VAMP8 double knockout cells showed an abnormal number of small vesicles accumulating around the periphery of late endocytic organelles (Figure 4.8B) which also does not usually occur in wild type HeLa cells.

Figure 4.8

A

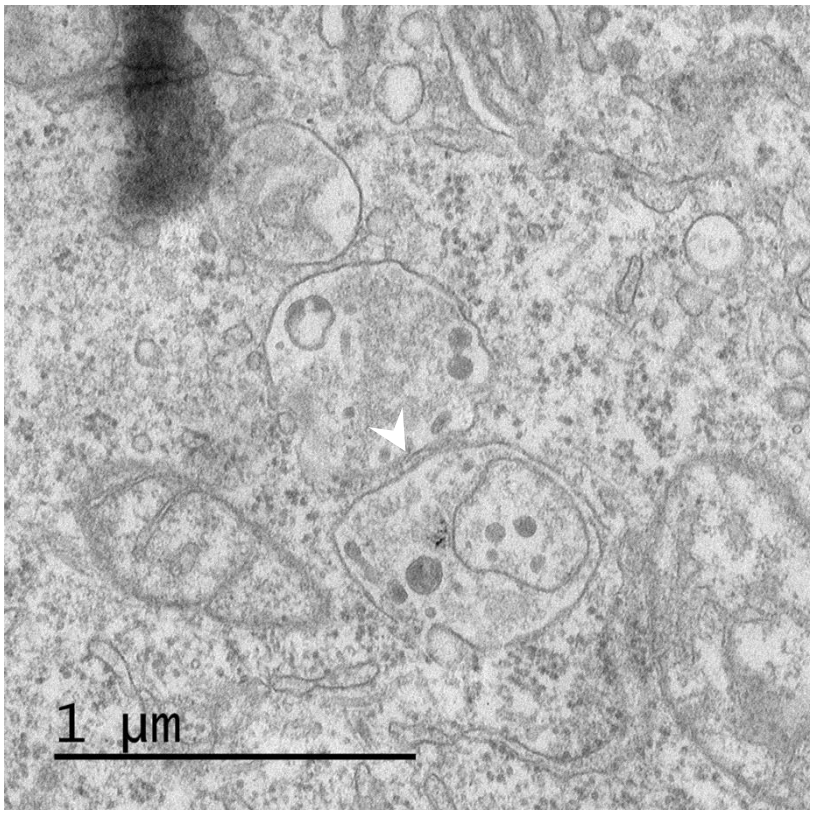

B

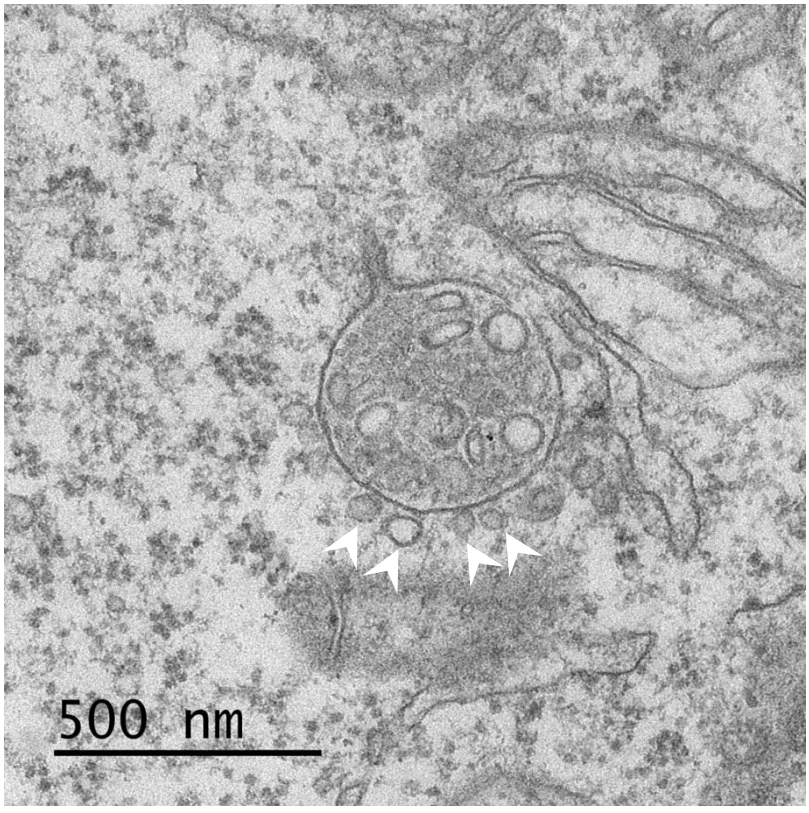

Figure 4.8: EM of late endocytic organelles in double VAMP7 and VAMP8 knockout cells (Images from Dr Nick Bright)

VAMP7+VAMP8 double knockout cells were incubated with colloidal gold stabilised with BSA for 4 hours and chased with gold-free medium for 20 hours before fixation and processing for EM as described in (Bright, Davis and Luzio, 2016).

(A) EM of a thin section from a VAMP7+VAMP8 KO cell, showing extensive tethering between organelles of the late endocytic pathway (arrowhead).

(B) EM of a thin section from a VAMP7+VAMP8 KO cell showing abnormal accumulation of small vesicles around the periphery of a late endocytic organelle (arrowheads).

4.2.9 Alternative R-SNAREs do not change in abundance after double knockout of VAMP7 and VAMP8 in HeLa cells

Provided that concurrent depletion of VAMP7 and VAMP8 had little effect on delivery of endocytosed cargo to endolysosomes, it may be assumed that another alternative SNARE may be compensating for the lack of VAMP7. Potential alternative R-SNAREs (Figure 4.9 B) were analysed by western blot to assess if there was any measurable upregulation at the protein level. There were no significant changes in the protein levels of YKT6 or SEC22b between wild type and VAMP7+VAMP8 knockout cells.

Figure 4.9

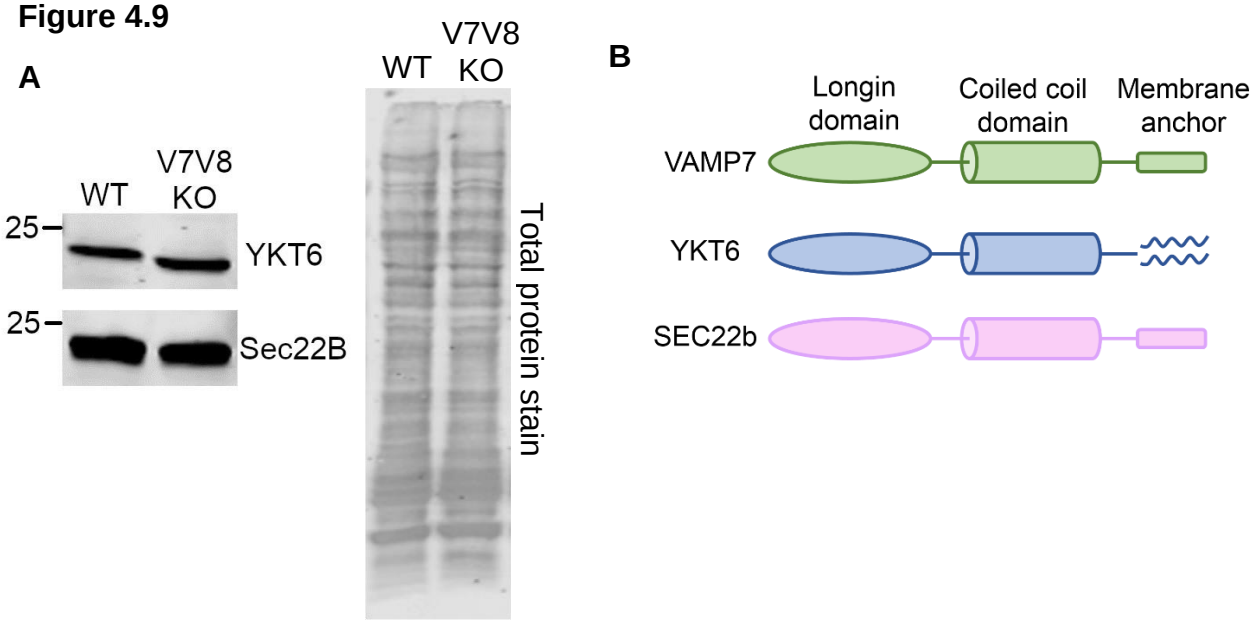

Figure 4.9: Alternative R-SNAREs do not change in abundance in individual or double knockout of VAMP7 and VAMP8

(A) HeLa WT and VAMP7+VAMP8 KO cells were analysed by Western blot to measure protein abundance of YKT6 or SEC22b. Cell lysates were run on a 15% polyacrylamide SDS gel, and transferred to PVDF membrane before measuring protein loading with REVERT™ Total Protein Stain. The membrane was immunoblotted with antibodies to YKT6 and SEC22b. Bands were quantified using Image Studio, and normalised to Total Protein Stain signal.

(B) A diagram depicting the domain similarities between VAMP7, YKT6 and SEC22b, as members of the longin group of R-SNAREs.

4.2.10 Endocytosed cargo delivery to endolysosomes is impeded in YKT6-depleted cells

As discussed in chapter 4.1, YKT6 represents a strong candidate for the replacement of VAMP7 in late endosome-lysosome fusion. Using siRNA mediated knockdown of YKT6 in both wild type and VAMP7+VAMP8 double knockout cells, the extent of endocytosed dextran delivery to lysosomes was analysed as for figure 4.2B. Using two different oligos, >85% YKT6 knockdown (Figure 4.10B) had a very mild inhibitory effect on delivery to lysosomes in wild type cells, however when YKT6 was knocked down in VAMP7+VAMP8 double knockout cells, there was a much greater inhibition of delivery of dextran to endolysosomes (Figure 4.10A and C). This shows that VAMP7+VAMP8 double knockout cells are more sensitive to YKT6 depletion than wild type, suggesting some specific involvement of YKT6 in endosome-lysosome fusion, and that the effect is not simply a consequence of reduced YKT6 function in other pathways affecting the whole cell.

Figure 4.10

A

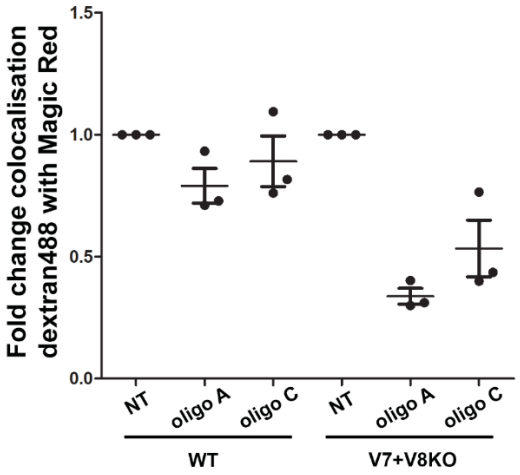

B

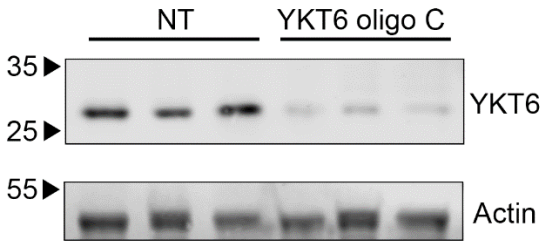

C

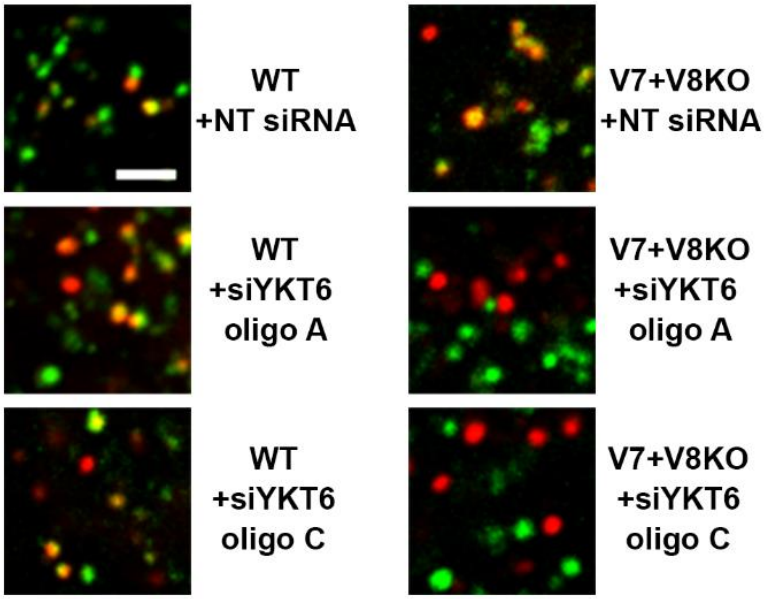

Figure 4.10: The effect of Ykt6 knockdown on dextran delivery to late endocytic compartments in VAMP7 and VAMP8 double knockout cells

(A) Wild type and VAMP7+VAMP8 double knockout cells were transfected with either non-targetting siRNA, YKT6-targetting siRNA oligo A, or YKT6-targetting siRNA oligo C. 96 hours post-transfection, cells were pulsed with 2 hours uptake of Dex488 followed by 1 hour chase in dextran-free medium, and incubated with Magic Red™ Cathepsin B for 2 minutes before capturing confocal images which were analysed for colocalisation analysis. Mander's (MRB: Dex488) correlation coefficients for colocalisation of pulsed Dex488 and MRB in wild type and VAMP7+VAMP8 double knockout cells are shown. Error bars represent the mean ± SEM of 3 experiments

(B) Representative blots of YKT6 knockdown in cells transfected with non-targetting or YKT6-targetting siRNA analysed by Western blot. Cell lysates were run on a 12% TruPAGE polyacrylamide SDS gel, and transferred to PVDF membrane before immunoblotting with antibodies to YKT6 and β-actin. Bands were quantified using Image Studio, and normalised to β-actin band signal.

(C) Live cell confocal image sections of cells analysed for colocalisation in (A), showing Dex488 in green and MRB in red. Scale bar represents 2.5µm.

4.2.11 The distribution of YKT6 is unaltered in VAMP7 and VAMP8 double knockout cells

Given that late endosome-lysosome fusion in VAMP7+VAMP8 double knockout cells appears to be more sensitive to YKT6 depletion, it could be assumed that in these cells, YKT6 is fulfilling the role of the R-SNARE in late endosome-lysosome trans SNARE complexes. In such a case, double knockout cells may display an increased distribution of YKT6 to lysosomes. To test this, wild type and VAMP7+VAMP8 double knockout cells were immunostained for YKT6, however in both cell lines YKT6 retained its predominantly perinuclear and partially cytoplasmic staining (Figure 4.11A) as previously reported (Fukasawa *et al.*, 2004). To quantify the YKT6 distribution relative to lysosomes, cells were co-stained for YKT6 and lysosomal marker LAMP1 then confocal images were taken and analysed to calculate Pearson's coefficients. This showed no significant difference in the colocalisation of YKT6 and LAMP1 between wild type or VAMP7+VAMP8 double knockout cells (Figure 4.11 B).

Figure 4.11

A

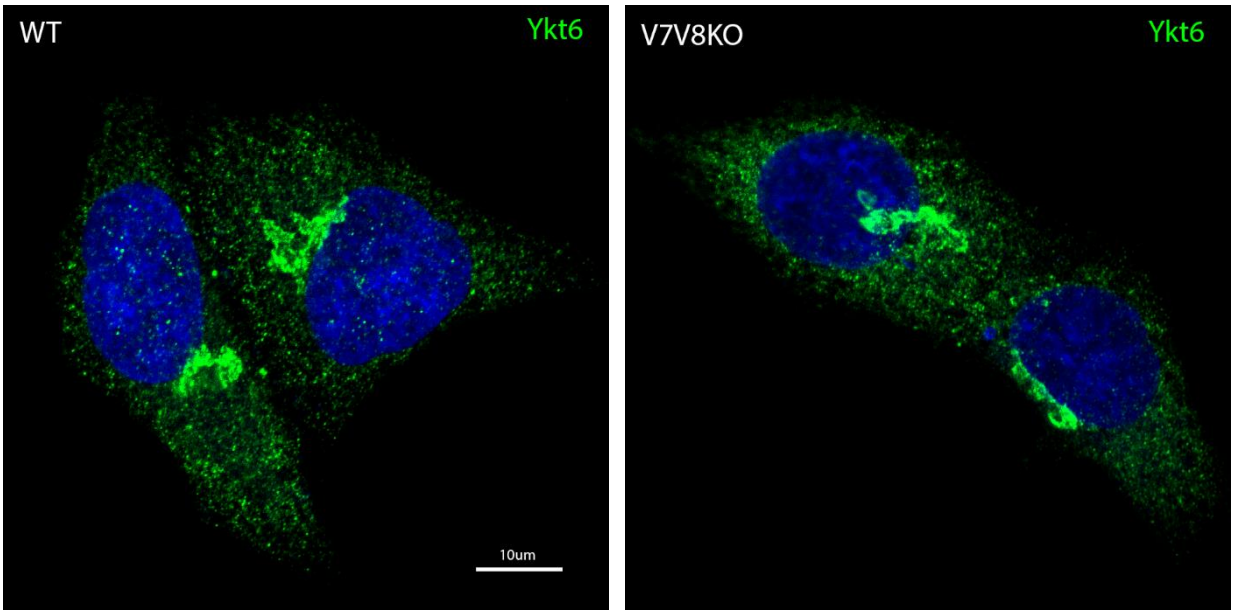

B

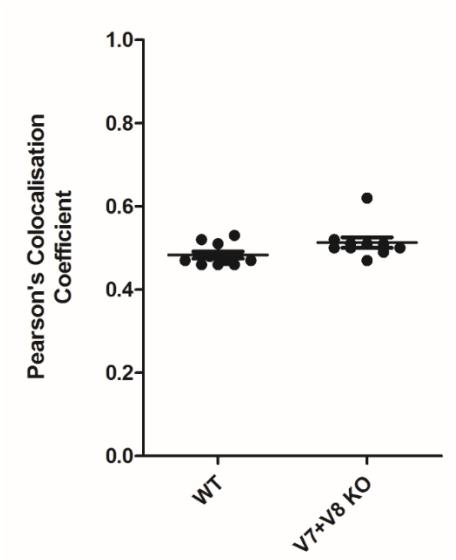

Figure 4.11: The distribution of Ykt6 in VAMP7 and VAMP8 double knockout cells

(A) Anti-YKT6 immunoreactivity in fixed wild type or VAMP7+VAMP8 double knockout cells showing endogenous YKT6 distribution. Nuclei were identified by Hoechst 33342 staining. Scale bar represents 10µm.

(B) Pearson's colocalisation analysis for colocalisation of YKT6 and LAMP1 immunofluorescence in fixed cells (single experiment). Error bars represent the mean ± SD.

4.2.12 Autophagy is not upregulated in VAMP7 and VAMP8 double knockout cells

In order to assess if the VAMP7 and VAMP8 double knockouts are impeding autophagic flux, whole cell lysate of HeLa VAMP7 and VAMP8 double knockout clone A1 cells was immunoblotted for LC3. The double knockout cell line showed no significant difference in LC3 accumulation relative to wild type HeLa cells, indicating normal levels of autophagy.

Figure 4.12

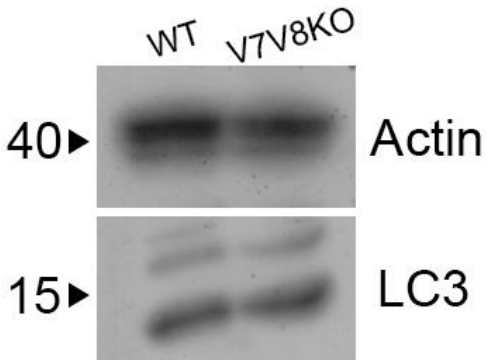

Figure 4.12: Immunoblotting of LC3 in R-SNARE depleted cells

HeLa VAMP7+VAMP8 double knockout cells were lysed and analysed by western blot to assess LC3 accumulation. Cell lysates were run on a 15% polyacrylamide SDS gel, and transferred to PVDF membrane before immunoblotting with an antibody to LC3. Anti-β-actin antibody was used to assess the levels of protein loading of each cell line.

4.2.13 The effect of YKT6 depletion on delivery to endolysosomes in VAMP7 and VAMP8 double knockout cells is rescued by VAMP7 reconstitution

The enhanced susceptibility of VAMP7+VAMP8 double knockout cells to YKT6 knockdown suggests that YKT6 may be replacing either VAMP7 or VAMP8 as the R-SNARE for late endosome-lysosome fusion. To further assess this, a VAMP7+VAMP8 double knockout cell line overexpressing HA-tagged VAMP7 was generated. In wild type, VAMP7+VAMP8 double knockout, and VAMP7-rescue double knockout cells, delivery of endocytosed dextran to endolysosomes was analysed with or without depletion of YKT6. While VAMP7+VAMP8 double knockout cells showed a significant impediment of delivery to lysosomes after YKT6 depletion, the knockout cells overexpressing VAMP7 showed a much less pronounced effect, very similar to wild type cells (Figure 4.13 A). The capacity of VAMP7 to reverse the sensitivity of double-knockout cells to YKT6 knockdown lends credence to the idea that these two R-SNAREs are to some extent interchangeable in their roles in late endosome-lysosome fusion.

Figure 4.13

A

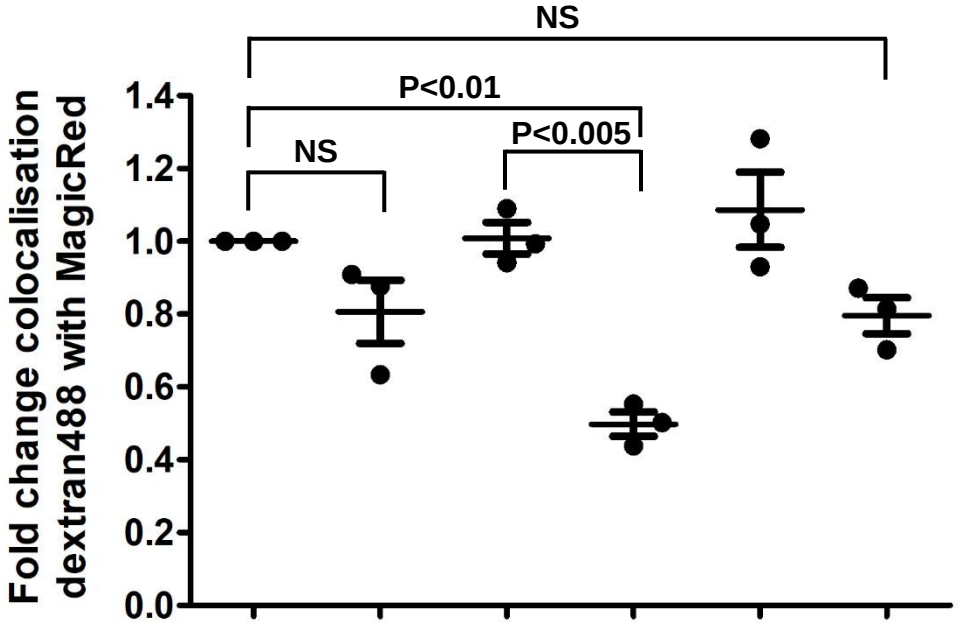

VAMP7	**+**	**+**	**--**	**--**	**++**	**++**
VAMP8	**+**	**+**	**--**	**--**	**--**	**--**
YKT6	**+**	**-**	**+**	**-**	**+**	**-**

B

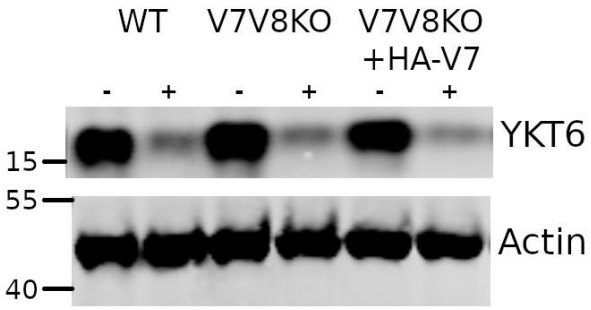

C

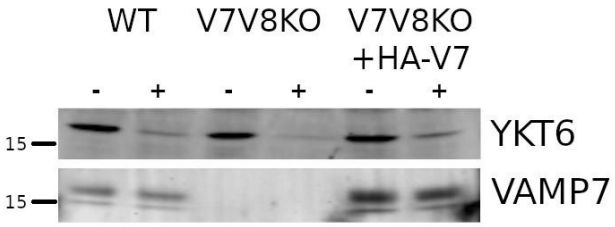

Figure 4.13: The effect of YKT6 depletion on delivery to endolysosomes in VAMP7 and VAMP8 double knockout cells is rescued by VAMP7

(A) Wild type HeLa cells, VAMP7+VAMP8 double knockout HeLa cells, and VAMP7+VAMP8 double knockout VAMP7-overexpressing HeLa cells were transfected with either non-targetting siRNA, or YKT6-targetting siRNA oligo C. 96 hours post-transfection, cells were pulsed with 2 hours uptake of Dex488 followed by 1 hour chase in dextran-free medium, and incubated with Magic Red™ Cathepsin B for 2 minutes before capturing confocal images which were analysed for colocalisation analysis. Fold change of Mander's (MRB: Dex488) correlation coefficients for colocalisation of pulsed Dex488 and MRB relative to wild type non-targetting siRNA are shown. Error bars represent the mean ± SEM of 3 experiments. P values determined by unpaired t-test. NS = not significant.

+: endogenous protein present

++: stably overexpressed protein present

- : siRNA mediated knockdown of protein

- - : complete knockout of protein

(B) WT, VAMP7+VAMP8 KO, and VAMP7+VAMP8 KO HA-VAMP7-expressing cells transfected with non-targetting (-) or YKT6-targetting (+) siRNA were analysed by Western blot. Cell lysates were run on a 10% TruPAGE polyacrylamide SDS gel, and transferred to PVDF membrane before immunoblotting with antibodies to YKT6 and β-actin. Bands were quantified using Image Studio, and normalised to β-actin band signal.

(C) The same cell lysates were ran as in (B) and immunoblotted with antibodies to YKT6 and VAMP7 to show the levels of VAMP7 expression of each cell line.

4.3 Discussion

While it has been reported that concurrent depletion of VAMP7 and VAMP8 in cells may have a significant impact on late endosome-lysosome fusion, the data presented here show that not necessarily to be the case. Consistent with published data in cultured cells and knockout mice, this study showed little effect of VAMP7 or VAMP8 individual knockouts on late endosome-lysosome fusion. VAMP7 knockout cells did however show a very subtle increase in diameter of LAMP1-positive puncta, suggestive of slight lysosomal swelling, or some extent of clustered/tethered LAMP1-positive membrane structures. Simultaneous depletion of VAMP7 and VAMP8 did not appear to impede endosomal trafficking, as there was no major defects in distribution or morphology of intracellular compartments, and delivery of endocytosed cargo to endolysosomes remained intact. This challenges the role of VAMP8 as a sole compensatory R-SNARE after loss of VAMP7, and contrasts with the reported block of lysosomal delivery when cells are depleted of VAMP7 and VAMP8. These different outcomes may be a product of the timeframe of SNARE depletion, with knockout cell lines having a longer time to adapt and redistribute SNAREs compared to the short duration of siRNA-mediated knockdown. The greater effect of YKT6 depletion on late endosome-lysosome fusion in double knockout cells compared to wild type cells, and the reversal of this effect after VAMP7 rescue suggests that YKT6 is compensating for the loss of VAMP7. This is in line with the recent study showing Ykt6 to localise to lysosomes and compete with VAMP7 to join a trans-SNARE complex between autophagosomes and lysosomes in drosophila (Takáts *et al.*, 2018). Further investigation of the contribution of YKT6 to the SNARE-mediated fusion of late endosomes and lysosomes should address whether expression of siRNA-resistant YKT6 rescues the knockdown effect, however YKT6 expression is complicated by the mostly cytoplasmic localisation after overexpression (Gordon *et al.*, 2017). Indeed, the post-Golgi role of YKT6 reported by Gordon *et al*. (2017) further urges caution when interpreting results of YKT6-knockdown due to its widespread functions in the cell.

The extensively tethered late endocytic organelles observed in VAMP7+VAMP8 double knockout cells by EM may be a result of slowed or frustrated fusion between these organelles, such as occurs after knockdown of CHMP6 (Parkinson *et al.*, 2015). The unimpeded ability to deliver dextran to endolysosomes in

VAMP7+VAMP8 knockout cells suggests that there is some degree of late endosome-lysosome fusion still occurring despite the frustrated fusion observed in some of these organelles. While the identity of the small vesicles that accumulate and tether around the periphery of endolysosomes in VAMP7+VAMP8 double knockout cells remains unknown, a subpopulation of them match the reported sizes of LAMP-carriers (Pols *et al.*, 2013b). The apparent lack of ability of these vesicles to fuse with organelles of the late endocytic pathway, as indicated by the clustering and tethering, is in line with the requirement of VAMP7 for LAMP-carrier fusion with lysosomes. The questions of whether the extensive inter-organellar tethering is comprised of HOPS complexes could be addressed with further immuno-EM study of these cells, however the lack of EM-compatible antibodies to HOPS subunits would necessitate genetically-encoded tagging. To this end, I am in the process of generating CRISPR-Cas9-mediated knock-in of a 2xHA tag to the endogenous locus of VPS18, to increase the ability of antibody-based detection of HOPS complex in the tethers, while leaving the protein expression at endogenous levels. Immuno-EM may also be employed to detect whether the vesicles clustered around late endocytic organelles are marked by LAMP proteins, however this approach is inhibited by the density of LAMP proteins on such small structures.

Chapter 5 – Developing tools to study the dynamics of V-ATPase during lysosome reformation from endolysosomes

5.1 Introduction

In the lysosome regeneration cycle proposed in Chapter 3 (Section 3.3, Figure 3.9, (Bright, Davis and Luzio, 2016)), the organelles involved span a wide range of pH values. There is a decrease in pH as endosomes and acid hydrolase-storage lysosomes fuse to form endolysosomes, and conversely there is an increase in pH when lysosomes are reformed from endolysosomes. Luminal acidification is critical for a number of functions of both endosomes and endolysosomes, and is largely controlled by the membrane-embedded V-ATPase complex. Manipulations of the V-ATPase complex represents a major route of regulating organelle acidity by fine-tuning the influx of protons across the membrane, as discussed in Chapter 1 (section 1.10.2). This can occur through incorporation of different subunit isoforms, or on a larger scale, differential recruitment of whole V1 sectors onto membrane-resident Vo sectors. The controlled loss of acidity and increase of pH from ~4.5 to ~7 seen in reforming storage lysosomes is poorly understood. As discussed in Chapter 1, V-ATPases can be negatively regulated by reversible V1 dissociation, and this mechanism has been observed in mammalian cells. To address the mechanism by which the reformed lysosomal lumen is neutralised, we need to test the hypothesis that the reforming storage lysosome employs this mechanism, and that dissociation of the V1 sectors from the V-ATPase complexes occurs on the limiting membrane of the reforming lysosome, thereby inhibiting inward proton pumping while passive proton leakage continues to occur.

In order to study the integrity and dynamics of the V-ATPase complex, I attempted to use commercially available antibodies (Table 5.1) to assess V-ATPase subunit localisation by immunofluorescence, but found that none of those tried gave good signals. This has also been the experience of others. Generating stable cell lines expressing fluorescently tagged V-ATPase subunits at close to endogenous levels seemed a more promising approach, despite a previous report that in slime mould, co-expressing GFP-tagged V1 and RFP-tagged Vo was impossible (Carnell *et al.*, 2011). In NRK cells, the co-expression of differently tagged subunits of the V1 and Vo sectors should allow the use of the sucrosome/invertase system described in Chapter 3 (section 3.1) to investigate the dynamics of the V-ATPase sectors (Figure 5.1) during lysosome reformation, using live cell fluorescence microscopy. The applications of this method are, however, limited by the ease with which cells can

form sucrosomes, and the complications associated with upregulation of TFEB translocation to the nucleus. In the experiments described below, I aimed to tag a V1 subunit that did not constitute part of the rotor, and to tag the cytosolic side of the Vo sector. The V1G1 stator subunit was selected as an appropriate reporter for the V1 sector due to its peripheral and static position outside of the rotor, reducing the likelihood that a fluorescent protein tag impedes function. V1G1 is also important in V-ATPase regulation via binding to the Rab7 effector RILP (De Luca *et al.*, 2014). In this context it is interesting to note that whereas acidic juxtanuclear lysosomes/endolysosomes are Rab 7-positive, less acidic and more peripheral lysosomes are Rab7-negative (Chapter 3, section 3.2.2, (Johnson *et al.*, 2016). The Voa3 subunit isoform was selected for tagging the Vo sector as both termini of the a-subunit are thought to be cytosolic (Kartner *et al.*, 2013), allowing the tag to avoid the degradation or quenching effects of the acidic lysosomal lumen. Additionally, the a3 isoform is reported to be more endolysosomal/lysosomal in localisation than a1, a2, or a4 (Toyomura *et al.*, 2003) and it has in the past been successfully tagged with fluorescent proteins on its C-terminus in cultured cells (Bhargava *et al.*, 2012) and in whole mice (Sun-Wada *et al.*, 2009).

Table 5.1 V-ATPase Subunit Antibodies assessed for Immunofluorescence

Antigen	Antibody I.D.	Host species	Source	Dilution
Human V1A	17115-1-AP	Rabbit polyclonal	Proteintech	1:100
Human V1D	D-4	Mouse monoclonal	Santa Cruz Biotechnology	1:100
Human V1G1	16143-1-AP	Rabbit polyclonal	Proteintech	1:100
Human V1G1	D-5	Mouse monoclonal	Santa Cruz Biotechnology	1:100
Human Voa1	E-8	Mouse monoclonal	Santa Cruz Biotechnology	1:100

Figure 5.1

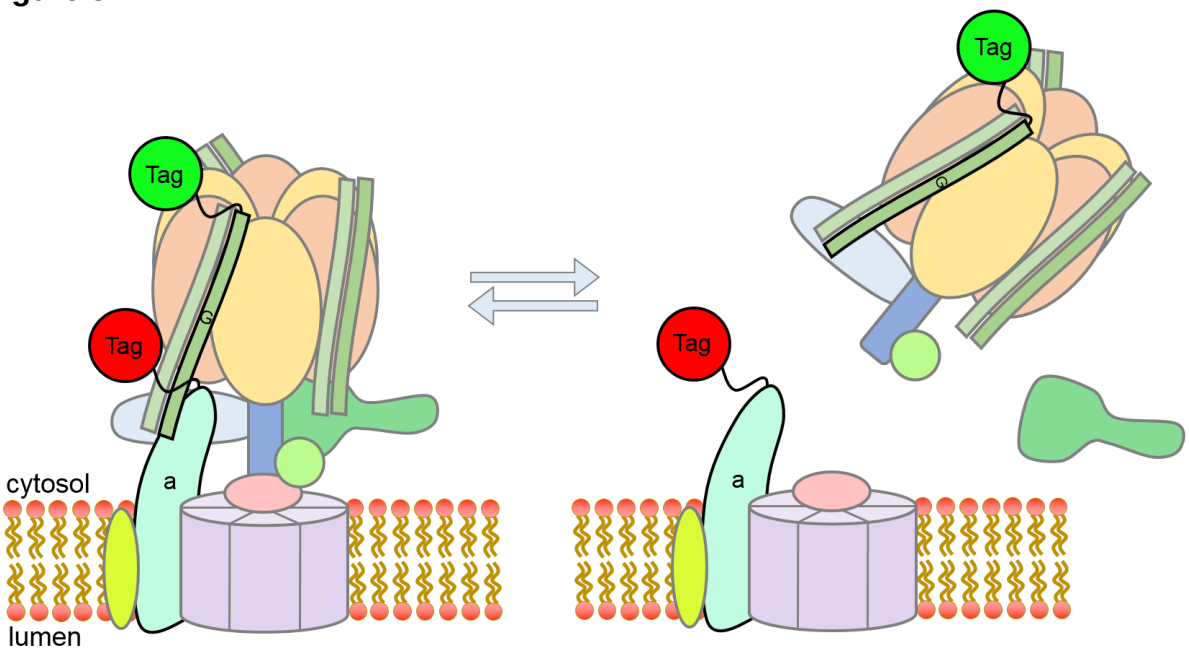

Figure 5.1: Schematic of the V-ATPase regulation by sector dissociation

Diagram illustrating the separation of the V1 and V0 sectors of V-ATPase complexes as a method of regulating V-ATPase function. Where the V-ATPase is fully assembled, the fluorescently tagged V1G1 and V0a3 subunits should remain in close proximity and their respective fluorophores should colocalise. Under conditions where the V1 sector dissociates from the V0 sector, the fluorescently tagged V1G1 sector may hypothetically diffuse away, resulting in reduced proximity and colocalisation with tagged V0a3.

5.2 Results

5.2.1 Stably over-expressed GFP-tagged V1G1 distributes to acidic, cathepsin-active intracellular compartments and the cytosol

In order to trace V1 sectors of the V-ATPase complex in both live and fixed cells, clonal cell lines overexpressing V1G1-GFP were generated in both HeLa and NRK cells. In both cell lines, V1G1-GFP marked puncta which colocalised with LysoTracker (Figure 5.2A, Figure 5.2B, top rows) as well as Magic Red™ (Figure 5.2A, Figure 5.2B, bottom rows). V1G1-GFP also displayed a dispersed cytosolic distribution in both cell types which matches the largely cytosolic distribution of the wild type subunit. Due to the high cytosolic signal of the V1G1-GFP, accurate colocalisation analyses could not be performed.

The degree of overexpression of GFP-tagged V1G1 relative to endogenous V1G1 in the clonal NRK cell line was analysed by Western blot (Figure 5.2C). V1G1-GFP was identified by the band shift of ~25kDa, and was found to be 3.3-fold more abundant in whole cell lysate than endogenous V1G1.

5.2.2 Stably overexpressed V1G1-GFP localises to the cytosol and limiting membrane of sucrosomes in NRK cells

To test further how stably overexpressed V1G1- GFP distributes, and to determine its suitability as a marker of the V1 sector after manipulating the endolysosomal system, clonal NRK V1G1-GFP expressing cells were incubated with sucrose to form sucrosomes, depleting the cells of terminal/storage lysosomes in the process. After sucrosome formation, V1G1-GFP was clearly seen to mark the limiting membrane of the swollen endolysosomes, while retaining a cytosolic pool (Figure 5.3). This indicates that the V1G1-GFP expressed in these cells is successfully labelling the cytosolic facing endolysosomal membrane, and is capable of tracing V-ATPase complexes on endolysosomes and swollen sucrosomes.

Figure 5.2

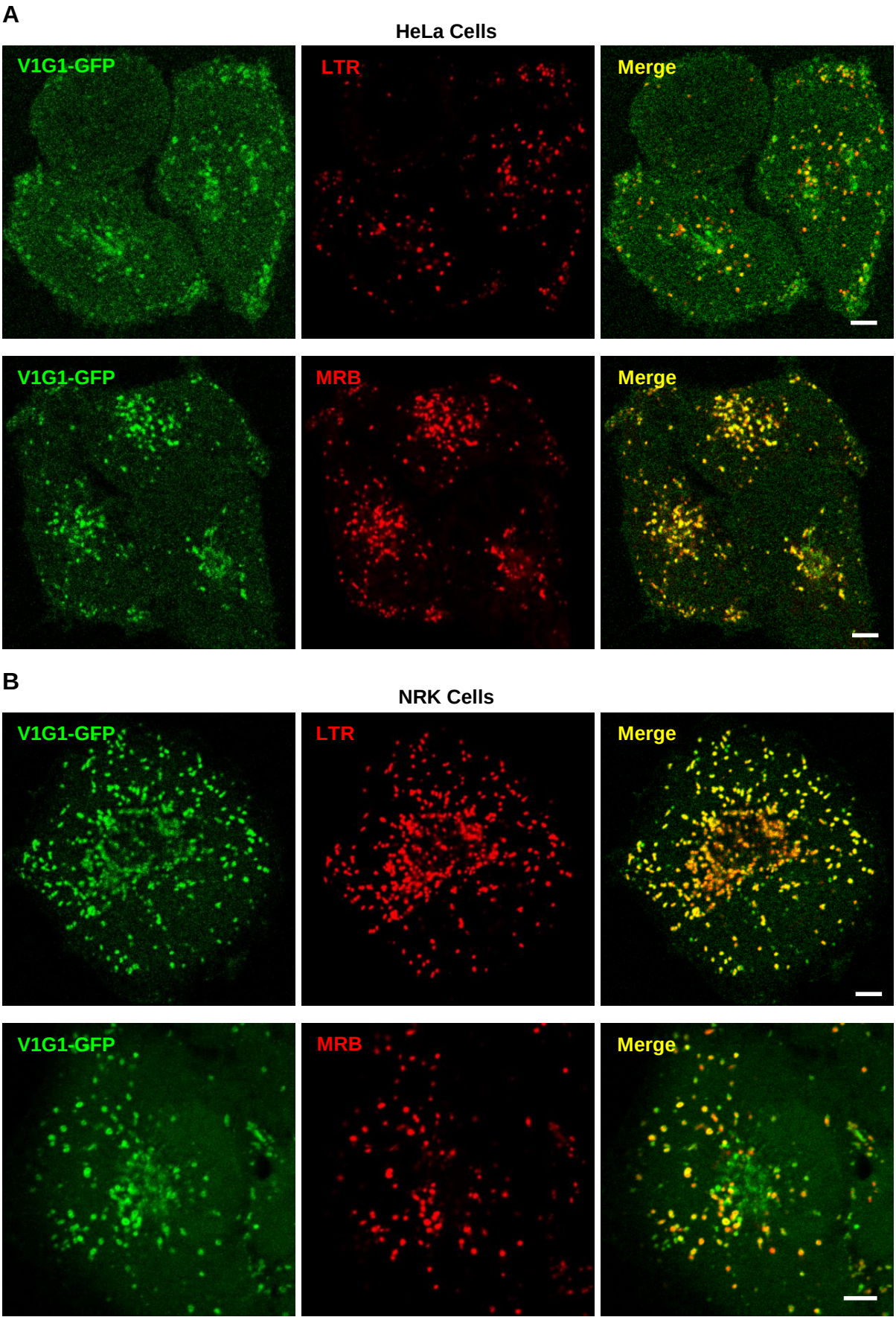
A
HeLa Cells
V1G1-GFP
LTR
Merge
V1G1-GFP
MRB
Merge
B
NRK Cells
V1G1-GFP
LTR
Merge
V1G1-GFP
MRB
Merge

C

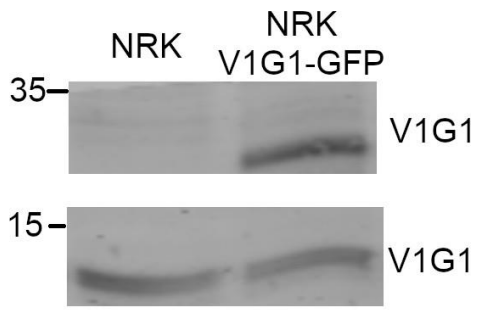

Figure 5.2: V1G1-GFP colocalises with LysoTracker and Magic Red™

(A) Confocal fluorescence microscopy images of live clonal HeLa cells stably expressing V1G1-GFP, after 5 min incubation with LysoTracker Red DND-99 (top row), or after 2 min incubation with MRB (bottom row).

(B) Confocal fluorescence microscopy images of live clonal NRK cells stably expressing V1G1-GFP, after 5 min incubation with LysoTracker Red DND-99 (top row), or after 2 min incubation with MRB (bottom row).

All scale bars represent 5µm.

(C) WT and V1G1-GFP-expressing clonal NRK cells were lysed and analysed by western blot to assess V1G1 overexpression. Cell lysates were run on a 15% polyacrylamide SDS gel, and transferred to PVDF membrane before immunoblotting with an antibody to V1G1. V1G1-GFP overexpression levels were calculated by measuring the ratio between the ~15kDa anti-V1G1 band (present in both wild type and V1G1-GFP cells) and the ~25kDa-shifted band (present exclusively in V1G1-GFP cells, in line with the size of the GFP tag). Blot fluorescence was scanned using an Odyssey CLx and band intensities were measured with background correction using Image Studio™.

Figure 5.3

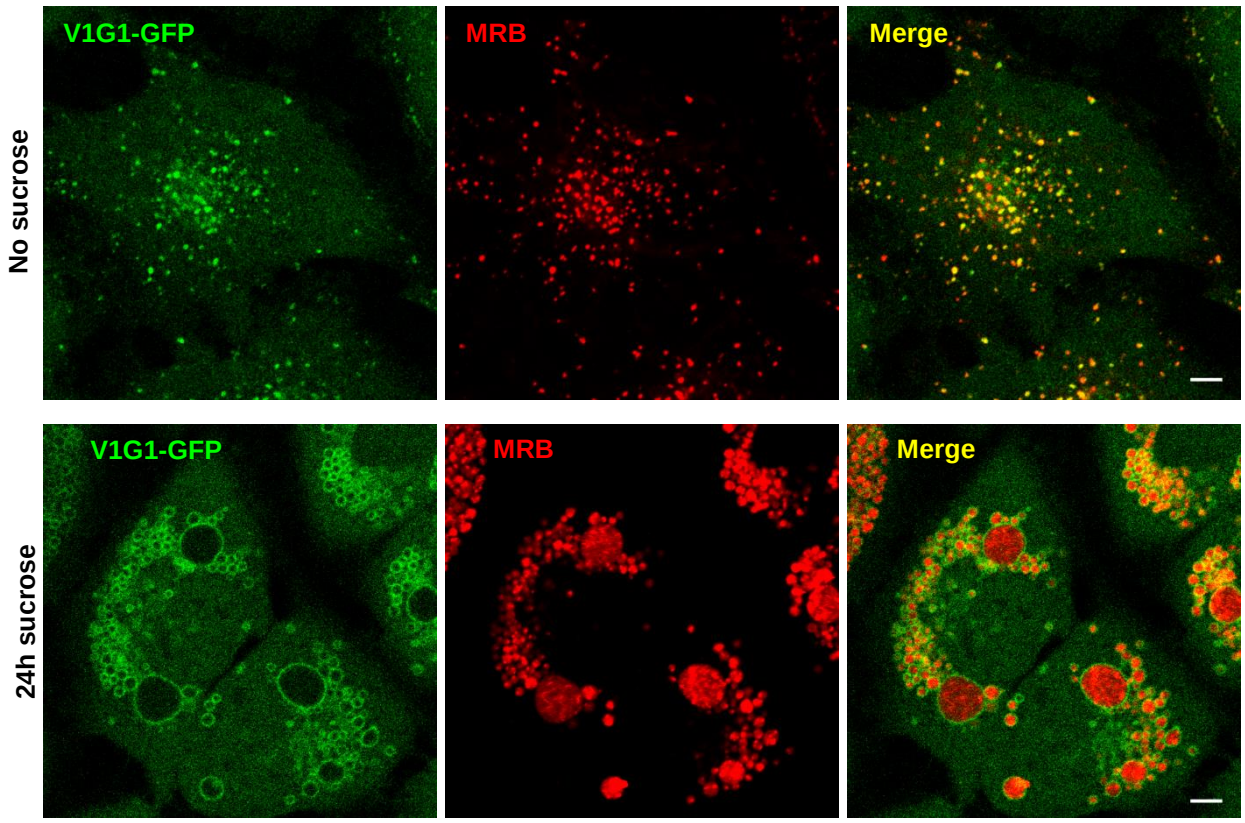

Figure 5.3: V1G1-GFP localisation in NRK cell sucrosomes

Confocal fluorescence microscopy images of clonal NRK cells stably expressing V1G1-GFP which were incubated with or without 30mM sucrose for 24 hr. The cells were then incubated with MRB for 2 min prior to imaging to mark cathepsin-active organelles. Scale bars represent 5µm.

5.2.3 The localisation of V1G1-GFP compared to lgp120 (rat LAMP1) and Voa3

If the hypothesis that V1/Vo sector dissociation occurs during lysosome reformation is correct, it is predicted that there should be a population of likely more peripheral lysosomes lacking V1 sector relative to more juxtanuclear, acidic endolysosomes. To test this, I first compared the overexpressed V1G1-GFP distribution against immunofluorescently-labelled endogenous lgp120 (rat LAMP1) in methanol-fixed clonal NRK V1G1-GFP cells (Figure 5.4). Lgp120 is an abundant lysosomal membrane glycoprotein, representing a suitable marker for all endolysosomes/lysosomes. In methanol-fixed cells, overexpressed V1G1-GFP shows a good degree of overlap with lgp120 nearer the perinuclear region of cells, however towards the cell periphery there appear to be more lgp120-positive (red) puncta with less V1G1-GFP (green) present (Figure 5.4A, arrowheads). The monoclonal antibody used to detect lgp120 in these experiments only gives a good signal in methanol-fixed cells. In cells fixed in this way, a 'background' of V1G1-GFP in the nuclei was often observed (Figure 5.4A), unlike the situation in live (Figures 5.2A, 5.3) or paraformaldehyde-fixed (Figure 5.4B) cells.

To address whether these peripheral lysosomes represent organelles with fewer V-ATPase complexes, or complexes with dissociated V1 sectors, clonal NRK V1G1-GFP cells were immunostained for Voa3 using an antibody raised against a mouse/rat Voa3 peptide (a gift from Dr. T. Jentsch, Berlin, see Chapter 2). In the PFA-fixed, saponin-permeabilised cells, Voa3 staining showed a similar distribution to that of lgp120, colocalising with V1G1 more centrally in the cell, but also marking peripheral organelles which had less or no V1G1-GFP present (Figure 5.4B). This provides preliminary evidence that there may exist a population of lysosomes with limiting membranes containing Vo sectors of the V-ATPase, but lacking the V1 sector.

Figure 5.4

A

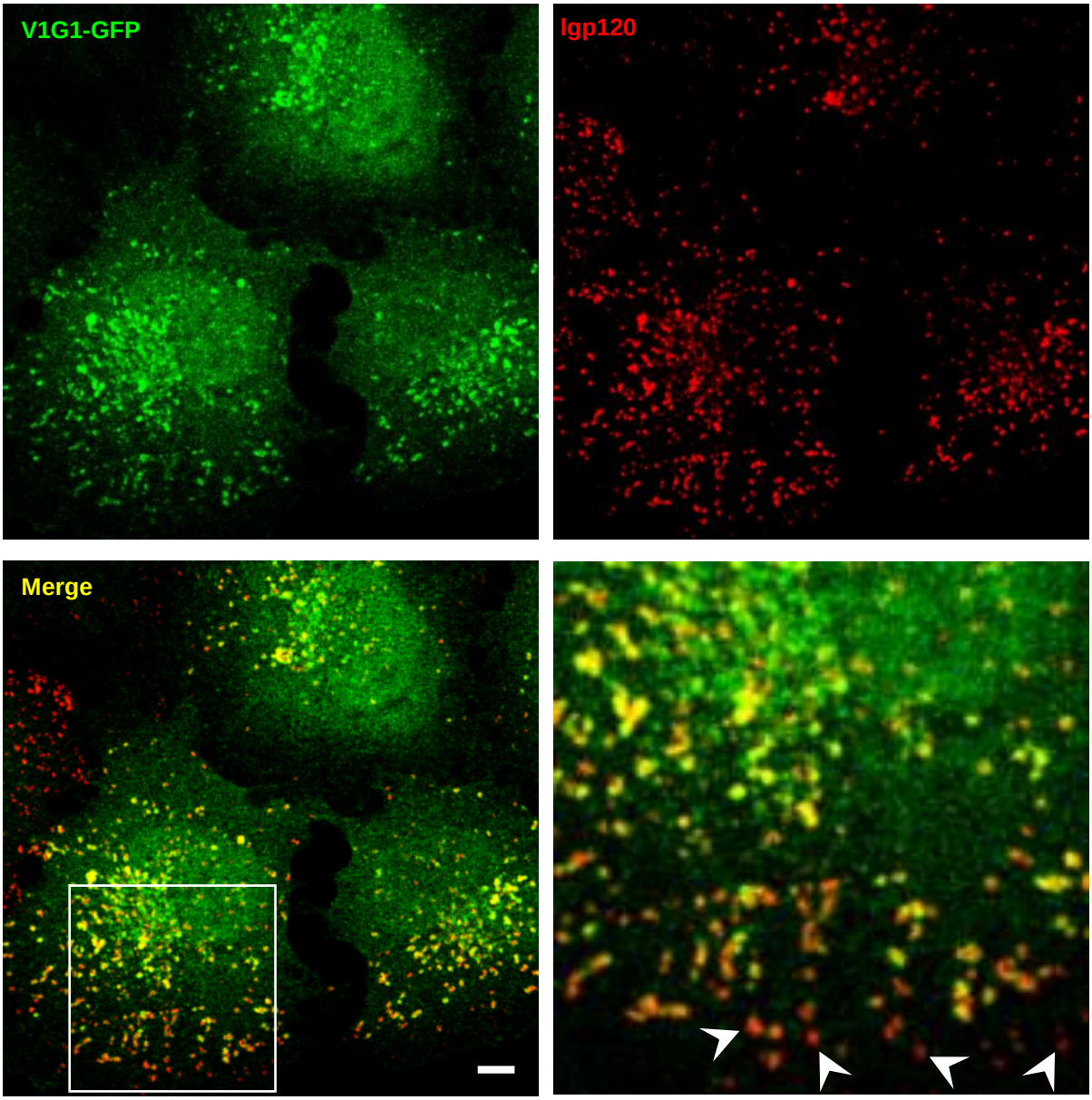

B

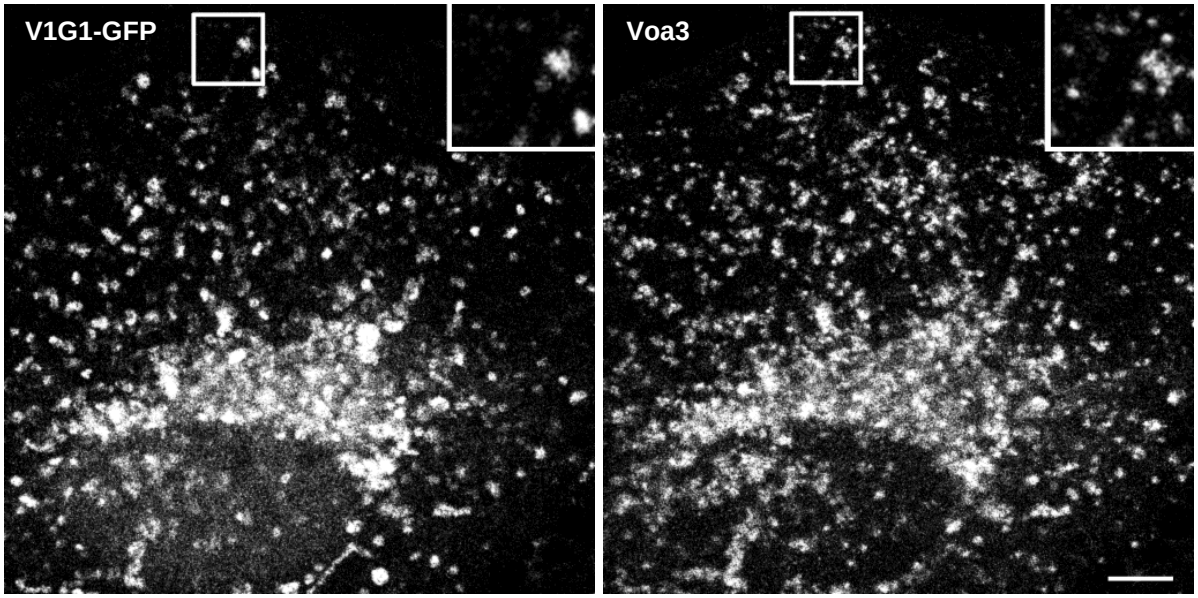

Figure 5.4: The localisation of V1G1-GFP compared to lgp120 and Voa3

(A) Anti-lgp120 immunoreactivity in methanol-fixed clonal NRK V1G1-GFP cells was used to mark all endolysosomes/lysosomes. Stably overexpressed V1G1 was used to mark V-ATPase complexes with associated V1 sectors. The boxed region in the bottom-left panel is enlarged and shown in the bottom-right panel.

(B) Anti-Voa3 immunoreactivity in PFA-fixed, saponin-permeabilised clonal NRK V1G1-GFP cells was used to mark Vo sectors of the V-ATPase complex. Stably overexpressed V1G1 was used to mark V-ATPase complexes with associated V1 sectors. Part of a single representative cell is shown. The boxed regions are enlarged and inlaid in the corner of each panel.

Scale bars represent 5µm**.**

5.2.4 Voa3-GFP localisation in NRK cell sucrosomes, and the localisation of V1G1-GFP and Voa3-GFP during lysosome reformation

Due to the very limited availability of an anti-Voa3 antibody which could be used for immunofluorescence, and to allow for future live-cell experiments, a stable NRK cell line expressing Voa3-GFP was generated to track the dynamics of the Vo sector of the V-ATPase complex in cells. Stably overexpressed Voa3-GFP in NRK cells almost exclusively localised to puncta, mostly those marked by Magic Red™ in the juxtanuclear region, while also localising to more peripheral smaller puncta which are less marked by Magic Red™, indicative of terminal/storage lysosomes (Figure 5.5A, arrowhead). These cells were also assessed after incubation with sucrose and subsequent sucrosome formation. Like V1G1-GFP, stably overexpressed Voa3-GFP localised to the limiting membranes of sucrosomes, suggesting that Voa3-GFP was successfully marking V-ATPase Vo sectors on the cytosolic face of the lysosomal membrane after sucrosome formation and terminal/storage lysosome depletion (Figure 5.5B).

The results from the cell lines expressing tagged V1G1 and Voa3 established that these subunits were successfully localising to endolysosome and sucrosome membranes. To address whether either or both of these V-ATPase subunits are also trafficked onto newly formed proto-lysosomal tubules, cells which had formed sucrosomes were allowed to uptake invertase, inducing tubulation of the sucrosomes. Both V1G1-GFP and Voa3-GFP could be seen along the length of tubules extending out of sucrosomes after invertase uptake (Figure 5.5C, arrowheads), suggesting that V1 and Vo sectors are associated together, and that whole V-ATPase complexes are sorted onto the forming protolysosomal tubule membrane.

Figure 5.5

A

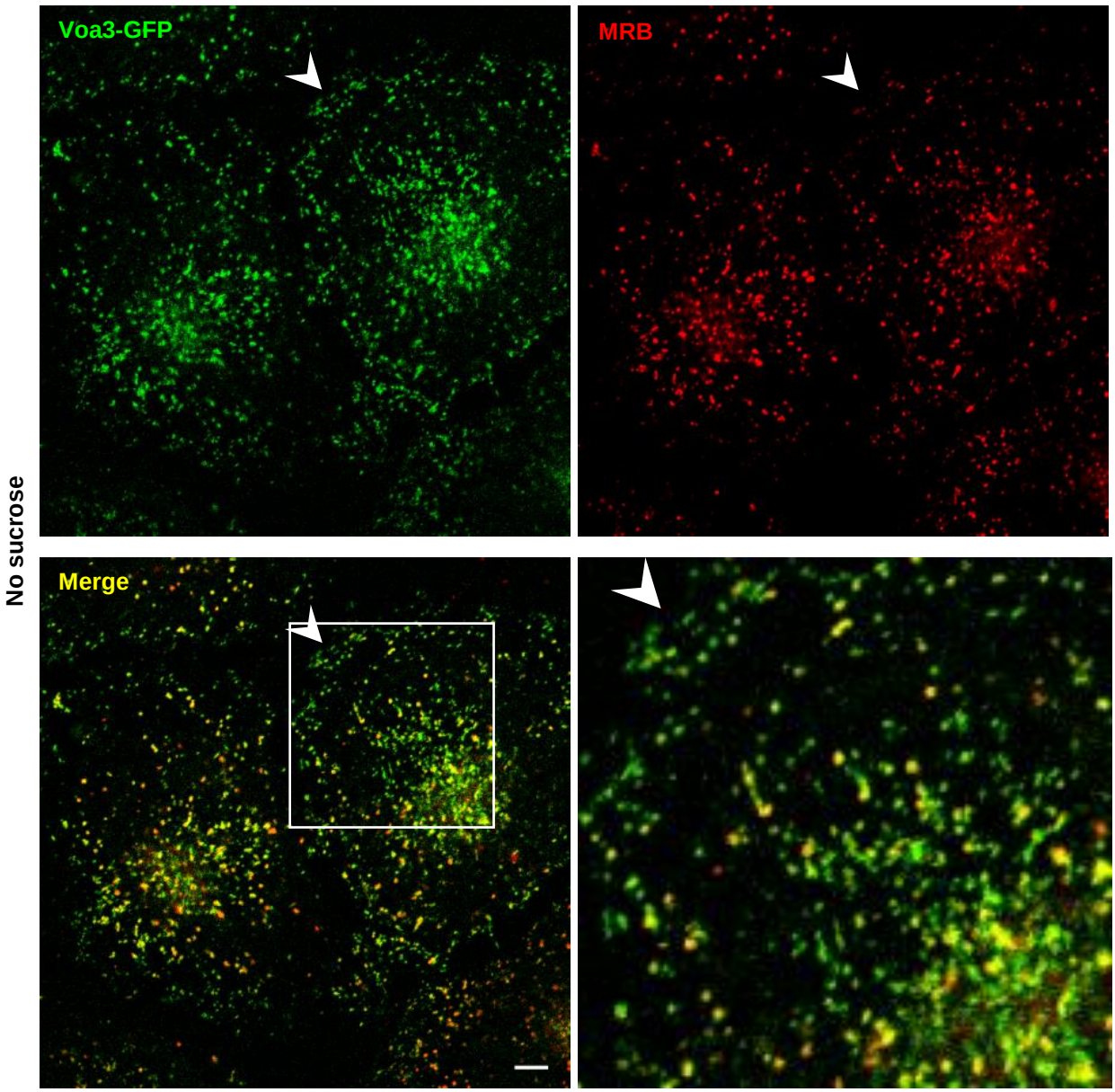

B

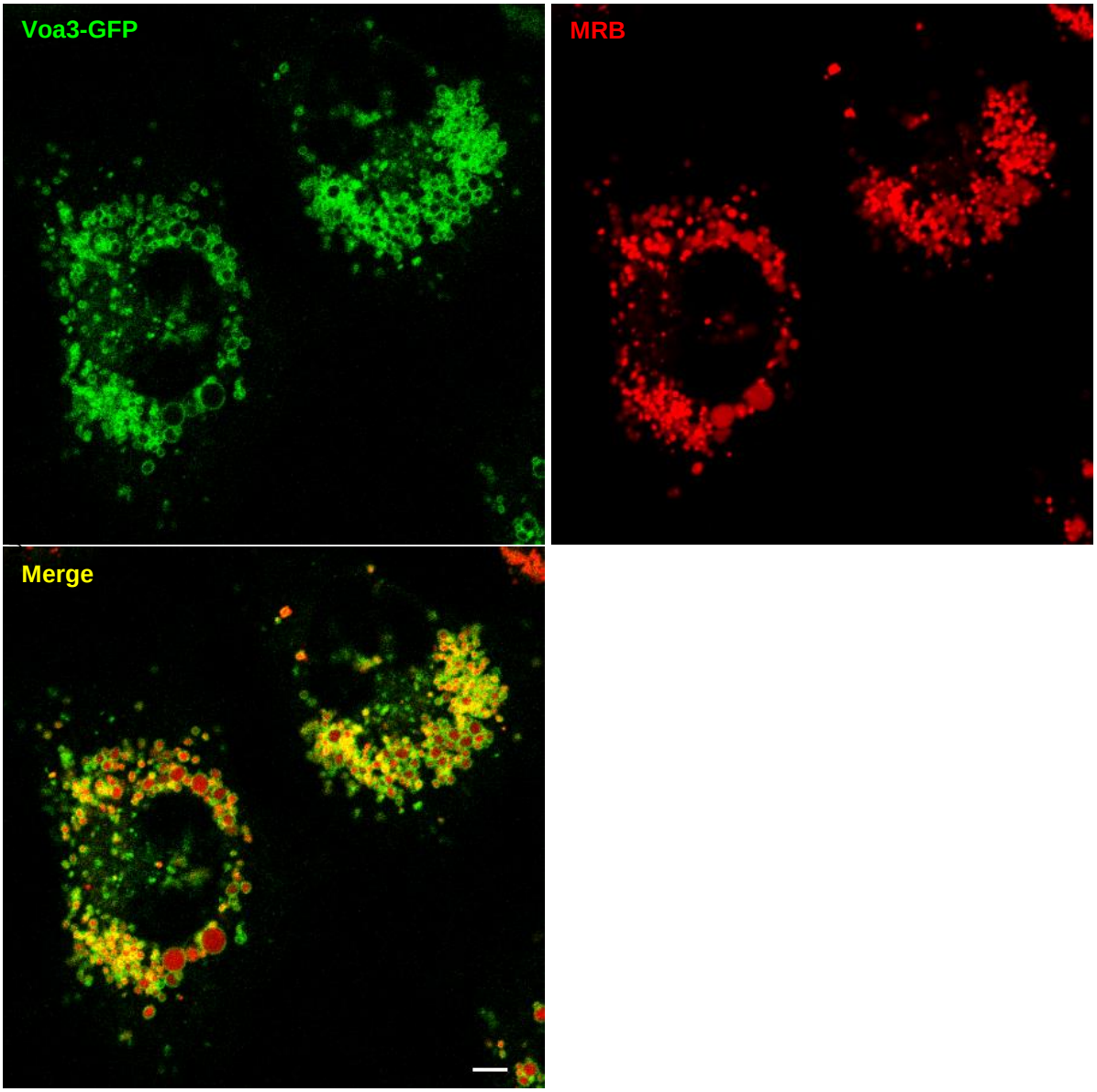

C

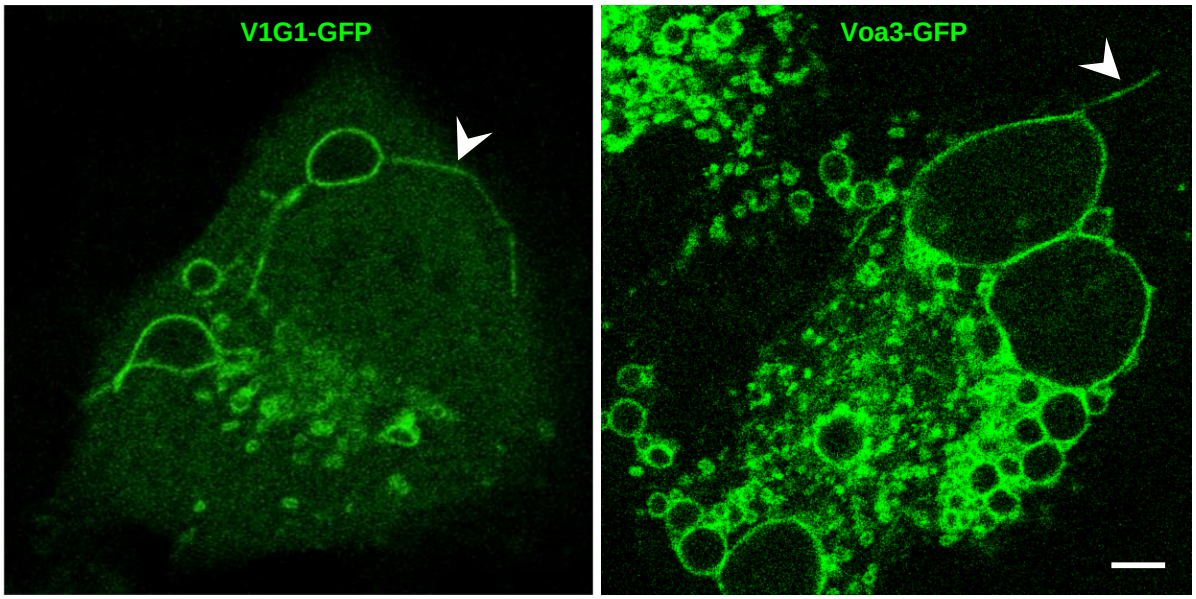

24h sucrose
+1h invertase

Figure 5.5: Voa3-GFP localisation in NRK cell sucrosomes, and the localisation of V1G1-GFP and Voa3-GFP during lysosome reformation

(A) Confocal fluorescence microscopy images of live clonal NRK cells stably expressing Voa3-GFP, after 2 min incubation with MRB.

(B) Confocal fluorescence microscopy images of live clonal NRK cells stably expressing Voa3-GFP which were incubated with or without 30mM sucrose for 24 hours. The cells were then incubated with MRB for 2 min prior to imaging to mark cathepsin-active organelles.

(C) Confocal fluorescence microscopy images of live clonal NRK cells expressing V1G1-GFP or Voa3-GFP which were incubated with 30mM sucrose for 24 hours before incubating with 0.5mg/ml invertase for 1 hour before imaging.

Scale bars represent 5µm.

5.2.5 Localisation of Coexpressed Fluorescently-Tagged V1G1 and Voa3 in NRK Cells With or Without Sucrosomes

Given that fluorescently tagged V1G1 and Voa3 have individually been shown to be traceable on endolysosomes, and on sucrosomes through to protolysosomal tubules, the next step to study their dynamics in relation to each other is to generate a cell expressing both subunits with spectrally separated fluorescent tags to allow simultaneous imaging of both sectors in real time. To this end, a clonal line of NRK cells expressing V1G1-GFP was further modified to express Voa3-TagRFP, allowing both subunits to be visualised simultaneously in the same cells. The co-expressed Voa3-TagRFP showed a very similar localisation to that seen with Voa3-GFP, in untreated cells (Figure 5.6A, top row). After sucrosome formation, however, Voa3-TagRFP could be seen on the sucrosome limiting membrane, but a significant proportion of the TagRFP signal was also seen in the sucrosome lumen (Figure 5.6A, bottom row). NRK cells stably overexpressing V1G1-TagRFP also displayed TagRFP fluorescence in the sucrosome lumen (Figure 5.6B). The degree of fluorescence in the lumen inhibits colocalisation analysis from providing meaningful data regarding V1-Vo association on the limiting membranes of endolysosomes/lysosomes.

Figure 5.6

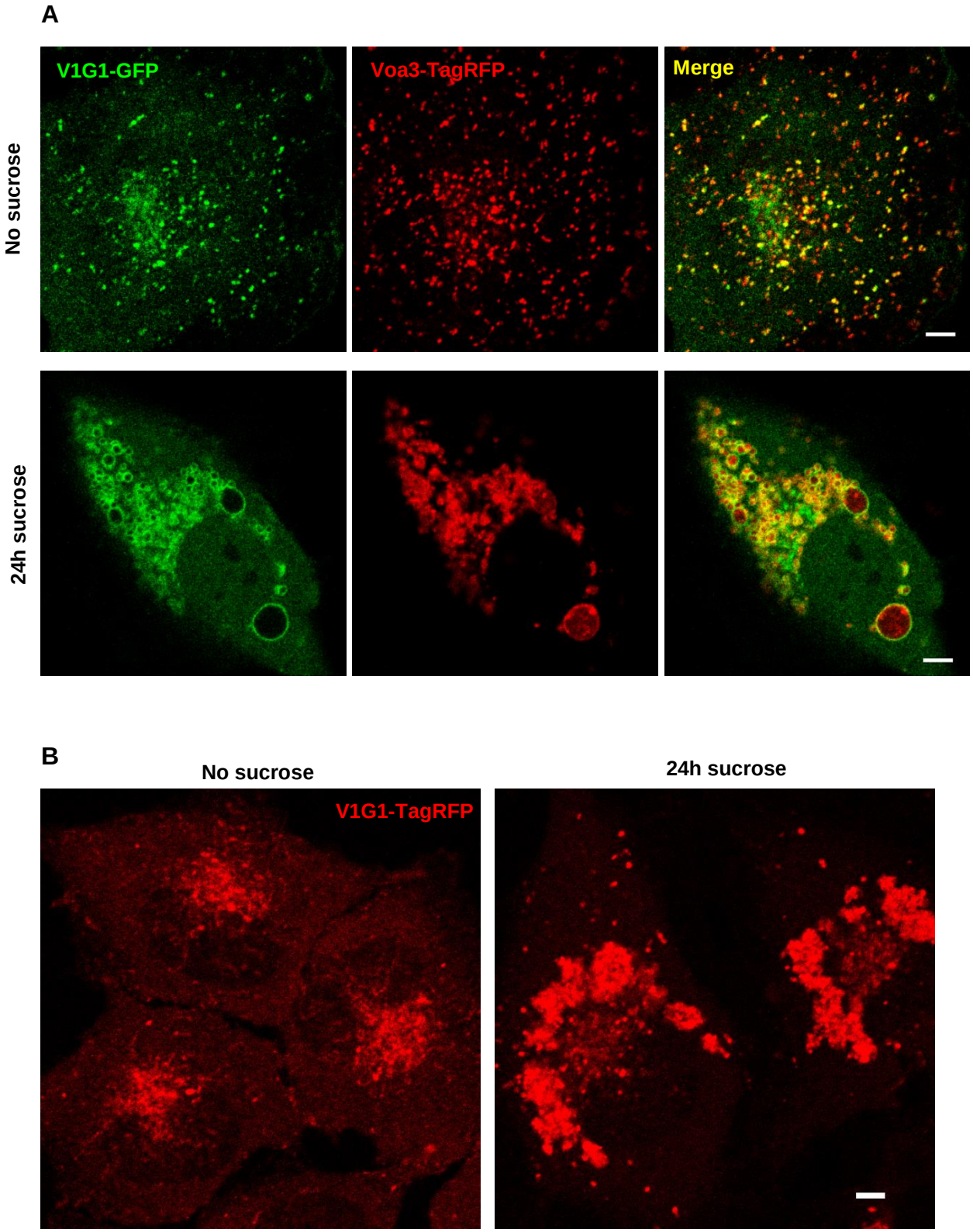
A
V1G1-GFP
Voa3-TagRFP
Merge
No sucrose
24h sucrose
B
No sucrose
24h sucrose
V1G1-TagRFP

Figure 5.6: Localisation of Coexpressed V1G1-GFP and Voa3-TagRFP in NRK Cells With or Without Sucrosomes

(A) Confocal fluorescence microscopy images of representative single live clonal NRK cells stably co-expressing V1G1-GFP and Voa3-TagRFP which were incubated with (bottom row) or without (top row) 30mM sucrose for 24 hours.

(B) Confocal fluorescence microscopy images of live clonal NRK cells stably co-expressing V1G1-TagRFP which were incubated with or without 30mM sucrose for 24 hours.

Scale bars represent 5µm.

5.2.6 Localisation of V1G1 Tagged with Acid Sensitive-mOrange2 M163K Fluorescent Tag, and Voa3-GFP in NRK Cells With or Without Sucrosomes

Because the difference in localisation between GFP- and TagRFP-tagged subunits was independent of which subunit the tag was associated with, and occurred even in cells only overexpressing a single tagged subunit, it is likely that differences between the fluorescent proteins themselves are responsible for the discrepancy. Additionally, the aberrant TagRFP fluorescence occurs in the lumen of sucrosomes which are swollen endolysosomes, and hence acidic (Bright, Davis and Luzio, 2016). GFP has a pK_a (pH at which fluorescence is 50% of maximum) value of ~5.6 (Patterson *et al.*, 1997) to ~5.8 (Haupts *et al.*, 1998) and as such its fluorescence would be quenched if present in the acidic sucrosome lumen. This is not the case for TagRFP, which has a pK_a of ~3.8 (Merzlyak *et al.*, 2007), so in its place, a more acid sensitive mutant (M163K) of mOrange2, with a reported pK_a ~7.4 (Shaner *et al.*, 2008) was used to tag V1G1. When expressed in NRK cells, V1G1-mOrange2 M163K showed a very similar localisation to V1G1-GFP and V1G1-TagRFP, and extensively colocalised with the stably co-expressed Voa3-GFP (Figure 5.7A, top row). However, after sucrosome formation, V1G1-mOrange2 M163K also gave significant signal in the lumens of sucrosomes. To compare the acid sensitivity of the two fluorophores expressed in these cells under imaging conditions, cells expressing V1G1-mOrange2 M163K and Voa3-GFP were incubated with sucrose and imaged before and after clamping at pH5 with monensin and nigericin-containin pH5-buffered medium. After acidifying the cytosol, Voa3-GFP which previously marked the cytosolic face of endolysosomal/lysosomal membranes was nearly completely quenched, however V1G1-mOrange2 M163K fluorescence was relatively unaffected (Figure 5.7B) which was unexpected, given its reported pK_a ~7.4.

Figure 5.7

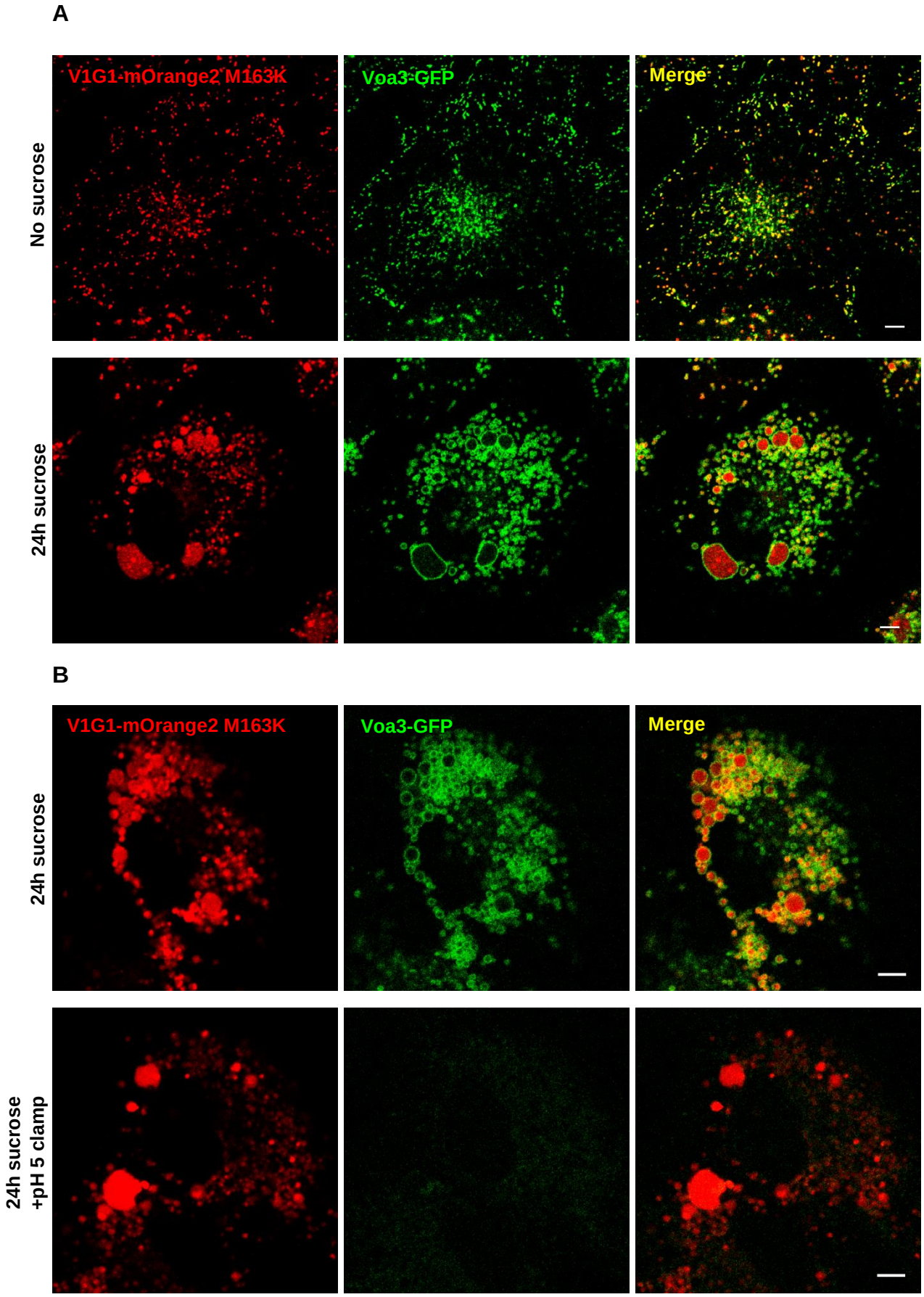
A
V1G1-mOrange2 M163K
Voa3-GFP
Merge
No sucrose
24h sucrose
B
V1G1-mOrange2 M163K
Voa3-GFP
Merge
24h sucrose
24h sucrose +pH 5 clamp

Figure 5.7: Localisation of Coexpressed V1G1-mOrange2 M163K and Voa3-GFP in NRK Cells With or Without Sucrosomes

(A) Confocal fluorescence microscopy images of representative single live clonal NRK cells stably co-expressing V1G1-mOrange2 M163K and Voa3-GFP which were incubated with (bottom row) or without (top row) 30mM sucrose for 24 hours.

(B) Confocal fluorescence microscopy images of representative single live clonal NRK cells stably co-expressing V1G1-mOrange2 M163K and Voa3-GFP which were incubated with 30mM sucrose for 24 hours, followed by imaging before (top row) or after (bottom row) 5 minutes incubation with pH5 clamping solution.

Scale bars represent 5µm.

5.3 Discussion

The dynamics and regulation of the V-ATPase, in particular the reversible dissociation of the V1 and Vo sectors during lysosome reformation in mammalian cells, is poorly understood. In this study, tools to independently and simultaneously visualise V1 and Vo sector subunits in real time were developed. Cells stably expressing fluorescently tagged candidate subunits V1G1 and Voa3 were generated to act as reporters of dynamics of the V1 and Vo sectors respectively, without impeding the function of the assembled V-ATPase complex. Both tagged V1G1 and Voa3 subunits localised to the limiting membranes of acidic and cathepsin B-active compartments, indicative of incorporation into, and normal function of, V-ATPase complexes. Both subunits, when tagged with GFP, decorated the limiting membrane of endolysosomes before and after the recruitment of terminal lysosomes to form sucrosomes, and both marked protolysosomal tubules extending from sucrosomes after invertase uptake. These tagged subunits, while expressed at relatively low levels (~3.3 fold endogenous V1G1) allowed the localisation of V1 and Vo sectors to be studied throughout manipulations of the endolysosomal-lysosomal equilibrium. Immunofluorescence experiments also generated preliminary evidence that V1G1 may localise to more peripheral lysosomes to a lesser degree when compared to lgp120 (rat LAMP1) or Voa3. Given that V1G1-GFP entered the tubules emanating from sucrosomes after invertase uptake, the preliminary data suggest that dissociation of the V1 and Vo sectors of the V-ATPase occurs at a later stage in the reformation and maturation of lysosomes. Co-expression of V1G1 and Voa3 with spectrally separable fluorescent tags revealed TagRFP- and mOrange2 M163K-tagged subunits to exhibit fluorescence in the lumens of sucrosomes, which has so far inhibited the use of sensitive colocalisation experiments to estimate the degree of V1-Vo association.

Results from cells overexpressing tagged V-ATPase subunits need to be interpreted with caution, even with the relatively low overexpression achieved in this study with retroviral methods of stable cell line generation. Overexpression of individual V-ATPase subunits can have measurable effects on cellular function, such as overexpression of V1C1 in fruit fly cells increasing endolysosomal acidity and affecting the levels of other V-ATPase subunits (Petzoldt *et al.*, 2013) or overexpression of VoB increasing V-ATPase activity and increasing mTORC1

activation (Meo-Evoli *et al.*, 2015). In addition, overexpression of V1G1 itself was shown to inhibit maturation of cathepsin D (De Luca *et al.*, 2014). With regards to expression levels, perhaps a better method to produce cells expressing fluorescently tagged V-ATPase subunits would be CRISPR-Cas9-mediated knock-in. Recently, a CRISPR-Cas9-mediated, homology-independent, PCR-product integration approach has been developed by Paul Manna (personal communication) in Margaret Robinson's laboratory and provides a fast and cloning-free strategy for genomic editing of mammalian cells. Using this method, I am currently generating cells with an Emerald-GFP tag knocked in to the C-terminus of V1G1 to achieve expression of the tagged protein at endogenous levels, under the control of the endogenous promoter. Alongside the advantages that come with studying proteins at endogenous levels, there are potential drawbacks such as microscopy applications being limited because the fluorescence is produced at endogenous tagged-protein quantities, particularly in monoallelic knock-ins.

The localisation of the overexpressed tagged V-ATPase subunits to intracellular membranes was indicative of their successful incorporation into whole V-ATPase complexes. Additionally, the organelles to which the tagged subunits were recruited are positive for LysoTracker® and Magic Red™ which shows that the endolysosomes they marked were successfully acidifying and catalytically active. Assuming incorporation into V-ATPase complexes reflects the approximate 3:1 ratio of abundance between tagged and endogenous V1G1, this suggests tagged subunits were able to form functional V-ATPase complexes. Future experiments could employ co-immunoprecipitation to confirm that tagged subunits are associated with other complex components. To address the function of the V-ATPase complexes with tagged subunits, a comparison of whole cell LysoTracker® fluorescence between wild type and these stable cell lines would provide a qualitative measure of any impact on acidification. For a more quantitative study of the effect on V-ATPase function, lysosomal reacidification could be measured using ratiometric fluorescence after the uptake of appropriate fluorescent dextrans together with addition and removal of a protonophore (Johnson *et al.*, 2016).

The sucrosome lumenal fluorescence exhibited by the TagRFP- and mOrange2 M163K-tagged subunits was possibly a product of the steady state turnover of V-ATPase components, reflecting unquenched tagged subunits in the process of

lysosomal degradation. In any case, such aberrant fluorescence presents a major obstacle to colocalisation-based studies as the intraluminal fraction of total fluorescence will confound the interpretation of any colocalisation coefficient applied. Given the successful membrane localisation of the GFP-tagged subunits in live cells, and the demonstrable pH-sensitivity of GFP by pH clamping, a spectrally viable second fluorescent tag with a greater pH-sensitivity than mOrange2 M163K should be sought. A particularly good candidate fluorophore is mApple-derived pHuji, which has a higher pK_a value than mOrange M163K, of 7.7, and exhibits a 22-fold change in fluorescence between pH 5.5 and 7.5 (Shen *et al.*, 2014) which approaches the range between cytosolic and endolysosomal pH. The next experiments will involve the generation of NRK Voa3-GFP cells stably expressing V1G1-pHuji and analysing the distribution of pHuji fluorescence after generating sucrosomes. If there is insignificant pHuji in the sucrosome lumen, the degree of colocalisation of Voa3-GFP and V1G1-pHuji can be measured to give an estimation of V1-Vo association after reversibly manipulating the endolysosome-terminal lysosome equilibrium using sucrose and invertase.

Chapter 6 – Lysosome signalling to the cell nucleus and the assessment of lysosomal stress

6.1 Introduction

Over the last decade, there have been a great number of studies on the emerging role of lysosomes in signalling and homeostasis, enacted through the mTORC1-TFEB signalling hub on the lysosomal membrane, as detailed in Chapter 1.12.1. The dynamics of TFEB itself are easily observed, not least because TFEB is amenable to tagging, including with fluorescent proteins, with nuclear translocation reporting its activation (Sardiello *et al.*, 2009; Settembre *et al.*, 2012; Roczniak-Ferguson *et al.*, 2012). However, the machinery and mechanism governing the movement of TFEB is not fully understood. TFEB activation and transfer to the nucleus to activate CLEAR network genes occurs as a response to a number of conditions of lysosomal stress, including starvation (Settembre *et al.*, 2011), lysosomal damage (Jia *et al.*, 2018), and lysosome neutralisation (Roczniak-Ferguson *et al.*, 2012) including that occurring as a result of V-ATPase inhibition (Settembre *et al.*, 2011). Neutralisation of lysosomes can occur by accumulation of cationic amphiphilic drugs (CADs) which freely diffuse across the membranes of lysosomes into the acidic lumen, where their basic amine groups become protonated, simultaneously trapping the CAD in the lysosome, and cumulatively quenching the acid in the lysosome. This lysosomal trapping and neutralising effect is associated with the development of phospholipidosis, an aberrant over-accumulation of phospholipids within lysosomes (Anderson and Borlak, 2006; Shayman and Abe, 2013; Glock *et al.*, 2016), predicted to be caused by inhibition of lysosomal phospholipase A2 (Glukhova *et al.*, 2015). Given that over half of all commercially available drugs contain at least one basic amine group (Goldman *et al.*, 2009), the association of basic amine-containing drugs with phospholipidosis represents a potential obstacle in the development of small molecule pharmaceutical compounds. Knowing that TFEB is translocated to the nucleus, and upregulates CLEAR element-containing genes in response to the lysosome acid-quenching effects of CADs, I have attempted to develop robust high throughput assays to assess the lysosome stress response to a number of stimuli including, but not limited to, CADs.

6.2 Results

6.2.1 Localisation of stably overexpressed TFEB-GFP in cells

Transiently over-expressed C-terminally GFP-tagged TFEB was previously used and shown to function correctly (Settembre *et al.*, 2012). Cell lines of HeLa and NRK cells were generated to stably express TFEB-GFP using the pLXIN and Phoenix packaging cell system. To confirm that GFP-tagged TFEB was responding correctly in these cell lines, they were imaged with or without incubation with torin1, a potent and selective inhibitor of mTOR. Untreated stable cell lines of both HeLa and NRK exhibited an almost exclusively cytoplasmic pool of TFEB-GFP, while torin1-treated cells showed a significant translocation of TFEB-GFP to the nucleus, indicating a functional response to the inhibition of mTOR. Whilst most of the TFEB-GFP in the untreated HeLa and NRK cell lines was cytosolic, a small proportion localised to punctate structures, and after releasing the cytosolic pool of TFEB-GFP by Saponin-permeabilisation of the plasma membrane, these have been shown to be endolysosomes and lysosomes (Bright, Davis and Luzio, 2016). Following torin1 treatment, some TFEB-GFP remained associated with punctate structures (Figure 6.1A) which have been previously identified as endolysosomes and lysosomes (Settembre *et al.*, 2012; Bright, Davis and Luzio, 2016). Settembre *et al*. (2012) suggested that in the torin1 treated cells, this TFEB was bound to inactive mTORC1 on the lysosomal membrane. A proportion of TFEB-GFP is localised to lysosomes in fed unperturbed cells, but can only be visualised by removing the cytosolic pool. In NRK cells preloaded with dextran and incubated with MRL, cytosolic TFEB-GFP was washed out of cells using Saponin incubation before fixation (Figure 6.1B). TFEB-GFP showed much more widespread punctate localisation than MRL, indicating that its localisation is not limited to endolysosomes. The colocalisation of TFEB-GFP with preloaded DexA and MRL was analysed using Manders' colocalisation coefficient (Figure 6.1C). The difference between the proportion of DexA-loaded lysosomes and MRL-marked endolysosomes that colocalised with TFEB-GFP was not significant.

Figure 6.1

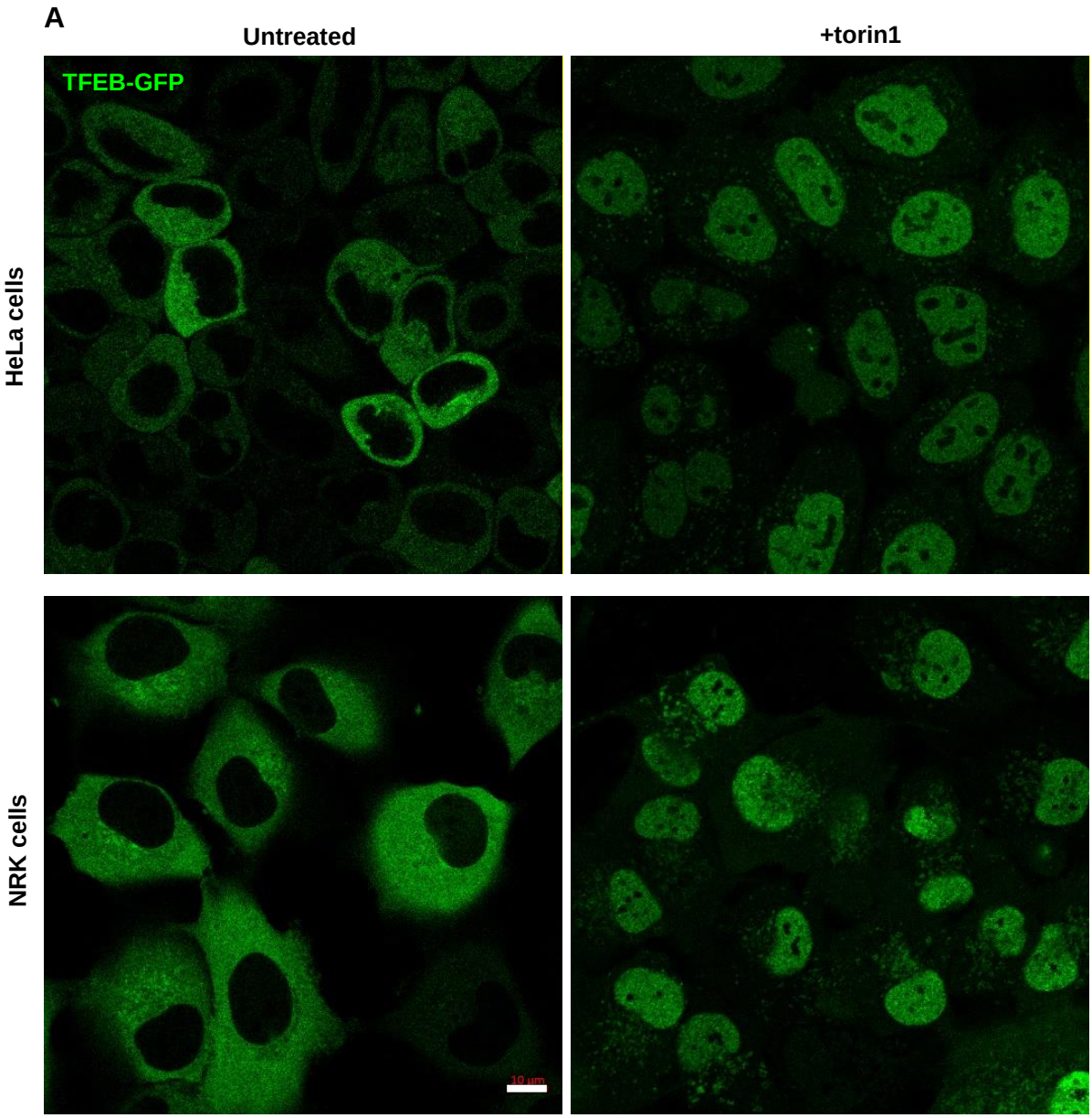

B

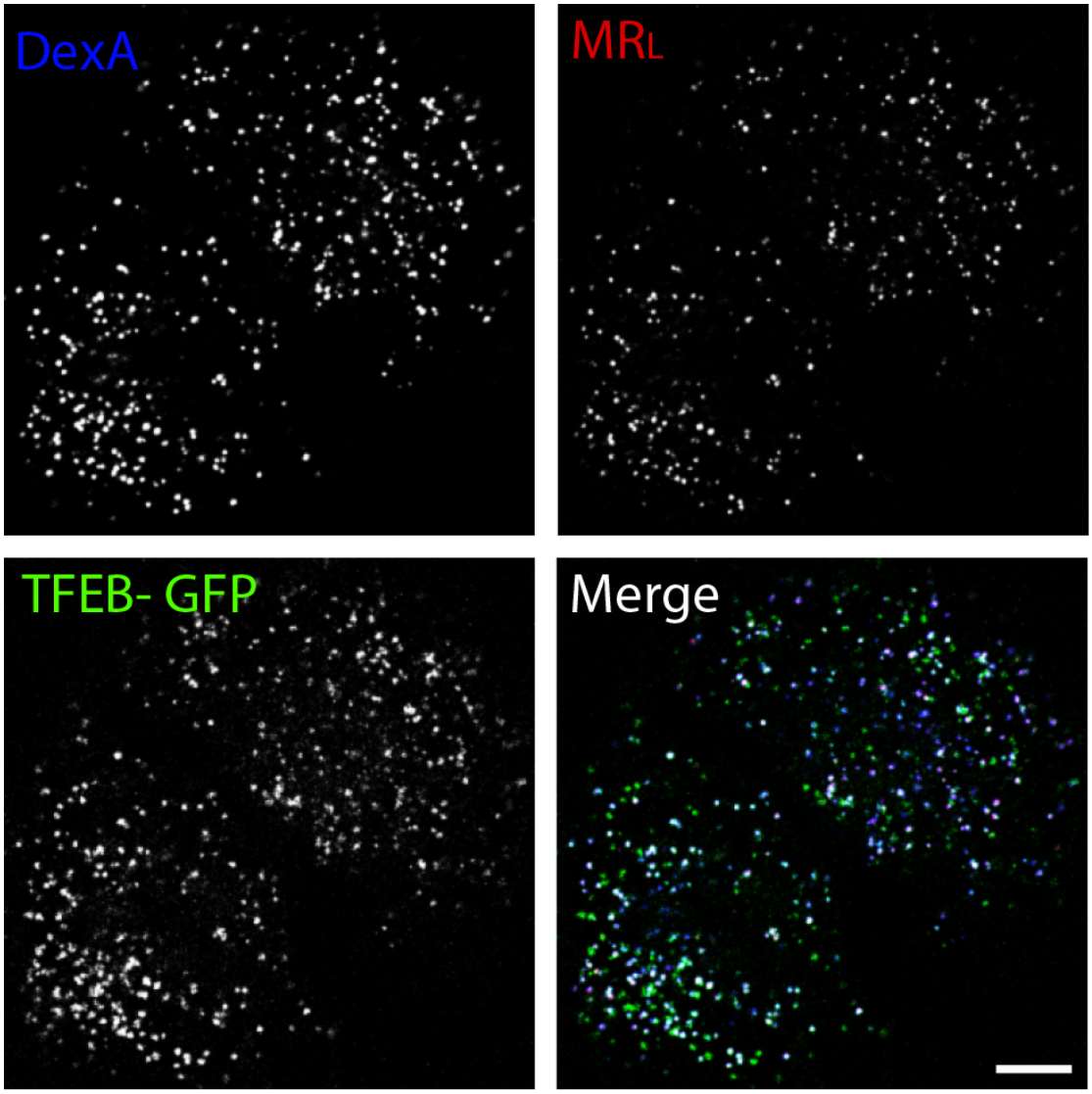
DexA
MRL
TFEB- GFP
Merge

C

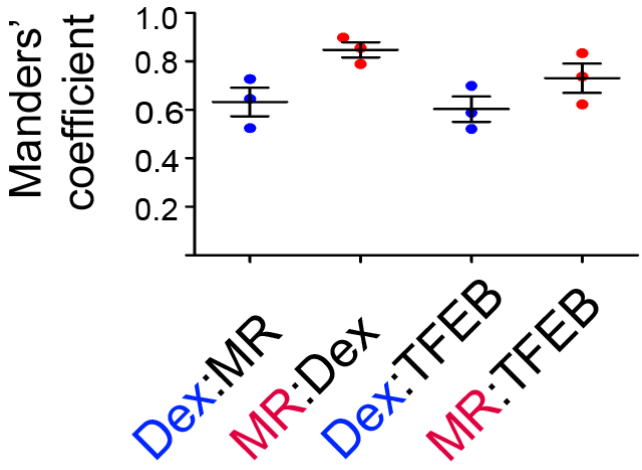
Manders' coefficient
1.0
0.8
0.6
0.4
0.2
Dex:MR
MR:Dex
Dex:TFEB
MR:TFEB

Figure 6.1: Stable cell lines expressing TFEB-GFP

(A) Confocal fluorescence microscopy images of mixed population HeLa (top row) or NRK (bottom row) cells stably expressing TFEB-GFP, which were incubated with or without 250nM torin1 for 90 minutes.

(B) Confocal fluorescence microscopy images of NRK cells stably expressing TFEB-GFP, pre-loaded with DexA to label terminal endocytic compartments, incubated with MRL for 3 min and fixed after cytosol washout by incubating the cells in 0.05% Saponin for 30 seconds prior to PFA fixation. Scale bar represents 10µm.

(C) Mander's correlation coefficients for colocalisation of pre-loaded DexA with MRL or TFEB-GFP, or for colocalisation of 3 minutes-incubated MRL with DexA, or TFEB-GFP in NRK cells. Error bars represent the mean ± SEM of 3 experiments, each measuring >15 cells.

6.2.2 Nuclear translocation of TFEB-GFP is a quantifiable reporter for lysosomal stress

To quantify the degree of nuclear translocation of TFEB under different conditions, a high-throughput automated widefield microscopy assay was used. An automated programme was designed to image cells and analyse the fluorescence data to give a readout of the difference in mean GFP signal, and hence difference in TFEB-GFP concentration, between the nucleus and a sampled region of the cytoplasm (Figure 6.2A). Increases in NucCyt difference represent increased TFEB translocation.

A number of known TFEB-activating conditions were applied to clonal NRK TFEB-GFP cells to quantify the effects on TFEB translocation and validate the system. torin1 treatment caused a significant degree of TFEB nuclear translocation, and hence could be used as a positive control (Figure 6.2B). Cell starvation by incubation in Earle's Balanced Salt Solution (EBSS) for 1-4 hours caused approximately one third of the nuclear translocation of TFEB when compared to the effect of torin1 (Figure 6.2B). TFEB translocation in response to manipulations of lysosomal pH were also quantified. Inhibition of the V-ATPase by incubating cells overnight with BafA1 produced approximately one quarter of the response to torin1, while neutralising lysosomes by incubating with weak basic chloroquine overnight resulted in approximately half the translocation in response to torin1 (Figure 6.2C).

Figure 6.2

A

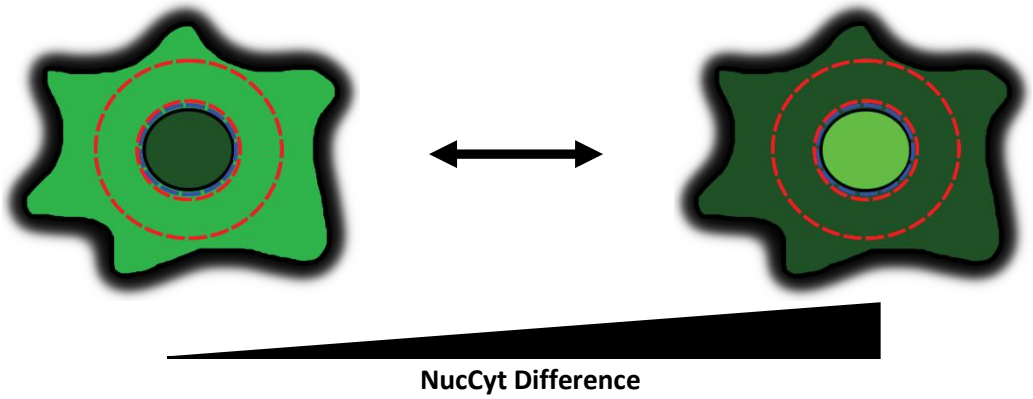

B

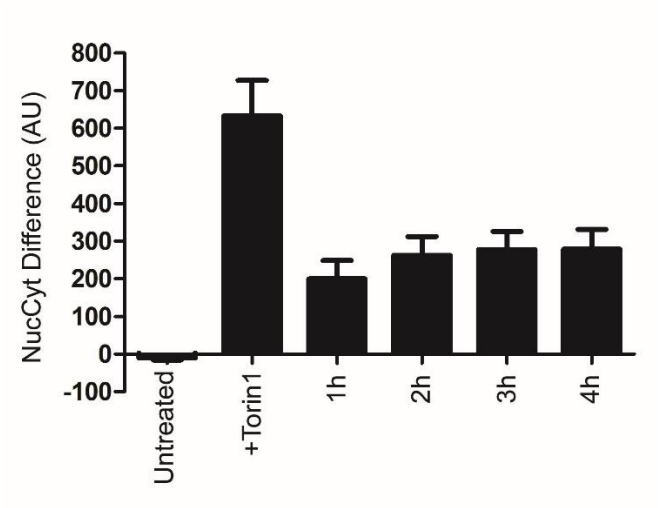

C

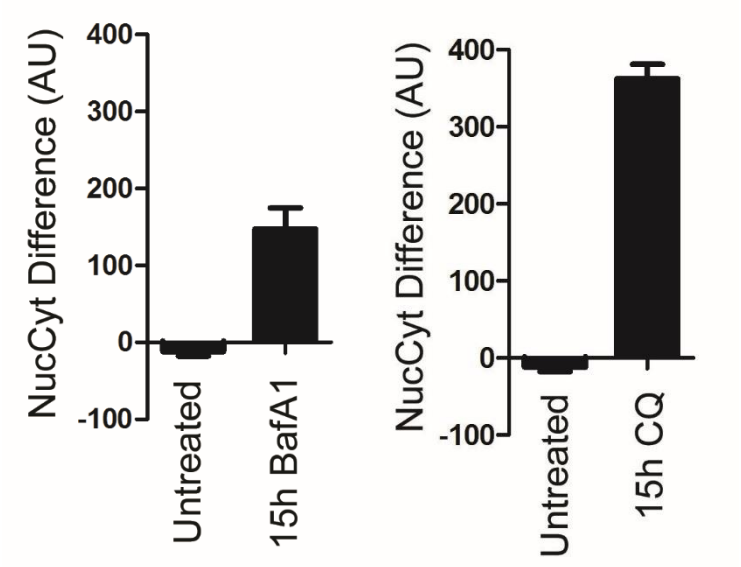

Figure 6.2: Nuclear translocation of TFEB-GFP as a reporter for lysosomal stress

(A) A schematic illustrating the cell regions measured during the automated TFEB-translocation quantification assay (Chapter 2.10). The blue, inner circle represents the nuclear region as determined by Hoechst staining, and the red, outer ring represents the cytoplasmic sample region. The NucCyt difference value is calculated by the nuclear GFP fluorescence intensity after subtracting the cytoplasmic GFP fluorescence intensity.

(B) Clonal NRK TFEB-GFP cells were untreated, incubated with 250nM torin1 for 90 minutes, or washed with, then incubated in EBSS for up to 4 hours. Cells were then fixed and processed for automated scanning. Error bars represent mean ± SEM of 3 experiments. >750 cells were measured per condition in each experiment.

(C) Clonal NRK TFEB-GFP cells were untreated, incubated with 100nM BafA1 for 15 hours, or incubated with 100µM chloroquine (CQ) for 15 hours. Cells were then fixed and processed for automated scanning. Error bars represent mean ± SEM of 3 experiments. >750 cells were measured per condition in each experiment.

6.2.3 TFEB-GFP acts as a dose-dependent reporter for R. equi VapA protein required for virulence

Some pathogens and their proteins can cause dysfunction of the host cell's lysosomal system. Once such pathogen, *Rhodococcus equi* (*R. equi*) is a foal-infecting bacterium capable of expressing a number of virulence-associated proteins (Vaps), including VapA which allows the bacterium to survive inside macrophages by perturbing endolysosomal function. In particular, VapA causes some lysosomal swelling and reduces the fusion of *R. equi*-containing phagosomes with lysosomes (Fernandez-Mora *et al.*, 2005; von Bargen and Haas, 2009; Rofe *et al.*, 2017). VapA is necessary for *R. equi* virulence and it alone can restore virulence to VapA, C, D, E, or F depletion mutants (JainBloom and Hondalus, 2003). *R. equi* can infect NRK cells but at a lower efficiency than macrophage cell lines (Rofe *et al.*, 2017). To investigate whether TFEB was activated in response to the lysosome-perturbing effects of *R. equi* Vaps, NRK TFEB-GFP cells were incubated with recombinant VapA (provided by Dr Adam Rofe and Dr Paul Pryor, University of York), which entered the cells by fluid phase endocytosis and caused a concentration-dependent increase in TFEB translocation. This reached approximately one quarter of the response to torin1 (250nM for 90 minutes) when cells were incubated for 24 hours with 200µg/ml VapA (Figure 6.3A). Incubation with recombinant virulence proteins VapD and VapG, despite the high degree of sequence homology of their core regions with that of VapA (Rofe *et al.*, 2017), showed no effect on TFEB translocation compared to untreated cells (Figure 6.3A).

To further investigate the timescale of the VapA-mediated activation of TFEB, and to determine the domain of VapA that is important in such activation, a timecourse experiment was performed. NRK TFEB-GFP cells were incubated with recombinant VapA, VapD, VapG, chimeric VapA (N-terminal)-VapD (core), or chimeric VapD (N-terminal)-VapA (core) proteins. TFEB nuclear translocation was only observed in VapA-incubated cells, and VapD (N-terminal)-VapA (core) chimera-incubated cells, which both reached a peak response after 16 hours incubation (Figure 6.3B). The fact that the VapD-VapA chimera, and not the VapA-VapD chimera, induced TFEB translocation indicates that the core region of VapA is specifically responsible for lysosome perturbation.

Figure 6.3

A

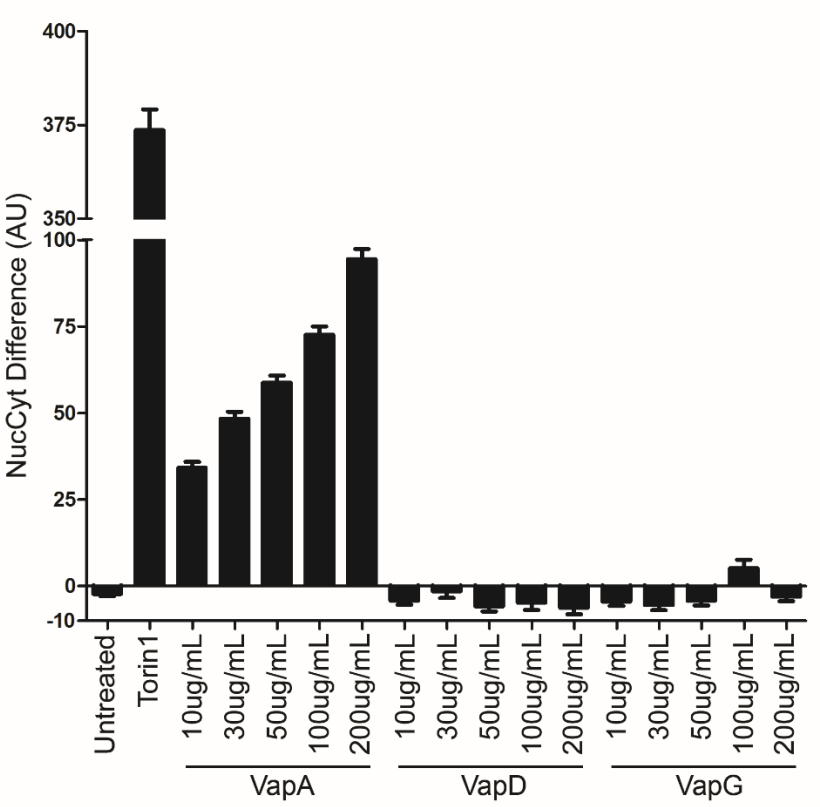
NucCyt Difference (AU)
400
375
350
100
75
50
25
0
-10
Untreated
Torin1
10ug/mL
30ug/mL
50ug/mL
100ug/mL
200ug/mL
VapA
VapD
VapG

B

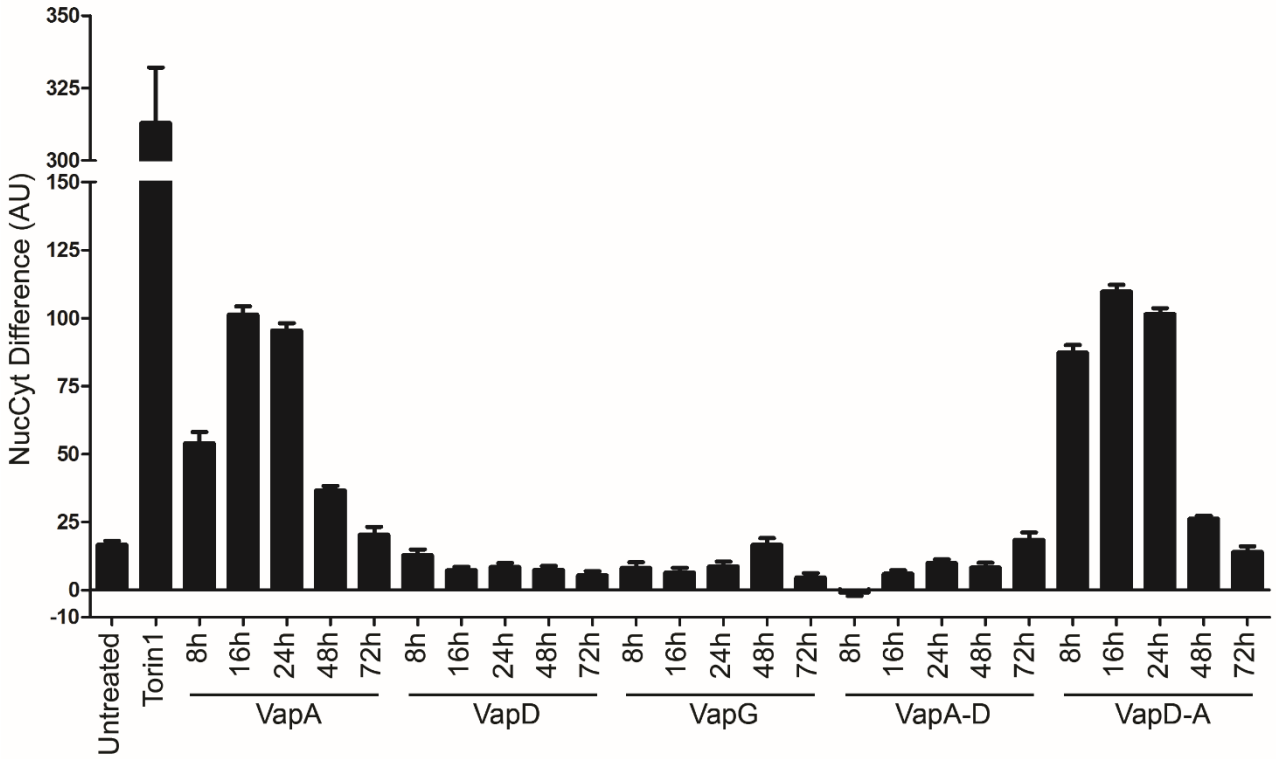
NucCyt Difference (AU)
350
325
300
150
125
100
75
50
25
0
-10
Untreated
Torin1
8h
16h
24h
48h
72h
VapA
VapD
VapG
VapA-D
VapD-A

Figure 6.3: TFEB-GFP nuclear translocation after incubation with R. equi virulence proteins

(A) Clonal NRK TFEB-GFP cells were untreated, incubated with 250nM torin1 for 90 minutes, or incubated with increasing concentrations of recombinant VapA, VapD, or VapG for 24 hours. Cells were then fixed and processed for automated scanning. Error bars represent mean ± SEM of 3 experiments. >750 cells were measured per condition in each experiment.

(B) Clonal NRK TFEB-GFP cells were untreated, incubated with 250nM torin1 for 90 minutes, or incubated with 100µg/ml of recombinant VapA, VapD, VapG, chimeric VapA-VapD, or chimeric VapD-VapA for 8-72 hours. Cells were then fixed and processed for automated scanning. Error bars represent mean ± SEM of 3 experiments. >750 cells were measured per condition in each experiment.

6.2.4 Using HEK293 cells stably expressing TFEB-GFP to determine optimal conditions to trigger TFEB translocation

Human embryonic kidney (HEK293) cells are a widely used human cell line for toxicity studies (see for example (Shukla *et al.*, 2010)). In order to study TFEB translocation in these cells in response so a variety of CADs and other drugs/drug precursors and in preparation for downstream analyses of TFEB-upregulated gene transcription using qPCR, clonal HEK293 cell lines stably expressing TFEB-GFP were generated. These cells were used in dose response and time course experiments with multiple TFEB-activating conditions to determine the temporal dynamics of TFEB translocation and to inform on the optimal conditions to treat cell samples for later qPCR applications. Maximum concentrations and durations where cell viability still exceeded 80% by resazurin-based assays were used. HEK293 TFEB-GFP cells were incubated with increasing concentrations of the CAD CQ for 1-18 hours, resulting in a peak in TFEB translocation between 3 and 6 hours with 100µM CQ (Figure 6.4A). After incubation with the V-ATPase inhibitor BafA1, HEK293 TFEB-GFP cells showed the greatest TFEB translocation after 18 hours incubation, with little difference between 25nM, 50nM, and 100nM concentrations (Figure 6.4B). ML-SA1 is an agonist which activates the TRPML1 lysosomal Ca^{2+} channel. This causes release of intra-lysosomal Ca^{2+} and resultant activation of calcineurin which dephosphorylates TFEB and allows it to be translocated into the nucleus (Medina *et al.*, 2015). ML-SA1 (Tocris Bioscience) demonstrated very potent concentration-dependent activation of TFEB in a short timescale, strongly inducing TFEB translocation when used at 200µM for 2 hours (Figure 6.4C).

Figure 6.4

A **CQ**

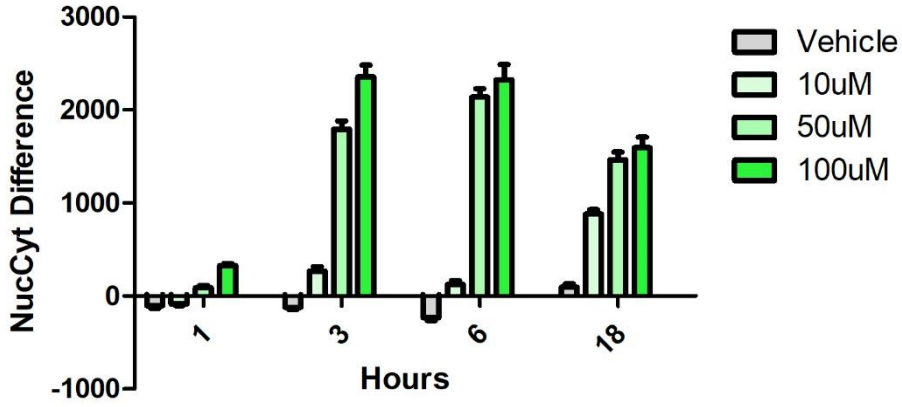

B **BafA1**

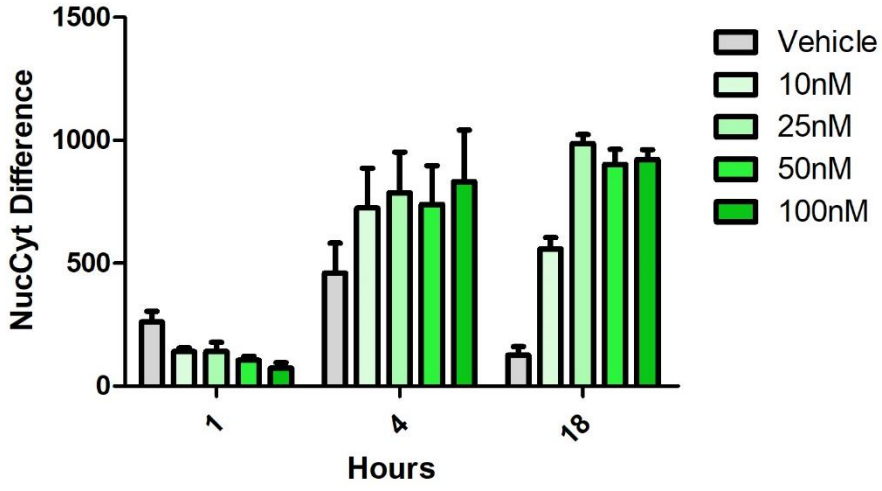

C **ML-SA1**

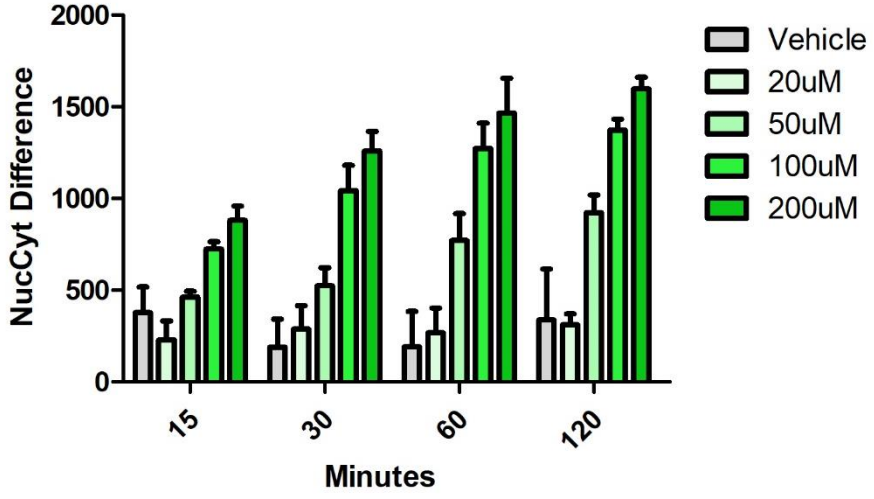

Figure 6.4: Using HEK293 cells stably expressing TFEB-GFP to determine optimal conditions to trigger TFEB translocation

(A) Clonal HEK293 TFEB-GFP cells were incubated with 1:1000 (v/v) DMSO vehicle, or increasing concentrations of CQ for 1, 3, 6, or 18 hours. Cells were then fixed and processed for automated scanning. Error bars represent mean ± SEM of 3 experiments. >750 cells were measured per condition in each experiment.

(B) Clonal HEK293 TFEB-GFP cells were incubated with 1:1000 (v/v) DMSO vehicle, or increasing concentrations of BafA1 for 1, 4, or 18 hours. Cells were then fixed and processed for automated scanning. Error bars represent mean ± SEM of 3 experiments. >750 cells were measured per condition in each experiment.

(C) Clonal HEK293 TFEB-GFP cells were incubated with 1:100 (v/v) DMSO vehicle, or increasing concentrations of ML-SA1 for 15, 30, 60, or 120 minutes. Cells were then fixed and processed for automated scanning. Error bars represent mean ± SEM of 3 experiments. >750 cells were measured per condition in each experiment.

Table 6.1 Applied Biosystems™ TaqMan® Gene Assays

Assay ID	Gene Symbol	Gene Name(s)	RefSeq(s)	GenBank mRNA(s)	Amplicon Length
Hs01060665_g1	ACTB	actin, beta;hCG15971 Celera Annotation	NM_001101.3	AK223055.1;BC013380.2;AK130062.1;DQ471327.1;BC002409.2;X00351.1;AK304552.1;BC012854.1;AK058019.1;BC001301.1;AK130157.1;AK223032.1;BC016045.1;BC004251.1;X63432.1;AK025375.1;AK309997.1;AK222925.1;BC014861.1;BC008633.1;BC013835.1;AK225414.1;EF095209.1	63
Hs04185629_g1	ARSA	arylsulfatase A;hCG16870 Celera Annotation	NM_001085425.2;NM_001085428.2;NM_001085427.2;NM_001085426.2;NM_000487.5	BM818814.1;AK315011.1;CA423492.1;AK092752.1;CR456383.1;X52151.1;AB448736.1;AK098659.1;BX648618.1;BC014210.2	60
Hs00940968_m1	ARSB	arylsulfatase B;hCG37743 Celera Annotation	NM_000046.3;NM_198709.2	BC029051.1;M32373.1;AK290865.1;AK314903.1;J05225.1	125
Hs01377254_m1	ATG9B	autophagy related 9B;hCG2039570 Celera Annotation	NM_173681.5	AY515311.1;AY316116.1	72
Hs00895280_g1	ATP6V1G1	ATPase, H^+ transporting, lysosomal 13kDa, V1 subunit G1;hCG29854 Celera Annotation	NM_004888.3	CR542237.1;CR456971.1;BC008452.1;AF038954.1	78
Hs00977530_m1	ATP6V1H	ATPase, H^+ transporting, lysosomal 50/57kDa, V1 subunit H;hCG27354 Celera Annotation	NM_213619.2;NM_213620.2;NM_015941.3	AK098305.1;AK308204.1;AF112204.1;AF113222.1;AK022345.1;AF125105.1;BC025275.1;AF298777.1;AK303229.1;AK094839.1	72
Hs01126462_m1	CLCN7	chloride channel, voltage-sensitive 7;hCG42716 Celera Annotation	NM_001287.5;NM_001114331.2	AK291404.1;AK304796.1;AK292136.1;AF224741.1;Z67743.1;AK056551.1;BC012737.2	69
Hs00264902_m1	CTSA	cathepsin A;hCG38374 Celera Annotation	NM_001167594.1;NM_001127695.1;NM_000308.2	AK307701.1;AB209705.2;AK097786.1;BC093009.1;AK312898.1;M22960.1;AK172808.1;BC000597.2;AK304536.1	65
Hs00947433_m1	CTSB	hCG1990887 Celera Annotation;cathepsin B	NM_147783.2;NM_147782.2;NM_147781.2;NM_147780.2;NM_001908.3	BX647952.1;L16510.1;AK296845.1;BX647765.1;AL543654.3;AK075393.1;BC095408.1;BG770805.1;AK130184.1;AK092070.1;BC010240.1;CB997355.1;AK290239.1;M14221.1;BM008741.1	73
Hs00157205_m1	CTSD	cathepsin D;hCG49857 Celera Annotation	NM_001909.4	BC001574.1;CR456947.1;BT020155.1;X05344.1;BT006910.1;AK130178.1;BC016320.2;M11233.1	103

Hs00186901_m1	CTSF	hCG20245 Celera Annotation;cathepsin F	NM_003793.3	AF088886.2;AF071748.1;AL137742.1;AF071749.1;BC036451.1;CR541680.1;AJ007331.1;BC011682.2;AF136279.1;AK313657.1	105
Hs00975732_m1	GALNS	hCG19109 Celera Annotation;galactosamine (N-acetyl)-6-sulfate sulfatase	NM_000512.4	AY129021.1;AK294390.1;AK308269.1;BC056151.1;BC050684.1;AK312655.1;AK131096.1	115
Hs02758991_g1	GAPDH	glyceraldehyde-3-phosphate dehydrogenase;hCG2005673 Celera Annotation	NM_002046.4;NM_001256799.1	BU155402.1;BC004109.2;BC013310.2;BC025925.1;BC020308.1;AF261085.1;BC009081.1;DQ403057.1;CR407671.1;M33197.1;EF036498.1;BC029340.1;BC023632.2;X53778.1;AY007133.1;BC001601.1;BC029618.1;BC026907.1;BT006893.1;AB062273.1;AK026525.1;BC083511.1;AK308198.1;X01677.1;M17851.1;AY633612.1	93
Hs00986836_g1	GBA	glucosidase, beta, acid;hCG1996349 Celera Annotation	NM_000157.3;NM_001171812.1;NM_001005742.2;NM_001171811.1;NM_001005741.2	BC003356.1;AK291911.1;AK302000.1;AK300876.1;BX648487.1;AK312502.1;AK300829.1;K02920.1;M19285.1;D13286.1;AK300186.1;AK301374.1;M16328.1	89
Hs00609238_m1	GLA	galactosidase, alpha;hCG20401 Celera Annotation	NM_000169.2	AK297148.1;BC002689.2;X05790.1;X16889.1;BT006864.1;D00039.1;AK291095.1	80
Hs00157741_m1	GNS	hCG1640559 Celera Annotation;glucosamine (N-acetyl)-6-sulfatase	NM_002076.3	AK223484.1;AK302443.1;BC012482.1;AK291771.1;BX537363.1;Z12173.1;AK304158.1;AK300350.1	60
Hs00166843_m1	HEXA	hexosaminidase A (alpha polypeptide);hCG40459 Celera Annotation	NM_000520.4	DC356933.1;BC084537.1;AK222502.1;M13520.1;AK301138.1;AK296528.1;BP356349.1;CR627386.1;BC018927.2;AK307770.1	91
Hs00174766_m1	LAMP1	hCG27880 Celera Annotation;lysosomal-associated membrane protein 1	NM_005561.3	BC021288.2;J04182.1;BC025335.1;BC093044.1;BU849686.1;AK301584.1;AK092398.1	93
Hs01548815_m1	LIPA	lipase A, lysosomal acid, cholesterol esterase;hCG24574 Celera Annotation	NM_001127605.1;NM_000235.2	AK091558.1;AK314665.1;U08464.1;Z31690.1;AK290241.1;AK125193.1;M74775.1;AK096406.1;BC012287.1;AK222760.1;X76488.1	118
Hs01100653_m1	MCOLN1	mucolipin 1;hCG22254 Celera Annotation	NM_020533.2	AK222673.1;AK294330.1;AK026102.1;AF249319.1;BC005149.2;AF287269.1;AJ293659.1;AJ293970.1;AF171088.1	86
Hs00165356_m1	NAGLU	N-acetylglucosaminidase, alpha;hCG16571 Celera Annotation	NM_000263.3	L78464.1;U40846.1;BC053991.1;U43573.1	80

Hs00902543_g1	NEU1	sialidase 1 (lysosomal sialidase);hCG43692 Celera Annotation	NM_000434.3	X78687.1;AF040958.1;AB209011.1;AK313006.1;U84246.1;BC000722.2;BC011900.2;CR541916.1;AK290966.1;BT007206.1	108
Hs00234592_m1	PPARG	peroxisome proliferator-activated receptor gamma;hCG26772 Celera Annotation	NM_015869.4; NM_005037.5; NM_138711.3; NM_138712.3	U63415.1;BC006811.1;U79012.1;AB451486.1;AB472042.1;AB307692.1;AB451337.1;X90563.1;AB565476.1;D83233.1;BT007281.1;AK290581.1;AK223528.1;HQ692866.1	77
Hs01016719_m1	PPARGC1A	hCG1811770 Celera Annotation;peroxisome proliferator-activated receptor gamma, coactivator 1 alpha	NM_013261.3	AB061325.1;AF159714.1;JQ772116.1;JQ772117.1;AF106698.1;AF186379.1;JQ772118.1;HQ695733.1;JQ772119.1;JQ772120.1	74
Hs01551096_m1	PSAP	prosaposin;hCG1787837 Celera Annotation	NM_002778.2; NM_001042465.1;NM_001042466.1	AK057878.1;J03015.1;BT006849.1;AK293672.1;M32221.1;M60255.1;M60257.1;J03077.1;CR456746.1;AK129790.1;AK299184.1;BC001503.2;M60258.1;BC007612.1;M81355.1;AB209776.1;D00422.1;AK223290.1;BC004275.1	74
Hs00222108_m1	SCPEP1	serine carboxypeptidase 1;hCG33381 Celera Annotation	NM_021626.2	AF282618.1;AK298161.1;DC344612.1;AY358559.1;AF113214.1;BC072405.1;AK027373.1	66
Hs00164924_m1	SGSH	N-sulfoglucosamine sulfohydrolase;hCG28568 Celera Annotation	NM_000199.3	DC319407.1;AK309927.1;BC047318.1;AK095969.1;AK222890.1;AK291257.1;U30894.1;AB209900.1	94
Hs00990751_m1	TCIRG1	T-cell, immune regulator 1, ATPase, H^+ transporting, lysosomal V0 subunit A3;hCG19345 Celera Annotation	NM_006053.3; NM_006019.3	U45285.1;BC018133.1;AF025374.1;BC032465.1	95
Hs01565444_g1	TMEM55B	hCG40483 Celera Annotation;transmembrane protein 55B	NM_144568.2; NM_001100814.1	AK314021.1;BC020947.1;BX248025.1;BC002867.1;BX161490.1	60
Hs00166099_m1	TPP1	hCG22005 Celera Annotation;tripeptidyl peptidase I	NM_000391.3	AK312388.1;AK295801.1;AK293741.1;AY358502.1;AF017456.1;AK300998.1;AK222538.1;AK293518.1;BP279860.1;AK222499.1;BC014863.1;AY268890.1	82
Hs00748673_s1	ATP6V0E1	ATPase, H^+ transporting, lysosomal 9kDa, V0 subunit e1;hCG41251 Celera Annotation	NM_003945.3	BF691381.1;Y15286.1	136

6.2.5 Lysosomal gene regulation in HEK293 cells after treatment with chloroquine

To investigate the effects of TFEB-activating conditions on gene regulation, a qPCR study was performed using a list of lysosomal genes with CLEAR elements (Table 6.1, modified from (Sardiello *et al.*, 2009)). Wild type HEK293 cells were treated with CQ or with acetaminophen as a non-lysosomotropic control compound before isolating RNA. TaqMan gene expression array card qPCR analysis showed very low levels of modulation of the selected lysosomal genes (Table 6.1) relative to untreated control conditions, with only 7 genes' expression increasing by >1.2 fold under any CQ treatment duration (Figure 6.5). ATP6V1H showed the greatest response with consistent 1.3-1.5 fold upregulation at all CQ treatment durations. For most genes, the greatest increase in mRNA copy number occurred after 16-18 hours treatment with CQ, suggesting that the time course of peak gene upregulation might be longer than investigated in this study. Acetaminophen consistently produces negligible effects on gene expression as anticipated.

6.2.6 Measuring gene regulation of a subset of CQ-responding genes using alternative TFEB-activating conditions

The 6 genes with the highest peaks in mRNA copy number upregulation from the initial qPCR study, together with RRAGD (Table 6.2) which has recently been reported to be capable of very high upregulation (Di Malta *et al.*, 2017), were further tested for their suitability as a reporter of lysosome stress by analysing their expression after applying different TFEB-activating stimuli.

Table 6.2 Applied Biosystems™ TaqMan® Gene Assay for RRAGD

Assay ID	Gene Symbol	Gene Name(s)	RefSeq(s)	GenBank mRNA(s)	Amplicon Length
Hs00222001_m1	RRAGD	Ras related GTP binding D	NM_021244	AF272036.1;AK289799.1;AL523999.3;BC003088.1	61

Wild type HEK293 cells were incubated with acetaminophen, torin1, ML-SA1, or amino acid (AA)-free medium before RNA isolation and qPCR analysis. Suprisingly, throughout the time course of torin1 incubation, all differences in expression were showing down-regulation of transcription of these genes (Figure 6.6A). ML-SA1

treatment caused similar downregulation of genes to that of torin1, with the exception of NEU1 which was strongly upregulated at 8 and 24 hours incubation (Figure 6.6B). Amino acid starvation of HEK293 cells produced the most dramatic response in the genes, resulting in significant upregulation of every gene except for RRAGD at 4 hours starvation (Figure 6.6C).

Figure 6.5

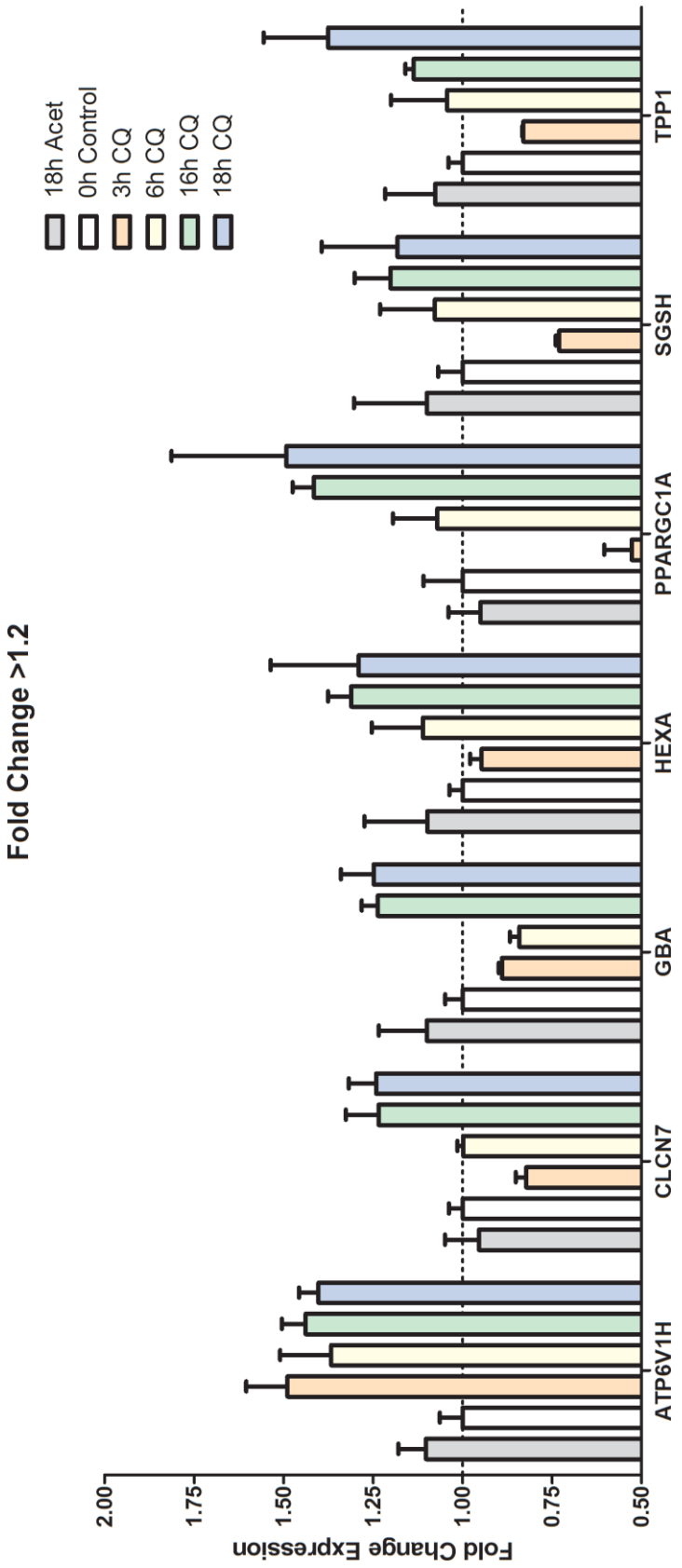
Fold Change >1.2
18h Acet
0h Control
3h CQ
6h CQ
16h CQ
18h CQ
Fold Change Expression
2.00
1.75
1.50
1.25
1.00
0.75
0.50
ATP6V1H
CLCN7
GBA
HEXA
PPARGC1A
SGSH
TPP1

Figure 6.5: Lysosomal gene regulation in HEK293 cells after treatment with chloroquine

Wild type HEK293 cells were incubated with normal growth medium, with 50µM CQ for 3, 6, 16 or 18 hours, or with 100µM acetaminophen for 18 hours. Cells were then lysed, RNA was isolated, reverse-transcribed and quantified using qPCR as described in Chapter 2, section 2.13. Graph representing the fold change in mRNA copy number relative to that of PBS treated control samples, normalised to β-actin expression. Error bars represent mean ± SEM of 3 experiments. Statistical analyses were unable to be performed due to faulty Array Card wells exhibiting anomalous fluorescence in a number of polymerase-negative control wells.

Figure 6.6

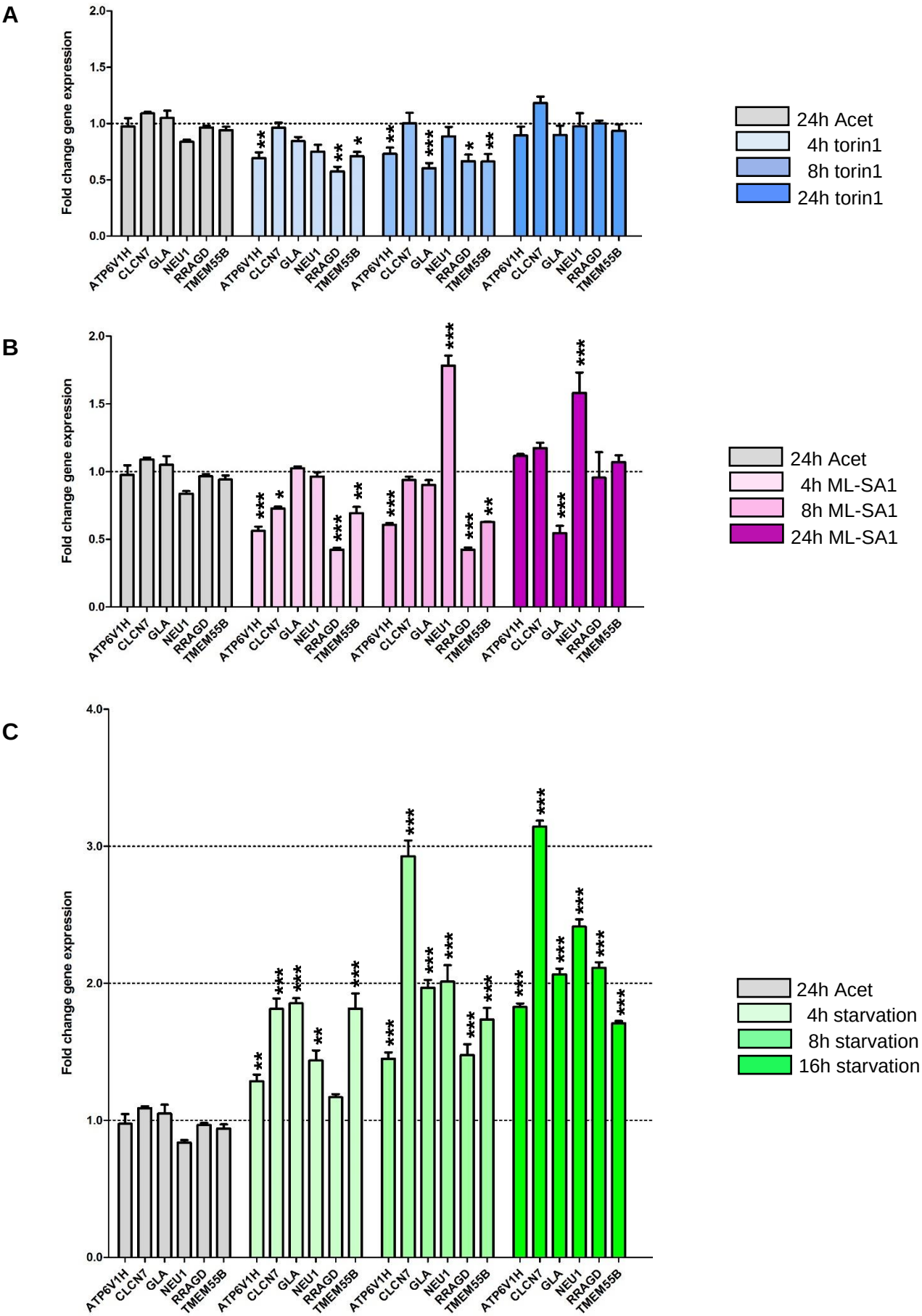
A
Fold change gene expression
2.0
1.5
1.0
0.5
0.0
ATP6V1H
CLCN7
GLA
NEU1
RRAGD
TMEM55B
24h Acet
4h torin1
8h torin1
24h torin1
B
Fold change gene expression
24h Acet
4h ML-SA1
8h ML-SA1
24h ML-SA1
C
Fold change gene expression
4.0
3.0
2.0
1.0
0.0
24h Acet
4h starvation
8h starvation
16h starvation

Figure 6.6: Measuring gene regulation of a subset of CQ-responding genes using alternative TFEB-activating conditions

Wild type HEK293 cells were incubated with 100µM acetaminophen for 24 hours, or (A) 30nM torin1 for 4, 8, or 24 hours, (B) 50µM ML-SA1 for 4, 8, or 24 hours, or (C) AA-free medium for 4, 8, or 16 hours before RNA was isolated, reverse-transcribed and quantified using qPCR as described in Chapter 2, section 2.13. Graphs represent the fold change in mRNA copy number relative to that of the vehicle control samples, normalised to β-actin expression. Statistical significance was determined using a one-way ANOVA analysis and Dunnett's multiple comparisons tests to determine statistically significant differences from the vehicle control.

*** $p<0.0001$, ** $p<0.001$, * $p<0.05$, unmarked means not significant from control.

6.3 Discussion

The data presented here shows that TFEB with C-terminally tagged GFP, when stably expressed in HeLa, NRK, or HEK293 cells, functions as expected by translocating into the nucleus in response to torin1-mediated mTOR inhibition. Through the use of high-throughput automated widefield fluorescence microscopy, GFP-tagged TFEB translocation has been quantified and shown to be a robust reporter for lysosomal stress caused by a variety of stimuli, including amino acid-deprivation, deacidification of lysosomes and bacterial virulence protein uptake. The dynamic range of the automated TFEB-GFP nuclear translocation assay provided a sensitive readout for lysosomal stress, as seen in the dose-dependent response to VapA incubation (Figure 6.3A) It even allowed mapping of the active domain of VapA, through studying the effects of chimeras of parts of VapA and of other Vap proteins (Figure 6.3A). The assay was also sufficiently sensitive to allow the generation of dose response and time course graphs for three small molecules, CQ, BafA1 and ML-SA1 that induce lysosomal stress by different mechanisms. It is therefore a potentially useful addition to the battery of tests, including LysoTracker®/LysoSensor™ staining to assess acidification, Magic Red™ to assess cathepsin activity, and LAMP staining currently available to assess the effects on lysosomal stress of known lysosomotropic compounds (Lu *et al.*, 2017) or pre-drugs during drug development. However, a caveat is that TFEB translocation can be activated by a range of pathways, including a mTOR-independent PKC-mediated pathway (Li *et al.*, 2016), and as such, cannot on its own be interpreted as a specific reporter or lysosomal status, or phospholipidotic potential of a compound.

My initial qPCR experiments showed that under the conditions of CQ incubation with HEK293 cells used to induce TFEB translocation to the nucleus, there was little, and inconsistent effect on the regulation of 29 selected CLEAR element genes. A subset of the 5 genes with the highest peak expression after CQ treatment, plus RRAGD, were taken forward to another qPCR experiment using cells treated with torin1, ML-SA1, or AA starvation.

The negative effects on CLEAR element gene regulation shown by torin1 and largely by shorter ML-SA1 incubations differ from the ~2 to ~6-fold changes previously reported for the same genes (Sardiello *et al.*, 2009) however the consistent

upregulation across all genes in the subset following amino acid starvation fits completely in line with previous reports. Low level effects on lysosome gene upregulation have been reported where a lysosomal gene transcriptional repressor, ZKSCAN3, was knocked down, and showed comparably mild <2.5 fold expression of lysosomal genes (Chauhan *et al.*, 2013), so the fact that only two lysosome perturbations tested here caused upregulation of >2.5 fold expression might not be an anomaly. Additionally, the greater amount of TFEB expressed in the TFEB-GFP reporter cell line compared to wild type may have predisposed the reporter cells to overestimate the degree of TFEB activation under any conditions of lysosomal stress. In such a situation, the wild type HEK293 cells treated the same way may exhibit less gene upregulation as the endogenous TFEB pathway isn't as strongly activated as estimated. Acetominophen again caused no change in lysosomal gene regulation, reflecting its lack of lysosomotropic character.

Chapter 7 – General discussion

7.1 General discussion

The overarching aim of the work reported in this thesis was to study the dynamics and function of organelles in the late endocytic pathway, focusing on the machinery that maintains the equilibrium of functionally heterogeneous organelles in the lysosome regeneration cycle. In particular, the roles of proteins involved in the interrelated aspects of late endosome-lysosome fusion to produce endolysosomes, and modulation of pH during reformation to regenerate acid hydrolase-storage lysosomes, were to be investigated. Additionally, a toolkit to report cell signalling in response to lysosomal damage or stress, was to be developed and tested.

In Chapter 3, live cell microscopy data demonstrated the endolysosome subpopulation of lysosomes to be acidic and cathepsin-active. Using the presence or absence of Magic Red™ in dextran loaded terminal endocytic compartments to distinguish endolysosomes from storage lysosomes respectively, the cross-sectional size of endolysosomes was on average greater than that of storage lysosomes. Dense core lysosomes, as identified by EM, are consumed during sucrosome formation (Bright *et al.*, 1997), and sucrosomes are endolysosomal in nature (Chapter 3, (Bright, Davis and Luzio, 2016)). Given that dextran-loaded Magic Red™-negative storage lysosomes appear smaller than endolysosomes, these storage lysosomes may very well represent dense core storage lysosomes observed by light microscopy. Endolysosomes were shown to strongly colocalise with Rab9 and Rab7, the latter of which is in alignment with the correlation between Rab7-presence and acidity of juxtanuclear lysosomes (Johnson *et al.*, 2016). Endolysosomes were also shown to be marked by ML1Nx2-GFP, a probe developed for the detection of the endolysosomal phosphoinositide $PI(3,5)P_2$ (Li *et al.*, 2013), however interpretation of these data is complicated by a dispute over the specificity of ML1Nx2-GFP binding to $PI(3,5)P_2$, particularly due to differing results from an experiment with a PIKFYVE inhibitor, YM201636, which is known to rapidly and specifically deplete $PI(3,5)P_2$ (Jefferies *et al.*, 2008). Hammond *et al*., 2015 questioned the specificity of ML1Nx2-GFP. They closely reproduced an experiment using ML1Nx2-GFP with or without YM201636, but instead of using separate cell populations, measured the same cell population throughout the duration, and observed no reduction in colocalisation of ML1Nx2-GFP with LAMP1 after $PI(3,5)P_2$ depletion (Hammond *et al.*, 2015). Hammond et al. 2015 suggest that their

experimental approach was more consistent as it avoided the effects of cell to cell differences in expression. ML1Nx2 consists of two copies of the N-terminal cytosolic domain of TRPML1 and one possibility is that it correctly recognises $PI(3,5)P_2$ but once localised to the membrane, ML1Nx2 interacts with protein binding partners of this cytosolic domain. Nevertheless the concerns about ML1Nx2-GFP suggest that a better probe should be developed.

To better understand the machinery involved in formation of endolysosomes by the fusion of late endosomes with endolysosomes/lysosomes, I investigated the roles played by the R-SNAREs VAMP7 and VAMP8. As described in Chapter 4, there is some evidence for the redundancy of VAMP7 and 8 in the delivery of endocytosed cargo to lysosomes by kiss-and-run or full fusion events. After depleting HeLa cells of VAMP7 or VAMP8 individually, no significant effect was observed on morphology of intracellular compartments, or on delivery of late endosome cargo to lysosomes, indicating some degree of functional redundancy in these cells, as endocytic trafficking was functional. CRISPR-Cas9-mediated knockout of each SNARE was employed to completely eliminate these SNAREs, as the remaining levels after individual siRNA-mediated knockdown of SNAREs has previously shown to be insufficient to impact a number of intracellular trafficking pathways (Bethani *et al.*, 2009). The unaffected lysosomal delivery observed in dual VAMP7 and VAMP8 knockout cells led to the investigation of the alternative R-SNARE YKT6, another longin R-SNARE which has been shown to be required for homotypic vacuole fusion (Ungermann *et al.*, 1999) and competes with Nyv1p, the yeast homologue of VAMP7, to bind to the vacuolar t-SNARE complex (Fukuda *et al.*, 2000). Yeast YKT6 (Ykt6p) has also been shown to be able to substitute for Nyv1p in in vitro yeast vacuole fusion (Thorngren *et al.*, 2004). Knockdown conditions in which YKT6 depletion did not affect wild type HeLa cells significantly impeded delivery of endocytic cargo to lysosomes in VAMP7 and VAMP8 dual knockdown cells (Chapter 4). Furthermore, stable expression of HA-VAMP7 in the dual knockout cells rescued the effect of YKT6 depletion on lysosome delivery, supporting the role of YKT6 as a compensatory R-SNARE, and an alternative to VAMP7 in lysosomal trans-SNARE complexes. Similarly, a recent study has demonstrated YKT6 and VAMP7 compete to bind with the Syntaxin17-SNAP29 complex required for autophagosome-lysosome fusion in fruit fly cells (Takáts *et al.*, 2018). These authors also provided evidence

that YKT6 is not part of the fusion-competent trans-SNARE complex in wild type cells, and instead plays a regulatory role. A study of HeLa cells, however, showed YKT6 to form a SNARE complex with SNAP29 and Syntaxin7, mediating autophagosome-lysosome fusion independently of Syntaxin17 (Matsui *et al.*, 2018). Taken together with an in vitro study suggesting YKT6 to be required for autophagosome-vacuole fusion in yeast (Bas *et al.*, 2018), the role of YKT6 in lysosome-autophagosome fusion appears to be evolutionarily conserved. The autoinhibitory state of farnesylated YKT6 (Wen *et al.*, 2010) and the reversible nature of YKT6 membrane association complicates the design of rescue experiments, particularly as overexpressed YKT6 has been reported to predominantly cytosolic (Gordon *et al.*, 2017). Without an easily approachable YKT6 rescue experiment, the specific role of YKT6 in endosome-lysosome fusion could be elucidated by co-immunoprecipitation experiments to determine if YKT6 complexes with lysosomal Q-SNAREs Vti1b, Syntaxin7 and Syntaxin8. Additionally, the effect of YKT6-knockdown on lysosomal delivery could be investigated in individual VAMP7- or VAMP8- knockdown cells to determine if YKT6 specifically compensates for VAMP7 as indicated by the VAMP7 rescue data. Introduction of a mutation into the zero ionic layer of YKT6 represents a useful tool that could be used to separate the regulatory or fusogenic roles of YKT6 in endolysosomal SNARE complexes.

After acidic, catalytically active endolysosomes are formed by fusion events, lysosomes must be reformed to maintain the equilibrium of neutral, storage lysosomes. As detailed in Chapter 1, studies of autolysosomes have provided the most information concerning machinery and requirements of lysosome reformation. To better address the specific question of how neutral lysosomes are derived from the highly acidic endolysosome source, I developed tools to study the V1 and Vo sectors of the V-ATPase complex. Differently fluorescently tagged V1G1 and Voa3 subunits were to be used to assess colocalisation as an estimation of V1-Vo association in the lysosome regeneration cycle. Both tagged V1G1 and Voa3 subunits independently localised to endolysosomal limiting membranes, to sucrosome limiting membranes, and to tubules protruding from sucrosomes after invertase uptake, indicating proto-lysosomes in the first stage of reformation. Both subunits individually localising to protolysosomal tubules may indicate that V1-Vo associated full V-ATPase complexes are trafficked onto the limiting membrane of the

newly forming lysosome, however due to the limitations faced with the secondary fluorophore, V1 and Vo sectors were not studied simultaneously. Preliminary evidence from immunofluorescence experiments showed V1G1 not to appear on the most peripheral Voa3-, or lgp120-marked lysosomes, which are assumed to be the least acidic lysosomes (Johnson *et al.*, 2016). The differences between the fluorescent signal in the sucrosome lumen produced by TagRFP or mOrange2 M163K compared to GFP may likely be avoidable with a tag as quenchable as GFP was demonstrated to be when the cells were clamped at pH 5. pHuji is likely to be a suitable tag to take forward due to its higher pK_a compared to mOrange2 M163K, and its greater fluorescence discrepancy between lysosomal and cytosolic pH values (Shen *et al.*, 2014). Provided pHuji fluorescence doesn't occur in the sucrosome lumen, cells co-expressing V1G1-pHuji Voa3-GFP should be taken forward. Confocal slices should be imaged in resting cells before sucrose uptake, after 24 hours sucrose incubation, when dense core lysosomes are depleted, and after a further 8 hours of invertase uptake when dense core lysosomes have been restored to the resting levels (Bright *et al.*, 1997). Manders' colocalisation coefficient should be used to calculate the proportion of Voa3-marked membrane which is also positive for V1G1, and used as a readout of the proportion of V1-Vo associated V-ATPase complexes at rest, when the terminal endocytic compartment is entirely comprised of swollen endolysosomes, or after reformation of less acidic, storage lysosomes. This proposed system employs overexpression of fluorescently tagged subunits, and as such, the dynamics of the non-fluorescent endogenous proteins will not be observed. In addition, the higher than endogenous levels of V1G1 and Voa3 may be affecting V-ATPase function and not be representative of wild type cells. To bypass these potential confounding factors, I am in the process of generating knock-in cell lines, thereby expressing tagged subunits under the control of the endogenous promoter. These cells, while avoiding any disadvantages of ectopic expression and truly representing the dynamics of endogenous V-ATPase complexes, are limited in fluorescence, as the tag is only present at endogenous protein levels. The lower brightness of knock-in tagged subunits may present a limitation in the application of microscopy and colocalisation analyses. The reversible dissociation of V1-Vo as a mechanism to control pH during lysosome reformation fits in to a network relating lysosome membrane composition, pH, and reformation. Endolysosomal phosphoinositide $PI(3,5)P_2$ has been shown in yeast to stabilise V1-Vo interaction (Li

et al., 2014). V1-Vo assembly is also promoted in HeLa cells by RILP (De Luca *et al.*, 2014), which is recruited to endolysosomes by Rab7, which is concentrated more on perinuclear, acidic lysosomes, compared to peripheral, neutral lysosomes in HeLa cells (Johnson *et al.*, 2016). It could therefore be predicted that reduction of V1-Vo assembly on reforming lysosomes occurs as a result of reduced Rab7 density, and reduced RILP-mediated V-ATPase stabilisation, leading to reduced acidification and eventual neutralisation from passive proton leakage observed in peripheral lysosomes (Johnson *et al.*, 2016). Beyond stabilising V1-Vo assembly, $PI(3,5)P_2$ activates TRPML1, which is required for lysosome reformation (Miller *et al.*, 2015), however a recent study using short-term manipulations of $PI(3,5)P_2$ suggests that PIKfyve-mediated generation of $PI(3,5)P_2$ may play a TRPML1-independent role in lysosome reformation (Bissig *et al.*, 2017).

The final aim of this thesis was to develop a set of tools that could report lysosomal health by measuring activity of the TFEB-CLEAR signalling network. First, a high throughput automated TFEB translocation assay was developed to use as a screen for lysosome perturbation by small molecule pharmacological agents. This assay gave a robust and reliable readout of a variety of lysosomal stress conditions, including V-ATPase inhibition, lysosomotropic drug accumulation, amino acid starvation, bacterial virulence protein uptake, and activation of lysosomal Ca^{2+} channels. Short and long TFEB-activating incubations with CQ were applied to cells which were then analysed for expression changes of a broad selection of lysosomal genes in response to TFEB activation across different time points. None of the genes analysed were consistently >1.5 fold upregulated, however a subset of genes that showed the greatest fold change at any single time point were taken forward as reporters for further experiments. Expression of the subset of reporter genes was analysed in cells starved of amino acids, treated with TRPML1 activator ML-SA1, or treated with mTOR inhibitor torin1. Torin1-treated cells showed only downregulation of gene expression, which seems counterintuitive compared to its powerful effect on TFEB translocation to the nucleus. A small downregulation of some genes was also observed in ML-SA1-treated incubation with ML-SA1, however these conditions also caused a significant upregulation of NEU1, so at the very least, the responses of these genes are not consistent with one another. Amino acid starvation induced

significant upregulation of every gene in the subset by 8 hours, and continued to 16 hours starvation. In this instance, the genes did show a consistent response.

These data suggest that gene regulation may not give a consistent response to different TFEB-activating conditions, but may be robust and consistent in reporting starvation. The relatively narrow dynamic range of gene upregulation along with the inconsistency of gene responses brings into question the utility of such a study as a universal reporter of lysosomal perturbation. The different responses to each mode of TFEB activation may be dependent on currently unknown TFEB-interacting machinery. In fact, much of the current understanding of how TFEB integrates signalling pathways to control TFEB translocation dynamics has only emerged in the last few years and there is undoubtedly more unidentified machinery involved. While phosphoproteomic studies show that TFEB undergoes phosphorylation at over 20 sites, only 9 of these sites have been shown to be phosphorylated in functional studies (reviewed in Puertollano 2018). TFEB activity can be controlled by changes in localisation in response to phosphorylation by a number of kinases including ERK1/2, GSK3β and AKT (Settembre *et al.*, 2011; Li *et al.*, 2016; Palmieri *et al.*, 2017), or ester binding, blocking the 14-3-3 binding site (Song *et al.*, 2016). TFEB phosphorylation has also been shown to affect TFEB stability by STUB1-mediated ubiquitylation and consequent promotion of its proteasomal degradation (Sha *et al.*, 2017). Phosphorylation-related effects on TFEB are also modulated by phosphatases, of which only calcineurin has yet been identified (Medina *et al.*, 2015). Beyond phosphorylation, TFEB also appears to be regulated at the level of nuclear export, as incubation with CRM1-mediated nuclear export inhibitor leptomycin B induced nuclear accumulation of TFEB-GFP in NRK cells (Figure 7.1). This effect was also recently reported in MCF7 (Li *et al.*, 2018), HeLa and HEK293T cells (Napolitano *et al.*, 2018), where the nuclear export sequence (NES) was determined to be adjacent to the mTORC1- and ERK1/2-phosphorylatable S142.

Figure 7.1

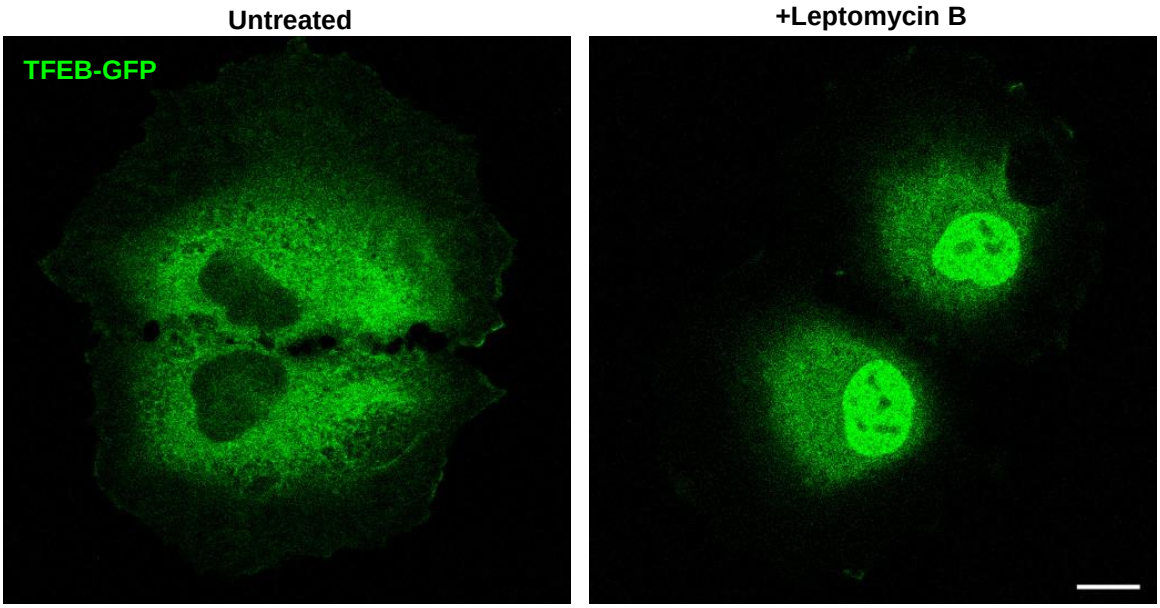

Figure 7.1: Leptomycin B treatment causes nuclear accumulation of TFEB-GFP in NRK cells

Confocal fluorescence microscopy images of clonal NRK cells stably expressing TFEB-GFP which were incubated with or without 20nM leptomycin B for 30 minutes. Scale bar represents 10µm.

By analysing full length human TFEB sequence using the NetNES 1.1 server to predict NES locations (la Cour *et al.*, 2004), the sequence starting at L435, reading as LMLLDDSLLPL, reached the threshold for NES detection (Figure 7.2A) and had the characteristics of a class 3 (Φ-X2-Φ-X3-Φ-X2-Φ) Kosugi NES consensus sequence (Xu *et al.*, 2012; Kosugi *et al.*, 2008). This suggests that in full length TFEB there may be an additional NES to that adjacent to S142. In future experiments to explore whether this additional predicted NES is functional, TFEB with L435A, L438A, L442A, and L445A mutations of the bulky hydrophobic residues (Figure 7.2B); based on NES-impairment of NS1 (TynellMelén and Julkunen, 2014), will be expressed in cells to determine the contribution of this NES to TFEB

localisation and dynamics. On a broader scale, additional machinery in the TFEB pathway could be identified using CRISPR library-based forward genetic screen. For this approach (see for example (Burr *et al.*, 2016)), a cell line expressing a fluorescently-labelled reporter for the downstream effects of TFEB transcription activity, such as a knock-in of a highly responsive CLEAR element gene, would need to be generated. These cells could be transfected with a CRISPR library, and clones which display reduced reporter fluorescence in response to stimulus would be sorted by FACS, then sequenced to reveal which genes' depletion reduced the function of TFEB, and are potentially involved in the function of the TFEB pathway.

Figure 7.2

A

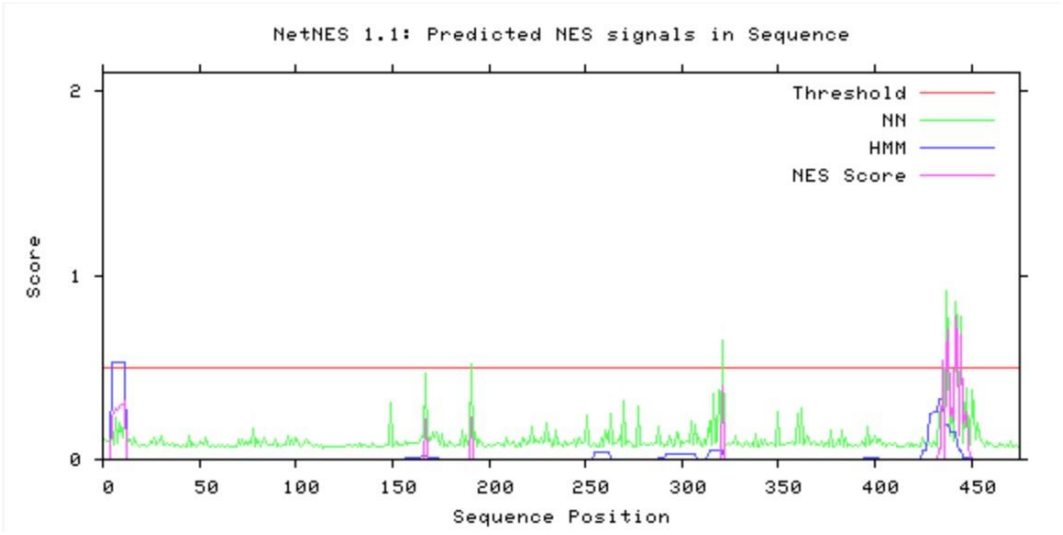

B

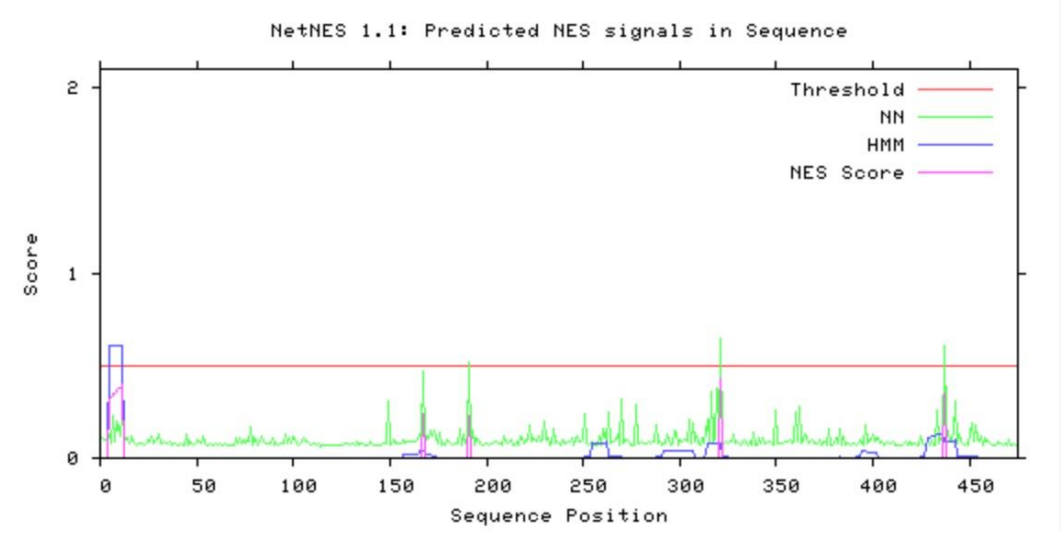

Figure 7.2: NetNES 1.1 prediction identifies a class 3 Kosugi consensus NES beginning at L435 in TFEB

(A) Computational prediction of NES signals in wild type full length human TFEB sequence.

(B) Computational prediction of NES signals in full length human TFEB after bulky hydrophobic residue mutations L435A, L438A, L442A, and L445A.

References

Anderson, N. and Borlak, J. (2006) 'Drug-induced phospholipidosis', *FEBS Lett,* 580(23), pp. 5533-40.

Antonin, W., Holroyd, C., Fasshauer, D., Pabst, S., Von Mollard, G. F. and Jahn, R. (2000) 'A SNARE complex mediating fusion of late endosomes defines conserved properties of SNARE structure and function', *EMBO J,* 19(23), pp. 6453-64.

Arighi, C. N., Hartnell, L. M., Aguilar, R. C., Haft, C. R. and Bonifacino, J. S. (2004) 'Role of the mammalian retromer in sorting of the cation-independent mannose 6-phosphate receptor', *J Cell Biol,* 165(1), pp. 123-33.

Avinoam, O., Schorb, M., Beese, C. J., Briggs, J. A. and Kaksonen, M. (2015) 'ENDOCYTOSIS. Endocytic sites mature by continuous bending and remodeling of the clathrin coat', *Science,* 348(6241), pp. 1369-72.

Bache, K. G., Stuffers, S., Malerød, L., Slagsvold, T., Raiborg, C., Lechardeur, D., Wälchli, S., Lukacs, G. L., Brech, A. and Stenmark, H. (2006) 'The ESCRT-III subunit hVps24 is required for degradation but not silencing of the epidermal growth factor receptor', *Mol Biol Cell,* 17(6), pp. 2513-23.

Baravalle, G., Schober, D., Huber, M., Bayer, N., Murphy, R. F. and Fuchs, R. (2005) 'Transferrin recycling and dextran transport to lysosomes is differentially affected by bafilomycin, nocodazole, and low temperature', *Cell Tissue Res,* 320(1), pp. 99-113.

Barriere, H., Nemes, C., Lechardeur, D., Khan-Mohammad, M., Fruh, K. and Lukacs, G. L. (2006) 'Molecular basis of oligoubiquitin-dependent internalization of membrane proteins in Mammalian cells', *Traffic,* 7(3), pp. 282-97.

Bas, L., Papinski, D., Licheva, M., Torggler, R., Rohringer, S., Schuschnig, M. and Kraft, C. (2018) 'Reconstitution reveals Ykt6 as the autophagosomal SNARE in autophagosome-vacuole fusion', *J Cell Biol*.

Bayer, M. J., Reese, C., Buhler, S., Peters, C. and Mayer, A. (2003) 'Vacuole membrane fusion: V0 functions after trans-SNARE pairing and is coupled to the Ca2+-releasing channel', *J Cell Biol,* 162(2), pp. 211-22.

Bethani, I., Werner, A., Kadian, C., Geumann, U., Jahn, R. and Rizzoli, S. O. (2009) 'Endosomal fusion upon SNARE knockdown is maintained by residual SNARE activity and enhanced docking', *Traffic,* 10(10), pp. 1543-59.

Bhargava, A., Voronov, I., Wang, Y., Glogauer, M., Kartner, N. and Manolson, M. F. (2012) 'Osteopetrosis mutation R444L causes endoplasmic reticulum retention and misprocessing of vacuolar H+-ATPase a3 subunit', *J Biol Chem,* 287(32), pp. 26829-39.

Bissig, C., Hurbain, I., Raposo, G. and van Niel, G. (2017) 'PIKfyve activity regulates reformation of terminal storage lysosomes from endolysosomes', *Traffic,* 18(11), pp. 747-757.

Bitsikas, V., Corrêa, I. R. and Nichols, B. J. (2014) 'Clathrin-independent pathways do not contribute significantly to endocytic flux', *Elife,* 3, pp. e03970.

Bonifacino, J. S. and Glick, B. S. (2004) 'The mechanisms of vesicle budding and fusion', *Cell,* 116(2), pp. 153-66.

Bonifacino, J. S. and Traub, L. M. (2003) 'Signals for sorting of transmembrane proteins to endosomes and lysosomes', *Annu Rev Biochem,* 72, pp. 395-447.

Brandhorst, D., Zwilling, D., Rizzoli, S. O., Lippert, U., Lang, T. and Jahn, R. (2006) 'Homotypic fusion of early endosomes: SNAREs do not determine fusion specificity', *Proc Natl Acad Sci U S A,* 103(8), pp. 2701-6.

Bright, N. A., Davis, L. J. and Luzio, J. P. (2016) 'Endolysosomes Are the Principal Intracellular Sites of Acid Hydrolase Activity', *Curr Biol,* 26(17), pp. 2233-45.

Bright, N. A., Gratian, M. J. and Luzio, J. P. (2005) 'Endocytic delivery to lysosomes mediated by concurrent fusion and kissing events in living cells', *Curr Biol,* 15(4), pp. 360-5.

Bright, N. A., Reaves, B. J., Mullock, B. M. and Luzio, J. P. (1997) 'Dense core lysosomes can fuse with late endosomes and are re-formed from the resultant hybrid organelles', *J Cell Sci,* 110 (Pt 17), pp. 2027-40.

Buckley, C. M. and King, J. S. (2017) 'Drinking problems: mechanisms of macropinosome formation and maturation', *FEBS J,* 284(22), pp. 3778-3790.

Burd, C. and Cullen, P. J. (2014) 'Retromer: a master conductor of endosome sorting', *Cold Spring Harb Perspect Biol,* 6(2).

Burr, S. P., Costa, A. S., Grice, G. L., Timms, R. T., Lobb, I. T., Freisinger, P., Dodd, R. B., Dougan, G., Lehner, P. J., Frezza, C. and Nathan, J. A. (2016) 'Mitochondrial Protein Lipoylation and the 2-Oxoglutarate Dehydrogenase Complex Controls HIF1α Stability in Aerobic Conditions', *Cell Metab,* 24(5), pp. 740-752.

Butor, C., Griffiths, G., Aronson, N. N. and Varki, A. (1995) 'Co-localization of hydrolytic enzymes with widely disparate pH optima: implications for the regulation of lysosomal pH', *J Cell Sci,* 108 (Pt 6), pp. 2213-9.

Cao, Q., Zhong, X. Z., Zou, Y., Murrell-Lagnado, R., Zhu, M. X. and Dong, X. P. (2015) 'Calcium release through P2X4 activates calmodulin to promote endolysosomal membrane fusion', *J Cell Biol,* 209(6), pp. 879-94.

Capel, R. A., Bolton, E. L., Lin, W. K., Aston, D., Wang, Y., Liu, W., Wang, X., Burton, R. A., Bloor-Young, D., Shade, K. T., Ruas, M., Parrington, J., Churchill, G. C., Lei, M., Galione, A. and Terrar, D. A. (2015) 'Two-pore Channels (TPC2s) and Nicotinic Acid Adenine Dinucleotide Phosphate (NAADP) at Lysosomal-Sarcoplasmic Reticular Junctions Contribute to Acute and Chronic β-Adrenoceptor Signaling in the Heart', *J Biol Chem,* 290(50), pp. 30087-98.

Carlton, J., Bujny, M., Peter, B. J., Oorschot, V. M., Rutherford, A., Mellor, H., Klumperman, J., McMahon, H. T. and Cullen, P. J. (2004) 'Sorting nexin-1 mediates tubular endosome-to-TGN transport through coincidence sensing of high- curvature membranes and 3-phosphoinositides', *Curr Biol,* 14(20), pp. 1791-800.

Carnell, M., Zech, T., Calaminus, S. D., Ura, S., Hagedorn, M., Johnston, S. A., May, R. C., Soldati, T., Machesky, L. M. and Insall, R. H. (2011) 'Actin polymerization driven by WASH causes V-ATPase retrieval and vesicle neutralization before exocytosis', *J Cell Biol,* 193(5), pp. 831-9.

Chauhan, S., Goodwin, J. G., Manyam, G., Wang, J., Kamat, A. M. and Boyd, D. D. (2013) 'ZKSCAN3 is a master transcriptional repressor of autophagy', *Mol Cell,* 50(1), pp. 16-28.

Christensen, K. A., Myers, J. T. and Swanson, J. A. (2002) 'pH-dependent regulation of lysosomal calcium in macrophages', *J Cell Sci,* 115(Pt 3), pp. 599-607.

Clague, M. J., Urbé, S., Aniento, F. and Gruenberg, J. (1994) 'Vacuolar ATPase activity is required for endosomal carrier vesicle formation', *J Biol Chem,* 269(1), pp. 21-4.

Clapper, D. L., Walseth, T. F., Dargie, P. J. and Lee, H. C. (1987) 'Pyridine nucleotide metabolites stimulate calcium release from sea urchin egg microsomes desensitized to inositol trisphosphate', *J Biol Chem,* 262(20), pp. 9561-8.

Cohn, Z. A. and Ehrenreich, B. A. (1969) 'The uptake, storage, and intracellular hydrolysis of carbohydrates by macrophages', *J Exp Med,* 129(1), pp. 201-25.

Colacurcio, D. J. and Nixon, R. A. (2016) 'Disorders of lysosomal acidification-The emerging role of v-ATPase in aging and neurodegenerative disease', *Ageing Res Rev,* 32, pp. 75-88.

Coonrod, E. M., Graham, L. A., Carpp, L. N., Carr, T. M., Stirrat, L., Bowers, K., Bryant, N. J. and Stevens, T. H. (2013) 'Homotypic vacuole fusion in yeast requires organelle acidification and not the V-ATPase membrane domain', *Dev Cell,* 27(4), pp. 462-8.

Danglot, L., Zylbersztejn, K., Petkovic, M., Gauberti, M., Meziane, H., Combe, R., Champy, M. F., Birling, M. C., Pavlovic, G., Bizot, J. C., Trovero, F., Della Ragione, F., Proux-Gillardeaux, V., Sorg, T., Vivien, D., D'Esposito, M. and Galli, T. (2012) 'Absence of TI-VAMP/Vamp7 leads to increased anxiety in mice', *J Neurosci,* 32(6), pp. 1962-8.

Daniel, W. A., Bickel, M. H. and Honegger, U. E. (1995) 'The contribution of lysosomal trapping in the uptake of desipramine and chloroquine by different tissues', *Pharmacol Toxicol,* 77(6), pp. 402-6.

Daniel, W. A. and Wójcikowski, J. (1999) 'The role of lysosomes in the cellular distribution of thioridazine and potential drug interactions', *Toxicol Appl Pharmacol,* 158(2), pp. 115-24.

de Duve, C. (2005) 'The lysosome turns fifty', *Nat Cell Biol,* 7(9), pp. 847-9.

De Leo, M. G., Staiano, L., Vicinanza, M., Luciani, A., Carissimo, A., Mutarelli, M., Di Campli, A., Polishchuk, E., Di Tullio, G., Morra, V., Levtchenko, E., Oltrabella, F., Starborg, T., Santoro, M., Di Bernardo, D., Devuyst, O., Lowe, M., Medina, D. L., Ballabio, A. and De Matteis, M. A. (2016) 'Autophagosome-lysosome fusion triggers a lysosomal response mediated by TLR9 and controlled by OCRL', *Nat Cell Biol,* 18(8), pp. 839-850.

De Luca, M., Cogli, L., Progida, C., Nisi, V., Pascolutti, R., Sigismund, S., Di Fiore, P. P. and Bucci, C. (2014) 'RILP regulates vacuolar ATPase through interaction with the V1G1 subunit', *J Cell Sci,* 127(Pt 12), pp. 2697-708.

Dell'Antone, P. (1979) 'Evidence for an ATP-driven "proton pump" in rat liver lysosomes by basic dyes uptake', *Biochem Biophys Res Commun,* 86(1), pp. 180-9.

Deriy, L. V., Gomez, E. A., Zhang, G., Beacham, D. W., Hopson, J. A., Gallan, A. J., Shevchenko, P. D., Bindokas, V. P. and Nelson, D. J. (2009) 'Disease-causing mutations in the cystic fibrosis transmembrane conductance regulator determine the functional responses of alveolar macrophages', *J Biol Chem,* 284(51), pp. 35926-38.

Di Malta, C., Siciliano, D., Calcagni, A., Monfregola, J., Punzi, S., Pastore, N., Eastes, A. N., Davis, O., De Cegli, R., Zampelli, A., Di Giovannantonio, L. G., Nusco, E., Platt, N., Guida, A., Ogmundsdottir, M. H., Lanfrancone, L., Perera, R. M., Zoncu, R., Pelicci, P. G., Settembre, C. and Ballabio, A. (2017) 'Transcriptional activation of RagD GTPase controls mTORC1 and promotes cancer growth', *Science,* 356(6343), pp. 1188-1192.

DiCiccio, J. E. and Steinberg, B. E. (2011) 'Lysosomal pH and analysis of the counter ion pathways that support acidification', *J Gen Physiol,* 137(4), pp. 385-90.

Doherty, G. J. and McMahon, H. T. (2009) 'Mechanisms of endocytosis', *Annu Rev Biochem,* 78, pp. 857-902.

Dong, X. P., Shen, D., Wang, X., Dawson, T., Li, X., Zhang, Q., Cheng, X., Zhang, Y., Weisman, L. S., Delling, M. and Xu, H. (2010) 'PI(3,5)P(2) controls membrane trafficking by direct activation of mucolipin Ca(2+) release channels in the endolysosome', *Nat Commun,* 1, pp. 38.

Doray, B., Ghosh, P., Griffith, J., Geuze, H. J. and Kornfeld, S. (2002) 'Cooperation of GGAs and AP-1 in packaging MPRs at the trans-Golgi network', *Science,* 297(5587), pp. 1700-3.

Dove, S. K., Dong, K., Kobayashi, T., Williams, F. K. and Michell, R. H. (2009) 'Phosphatidylinositol 3,5-bisphosphate and Fab1p/PIKfyve underPPIn endo-lysosome function', *Biochem J,* 419(1), pp. 1-13.

Du, W., Su, Q. P., Chen, Y., Zhu, Y., Jiang, D., Rong, Y., Zhang, S., Zhang, Y., Ren, H., Zhang, C., Wang, X., Gao, N., Wang, Y., Sun, L., Sun, Y. and Yu, L. (2016) 'Kinesin 1 Drives Autolysosome Tubulation', *Dev Cell,* 37(4), pp. 326-336.

Du, X., Kumar, J., Ferguson, C., Schulz, T. A., Ong, Y. S., Hong, W., Prinz, W. A., Parton, R. G., Brown, A. J. and Yang, H. (2011) 'A role for oxysterol-binding protein-related protein 5 in endosomal cholesterol trafficking', *J Cell Biol,* 192(1), pp. 121-35.

Dunn, K. W., Kamocka, M. M. and McDonald, J. H. (2011) 'A practical guide to evaluating colocalization in biological microscopy', *Am J Physiol Cell Physiol,* 300(4), pp. C723-42.

Edeling, M. A., Mishra, S. K., Keyel, P. A., Steinhauser, A. L., Collins, B. M., Roth, R., Heuser, J. E., Owen, D. J. and Traub, L. M. (2006) 'Molecular switches involving the AP-2 beta2 appendage regulate endocytic cargo selection and clathrin coat assembly', *Dev Cell,* 10(3), pp. 329-42.

Edgar, J. R., Eden, E. R. and Futter, C. E. (2014) 'Hrs- and CD63-dependent competing mechanisms make different sized endosomal intraluminal vesicles', *Traffic,* 15(2), pp. 197-211.

Egami, Y. (2016) 'Molecular imaging analysis of Rab GTPases in the regulation of phagocytosis and macropinocytosis', *Anat Sci Int,* 91(1), pp. 35-42.

Eltschinger, S. and Loewith, R. (2016) 'TOR Complexes and the Maintenance of Cellular Homeostasis', *Trends Cell Biol,* 26(2), pp. 148-159.

Fernandez-Mora, E., Polidori, M., Lührmann, A., Schaible, U. E. and Haas, A. (2005) 'Maturation of Rhodococcus equi-containing vacuoles is arrested after completion of the early endosome stage', *Traffic,* 6(8), pp. 635-53.

Folts, C. J., Scott-Hewitt, N., Pröschel, C., Mayer-Pröschel, M. and Noble, M. (2016) 'Lysosomal Re-acidification Prevents Lysosphingolipid-Induced Lysosomal Impairment and Cellular Toxicity', *PLoS Biol,* 14(12), pp. e1002583.

Friedman, J. R., Lackner, L. L., West, M., DiBenedetto, J. R., Nunnari, J. and Voeltz, G. K. (2011) 'ER tubules mark sites of mitochondrial division', *Science,* 334(6054), pp. 358-62.

Fujiwara, T., Ye, S., Castro-Gomes, T., Winchell, C. G., Andrews, N. W., Voth, D. E., Varughese, K. I., Mackintosh, S. G., Feng, Y., Pavlos, N., Nakamura, T., Manolagas, S. C. and Zhao, H. (2016) 'PLEKHM1/DEF8/RAB7 complex regulates lysosome positioning and bone homeostasis', *JCI Insight,* 1(17), pp. e86330.

Fukasawa, M., Varlamov, O., Eng, W. S., Söllner, T. H. and Rothman, J. E. (2004) 'Localization and activity of the SNARE Ykt6 determined by its regulatory domain and palmitoylation', *Proc Natl Acad Sci U S A,* 101(14), pp. 4815-20.

Fukuda, R., McNew, J. A., Weber, T., Parlati, F., Engel, T., Nickel, W., Rothman, J. E. and Söllner, T. H. (2000) 'Functional architecture of an intracellular membrane t-SNARE', *Nature,* 407(6801), pp. 198-202.

Futter, C. E., Pearse, A., Hewlett, L. J. and Hopkins, C. R. (1996) 'Multivesicular endosomes containing internalized EGF-EGF receptor complexes mature and then fuse directly with lysosomes', *J Cell Biol,* 132(6), pp. 1011-23.

Garrity, A. G., Wang, W., Collier, C. M., Levey, S. A., Gao, Q. and Xu, H. (2016) 'The endoplasmic reticulum, not the pH gradient, drives calcium refilling of lysosomes', *Elife,* 5.

Gatta, A. T. and Levine, T. P. (2017) 'Piecing Together the Patchwork of Contact Sites', *Trends Cell Biol,* 27(3), pp. 214-229.

Glock, M., Muehlbacher, M., Hurtig, H., Tripal, P. and Kornhuber, J. (2016) 'Drug-induced phospholipidosis caused by combinations of common drugs in vitro', *Toxicol In Vitro,* 35, pp. 139-48.

Glukhova, A., Hinkovska-Galcheva, V., Kelly, R., Abe, A., Shayman, J. A. and Tesmer, J. J. (2015) 'Structure and function of lysosomal phospholipase A2 and lecithin:cholesterol acyltransferase', *Nat Commun,* 6, pp. 6250.

Goldman, S. D., Funk, R. S., Rajewski, R. A. and Krise, J. P. (2009) 'Mechanisms of amine accumulation in, and egress from, lysosomes', *Bioanalysis,* 1(8), pp. 1445-59.

Goldman, S. D. and Krise, J. P. (2010) 'Niemann-Pick C1 functions independently of Niemann-Pick C2 in the initial stage of retrograde transport of membrane-impermeable lysosomal cargo', *J Biol Chem,* 285(7), pp. 4983-94.

Gordon, D. E., Chia, J., Jayawardena, K., Antrobus, R., Bard, F. and Peden, A. A. (2017) 'VAMP3/Syb and YKT6 are required for the fusion of constitutive secretory carriers with the plasma membrane', *PLoS Genet,* 13(4), pp. e1006698.
Gordon, D. E., Mirza, M., Sahlender, D. A., Jakovleska, J. and Peden, A. A. (2009) 'Coiled-coil interactions are required for post-Golgi R-SNARE trafficking', *EMBO Rep,* 10(8), pp. 851-6.

Graves, A. R., Curran, P. K., Smith, C. L. and Mindell, J. A. (2008) 'The Cl-/H+ antiporter ClC-7 is the primary chloride permeation pathway in lysosomes', *Nature,* 453(7196), pp. 788-92.

Grimm, C., Holdt, L. M., Chen, C. C., Hassan, S., Müller, C., Jörs, S., Cuny, H., Kissing, S., Schröder, B., Butz, E., Northoff, B., Castonguay, J., Luber, C. A., Moser, M., Spahn, S., Lüllmann-Rauch, R., Fendel, C., Klugbauer, N., Griesbeck, O., Haas, A., Mann, M., Bracher, F., Teupser, D., Saftig, P., Biel, M. and Wahl-Schott, C. (2014) 'High susceptibility to fatty liver disease in two-pore channel 2-deficient mice', *Nat Commun,* 5, pp. 4699.

Guardia, C. M., Farías, G. G., Jia, R., Pu, J. and Bonifacino, J. S. (2016) 'BORC Functions Upstream of Kinesins 1 and 3 to Coordinate Regional Movement of Lysosomes along Different Microtubule Tracks', *Cell Rep,* 17(8), pp. 1950-1961.

Haggie, P. M. and Verkman, A. S. (2007) 'Cystic fibrosis transmembrane conductance regulator-independent phagosomal acidification in macrophages', *J Biol Chem,* 282(43), pp. 31422-8.

Haggie, P. M. and Verkman, A. S. (2009a) 'Defective organellar acidification as a cause of cystic fibrosis lung disease: reexamination of a recurring hypothesis', *Am J Physiol Lung Cell Mol Physiol,* 296(6), pp. L859-67.

Haggie, P. M. and Verkman, A. S. (2009b) 'Unimpaired lysosomal acidification in respiratory epithelial cells in cystic fibrosis', *J Biol Chem,* 284(12), pp. 7681-6.

Hammond, G. R., Takasuga, S., Sasaki, T. and Balla, T. (2015) 'The ML1Nx2 Phosphatidylinositol 3,5-Bisphosphate Probe Shows Poor Selectivity in Cells', *PLoS One,* 10(10), pp. e0139957.

Harikumar, P. and Reeves, J. P. (1983) 'The lysosomal proton pump is electrogenic', *J Biol Chem,* 258(17), pp. 10403-10.

Hariri, H., Ugrankar, R., Liu, Y. and Henne, W. M. (2016) 'Inter-organelle ER-endolysosomal contact sites in metabolism and disease across evolution', *Commun Integr Biol,* 9(3), pp. e1156278.

Hasegawa, J., Strunk, B. S. and Weisman, L. S. (2017) 'PI5P and PI(3,5)P', *Cell Struct Funct,* 42(1), pp. 49-60.

Haupts, U., Maiti, S., Schwille, P. and Webb, W. W. (1998) 'Dynamics of fluorescence fluctuations in green fluorescent protein observed by fluorescence correlation spectroscopy', *Proc Natl Acad Sci U S A,* 95(23), pp. 13573-8.

Henne, W. M., Buchkovich, N. J., Zhao, Y. and Emr, S. D. (2012) 'The endosomal sorting complex ESCRT-II mediates the assembly and architecture of ESCRT-III helices', *Cell,* 151(2), pp. 356-71.

Hickey, C. M. and Wickner, W. (2010) 'HOPS initiates vacuole docking by tethering membranes before trans-SNARE complex assembly', *Mol Biol Cell,* 21(13), pp. 2297-305.

Higuchi, T., Nishikawa, J. and Inoue, H. (2015) 'Sucrose induces vesicle accumulation and autophagy', *J Cell Biochem,* 116(4), pp. 609-17.

Hirst, J., Edgar, J. R., Esteves, T., Darios, F., Madeo, M., Chang, J., Roda, R. H., Dürr, A., Anheim, M., Gellera, C., Li, J., Züchner, S., Mariotti, C., Stevanin, G., Blackstone, C., Kruer, M. C. and Robinson, M. S. (2015) 'Loss of AP-5 results in accumulation of aberrant endolysosomes: defining a new type of lysosomal storage disease', *Hum Mol Genet,* 24(17), pp. 4984-96.

Holland, P., Torgersen, M. L., Sandvig, K. and Simonsen, A. (2014) 'LYST affects lysosome size and quantity, but not trafficking or degradation through autophagy or endocytosis', *Traffic,* 15(12), pp. 1390-405.

Huotari, J. and Helenius, A. (2011) 'Endosome maturation', *EMBO J,* 30(17), pp. 3481-500.
Jain, S., Bloom, B. R. and Hondalus, M. K. (2003) 'Deletion of vapA encoding Virulence Associated Protein A attenuates the intracellular actinomycete Rhodococcus equi', *Mol Microbiol,* 50(1), pp. 115-28.

Jefferies, H. B., Cooke, F. T., Jat, P., Boucheron, C., Koizumi, T., Hayakawa, M., Kaizawa, H., Ohishi, T., Workman, P., Waterfield, M. D. and Parker, P. J. (2008) 'A selective PIKfyve inhibitor blocks PtdIns(3,5)P(2) production and disrupts endomembrane transport and retroviral budding', *EMBO Rep,* 9(2), pp. 164-70.

Jia, J., Abudu, Y. P., Claude-Taupin, A., Gu, Y., Kumar, S., Choi, S. W., Peters, R., Mudd, M. H., Allers, L., Salemi, M., Phinney, B., Johansen, T. and Deretic, V. (2018) 'Galectins Control mTOR in Response to Endomembrane Damage', *Mol Cell,* 70(1), pp. 120-135.e8.

Johnson, D. E., Ostrowski, P., Jaumouillé, V. and Grinstein, S. (2016) 'The position of lysosomes within the cell determines their luminal pH', *J Cell Biol,* 212(6), pp. 677-92.

Jongsma, M. L., Berlin, I., Wijdeven, R. H., Janssen, L., Janssen, G. M., Garstka, M. A., Janssen, H., Mensink, M., van Veelen, P. A., Spaapen, R. M. and Neefjes, J. (2016) 'An ER-Associated Pathway Defines Endosomal Architecture for Controlled Cargo Transport', *Cell,* 166(1), pp. 152-66.

Jordens, I., Fernandez-Borja, M., Marsman, M., Dusseljee, S., Janssen, L., Calafat, J., Janssen, H., Wubbolts, R. and Neefjes, J. (2001) 'The Rab7 effector protein RILP controls lysosomal transport by inducing the recruitment of dynein-dynactin motors', *Curr Biol,* 11(21), pp. 1680-5.

Jovic, M., Sharma, M., Rahajeng, J. and Caplan, S. (2010) 'The early endosome: a busy sorting station for proteins at the crossroads', *Histol Histopathol,* 25(1), pp. 99-112.

Kane, P. M. (1995) 'Disassembly and reassembly of the yeast vacuolar H(+)-ATPase in vivo', *J Biol Chem,* 270(28), pp. 17025-32.

Karim, M. A., Samyn, D. R., Mattie, S. and Brett, C. L. (2018) 'Distinct features of multivesicular body-lysosome fusion revealed by a new cell-free content-mixing assay', *Traffic,* 19(2), pp. 138-149.

Kartner, N., Yao, Y., Bhargava, A. and Manolson, M. F. (2013) 'Topology, glycosylation and conformational changes in the membrane domain of the vacuolar H+-ATPase a subunit', *J Cell Biochem,* 114(7), pp. 1474-87.

Kasper, D., Planells-Cases, R., Fuhrmann, J. C., Scheel, O., Zeitz, O., Ruether, K., Schmitt, A., Poët, M., Steinfeld, R., Schweizer, M., Kornak, U. and Jentsch, T. J. (2005) 'Loss of the chloride channel ClC-7 leads to lysosomal storage disease and neurodegeneration', *EMBO J,* 24(5), pp. 1079-91.

Kawai, A., Uchiyama, H., Takano, S., Nakamura, N. and Ohkuma, S. (2007) 'Autophagosome-lysosome fusion depends on the pH in acidic compartments in CHO cells', *Autophagy,* 3(2), pp. 154-7.

Kawasaki-Nishi, S., Nishi, T. and Forgac, M. (2001) 'Yeast V-ATPase complexes containing different isoforms of the 100-kDa a-subunit differ in coupling efficiency and in vivo dissociation', *J Biol Chem,* 276(21), pp. 17941-8.

Kazmi, F., Hensley, T., Pope, C., Funk, R. S., Loewen, G. J., Buckley, D. B. and Parkinson, A. (2013) 'Lysosomal sequestration (trapping) of lipophilic amine (cationic amphiphilic) drugs in immortalized human hepatocytes (Fa2N-4 cells)', *Drug Metab Dispos,* 41(4), pp. 897-905.

Kelly, B. T. and Owen, D. J. (2011) 'Endocytic sorting of transmembrane protein cargo', *Curr Opin Cell Biol,* 23(4), pp. 404-12.

Kerr, M. C. and Teasdale, R. D. (2009) 'Defining macropinocytosis', *Traffic,* 10(4), pp. 364-71.
Khatter, D., Raina, V. B., Dwivedi, D., Sindhwani, A., Bahl, S. and Sharma, M. (2015) 'The small GTPase Arl8b regulates assembly of the mammalian HOPS complex on lysosomes', *J Cell Sci,* 128(9), pp. 1746-61.

Kilpatrick, B. S., Eden, E. R., Schapira, A. H., Futter, C. E. and Patel, S. (2013) 'Direct mobilisation of lysosomal Ca2+ triggers complex Ca2+ signals', *J Cell Sci,* 126(Pt 1), pp. 60-6.

Kinchen, J. M. and Ravichandran, K. S. (2010) 'Identification of two evolutionarily conserved genes regulating processing of engulfed apoptotic cells', *Nature,* 464(7289), pp. 778-82.

Kornak, U., Kasper, D., Bösl, M. R., Kaiser, E., Schweizer, M., Schulz, A., Friedrich, W., Delling, G. and Jentsch, T. J. (2001) 'Loss of the ClC-7 chloride channel leads to osteopetrosis in mice and man', *Cell,* 104(2), pp. 205-15.

Kosugi, S., Hasebe, M., Tomita, M. and Yanagawa, H. (2008) 'Nuclear export signal consensus sequences defined using a localization-based yeast selection system', *Traffic,* 9(12), pp. 2053-62.

la Cour, T., Kiemer, L., Mølgaard, A., Gupta, R., Skriver, K. and Brunak, S. (2004) 'Analysis and prediction of leucine-rich nuclear export signals', *Protein Eng Des Sel,* 17(6), pp. 527-36.

Lafourcade, C., Sobo, K., Kieffer-Jaquinod, S., Garin, J. and van der Goot, F. G. (2008) 'Regulation of the V-ATPase along the endocytic pathway occurs through reversible subunit association and membrane localization', *PLoS One,* 3(7), pp. e2758.

Lange, P. F., Wartosch, L., Jentsch, T. J. and Fuhrmann, J. C. (2006) 'ClC-7 requires Ostm1 as a beta-subunit to support bone resorption and lysosomal function', *Nature,* 440(7081), pp. 220-3.

Larionov, A., Krause, A. and Miller, W. (2005) 'A standard curve based method for relative real time PCR data processing', *BMC Bioinformatics,* 6, pp. 62.

Lassen, K. G., McKenzie, C. I., Mari, M., Murano, T., Begun, J., Baxt, L. A., Goel, G., Villablanca, E. J., Kuo, S. Y., Huang, H., Macia, L., Bhan, A. K., Batten, M., Daly, M. J., Reggiori, F., Mackay, C. R. and

Xavier, R. J. (2016) 'Genetic Coding Variant in GPR65 Alters Lysosomal pH and Links Lysosomal Dysfunction with Colitis Risk', *Immunity,* 44(6), pp. 1392-405.

Lemmon, S. K. (2001) 'Clathrin uncoating: Auxilin comes to life', *Curr Biol,* 11(2), pp. R49-52.
Li, L., Friedrichsen, H. J., Andrews, S., Picaud, S., Volpon, L., Ngeow, K., Berridge, G., Fischer, R., Borden, K. L. B., Filippakopoulos, P. and Goding, C. R. (2018) 'A TFEB nuclear export signal integrates amino acid supply and glucose availability', *Nat Commun,* 9(1), pp. 2685.

Li, S. C., Diakov, T. T., Xu, T., Tarsio, M., Zhu, W., Couoh-Cardel, S., Weisman, L. S. and Kane, P. M. (2014) 'The signaling lipid PI(3,5)P_2 stabilizes V_1-V(o) sector interactions and activates the V-ATPase', *Mol Biol Cell,* 25(8), pp. 1251-62.

Li, X., Wang, X., Zhang, X., Zhao, M., Tsang, W. L., Zhang, Y., Yau, R. G., Weisman, L. S. and Xu, H. (2013) 'Genetically encoded fluorescent probe to visualize intracellular phosphatidylinositol 3,5-bisphosphate localization and dynamics', *Proc Natl Acad Sci U S A,* 110(52), pp. 21165-70.

Li, Y., Xu, M., Ding, X., Yan, C., Song, Z., Chen, L., Huang, X., Wang, X., Jian, Y., Tang, G., Tang, C., Di, Y., Mu, S., Liu, X., Liu, K., Li, T., Wang, Y., Miao, L., Guo, W., Hao, X. and Yang, C. (2016) 'Protein kinase C controls lysosome biogenesis independently of mTORC1', *Nat Cell Biol,* 18(10), pp. 1065-77.

Lin, X., Yang, T., Wang, S., Wang, Z., Yun, Y., Sun, L., Zhou, Y., Xu, X., Akazawa, C., Hong, W. and Wang, T. (2014) 'RILP interacts with HOPS complex via VPS41 subunit to regulate endocytic trafficking', *Sci Rep,* 4, pp. 7282.

Lippé, R., Miaczynska, M., Rybin, V., Runge, A. and Zerial, M. (2001) 'Functional synergy between Rab5 effector Rabaptin-5 and exchange factor Rabex-5 when physically associated in a complex', *Mol Biol Cell,* 12(7), pp. 2219-28.

Lloyd-Evans, E., Morgan, A. J., He, X., Smith, D. A., Elliot-Smith, E., Sillence, D. J., Churchill, G. C., Schuchman, E. H., Galione, A. and Platt, F. M. (2008) 'Niemann-Pick disease type C1 is a sphingosine storage disease that causes deregulation of lysosomal calcium', *Nat Med,* 14(11), pp. 1247-55.

Lloyd-Evans, E. and Platt, F. M. (2011) 'Lysosomal Ca(2+) homeostasis: role in pathogenesis of lysosomal storage diseases', *Cell Calcium,* 50(2), pp. 200-5.

Lu, S., Sung, T., Lin, N., Abraham, R. T. and Jessen, B. A. (2017) 'Lysosomal adaptation: How cells respond to lysosomotropic compounds', *PLoS One,* 12(3), pp. e0173771.

Luzio, J. P., Bright, N. A. and Pryor, P. R. (2007) 'The role of calcium and other ions in sorting and delivery in the late endocytic pathway', *Biochem Soc Trans,* 35(Pt 5), pp. 1088-91.

Luzio, J. P., Pryor, P. R. and Bright, N. A. (2007) 'Lysosomes: fusion and function', *Nat Rev Mol Cell Biol,* 8(8), pp. 622-32.

López-Sanjurjo, C. I., Tovey, S. C., Prole, D. L. and Taylor, C. W. (2013) 'Lysosomes shape Ins(1,4,5)P3-evoked Ca2+ signals by selectively sequestering Ca2+ released from the endoplasmic reticulum', *J Cell Sci,* 126(Pt 1), pp. 289-300.

Maekawa, M., Terasaka, S., Mochizuki, Y., Kawai, K., Ikeda, Y., Araki, N., Skolnik, E. Y., Taguchi, T. and Arai, H. (2014) 'Sequential breakdown of 3-phosphorylated phosphoinositides is essential for the completion of macropinocytosis', *Proc Natl Acad Sci U S A,* 111(11), pp. E978-87.

Marshansky, V. and Futai, M. (2008) 'The V-type H+-ATPase in vesicular trafficking: targeting, regulation and function', *Curr Opin Cell Biol,* 20(4), pp. 415-26.

Martina, J. A., Diab, H. I., Brady, O. A. and Puertollano, R. (2016) 'TFEB and TFE3 are novel components of the integrated stress response', *EMBO J,* 35(5), pp. 479-95.

Martina, J. A. and Puertollano, R. (2013) 'Rag GTPases mediate amino acid-dependent recruitment of TFEB and MITF to lysosomes', *J Cell Biol,* 200(4), pp. 475-91.

Matsui, T., Jiang, P., Nakano, S., Sakamaki, Y., Yamamoto, H. and Mizushima, N. (2018) 'Autophagosomal YKT6 is required for fusion with lysosomes independently of syntaxin 17', *J Cell Biol*.

Mauvezin, C., Nagy, P., Juhász, G. and Neufeld, T. P. (2015) 'Autophagosome-lysosome fusion is independent of V-ATPase-mediated acidification', *Nat Commun,* 6, pp. 7007.

McNally, K. E., Faulkner, R., Steinberg, F., Gallon, M., Ghai, R., Pim, D., Langton, P., Pearson, N., Danson, C. M., Nägele, H., Morris, L. L., Singla, A., Overlee, B. L., Heesom, K. J., Sessions, R., Banks, L., Collins, B. M., Berger, I., Billadeau, D. D., Burstein, E. and Cullen, P. J. (2017) 'Retriever is a multiprotein complex for retromer-independent endosomal cargo recycling', *Nat Cell Biol,* 19(10), pp. 1214-1225.

Medina, D. L., Di Paola, S., Peluso, I., Armani, A., De Stefani, D., Venditti, R., Montefusco, S., Scotto-Rosato, A., Prezioso, C., Forrester, A., Settembre, C., Wang, W., Gao, Q., Xu, H., Sandri, M., Rizzuto, R., De Matteis, M. A. and Ballabio, A. (2015) 'Lysosomal calcium signalling regulates autophagy through calcineurin and TFEB', *Nat Cell Biol,* 17(3), pp. 288-99.

Melchionda, M., Pittman, J. K., Mayor, R. and Patel, S. (2016) 'Ca2+/H+ exchange by acidic organelles regulates cell migration in vivo', *J Cell Biol,* 212(7), pp. 803-13.

Mellman, I., Fuchs, R. and Helenius, A. (1986) 'Acidification of the endocytic and exocytic pathways', *Annu Rev Biochem,* 55, pp. 663-700.

Mellman, I. and Warren, G. (2000) 'The road taken: past and future foundations of membrane traffic', *Cell,* 100(1), pp. 99-112.

Meo-Evoli, N., Almacellas, E., Massucci, F. A., Gentilella, A., Ambrosio, S., Kozma, S. C., Thomas, G. and Tauler, A. (2015) 'V-ATPase: a master effector of E2F1-mediated lysosomal trafficking, mTORC1 activation and autophagy', *Oncotarget,* 6(29), pp. 28057-70.

Merzlyak, E. M., Goedhart, J., Shcherbo, D., Bulina, M. E., Shcheglov, A. S., Fradkov, A. F., Gaintzeva, A., Lukyanov, K. A., Lukyanov, S., Gadella, T. W. and Chudakov, D. M. (2007) 'Bright monomeric red fluorescent protein with an extended fluorescence lifetime', *Nat Methods,* 4(7), pp. 555-7.

Metcalf, D. and Isaacs, A. M. (2010) 'The role of ESCRT proteins in fusion events involving lysosomes, endosomes and autophagosomes', *Biochem Soc Trans,* 38(6), pp. 1469-73.

Meyer, C., Zizioli, D., Lausmann, S., Eskelinen, E. L., Hamann, J., Saftig, P., von Figura, K. and Schu, P. (2000) 'mu1A-adaptin-deficient mice: lethality, loss of AP-1 binding and rerouting of mannose 6-phosphate receptors', *EMBO J,* 19(10), pp. 2193-203.

Miller, A., Schafer, J., Upchurch, C., Spooner, E., Huynh, J., Hernandez, S., McLaughlin, B., Oden, L. and Fares, H. (2015) 'Mucolipidosis type IV protein TRPML1-dependent lysosome formation', *Traffic,* 16(3), pp. 284-97.
Morgan, A. J., Platt, F. M., Lloyd-Evans, E. and Galione, A. (2011) 'Molecular mechanisms of endolysosomal Ca2+ signalling in health and disease', *Biochem J,* 439(3), pp. 349-74.

Mousavi, S. A., Malerød, L., Berg, T. and Kjeken, R. (2004) 'Clathrin-dependent endocytosis', *Biochem J,* 377(Pt 1), pp. 1-16.

Mullock, B. M., Bright, N. A., Fearon, C. W., Gray, S. R. and Luzio, J. P. (1998) 'Fusion of lysosomes with late endosomes produces a hybrid organelle of intermediate density and is NSF dependent', *J Cell Biol,* 140(3), pp. 591-601.

Munro, S. (2003) 'Lipid rafts: elusive or illusive?', *Cell,* 115(4), pp. 377-88.

Napolitano, G. and Ballabio, A. (2016) 'TFEB at a glance', *J Cell Sci,* 129(13), pp. 2475-81.

Napolitano, G., Esposito, A., Choi, H., Matarese, M., Benedetti, V., Di Malta, C., Monfregola, J., Medina, D. L., Lippincott-Schwartz, J. and Ballabio, A. (2018) 'mTOR-dependent phosphorylation controls TFEB nuclear export', *Nat Commun,* 9(1), pp. 3312.

Naufer, A., Hipolito, V. E. B., Ganesan, S., Prashar, A., Zaremberg, V., Botelho, R. J. and Terebiznik, M. R. (2018) 'pH of endophagosomes controls association of their membranes with Vps34 and PtdIns(3)P levels', *J Cell Biol,* 217(1), pp. 329-346.

Nguyen, O. N., Grimm, C., Schneider, L. S., Chao, Y. K., Atzberger, C., Bartel, K., Watermann, A., Ulrich, M., Mayr, D., Wahl-Schott, C., Biel, M. and Vollmar, A. M. (2017) 'Two-Pore Channel Function Is Crucial for the Migration of Invasive Cancer Cells', *Cancer Res,* 77(6), pp. 1427-1438.

Nordmann, M., Cabrera, M., Perz, A., Bröcker, C., Ostrowicz, C., Engelbrecht-Vandré, S. and Ungermann, C. (2010) 'The Mon1-Ccz1 complex is the GEF of the late endosomal Rab7 homolog Ypt7', *Curr Biol,* 20(18), pp. 1654-9.

Ohkuma, S., Moriyama, Y. and Takano, T. (1982) 'Identification and characterization of a proton pump on lysosomes by fluorescein-isothiocyanate-dextran fluorescence', *Proc Natl Acad Sci U S A,* 79(9), pp. 2758-62.

Ostrowski, P. P., Fairn, G. D., Grinstein, S. and Johnson, D. E. (2016) 'Cresyl violet: a superior fluorescent lysosomal marker', *Traffic,* 17(12), pp. 1313-1321.

Palmieri, M., Impey, S., Kang, H., di Ronza, A., Pelz, C., Sardiello, M. and Ballabio, A. (2011) 'Characterization of the CLEAR network reveals an integrated control of cellular clearance pathways', *Hum Mol Genet,* 20(19), pp. 3852-66.

Palmieri, M., Pal, R., Nelvagal, H. R., Lotfi, P., Stinnett, G. R., Seymour, M. L., Chaudhury, A., Bajaj, L., Bondar, V. V., Bremner, L., Saleem, U., Tse, D. Y., Sanagasetti, D., Wu, S. M., Neilson, J. R., Pereira, F. A., Pautler, R. G., Rodney, G. G., Cooper, J. D. and Sardiello, M. (2017) 'mTORC1-independent TFEB activation via Akt inhibition promotes cellular clearance in neurodegenerative storage diseases', *Nat Commun,* 8, pp. 14338.

Parkinson, M. D., Piper, S. C., Bright, N. A., Evans, J. L., Boname, J. M., Bowers, K., Lehner, P. J. and Luzio, J. P. (2015) 'A non-canonical ESCRT pathway, including histidine domain phosphotyrosine phosphatase (HD-PTP), is used for down-regulation of virally ubiquitinated MHC class I', *Biochem J,* 471(1), pp. 79-88.
Parra, K. J., Keenan, K. L. and Kane, P. M. (2000) 'The H subunit (Vma13p) of the yeast V-ATPase inhibits the ATPase activity of cytosolic V1 complexes', *J Biol Chem,* 275(28), pp. 21761-7.

Parton, R. G. and Simons, K. (2007) 'The multiple faces of caveolae', *Nat Rev Mol Cell Biol,* 8(3), pp. 185-94.

Parton, R. G., Tillu, V. A. and Collins, B. M. (2018) 'Caveolae', *Curr Biol,* 28(8), pp. R402-R405.

Patterson, G. H., Knobel, S. M., Sharif, W. D., Kain, S. R. and Piston, D. W. (1997) 'Use of the green fluorescent protein and its mutants in quantitative fluorescence microscopy', *Biophys J,* 73(5), pp. 2782-90.

Penny, C. J., Kilpatrick, B. S., Eden, E. R. and Patel, S. (2015) 'Coupling acidic organelles with the ER through Ca^{2+} microdomains at membrane contact sites', *Cell Calcium,* 58(4), pp. 387-96.

Perera, R. M. and Zoncu, R. (2016) 'The Lysosome as a Regulatory Hub', *Annu Rev Cell Dev Biol,* 32, pp. 223-253.

Perini, E. D., Schaefer, R., Stöter, M., Kalaidzidis, Y. and Zerial, M. (2014) 'Mammalian CORVET is required for fusion and conversion of distinct early endosome subpopulations', *Traffic,* 15(12), pp. 1366-89.

Peters, C., Bayer, M. J., Bühler, S., Andersen, J. S., Mann, M. and Mayer, A. (2001) 'Trans-complex formation by proteolipid channels in the terminal phase of membrane fusion', *Nature,* 409(6820), pp. 581-8.

Petzoldt, A. G., Gleixner, E. M., Fumagalli, A., Vaccari, T. and Simons, M. (2013) 'Elevated expression of the V-ATPase C subunit triggers JNK-dependent cell invasion and overgrowth in a Drosophila epithelium', *Dis Model Mech,* 6(3), pp. 689-700.

Pitt, S. J., Funnell, T. M., Sitsapesan, M., Venturi, E., Rietdorf, K., Ruas, M., Ganesan, A., Gosain, R., Churchill, G. C., Zhu, M. X., Parrington, J., Galione, A. and Sitsapesan, R. (2010) 'TPC2 is a novel NAADP-sensitive Ca2+ release channel, operating as a dual sensor of luminal pH and Ca2+', *J Biol Chem,* 285(45), pp. 35039-46.

Platt, F. M., Boland, B. and van der Spoel, A. C. (2012) 'The cell biology of disease: lysosomal storage disorders: the cellular impact of lysosomal dysfunction', *J Cell Biol,* 199(5), pp. 723-34.

Polo, S., Sigismund, S., Faretta, M., Guidi, M., Capua, M. R., Bossi, G., Chen, H., De Camilli, P. and Di Fiore, P. P. (2002) 'A single motif responsible for ubiquitin recognition and monoubiquitination in endocytic proteins', *Nature,* 416(6879), pp. 451-5.

Pols, M. S., ten Brink, C., Gosavi, P., Oorschot, V. and Klumperman, J. (2013a) 'The HOPS proteins hVps41 and hVps39 are required for homotypic and heterotypic late endosome fusion', *Traffic,* 14(2), pp. 219-32.

Pols, M. S., van Meel, E., Oorschot, V., ten Brink, C., Fukuda, M., Swetha, M. G., Mayor, S. and Klumperman, J. (2013b) 'hVps41 and VAMP7 function in direct TGN to late endosome transport of lysosomal membrane proteins', *Nat Commun,* 4, pp. 1361.

Popova, N. V., Deyev, I. E. and Petrenko, A. G. (2013) 'Clathrin-mediated endocytosis and adaptor proteins', *Acta Naturae,* 5(3), pp. 62-73.

Poteryaev, D., Datta, S., Ackema, K., Zerial, M. and Spang, A. (2010) 'Identification of the switch in early-to-late endosome transition', *Cell,* 141(3), pp. 497-508.

Poupon, V., Stewart, A., Gray, S. R., Piper, R. C. and Luzio, J. P. (2003) 'The role of mVps18p in clustering, fusion, and intracellular localization of late endocytic organelles', *Mol Biol Cell,* 14(10), pp. 4015-27.

Pryor, P. R., Mullock, B. M., Bright, N. A., Gray, S. R. and Luzio, J. P. (2000) 'The role of intraorganellar Ca(2+) in late endosome-lysosome heterotypic fusion and in the reformation of lysosomes from hybrid organelles', *J Cell Biol,* 149(5), pp. 1053-62.

Pryor, P. R., Mullock, B. M., Bright, N. A., Lindsay, M. R., Gray, S. R., Richardson, S. C., Stewart, A., James, D. E., Piper, R. C. and Luzio, J. P. (2004) 'Combinatorial SNARE complexes with VAMP7 or VAMP8 define different late endocytic fusion events', *EMBO Rep,* 5(6), pp. 590-5.

Pu, J., Schindler, C., Jia, R., Jarnik, M., Backlund, P. and Bonifacino, J. S. (2015) 'BORC, a multisubunit complex that regulates lysosome positioning', *Dev Cell,* 33(2), pp. 176-88.

Raben, N. and Puertollano, R. (2016) 'TFEB and TFE3: Linking Lysosomes to Cellular Adaptation to Stress', *Annu Rev Cell Dev Biol,* 32, pp. 255-278.

Raffaello, A., Mammucari, C., Gherardi, G. and Rizzuto, R. (2016) 'Calcium at the Center of Cell Signaling: Interplay between Endoplasmic Reticulum, Mitochondria, and Lysosomes', *Trends Biochem Sci,* 41(12), pp. 1035-1049.

Rahman, S., Yamato, I., Saijo, S., Mizutani, K., Takamuku, Y., Ishizuka-Katsura, Y., Ohsawa, N., Terada, T., Shirouzu, M., Yokoyama, S. and Murata, T. (2016) 'Binding interactions of the peripheral stalk subunit isoforms from human V-ATPase', *Biosci Biotechnol Biochem*, pp. 1-13.

Raymond, C. K., Howald-Stevenson, I., Vater, C. A. and Stevens, T. H. (1992) 'Morphological classification of the yeast vacuolar protein sorting mutants: evidence for a prevacuolar compartment in class E vps mutants', *Mol Biol Cell,* 3(12), pp. 1389-402.

Richo, G. R. and Conner, G. E. (1994) 'Structural requirements of procathepsin D activation and maturation', *J Biol Chem,* 269(20), pp. 14806-12.

Rink, J., Ghigo, E., Kalaidzidis, Y. and Zerial, M. (2005) 'Rab conversion as a mechanism of progression from early to late endosomes', *Cell,* 122(5), pp. 735-49.

Roczniak-Ferguson, A., Petit, C. S., Froehlich, F., Qian, S., Ky, J., Angarola, B., Walther, T. C. and Ferguson, S. M. (2012) 'The transcription factor TFEB links mTORC1 signaling to transcriptional control of lysosome homeostasis', *Sci Signal,* 5(228), pp. ra42.

Rofe, A. P., Davis, L. J., Whittingham, J. L., Latimer-Bowman, E. C., Wilkinson, A. J. and Pryor, P. R. (2017) 'The Rhodococcus equi virulence protein VapA disrupts endolysosome function and stimulates lysosome biogenesis', *Microbiologyopen,* 6(2).

Ronco, V., Potenza, D. M., Denti, F., Vullo, S., Gagliano, G., Tognolina, M., Guerra, G., Pinton, P., Genazzani, A. A., Mapelli, L., Lim, D. and Moccia, F. (2015) 'A novel Ca^{2+}-mediated cross-talk between endoplasmic reticulum and acidic organelles: implications for NAADP-dependent Ca^{2+} signalling', *Cell Calcium,* 57(2), pp. 89-100.

Rong, Y., Liu, M., Ma, L., Du, W., Zhang, H., Tian, Y., Cao, Z., Li, Y., Ren, H., Zhang, C., Li, L., Chen, S., Xi, J. and Yu, L. (2012) 'Clathrin and phosphatidylinositol-4,5-bisphosphate regulate autophagic lysosome reformation', *Nat Cell Biol,* 14(9), pp. 924-34.

Rong, Y., McPhee, C. K., McPhee, C., Deng, S., Huang, L., Chen, L., Liu, M., Tracy, K., Baehrecke, E. H., Baehreck, E. H., Yu, L. and Lenardo, M. J. (2011) 'Spinster is required for autophagic lysosome reformation and mTOR reactivation following starvation', *Proc Natl Acad Sci U S A,* 108(19), pp. 7826-31.

Rosa-Ferreira, C. and Munro, S. (2011) 'Arl8 and SKIP act together to link lysosomes to kinesin-1', *Dev Cell,* 21(6), pp. 1171-8.

Rowland, A. A., Chitwood, P. J., Phillips, M. J. and Voeltz, G. K. (2014) 'ER contact sites define the position and timing of endosome fission', *Cell,* 159(5), pp. 1027-1041.

Saarikangas, J., Zhao, H. and Lappalainen, P. (2010) 'Regulation of the actin cytoskeleton-plasma membrane interplay by phosphoinositides', *Physiol Rev,* 90(1), pp. 259-89.

Saftig, P. and Klumperman, J. (2009) 'Lysosome biogenesis and lysosomal membrane proteins: trafficking meets function', *Nat Rev Mol Cell Biol,* 10(9), pp. 623-35.

Sakurai, Y., Kolokoltsov, A. A., Chen, C. C., Tidwell, M. W., Bauta, W. E., Klugbauer, N., Grimm, C., Wahl-Schott, C., Biel, M. and Davey, R. A. (2015) 'Ebola virus. Two-pore channels control Ebola virus host cell entry and are drug targets for disease treatment', *Science,* 347(6225), pp. 995-8.

Sancak, Y., Peterson, T. R., Shaul, Y. D., Lindquist, R. A., Thoreen, C. C., Bar-Peled, L. and Sabatini, D. M. (2008) 'The Rag GTPases bind raptor and mediate amino acid signaling to mTORC1', *Science,* 320(5882), pp. 1496-501.

Sardiello, M., Palmieri, M., di Ronza, A., Medina, D. L., Valenza, M., Gennarino, V. A., Di Malta, C., Donaudy, F., Embrione, V., Polishchuk, R. S., Banfi, S., Parenti, G., Cattaneo, E. and Ballabio, A. (2009) 'A gene network regulating lysosomal biogenesis and function', *Science,* 325(5939), pp. 473-7.

Sato, M., Yoshimura, S., Hirai, R., Goto, A., Kunii, M., Atik, N., Sato, T., Sato, K., Harada, R., Shimada, J., Hatabu, T., Yorifuji, H. and Harada, A. (2011) 'The role of VAMP7/TI-VAMP in cell polarity and lysosomal exocytosis in vivo', *Traffic,* 12(10), pp. 1383-93.

Sbano, L., Bonora, M., Marchi, S., Baldassari, F., Medina, D. L., Ballabio, A., Giorgi, C. and Pinton, P. (2017) 'TFEB-mediated increase in peripheral lysosomes regulates store-operated calcium entry', *Sci Rep,* 7, pp. 40797.

Schmid, S. L., McNiven, M. A. and De Camilli, P. (1998) 'Dynamin and its partners: a progress report', *Curr Opin Cell Biol,* 10(4), pp. 504-12.

Schmidt, O. and Teis, D. (2012) 'The ESCRT machinery', *Curr Biol,* 22(4), pp. R116-20.
Schulze, R. J., Weller, S. G., Schroeder, B., Krueger, E. W., Chi, S., Casey, C. A. and McNiven, M. A. (2013) 'Lipid droplet breakdown requires dynamin 2 for vesiculation of autolysosomal tubules in hepatocytes', *J Cell Biol,* 203(2), pp. 315-26.

Seaman, M. N. (2004) 'Cargo-selective endosomal sorting for retrieval to the Golgi requires retromer', *J Cell Biol,* 165(1), pp. 111-22.

Seaman, M. N., Ball, C. L. and Robinson, M. S. (1993) 'Targeting and mistargeting of plasma membrane adaptors in vitro', *J Cell Biol,* 123(5), pp. 1093-105.

Settembre, C., De Cegli, R., Mansueto, G., Saha, P. K., Vetrini, F., Visvikis, O., Huynh, T., Carissimo, A., Palmer, D., Klisch, T. J., Wollenberg, A. C., Di Bernardo, D., Chan, L., Irazoqui, J. E. and Ballabio, A. (2013) 'TFEB controls cellular lipid metabolism through a starvation-induced autoregulatory loop', *Nat Cell Biol,* 15(6), pp. 647-58.

Settembre, C., Di Malta, C., Polito, V. A., Garcia Arencibia, M., Vetrini, F., Erdin, S., Erdin, S. U., Huynh, T., Medina, D., Colella, P., Sardiello, M., Rubinsztein, D. C. and Ballabio, A. (2011) 'TFEB links autophagy to lysosomal biogenesis', *Science,* 332(6036), pp. 1429-33.

Settembre, C., Zoncu, R., Medina, D. L., Vetrini, F., Erdin, S., Huynh, T., Ferron, M., Karsenty, G., Vellard, M. C., Facchinetti, V., Sabatini, D. M. and Ballabio, A. (2012) 'A lysosome-to-nucleus signalling mechanism senses and regulates the lysosome via mTOR and TFEB', *EMBO J,* 31(5), pp. 1095-108.

Sha, Y., Rao, L., Settembre, C., Ballabio, A. and Eissa, N. T. (2017) 'STUB1 regulates TFEB-induced autophagy-lysosome pathway', *EMBO J,* 36(17), pp. 2544-2552.

Shalem, O., Sanjana, N. E., Hartenian, E., Shi, X., Scott, D. A., Mikkelson, T., Heckl, D., Ebert, B. L., Root, D. E., Doench, J. G. and Zhang, F. (2014) 'Genome-scale CRISPR-Cas9 knockout screening in human cells', *Science,* 343(6166), pp. 84-87.

Shaner, N. C., Lin, M. Z., McKeown, M. R., Steinbach, P. A., Hazelwood, K. L., Davidson, M. W. and Tsien, R. Y. (2008) 'Improving the photostability of bright monomeric orange and red fluorescent proteins', *Nat Methods,* 5(6), pp. 545-51.

Shayman, J. A. and Abe, A. (2013) 'Drug induced phospholipidosis: an acquired lysosomal storage disorder', *Biochim Biophys Acta,* 1831(3), pp. 602-11.

Shen, Y., Rosendale, M., Campbell, R. E. and Perrais, D. (2014) 'pHuji, a pH-sensitive red fluorescent protein for imaging of exo- and endocytosis', *J Cell Biol,* 207(3), pp. 419-32.

Shim, J. H., Xiao, C., Hayden, M. S., Lee, K. Y., Trombetta, E. S., Pypaert, M., Nara, A., Yoshimori, T., Wilm, B., Erdjument-Bromage, H., Tempst, P., Hogan, B. L., Mellman, I. and Ghosh, S. (2006) 'CHMP5 is essential for late endosome function and down-regulation of receptor signaling during mouse embryogenesis', *J Cell Biol,* 172(7), pp. 1045-56.

Shukla, S. J., Huang, R., Austin, C. P. and Xia, M. (2010) 'The future of toxicity testing: a focus on in vitro methods using a quantitative high-throughput screening platform', *Drug Discov Today,* 15(23-24), pp. 997-1007.
Sigismund, S., Woelk, T., Puri, C., Maspero, E., Tacchetti, C., Transidico, P., Di Fiore, P. P. and Polo, S. (2005) 'Clathrin-independent endocytosis of ubiquitinated cargos', *Proc Natl Acad Sci U S A,* 102(8), pp. 2760-5.

Song, J. X., Sun, Y. R., Peluso, I., Zeng, Y., Yu, X., Lu, J. H., Xu, Z., Wang, M. Z., Liu, L. F., Huang, Y. Y., Chen, L. L., Durairajan, S. S., Zhang, H. J., Zhou, B., Zhang, H. Q., Lu, A., Ballabio, A., Medina, D. L., Guo, Z. and Li, M. (2016) 'A novel curcumin analog binds to and activates TFEB in vitro and in vivo independent of MTOR inhibition', *Autophagy,* 12(8), pp. 1372-89.

Sorkin, A. and Goh, L. K. (2009) 'Endocytosis and intracellular trafficking of ErbBs', *Exp Cell Res,* 315(4), pp. 683-96.

Steinberg, B. E., Huynh, K. K., Brodovitch, A., Jabs, S., Stauber, T., Jentsch, T. J. and Grinstein, S. (2010) 'A cation counterflux supports lysosomal acidification', *J Cell Biol,* 189(7), pp. 1171-86.

Sumner, J. P., Dow, J. A., Earley, F. G., Klein, U., Jäger, D. and Wieczorek, H. (1995) 'Regulation of plasma membrane V-ATPase activity by dissociation of peripheral subunits', *J Biol Chem,* 270(10), pp. 5649-53.

Sun-Wada, G. H., Tabata, H., Kawamura, N., Aoyama, M. and Wada, Y. (2009) 'Direct recruitment of H+-ATPase from lysosomes for phagosomal acidification', *J Cell Sci,* 122(Pt 14), pp. 2504-13.

Swift, S., Lorens, J., Achacoso, P. and Nolan, G. P. (2001) 'Rapid production of retroviruses for efficient gene delivery to mammalian cells using 293T cell-based systems', *Curr Protoc Immunol,* Chapter 10, pp. Unit 10.17C.

Takáts, S., Glatz, G., Szenci, G., Boda, A., Horváth, G. V., Hegedűs, K., Kovács, A. L. and Juhász, G. (2018) 'Non-canonical role of the SNARE protein Ykt6 in autophagosome-lysosome fusion', *PLoS Genet,* 14(4), pp. e1007359.

Thorngren, N., Collins, K. M., Fratti, R. A., Wickner, W. and Merz, A. J. (2004) 'A soluble SNARE drives rapid docking, bypassing ATP and Sec17/18p for vacuole fusion', *EMBO J,* 23(14), pp. 2765-76.

Tian, X., Gala, U., Zhang, Y., Shang, W., Nagarkar Jaiswal, S., di Ronza, A., Jaiswal, M., Yamamoto, S., Sandoval, H., Duraine, L., Sardiello, M., Sillitoe, R. V., Venkatachalam, K., Fan, H., Bellen, H. J. and Tong, C. (2015) 'A voltage-gated calcium channel regulates lysosomal fusion with endosomes and autophagosomes and is required for neuronal homeostasis', *PLoS Biol,* 13(3), pp. e1002103.

Toyomura, T., Murata, Y., Yamamoto, A., Oka, T., Sun-Wada, G. H., Wada, Y. and Futai, M. (2003) 'From lysosomes to the plasma membrane: localization of vacuolar-type H+ -ATPase with the a3 isoform during osteoclast differentiation', *J Biol Chem,* 278(24), pp. 22023-30.

Traub, L. M. and Bonifacino, J. S. (2013) 'Cargo recognition in clathrin-mediated endocytosis', *Cold Spring Harb Perspect Biol,* 5(11), pp. a016790.

Trombetta, E. S., Ebersold, M., Garrett, W., Pypaert, M. and Mellman, I. (2003) 'Activation of lysosomal function during dendritic cell maturation', *Science,* 299(5611), pp. 1400-3.

Tynell, J., Melén, K. and Julkunen, I. (2014) 'Mutations within the conserved NS1 nuclear export signal lead to inhibition of influenza A virus replication', *Virol J,* 11, pp. 128.
Ungermann, C., von Mollard, G. F., Jensen, O. N., Margolis, N., Stevens, T. H. and Wickner, W. (1999) 'Three v-SNAREs and two t-SNAREs, present in a pentameric cis-SNARE complex on isolated vacuoles, are essential for homotypic fusion', *J Cell Biol,* 145(7), pp. 1435-42.

Ungermann, C., Wickner, W. and Xu, Z. (1999) 'Vacuole acidification is required for trans-SNARE pairing, LMA1 release, and homotypic fusion', *Proc Natl Acad Sci U S A,* 96(20), pp. 11194-9.

Urwin, H., Authier, A., Nielsen, J. E., Metcalf, D., Powell, C., Froud, K., Malcolm, D. S., Holm, I., Johannsen, P., Brown, J., Fisher, E. M., van der Zee, J., Bruyland, M., Van Broeckhoven, C., Collinge, J., Brandner, S., Futter, C., Isaacs, A. M. and Consortium, F. (2010) 'Disruption of endocytic trafficking in frontotemporal dementia with CHMP2B mutations', *Hum Mol Genet,* 19(11), pp. 2228-38.

van der Kant, R., Jonker, C. T., Wijdeven, R. H., Bakker, J., Janssen, L., Klumperman, J. and Neefjes, J. (2015) 'Characterization of the Mammalian CORVET and HOPS Complexes and Their Modular Restructuring for Endosome Specificity', *J Biol Chem,* 290(51), pp. 30280-90.

van Deurs, B., Holm, P. K., Kayser, L. and Sandvig, K. (1995) 'Delivery to lysosomes in the human carcinoma cell line HEp-2 involves an actin filament-facilitated fusion between mature endosomes and preexisting lysosomes', *Eur J Cell Biol,* 66(4), pp. 309-23.

Van Dyke, R. W. (1993) 'Acidification of rat liver lysosomes: quantitation and comparison with endosomes', *Am J Physiol,* 265(4 Pt 1), pp. C901-17.

van Weert, A. W., Dunn, K. W., Geuze, H. J., Maxfield, F. R. and Stoorvogel, W. (1995) 'Transport from late endosomes to lysosomes, but not sorting of integral membrane proteins in endosomes, depends on the vacuolar proton pump', *J Cell Biol,* 130(4), pp. 821-34.

Vega-Rubin-de-Celis, S., Peña-Llopis, S., Konda, M. and Brugarolas, J. (2017) 'Multistep regulation of TFEB by MTORC1', *Autophagy,* 13(3), pp. 464-472.

von Bargen, K. and Haas, A. (2009) 'Molecular and infection biology of the horse pathogen Rhodococcus equi', *FEMS Microbiol Rev,* 33(5), pp. 870-91.

Wang, C. C., Ng, C. P., Lu, L., Atlashkin, V., Zhang, W., Seet, L. F. and Hong, W. (2004) 'A role of VAMP8/endobrevin in regulated exocytosis of pancreatic acinar cells', *Dev Cell,* 7(3), pp. 359-71.

Wang, T., Li, L. and Hong, W. (2017) 'SNARE proteins in membrane trafficking', *Traffic,* 18(12), pp. 767-775.

Ward, D. M., Pevsner, J., Scullion, M. A., Vaughn, M. and Kaplan, J. (2000) 'Syntaxin 7 and VAMP-7 are soluble N-ethylmaleimide-sensitive factor attachment protein receptors required for late endosome-lysosome and homotypic lysosome fusion in alveolar macrophages', *Mol Biol Cell,* 11(7), pp. 2327-33.

Wartosch, L., Günesdogan, U., Graham, S. C. and Luzio, J. P. (2015) 'Recruitment of VPS33A to HOPS by VPS16 Is Required for Lysosome Fusion with Endosomes and Autophagosomes', *Traffic,* 16(7), pp. 727-42.

Watts, C. and Marsh, M. (1992) 'Endocytosis: what goes in and how?', *J Cell Sci,* 103 (Pt 1), pp. 1-8.

Wee, Y. S., Roundy, K. M., Weis, J. J. and Weis, J. H. (2012) 'Interferon-inducible transmembrane proteins of the innate immune response act as membrane organizers by influencing clathrin and v-ATPase localization and function', *Innate Immun,* 18(6), pp. 834-45.

Wen, W., Yu, J., Pan, L., Wei, Z., Weng, J., Wang, W., Ong, Y. S., Tran, T. H., Hong, W. and Zhang, M. (2010) 'Lipid-Induced conformational switch controls fusion activity of longin domain SNARE Ykt6', *Mol Cell,* 37(3), pp. 383-95.

Wenzel, E. M., Schultz, S. W., Schink, K. O., Pedersen, N. M., Nähse, V., Carlson, A., Brech, A., Stenmark, H. and Raiborg, C. (2018) 'Concerted ESCRT and clathrin recruitment waves define the timing and morphology of intraluminal vesicle formation', *Nat Commun,* 9(1), pp. 2932.

White, I. J., Bailey, L. M., Aghakhani, M. R., Moss, S. E. and Futter, C. E. (2006) 'EGF stimulates annexin 1-dependent inward vesiculation in a multivesicular endosome subpopulation', *EMBO J,* 25(1), pp. 1-12.

Wijdeven, R. H., Janssen, H., Nahidiazar, L., Janssen, L., Jalink, K., Berlin, I. and Neefjes, J. (2016) 'Cholesterol and ORP1L-mediated ER contact sites control autophagosome transport and fusion with the endocytic pathway', *Nat Commun,* 7, pp. 11808.

Woodman, P. G. and Futter, C. E. (2008) 'Multivesicular bodies: co-ordinated progression to maturity', *Curr Opin Cell Biol,* 20(4), pp. 408-14.

Xu, D., Farmer, A., Collett, G., Grishin, N. V. and Chook, Y. M. (2012) 'Sequence and structural analyses of nuclear export signals in the NESdb database', *Mol Biol Cell,* 23(18), pp. 3677-93.

Yamasaki, M., Thomas, J. M., Churchill, G. C., Garnham, C., Lewis, A. M., Cancela, J. M., Patel, S. and Galione, A. (2005) 'Role of NAADP and cADPR in the induction and maintenance of agonist-evoked Ca2+ spiking in mouse pancreatic acinar cells', *Curr Biol,* 15(9), pp. 874-8.

Yamashiro, D. J. and Maxfield, F. R. (1987) 'Acidification of morphologically distinct endosomes in mutant and wild-type Chinese hamster ovary cells', *J Cell Biol,* 105(6 Pt 1), pp. 2723-33.

Yu, L., McPhee, C. K., Zheng, L., Mardones, G. A., Rong, Y., Peng, J., Mi, N., Zhao, Y., Liu, Z., Wan, F., Hailey, D. W., Oorschot, V., Klumperman, J., Baehrecke, E. H. and Lenardo, M. J. (2010) 'Termination of autophagy and reformation of lysosomes regulated by mTOR', *Nature,* 465(7300), pp. 942-6.

Zerial, M. and McBride, H. (2001) 'Rab proteins as membrane organizers', *Nat Rev Mol Cell Biol,* 2(2), pp. 107-17.

Zhang, H. and Hu, J. (2016) 'Shaping the Endoplasmic Reticulum into a Social Network', *Trends Cell Biol,* 26(12), pp. 934-943.

Zou, J., Hu, B., Arpag, S., Yan, Q., Hamilton, A., Zeng, Y. S., Vanoye, C. G. and Li, J. (2015) 'Reactivation of Lysosomal Ca2+ Efflux Rescues Abnormal Lysosomal Storage in FIG4-Deficient Cells', *J Neurosci,* 35(17), pp. 6801-12.